Prestress and Deformation Control in Flexible Structures

Thesis submitted in partial fulfilment of the requirements

for the degree of Doctor of Philosophy (PhD)

Najmadeen Mohammed Saeed

B.Sc. & M.Sc., Structural Engineering

Cardiff School of Engineering

Cardiff University

United Kingdom

December 2014

ACKNOWLEDGEMENTS

Dedicated to

➢ *Kurdistan Regional Government*

➢ *My Parents Mohammed and Hamin*

➢ *My Wife Paiman*

➢ *My Children Zhwan, Shwan, Tnok and Asman*

Najmadeen

ABSTRACT

A direct method for controlling nodal displacements and/or internal bar forces has been developed for prestressable structural assemblies including complex elements ("macro-elements", e.g. the pantographic element), involving Matrix Condensation. The method is aimed at static shape control of geometrically sensitive structures. The dissertation discusses identification of the most effective bars for actuation, without incurring violation in bar forces, and also with objective of minimal number of actuators or minimum actuation. The method can also be used for adjustment of bar forces to either reduce instances of high forces or increase low forces (*e.g.* in a cable nearing slack).

The techniques of controlling nodal displacement, bar force and simultaneously nodal displacement and bar force for a structure made of non-complex elements have been verified by experiments on the physical model of a cable-stayed bridge. Likewise the technique of joint displacement controlling of structures constructed from complex structural elements, has been also been confirmed by experiments on the physical model of an aerofoil shaped morphing pantographic structure. Overall, experimental results agree well with theoretical prediction.

This dissertation also concerns with morphing structures, *e.g.* as applied in the aerospace industry. A morphing aerofoil structure capable of variable geometry was developed, which was shown to be able to cater for the different aerodynamic requirements at different stages of flight. In this thesis, two suitable morphing aerofoil structures were made of curved pantographic units. Results show that the configuration with a large number of small pantograph elements exhibits a wider range of Lift Coefficient (C_L) and Drag Coefficient (C_D) than achievable by the first, and also by the standard NACA2415 aerofoil with flaps. In addition, it was found that the morphing aerofoil can decrease the drag by more than 18%, especially in the early stages of morphing.

Finally, two useful and relatively simple methods have been presented in this dissertation which provide a direct method for calculating required morphing shape displacements and calculating set of length actuations for bar assembly to adjust shape imperfection.

Keywords: Static shape control, Prestress control, Displacement control, Actuator placement, Force Method, Pantographic unit, Morphing structure, Morphing aerofoil, NACA aerofoil, Aerodynamic characteristics.

PhD THESIS RESEARCH ACHIEVEMENTS

- Saeed, N. M. & Kwan, A. S. K. 2014. *Concepts for morphing aerofoil sections using pantographic structures.* Proceedings of Mobile and Rapidly Assembled Structures IV. Ostend, Belgium, 11–13 June 2014. WIT Press, pp. 279-289.

TABLE OF CONTENTS

LIST OF FIGURES

LIST OF TABLES

LIST OF NOTATIONS

The following is a list of the most important symbols that appear in the thesis. Symbols not included in this list are defined when they first appear.

A	Equilibrium matrix
$\mathbf{A}^*$	Condensed equilibrium matrix
a, a₁, b, b₁, c,	Semi-bars (semi-lengths)
$\mathbf{A}^+$	Pseudo-inverse of **A**
$\mathbf{A_{mn}}$	Equilibrium sub-matrix
A_r	Surface area of wing
$\mathbf{A^T}$	Transposes of equilibrium matrix
axial	Bar/beam tension (elongation)
b	Number of bars
B	Compatibility matrix
$\mathbf{B}^*$	Condensed compatibility matrix
Bar36	Morphing control bar
$\mathbf{B_{nm}}$	Compatibility sub-matrix
$\mathbf{B^T}$	Transposes of compatibility matrix
c	Degrees of freedom
c	Chord line
C_D	Coefficient of Drag
C_L	Coefficient of Lift
Cm	Moment coefficient
Cp	Pressure coefficient
d	External nodal displacements
D, E, D', E'	Additional revolute joints of pantograph
$\mathbf{d_c}$	External nodal displacement vanishing and non-vanishing
$\mathbf{d_m}$	External displacement correspond directly to $\mathbf{p_m}$
$\mathbf{d_P}$	Nodal displacements due to only load
$\mathbf{d_p}$	External displacement correspond directly to $\mathbf{p_p}$ P.69
$\mathbf{d_{pc}}$	Nodal displacements due to only load vanishing and non-vanishing
e	Internal bar elongation
E	Young's modulus
$\mathbf{e}^*$	Condensed internal bar elongation
e'	Eccentricity
EA	The axial stiffness of members
EI	The bending stiffness of members

$\mathbf{e_n}$	Non-vanishing internal bar elongation actuation
$\mathbf{e_o}$	Elongation actuation vector
$\mathbf{e_o}^*$	Condensed elongation actuation vector
$\mathbf{e_{oc}}$	Elongation actuation vector vanishing and non-vanishing member
$\mathbf{e_p}$	Vanishing internal bar elongation actuation
ESPS	Exhaustive-single point substitution
$\mathbf{F}$	Flexibility matrix
$\mathbf{F}^*$	Condensed flexibility matrix
FA	Flap angle
F_D	Drag force on the aerofoil
F_L	Lift force on the aerofoil
F_{total}	Total force on the aerofoil
GA	Genetic algorithms
GA2	Modified Genetic Algorithm
i	Dimension of the structure
ISA	Improved simulated annealing
j	Number of joints of the structure
$\mathbf{K}$	Stiffness matrix
LE	Leading edge
LPA	Laminated piezoelectric actuator
MAS1	Morphing aerofoil structure one
MAS2	Morphing aerofoil structure two
MAS3	Morphing aerofoil structure three
Mc	Mach number
NACA	National Advisory Committee for Aeronautics
$\mathbf{p}$	External loads
p	Normal stress (air pressure)
$\mathbf{p}^*$	Condensed external (non-zero) load
$\mathbf{p_m}$	Non-zero components of external joint load
$\mathbf{p_p}$	Zero components of external joint load
QTM	Qualisys track manager
Re	Reynolds number
rms	Root mean square
rot.1 & rot.2	Beam moment (rotation) at ends 1 and 2
$\mathbf{S}$	States of self-stress
$\mathbf{S}^*$	Condensed states of self-stress
SA	Simulated annealing
SD	Skelton and delorenzo algorithm
SLE	Scissor-like elements
SMA	Shape memory alloy
SPEC	Successive peak error correction

SVD	Singular value decomposition
$\mathbf{t}$	Internal bar forces
$\mathbf{t}^*$	Condensed internal bar forces
t, t_1, t_2	Unit thickness
$\mathbf{t_c}$	Internal bar force vanishing and non-vanishing member
TE	Trailing edge
$\mathbf{t_H}$	The particular solution internal bar forces
$\mathbf{t_n}$	Non-vanishing internal bar force
$\mathbf{t_o}$	Initial internal force of the cables
$\mathbf{t_P}$	Internal force due to the applied load only
$\mathbf{t_p}$	Vanishing internal bar force
U	Wind speed
VGT	Variable geometry truss
WOBI	Worst-out-best-in
x/c	Normalised aerofoil length
$\mathbf{Y}\, \mathbf{e_o}$	Nodal displacements due to $\mathbf{e_o}$
$\mathbf{Y}^+$	Pseudoinverse of $\mathbf{Y}$
$\mathbf{Z}\, \mathbf{e_o}$	Internal force due to $\mathbf{e_o}$
z/c	Normalised aerofoil thickness
α	Set of s combinatorial constants for the vectors of $\mathbf{S}$
α	Angle of attack
β	Kink angle
γ	Unit angle
θ	Deployment angle
ρ	Air density
τ_w	Shear stress (viscosity effects)
$\psi 1\ \&\ \psi 2$	Beam rotation at ends 1 and 2

Chapter 1

Introduction and Overview

1.1   Introduction

The construction industry, by the scale of typical projects and the more imprecise nature of loadings, usually works to a less exacting standard of tolerance than most of other branches of engineering. Nonetheless, there are applications of structural engineering where tolerances of structural shape and internal forces, under changing service conditions, are not only important but actually impinge on the structure's serviceability limit state. Such structures could be supporting sensitive scientific or communications equipment, which demands challenging structural performance, or be deployed in harsh environments (e.g. space). Such structures are typically pin-jointed assemblies, or have characteristics very similar to pin-jointed assemblies, since length actuations, which bring about the shape and/or bar force changes can be more readily incorporated into pin-jointed assemblies.

On the other hand, structures composed of beam members such as cable-stayed bridges could undergo a big deflection under the load or may be required to control internal force of a specific cable. In this case, the displacement must be restored and/or the cable force must be controlled and limited according to the desired target. In addition, the application of pantographic structures, which are made from pantographic units that

1

consist of two coplanar, straight beams, joined by a shear connector, could be very delicate and sensitive to distortion.

Morphing structures are a type of structure which can change their shape according to applications and conditions. The applications of morphing structures are in the aerospace industry rather than other branches of engineering. For example, the ability of engineers to improve designs of wing will be increased by morphing aerofoil structures. Since the shape of the aerofoil section is the principal and most responsive parameter for changing the flight characteristics of an aeroplane, researchers working on "smart wings" have focused on finding different ways to change the flight efficiency and achieve the same aerodynamic effects in different flight conditions and environments.

1.2   Aim and Objectives of Study

There are two main related aims of the present dissertation. The first is to provide a method to directly control nodal displacements and bar forces via bar length actuations. Although displacement requirements can make demands on actuations that are in conflict with those required by bar forces, there is yet the possibility that solutions, or approximate solutions, exist that adjust the shape or stress-state of a structure from a current undesirable position to a desired one.

The second aim of this work is to propose a suitable morphing structure in the form of an aerofoil to allow shape re-configuration in order to replace the traditional aerofoil while still retaining the required aerodynamic characteristics. In addition, it is also an aim to have both first and second aims simultaneously *i.e.* directly control nodal position/displacements of a morphing aerofoil during morphing via bar length actuation. These aims are realized through achieving the following nine steps.

1- To review the available literature on analytical and numerical techniques on shape control, with a view to finding efficient and comprehensive techniques for shape control.

2- To derive a direct method for control of nodal displacements, bar forces and simultaneous nodal displacements and bar forces, for a structural assembly.

3- To develop a direct method for adjusting nodal displacements, bar forces and

simultaneously nodal displacement and bar force together, for structures made up of more complex structural components (*i.e.* those with "macro-elements"), *e.g.* the pantographic element.

4- To identify the best locations for actuators and to determine how to achieve target with minimum actuation.

5- To correct manufacture or assembly imperfections, or restore structural shape or internal force due to environmental effects or prestressing.

6- To propose a morphing aerofoil structure as an effective way to enhance/replace the tradition aerofoil.

7- To study methods for calculating theoretical nodal displacement of the pantographic morphing structure.

8- To examine and test shape adjustment of a morphing structure.

9- To experimentally verify achievements of the objectives 2 to 7.

1.3   General Layout of the Dissertation

This dissertation is separated into the following chapters.

Chapter 1 introduces the dissertation and sets out the aim and objectives. It includes a brief introduction to the problem of controlling displacement and bar force of structures, morphing pantographic structure and it role in aerospace. A summary of the organisation of the dissertation is also provided.

Chapter 2 gives details about the literature review of the topics for this dissertation, in the area of controlling structures, morphing structures, and pantographic structures with different types of pantographic units.

Chapter 3 provides theoretical analysis for the controlling equations for controlling joint displacement, bar force and simultaneously joint displacement and bar force, through using matrices of force method in ordinary and condensed form. The force method, on which the current work is based, is briefly summarised to establish notations and terminology. Finding length actuations for bars where joint displacements, and separately bar forces, are required to be controlled is carried out. Furthermore, work is also done to

find length actuations for bars where both displacements and bar forces are to be simultaneously controlled.

Chapter 4 describes the experimental work of structural joint displacement and bar force controlling, on a cable stayed bridge model and explains the experimental work carried out. Experimental results are then compared to theoretically derived results following Chapter 3.

Chapter 5 concerns the changing aerodynamic characteristics of a morphing wing structure based on pantographic structures. In this chapter, two concepts for morphing aerofoil sections are presented using pantographic structures. A brief introduction of the terminology and aerodynamic forces of aerofoil as well as a standard aerofoil shape are provided. The performance of the proposed morphing aerofoils is then explored alongside that of the standard aerofoil.

Chapter 6 illustrates an experiment carried out on a morphing pantographic structure for controlling structural joint displacements. Experimental results are compared with the theoretical results obtained from the condensed matrix technique developed in Chapter 3. The technique of morphing shape calculation as also covered alongside experimental and theoretical result comparison.

Chapter 7 collects up the conclusions of this study in line with the original aim and objectives and also suggests directions for further work to be done in this area.

For more clarity, a flowchart presenting the interrelations between different chapters is shown in Figure 1.1
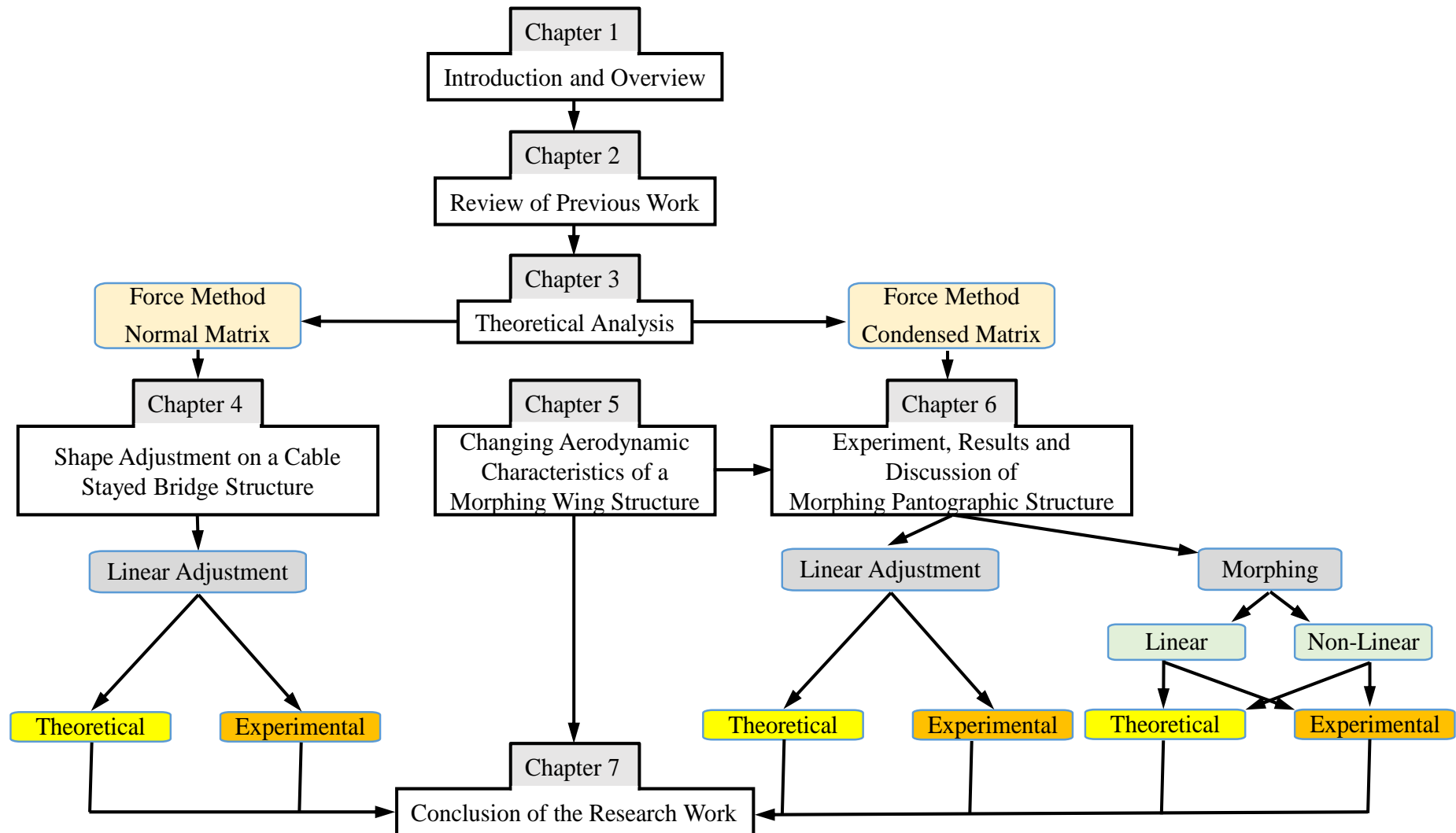
Figure 1.1: Organisation of dissertation.

Chapter 2

Review of Previous Work

2.1 Introduction

This chapter reviews previous work that is relevant to this dissertation and is divided into two main subjects, namely controlling and morphing of the structures. The first subject is a detailed overview of the relevant literature on adjustment or controlling of the structures, which explains why controlling of the structures is required. Controlling of structures has three main categories: control of joint displacements; control of bar forces; and simultaneous control of both joint displacements and bar forces. Each category is reviewed separately with illustrations of the different approaches proposed by different researchers. Furthermore, an overview will also be provided for showing methods used to limit the number of actuators, and the placement of actuators for optimal control of structures, due to the cost of employing a high number of actuators. The different types of actuators are also presented.

The second subject of this chapter deals with morphing and deployable structures, with examples in this field. A review is given of existing pantographic structures and types of pantograph units such as translational units, polar units and angulated units. All of these pantographic units will be used in the morphing structure based on the pantograph that will proposed in this thesis, except for angulated units. The last sections give a review of conditions for deployability and analysis of a pantographic structure.

2.2   Adjustment/Controlling of the Structure

In general, an adjustment can be defined as the process of small changes or movement that improves the current performance or achieves a desired outcome. More simply, shape control can be defined as reduction or even elimination of the structural deformation caused by external disturbances (Ziegler, 2005). Therefore, some structures are designed to have the ability of changing their shapes by adjusting some of the member lengths or forces (Shea *et al.*, 2002). Structural control can be divided into three subdomain categories as active control, adaptive control and intelligent control (Korkmaz, 2011) as shown in Figure 2.1.
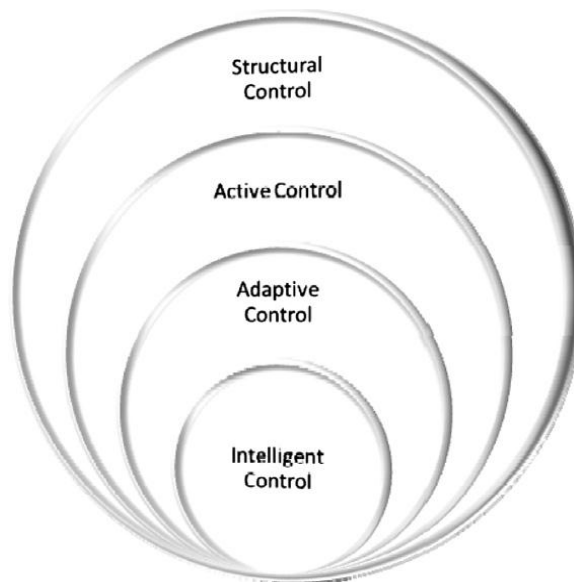
Figure 2.1: Three subdomain categories of structural control. Source: Korkmaz (2011).

Active control is the controlling in real time of an "active" structure, which contains sensors and actuators that, when active, modify the structure in response to its environment. Adaptive control is thus the engineering that improves structure's response to changing environments over time without reference to behaviour modelling and actions such as loading and temperature. Intelligent control is the control whereby an engineering structure monitor and maintains, or improves its structural performance by recognizing changes in behaviour and actions, and adapting the structure to meet performance goals, and using rules developed from past events to improve future performance (Korkmaz, 2011).

The controlling or adjustment process in structural engineering can be done via elongations of active members capable of length extension/contraction. The element elongations can be done using devices embedded in these members, called actuators, which produce the length extension/contraction (Sener *et al.*, 1994). For achieving an exact solution of static and dynamic shape control, the shape actuators must be capable of extension and contraction (Ziegler, 2005).

In this work, adjustment means "small" changes in external nodal displacements or internal member forces in order to control them to the desired target thus both "adjustment" and "control" words can be used. Even though the concept of length actuation as the cause of static shape change is simple, work on the associated analytical/computational techniques is not extensive, and this is especially the case for direct approaches. For more clarity, the previous work in this area can be divided under three categories as displacement control, bar force control and simultaneous control of both displacements and bar forces.

2.2.1 Displacement Control

In general, the structural geometric shape is very significant in most structural engineering. The shape of a structure is usually defined by its nodal positions. Such structures could be supporting sensitive scientific or communications equipment that require very high geometric accuracy, which demands good structural performance, or are deployed in harsh environments (*e.g.* space). Since space structures are designed to be as light in weight as possible, they also tend to be very flexible. These structures might have shape imperfections from manufacturing errors, errors due to unexpected transport loading, unexpected loads, and thermal distortion *etc.* and hence they require adjustment with suitable correction to accurately maintain their shapes as far as possible.

The aim of shape control is to abolish/reduce the effects of external disturbances on the structural deformation through appropriate actuation as stated by Irschik (2002) and Haftka and Adelman (1985a). In addition, they also pointed out that shape control could be a branch of structural engineering that was closely related to control engineering.

The process of controlling external displacement can be done by changing the length actuation of some active members. To achieve this, it is very necessary to find the sites of the most active members (Section 2.4) and amount of the length actuation for those members. Therefore, for attaining the previous requirement to nullify unwanted shape imperfection an attempts were made by some researchers. Earlier and recent studies on the structural control has been reviewed in detail and a number of articles have been cited by Korkmaz (2011). In addition, Burdisso and Haftka (1990) have also studied static shape control methods. Furthermore, Ziegler (2005) presented a short historical review of structural shape control, while a detailed discussion and review on shape control with piezoelectric actuators was presented by Irschik (2002), and Sunar and Rao (1999).

When the shape distortion becomes undesirable, the nodal positions have to be adjusted to restore the shape, the adjustment process is often achieved by controlling the length of the structural members (Edberg, 1987; Du *et al.*, 2013). It seems that subject of shape control was introduced firstly by Weeks (1984a; 1984b). Weeks (1984a; 1984b) described the approach for both static shape determination and control for large space structures using Green's functions. In the beginning, he developed the static shape control and determination algorithms for one-dimensional models, using a flexible simply supported beam as an example (Weeks, 1984a). He noted that the shape control problem could not be separated from the problem of shape determination since shape determination was followed by shape control. In a subsequent paper, Weeks (1984b) derived the solutions of static shape determination and control for large space structures, which was explained using the finite element model of a large space antenna.

One year later, the subject of shape control was developed by Haftka and Adelman (1985a). They presented an analytical procedure for static shape control of flexible space structures by changing the temperature of control elements so as to minimize the overall static distortion of a large space structure. Their displacement control procedure was based on using higher coefficients of thermal expansion elements as an active member for controlling/minimizing the overall distortion of the large space structure. They noted that the shape distortion of the structures could be either transient, *i.e.* changes to the structure gradually dampen out, or those that remain fixed over time.

Haftka and Adelman (1985a) derived two different equations for shape control, the first one was for continuous structures on the basis of a differential equation, which

they then applied to control the distorted shape of a simple beam due to non-uniform heating. Their second formulation procedure was based on the finite element model for discrete structures. They performed this procedure for the 55m space-truss-parabolic antenna in Figure 2.2 to estimate effectiveness of thermal shape control. After Haftka and Adelman (1985a), other researchers appeared gradually who took an interest in the field of shape control.
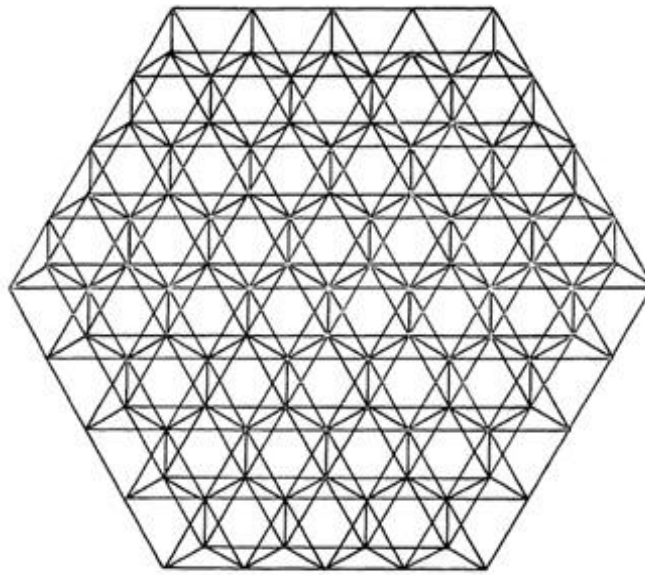
Figure 2.2: Tetrahedral truss antenna reflector. Source: Haftka & Adelman (1985a).

Indirect approaches for static shape control problem of flexible structures have also been tested, e.g. by Subramanian and Mohan (1996) with an algorithm of successive correction based on heuristics. Their algorithm (termed successive peak error correction, SPEC) starts with the procedure of applying the first adjustment at the location which has the peak deformation in the structure. Then the correction is done in the second location, which has the peak deformation after correcting in the first location of the structure and so on. This process is repeated until the target is achieved. They concluded that their technique is very economical and effective, since it requires only a small fraction of the time taken by the more established Skelton and DeLorenzo (1983) algorithm, as will be explained in Section 2.4.

Simulated annealing in combination with a linear finite-element evaluation of control of a precision truss structure was used by Salama *et al.* (1993) who concluded that their search was effective, but observed nonlinear behaviour led to inaccuracies. Chee *et al.* (2001; 2002) investigated a novel static shape control algorithm for structures taking into account the curvatures and slopes in the objective functions as the fine-tuning criteria. A three-dimensional solution of the static shape control by eigenstrain actuation has been derived by Irschik and Ziegler (2001).

Shape control has been done on the different types of structures in order to nullify the distortion of the shape of structure. The shape control of beam by piezoelectric actuator patches was analytically addressed by Yang and Ngoi (2000). They derived the analytical solution of a beam deflection due to both piezoelectric actuation and external loads. In their work, different boundary conditions were measured and several case studies were presented in order to show how analytical solutions could achieve shape control of the structure. Their prediction results showed that it was difficult to approach the desired shape of a beam locally with piezoelectric actuators due to the limitation of actuation forces of the piezoelectric actuators (Yang and Ngoi, 2000). Based on Timoshenko beam theory and induced strain actuation theory, Hadjigeorgiou *et al.* (2006) showed the shape control and damage identification of a cantilever composite beam using piezoelectric actuators and genetic algorithms optimization procedure. Yu *et al.* (2009) also considered the static shape control of a cantilever beam by laminated piezoelectric actuators.

The reflector surfaces of cable mesh antennas have to be sensibly adjusted to attain required accuracy either to achieve high gain or high directivity (which allows miniaturization of ground terminals) or to reform their shapes (which allows collection of weak signals) by changing the length of some cables capable of adjustment (Du *et al.*, 2013). The surface adjustment mechanism is used to correct the original deformation. Many research groups have carried out shape adjustment of cable mesh space antennas (Mitsugi *et al.*, 1990; Tanaka and Natori, 2004; Tanaka, 2011; Du *et al.*, 2014).

The direct method was studied by Mitsugi *et al.* (1990) who used the pseudo-inverse of a sensitivity matrix of surface error with respect to cable length variations that related control inputs to antenna deformations in order to determine the inputs for shape control. Tanaka and Natori (2004) also presented a direct method for adjustment and to

increase the surface precision by changing the length of boundary cables or tie cables in a mesh reflector shown in Figure 2.3.
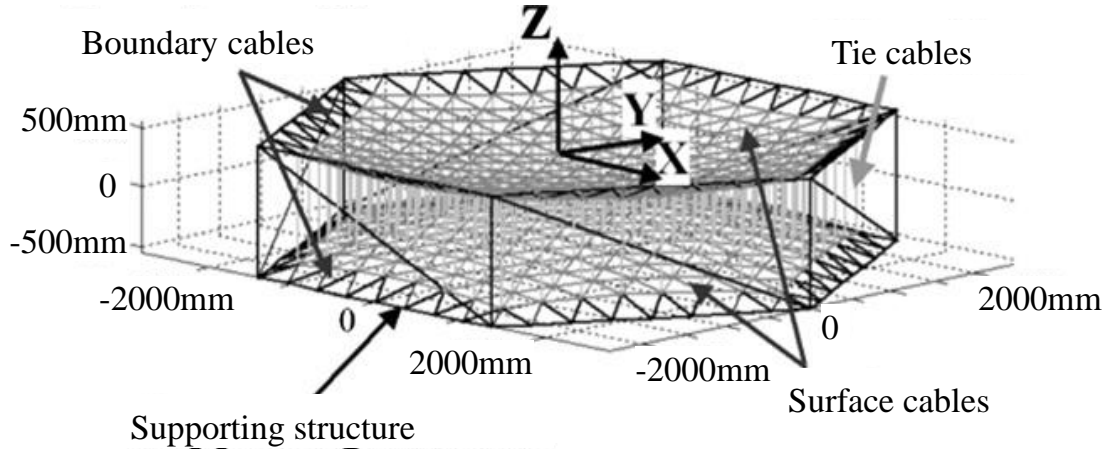
Figure 2.3: Antenna consisting of cable networks. Adapted from Tanaka (2011)

Tanaka (2011) developed a novel method for the estimation and correction of antenna surface deformations called the "surface adjustment mechanisms" method. In this method, firstly relationships between antenna surface errors and changes in antenna gains caused by intentional deformations were found. Then the deformations were corrected after estimating the original deformation of the antenna surface, on the basis of monitoring the impact on the signal gains of the antenna due to adjustments carried out (Tanaka, 2011). Tanaka (2011) concluded that calculation costs were reduced and applicability was improved in this method. Earlier Burdisso and Haftka (1990) also addressed the problem of efficient analysis of the statistics of initial and corrected shape distortion in antenna structures.

A shape adjustment procedure based on optimization was presented by Du *et al.* (2013). This method presents the relationship between the reflector surface error and the length variation of adjustable cables. Du *et al.* (2013) pointed out that some cables would be slack when the location of the required parabolic surface was not properly determined. The finite element model of an active cable structure was established and an active shape adjustment method was investigated by Wang *et al.* (2013) to achieve the active surface control of a cable net. On the other hand, shape control of deployable cable net reflectors

has been investigated by Tanaka and Natori (2006) on the basis of self-equilibrated stresses concept, where shape control was achieved without iteration.

There has been work on shape control of intelligent structures. A finite element analysis for static shape control of intelligent structures with distributed piezoelectric sensors/actuators has been proposed by Wang *et al.* (1997). Moreover, Trak and Melosh (1992) addressed the shape control of a truss through choosing nodal coordinates to compensate for deformation. For this purpose, they utilized a tetrahedral truss in different cases of structural loading and surface geometry, which showed that the determinate truss bar forces were not affected significantly by change in the geometry due to smallness of this geometry change.

Tensegrity structures are sensitive to a small environmental changes so Shea *et al.* (2002) described adaptive changes in a tensegrity-like grid structure. Through using stochastic search algorithms, feasible actuations have been found to adjust the structure from the initial shape to the target shape. Since the main problem in shape control of tensegrity is the determination of the actuations, according to Shea *et al.* (2002), they consequently proposed a system for intelligent structural control of tensegrity structures, as shown in Figure 2.4.
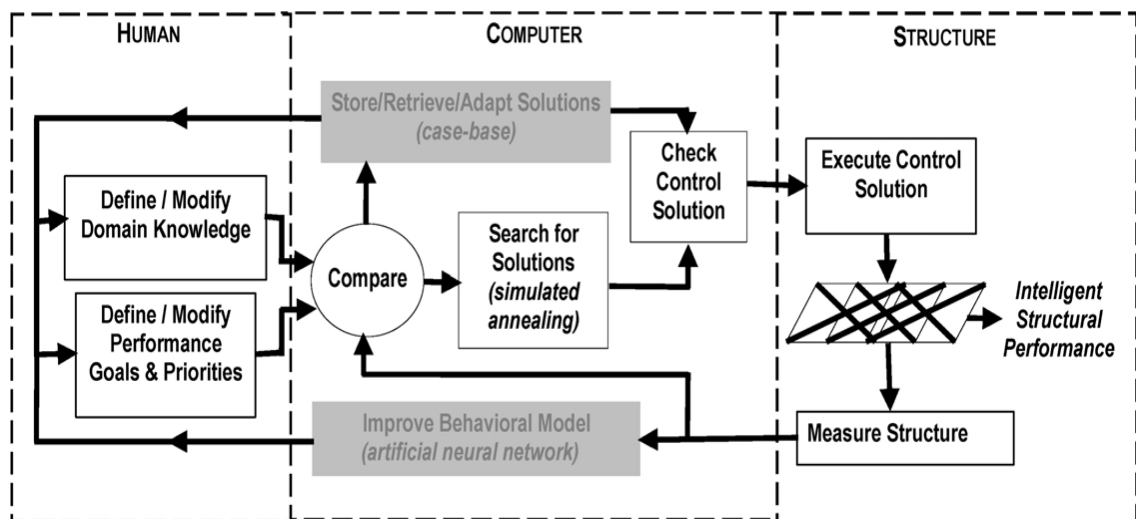
Figure 2.4: System for intelligent computational structural control of a tensegrity structure. Source: Shea *et al.* (2002).

2.2.2 Bar Forces Control

For some structures, or for some loads, the internal forces in the structural members might require control more than the displacements. For example, structures with cable members can have those members approaching slack under some loading conditions, and they thus need to be tightened to remain structurally existent. On the other hand, a slender strut could be approaching instability due to buckling failure and thus needs its compressive force reduced. Of course, bar length actuation has effect on internal bar forces only in statically indeterminate structures.

The current concern is about controlling the axial force of some of the structural members, which are over- or under-stressed as a result of loading, to avoid structural failure. However, the specific issue of control of internal force in structures has not had much study, thus some works are reviewed and summarised in this section which deal with the more general case of prestressing of structures. Strictly, a prestressing process can be done only in the indeterminate structures though, for all structures, there is a certain amount of "pre-stressing" due to the weight of the structure. On the other hand, large space structures can be prestressed in a certain way in order to reduce the weight of the structure (*e.g.* by shifting the balance of the predominant internal forces towards tensile, thus reducing the need for bulky compression struts) and for covering a larger span (Levy *et al.*, 1994) hence such structure are generally indeterminate structures. The prestressing technique has direct connection with the length actuation of the structure members. On the basis of the force method, Kwan & Pellegrino (1993) addressed methods to calculate length actuation in the case of trying to achieve a specific prestress pattern before loading. In addition, they also addressed the issue of finding the best prestress actuator sites, and the best actuator adjustments to improve an existing, incorrect prestress state in pin-jointed trusses.

The amount of the force in the prestressed structures can be also controlled via pre-tensioning prestress member to a desired value as discussed by Dong and Yuan (2007). Their initial internal force method for pre-tension analysis of a prestressed space grid structure was based on the principle of linear superposition. Their numerical results show that their technique is correct, reliable and effective, and applicable for the analysis of prestressed structures.

2.2.3 Simultaneous Displacement and Bar Force Control

In practice, it is difficult to control of one variable without at the same time affecting some other variables. For instance, in restoring the shape of an antenna to the predefined target through changing some member lengths, we have to be very careful that the resultant set of actuations do not also change strut forces to reach dangerous levels, or to bring some cables to slack due to reduction of their internal force. In this case, there is necessity to be able to control both the nodal displacement as well as the bar forces. In practice, it is not typically easy to control both the shape and forces at the same time.

On the control of both shape and internal forces, little work has been done. An analytical scheme of shape and stress control of pin-jointed prestressed truss structures, using a linear force method of analysis, was investigated by Kawaguchi *et al.* (1996). For validation of the proposed scheme, they compared computed results of the proposed scheme with experimental results from a tension stabilized truss structure shown in Figure 2.5. The tests were conducted without applying any external loads on the system, and they focussed on identifying difficulties regarding control of the displacement components.
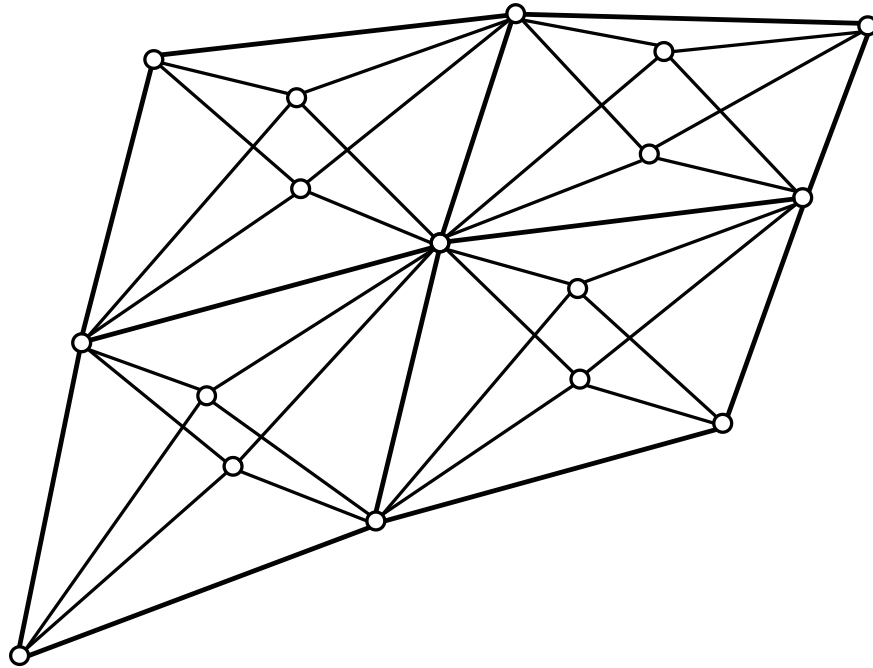
Figure 2.5: Tension stabilized truss structure: Adapted from Kawaguchi *et al.* (1996).

Based on the force method and for small linear elastic deformations, the displacement control scheme for prestressed cable structures by altering the length of some structural members was proposed by You (1997). You (1997) dealt with the problem directly, and showed the direct link between length actuations and displacements for prestressed structures. In his work, it was shown that the displacement of the prestressed truss/cable network structures could be controlled via changing the length of some structural members while simultaneously keeping the prestress level above a chosen lower bound. The validation and practicability of his technique was proved through good agreement between the computational and the experimental results in his experiment on the prestressable two-dimensional cable network shown in Figure 2.6. You's technique consists of: firstly finding a set of members capable of actuation in order to achieve any displacements within a given range, and at the same time their actuation has no effect on keeping the prestress level above a chosen lower bound for any member of the given structure. The second step is the calculation of the amount of actuation for those members required for getting the target displacement in the given range. However, the method is only appropriate for the case of small deformation of structures made of linearly elastic materials. Likewise, the shape and stress control analysis of pin-jointed prestressed truss structures was also investigated by Kawaguchi *et al.* (1996) where a simple analytical scheme based on the linear force method of analysis was proposed. However, difficulties were identified in validating numerical results through experimental testing.
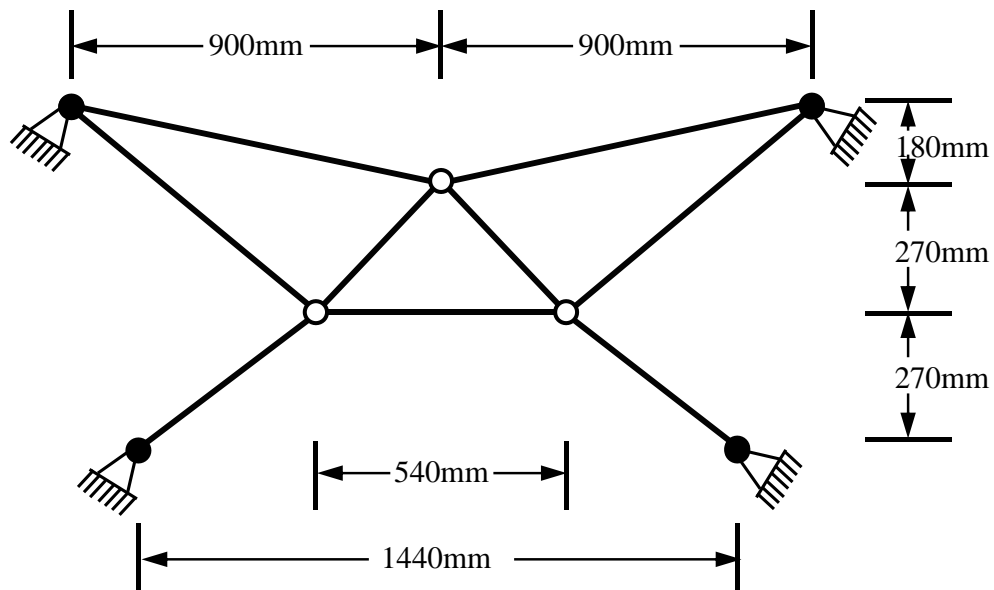
Figure 2.6: A two-dimensional cable network. Adapted from You (1997).

Smart structures, which are a type of engineering structure containing sensors and actuators, can change their geometry, stiffness and damping to adjust to changes in the environment (Korkmaz, 2011). They are often used in high accuracy space structures such as reflectors. Normally low damping, varying thermal loading conditions, and joint looseness, etc. affect such structures. These effects can be nullified or reduced by actuator control. Geometry control in prestressed adaptive space trusses was discussed by Sener *et al.* (1994) in order to satisfy the precision requirements of the instruments supported by them. They noted that approximate methods of geometry control were not satisfactory and exact control methods had to be emphasized since the required precision of the sensitive measurement equipment supported by the adaptive space truss demanded geometry control at the level of micrometres. In their work, two methods were used for shape control, stress-free control and stressed control, and both methods were applied to the two structures shown in Figures 2.7 and 2.8.
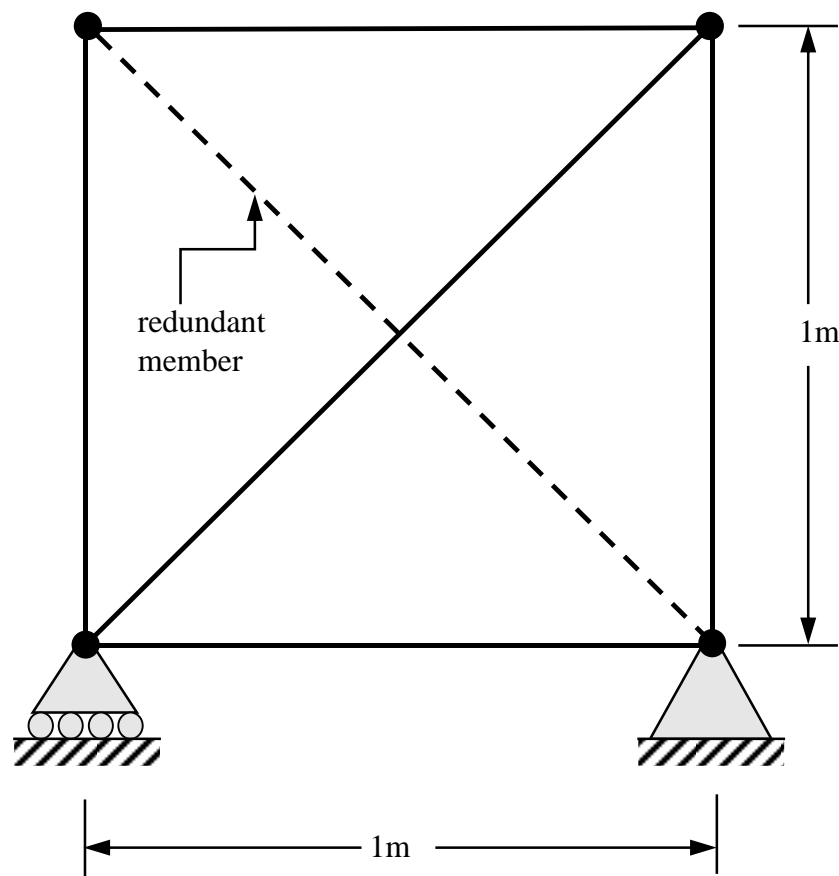
Figure 2.7: Planar indeterminate truss. Source: Sener *et al.* (1994).
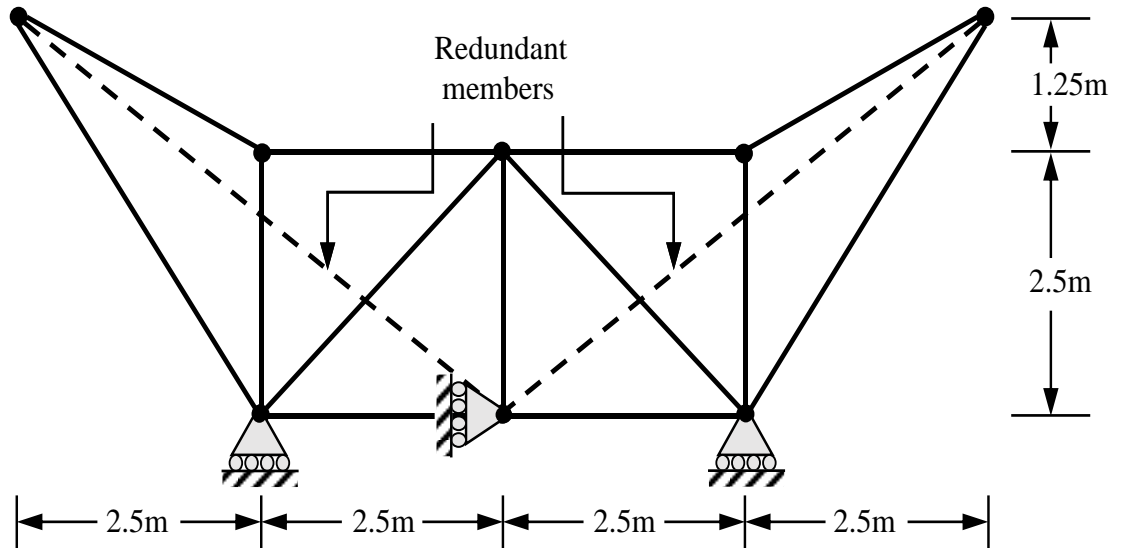
Figure 2.8: Planar antenna support structure. Source: Sener *et al.* (1994).

Shape control of a prestressed cable structure was proposed as a multi-objective optimization problem which was solved using a genetic algorithm by Xu and Luo (2008). In contrast, Wang *et al.* (2013) argued, for cable net structures with high surface accuracy requirements, multi-objective optimization methods were not appropriate due to the low precision of the solution and large computational effort for large and/or flexible truss structures. Sometimes significant shape errors or undesired bar forces result. Greene and Haftka (1990) proposed a member and joint exchange algorithm method to reduce both surface errors and member forces through finding alternative arrangements of members and joints.

Moreover, Xu and Luo (2009) proposed an iterative procedure to perform nonlinear shape control of prestressed cable structures on the basis of linear displacement control technique and the non-linear force method. After conducting their procedure they found that the computational results of their non-linear control method were in good agreement with the target values, however the corresponding results of the linear control method had considerable errors. They concluded also that the non-linear displacement control method kept the prestress level of the structural members much closer to the initial level than the linear displacement control method.

2.3   Number of Actuators

To control a particular structure, the number of actuators is very important to nullify undesired shape or bar force. That number depends on the structure, and what/how many joint displacements and bar forces are to be controlled. Salama *et al.* (1993) discussed that increasing the number of actuators could produce desired shape correction with successively increasing degree of accuracy. At the same time, due to the cost of employing a high number of actuators for the controlling resolution, generally the number of the actuators is limited. It is thus very important to find the optimal number of actuators for a given problem/structure.

The problem of selecting *n* actuator locations from a larger set of *m* available sites, was considered by Haftka and Adelman (1985b) for static shape control of large space structures. Haftka (1991) presented the concept of "ideal actuators" for correction of shape distortion. The concept of "ideal actuators" is used to estimate the number of actuators needed for a particular application for reducing shape error and characterization of the suitability of an actuator in term of effectiveness to reduce the number of truss members with actuators. The "ideal actuators" concept was tested on a 55-m radiometer antenna truss structure (Haftka, 1991). Furthermore, Kincaid (1993) used simulated annealing to achieve a nearby optimal solution for actuator placement for structures with a large number of members. Simulated annealing was found to be a sensible calculation technique to avoid a huge number of possible configuration calculations.

2.4   Actuators Placement

Placement of actuators for optimal control of a structure is of essential significance. Therefore, the optimisation to reduce/eliminate the distortion of the structure shape has been done via finding minimum amount of actuation by finding the best location for actuators (*i.e.* the location of the most effective actuators).

$$\min \sum_{i=1}^{b} \left(e_{\mathrm{o}} \right)_i^2 \qquad \text{or} \qquad \text{minimize the number of actuators } (i\,)$$

subject to $\qquad \mathbf{d} - \mathbf{d}_{\mathrm{P}} = 0$

where $\mathbf{d}_p$ is the vector of nodal displacements of the structure due only to load, and $\mathbf{d}$ is the resultant nodal displacements after some elongation actuation $\mathbf{e_o}$ has been applied.

Furuya and Haftka (1995a) reported that the number of possible combinations for placement of controllers, even for small structures, could be very large. Due to the cost of placing high number of actuators for the controlling purpose, mostly, the number of the actuators is limited. For this reason it is very important to find optimal locations of the actuators. Several researchers have earlier attempted the problem of selecting the positions of actuators to achieve a global optimal or a near-global optimum solution. Kwan and Pellegrino (1993) pointed out the role of location of actuators in adjusting an incorrect prestress distribution, as well as their required actuation and the best actuator adjustments.

Haftka (1984) investigated analytical procedures for placement of thermal and force actuators in the optimal locations for shape control against static deformations of large space structures. Expressions were derived based on the design against the worst disturbances and the analytical effort was minimized numerically. It was found that control placement is of greater importance for force actuators, so was of significance for thermal actuators.

Skelton and DeLorenzo (1983) developed a heuristic algorithm (SD algorithm) to determine the optimal control sites for actuators and sensors. This technique starts from an evaluation the effect of adding or eliminating actuators by quadratic performance criteria in all available sites, and then removes the least influential sites one by one, until the best sensors and actuators are selected with the permissible number of control sites. Subramanian and Mohan (1996) claimed a new, simple, heuristic algorithm method called the successive peak error correction to be faster than the SD method for static shape control of flexible structures but still with a comparable accuracy.

In another major study, Haftka and Adelman (1985b) studied the problem of placement of actuators with heuristic integer programing in large structures for the purpose of shape control. Two iterative heuristic algorithms under names of the Worst-Out-Best-In (WOBI) and Exhaustive-Single Point Substitution (ESPS) were formulated in their work. They were concerned with how to find the optimal locations of actuators from a high number of available locations. It was proven that both WOBI and ESPS heuristic algorithms were able to achieve shape adjustment by relocating actuators, but

the results depended somewhat on the initial guess. Furthermore, they compared their results from WOBI and ESPS with those obtained by SD algorithm of Skelton and DeLorenzo (1983), using the example of shape control of an antenna reflector. It was found that WOBI and ESPS results were better than those of SD when a relatively small number of the available sites was selected. However, the SD technique was computationally cheaper than the WOBI and ESPS algorithms when a large fraction of the available sites had to be selected. In addition, it was difficult to achieve high surface accuracy with just a few actuators even if these were optimally placed.

After Haftka and Adelman (1985b) several researchers proposed new approaches for actuator placement, for instance, using genetic algorithms (GA). Rao *et al.* (1991) presented the discrete optimal actuator location selection problem in actively controlled structures using a genetic algorithms (GA) approach to solve this as a binary encoding optimization problem and claimed that that their approach could produce a global-optimal solution or a near-global-optimal solution if a sufficient number of generations were considered. The formulation was also applied to find optimal locations of actuators in a two-bay truss (Rao *et al.*, 1991). In the same way, Furuya and Haftka (1995a; 1995b) used genetic algorithms and effectiveness indices in solving optimization problems to locate good locations for actuators within large space structural systems.

Another algorithm for the optimal placement of actuators was Simulated Annealing (SA). An attempt was made with static distortion minimization problem through the optimization of actuator placement in truss structures by applying SA, as applied on a large tetrahedral truss for minimum surface distortion (Kincaid, 1993). In addition, Chen *et al.* (1991) also applied SA to study the problem of the optimal placement of active and passive members in complex truss structures. Meanwhile, Onoda and Hanawa (1993) applied a Genetic Algorithm (GA), a modified Genetic Algorithm (GA2), and Improved Simulated Annealing approach (ISA) to the actuator placement optimization problem in shape control of space trusses. They concluded that GA, GA2 and ISA performed better than ESPS, WOBI and SA when the comparison was done on a three-ring tetrahedral truss example.

Maghami and Joshi (1993) outlined an optimal actuator and sensor location selection method in the active control for large flexible space structure. They optimized the location of actuators and sensors in order to move the transmission zeros from the

right-half-plane to the left-half-plane of the imaginary axis. This was a problem that especially needed for fast optimal regulation and tracking problems. Additionally this method was successfully applied to a large flexible structure (Maghami and Joshi, 1993).

The problem of actuator placement for controlling displacement of a force loaded beam was also discussed by Irschik and Nader (2009). The Mohr analogy extension has been applied to remove displacement and cross-sectional rotation at certain pre-selected places on the beam (smart structure) via piezoelectric actuators. They compared their proposed beam-type methodology of actuator placement with a two dimensional finite element computation with a good response. The optimal placements problem for the actuators was also identified by Matunaga and Onada (1995).

No doubt, in designing smart structures, engineers have to very carefully select the appropriate type of actuators with their locations on the structure and the amount of actuation to be applied to the actuators. For instance, controlling the bending shape distortion of beam structures should be done via piezoelectric patch actuators. Hadjigeorgiou *et al.* (2006) developed a finite element model and genetic optimization procedure for controlling and damage identification of a cantilever composite beam shown in Figure 2.9, via distributed piezoelectric patch actuators. The mathematical formulation of the model was based on the shear formulation beam theory (Timoshenko beam theory) and the linear theory of piezoelectricity. The investigators said that in general a large number of actuators was needed to be placed along the beam and especially in high strain regions. However Hadjigeorgiou *et al.* proved that a small number of actuators with optimal placement and optimal voltage values could also achieve shape control of the beam effectively.
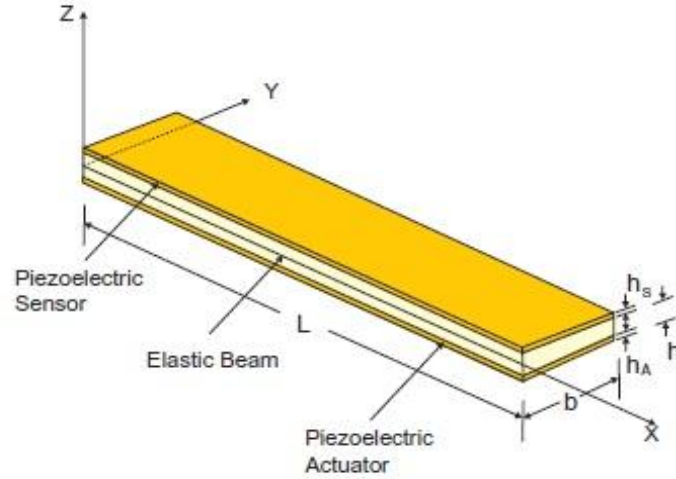
Figure 2.9: A laminated beam with piezoelectric sensor/actuator. Source: Hadjigeorgiou *et al.* (2006).

In order to reduce the cost of the optimization of actuator location, Burdisso and Haftka (1989) presented a continuum approximation technique for calculating statistical properties of the corrected shape. They showed that the comparison of their method with the exact statistical analysis was very good. In addition, they noted that the use of continuous optimization techniques was much cheaper than the integer programing methods by Haftka and Adelman (1985b). Furthermore, they concluded that the position of the actuators was optimized to minimize the weighted rms of the distortion using the continuum analysis also they showed that the optimum design was much better than a design with uniformly spaced actuators for parabolic weighting function. Finally, they found that actuators located on the beam face elements of the truss-beam structure in Figure 2.10 were more effective than the actuators located on the diagonal elements connecting the two surfaces.
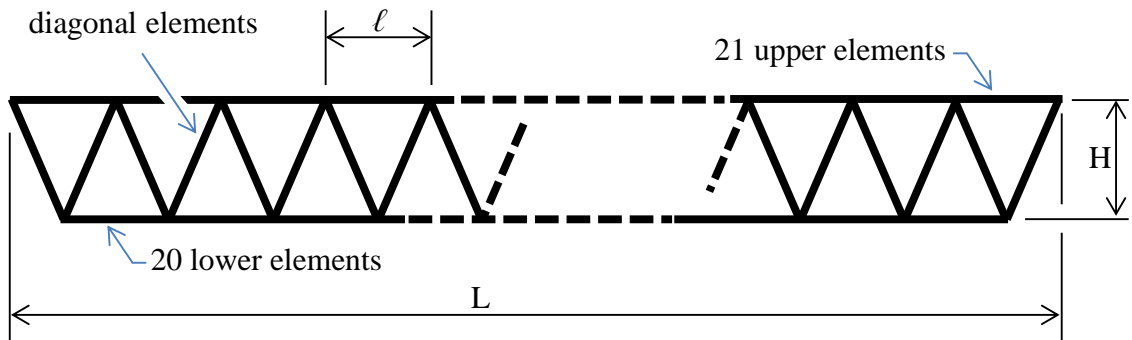
Figure 2.10: Truss-beam geometry. Source: Burdisso and Haftka (1989).

2.5 Types of Actuators

2.5.1 Piezoelectric Actuator

Shape control of flexible structures by piezoelectric actuators is one of the exciting applications of piezoelectric material (Chee *et al.*, 1998). To date, piezoelectric materials have been the most widely used smart material to control the shape of a structure. Detailed discussions and review on shape control of by piezoelectric actuation were presented by Irschik (2002), and Sunar and Rao (1999). Many researchers have used piezoelectric actuators for the purpose of shape control of flexible structures. For instance, they were used for shape control and damage identification of a cantilever composite beam by Hadjigeorgiou *et al.* (2006), and also by Yang and Ngoi (2000) for the shape control of a beam. In addition, a piezoelectric actuator was also used for static shape control of intelligent structures by Koconis *et al.* (1994a; 1994b), Wang *et al.* (1997) and Chee *et al.* (2001; 2002).

A new type of piezoelectric actuator called the laminated piezoelectric actuator (LPA) has been used by Yu *et al.* (2009) in the shape control of a cantilever beam. This type of piezoelectric actuator is made up of several piezoelectric patches with the same geometric and material parameters.

Despite the fact that piezoelectric actuators have been the most widely considered for shape control, they still have some certain disadvantages, such as being prove to damage and having limited ability to conform to curved structures (Binette *et al.*, 2009).

2.5.2 Thermal Effect

Using thermal effect as actuation can be an option whereby changing the temperature of the control elements can reduce the overall static distortion of a large space structure from its deformed shape. The chosen element as an active member must have a high coefficient of thermal expansion. Static shape control of flexible space structures using heat was done by Haftka and Adelman (1985a), who also (1987) performed a study to predict and assess the effect of actuator errors on the performance of a shape control procedure for flexible space structures using applied temperatures.

2.5.3 Shape Memory Alloy (SMA)

Shape memory alloy (SMA) is a relatively new and useful material and has found increasing applications in many different areas due to their unique properties such as high force, long stroke, small size, light weight, and silent operation (Peng *et al.*, 2008). Recently, research efforts have been extended to using SMA for control of the structures. The detailed review of applications of SMA materials for controls of structures was done by Song *et al.* (2006) . However, Peng *et al.* (2008) claimed that the poor stability and controllability of the shape memory alloy (SMA) made it a challenge to achieve accurate actuation.

2.5.4 Lead Screw Active Members

Salama *et al.* (1993) used lead-screw active members as actuators in controlling structures (as shown in Figure 2.11) as part of a complete assembly with adapters, a load cell and erectable joints. Salama *et al.* (1993) noted that this lead-screw active member was more suitable for full scale space-erectable truss structure than piezoelectrically driven active members, since actuator gains of the order of 1 mm were needed for this application, which could not be provided by piezoelectric active members.
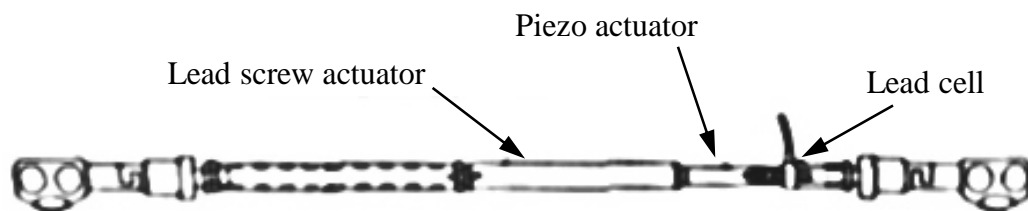
Figure 2.11: Lead screw active member. Adapted from Salama *et al.* (1993).

The combination of lead screws and piezo-actuators for demonstration of shape control of an erectable, experimental doubly curved tetrahedral truss structure was used by Salama *et al.* (1993). The structural changes in structures like parabolic tetrahedral truss structures resulting from launch loads or during operations in a space environment can be compensated precisely and controlled with high precision by substituting some of the truss members with actuators according to Haftka and Adelman (1985b) and Matunaga and Onoda (1995).

2.6   Shape Morphing

In the past few decades, interest in morphing structures has increased commonly due to the greater benefits they can provide, particularly within aerospace research, because of their variable geometry, low weight and reduced overall complexity of structure (Lachenal *et al.*, 2012). Iannucci and Fontanazza (2008) defined a morphing structure as a structure capable of modifying its geometric characteristics, dimensions or tune its properties (stiffness and damping) in order to its operating conditions, change its interaction with the surrounding environment adapt to different load conditions. The shape morphing truss structure has the ability of bending, twisting and undulating deformations (Sofla *et al.*, 2009).

Originally, in the last decade an increasing variety of attractive structures and buildings with movable functions have been seen worldwide, for instance in bridges that open to allow ships to pass, revolving restaurants on tops of buildings, sliding roofs of baseball and soccer dome stadiums, and artistic monuments (Inoue, 2007). These types of moveable structures can have a very simple movement on rails, or turn around a hinge. Their behaviours are repeatable without changing structural shape. Later, Inoue (2007) progressed the movable structures that includes change in the behaviour of the structures simultaneously with the changing the geometric shape of the structures with a lively motion. The first application of an adaptive structure using a variable geometry truss (VGT) mechanism was presented by Inoue (2007) at the International Expo 2005, Aichi, Japan. He presented a large-scale movable monument shown in Figure 2.12.   This monument is composed of three identical movable towers comprising four actuating truss members. Since shape morphing can be easily converted from well-known traditional truss structures by substituting some of the trusses with linear displacement actuators (Sofla *et al.*, 2009) through controlling the length of each of its extendable member (extensible actuator), the monument's shape can be changed to the various truss shapes as presented in Figure 2.13, which shows the monument's shape changes according to performance patterns (Inoue *et al.*, 2006).

In 2012, a novel type of morphing structure capable of large deformations was presented by Lachenal *et al.* (2012) as shown in Figure 2.14. Their morphing structure was made of two pre-stressed flanges joined together to have two stable configurations. In each flange, five holes were made along the length of each flange with equal space to

accommodate the rods. The steel rods were machined at their ends. In order to allow the device to twist freely, the flanges were loosely connected to the rods. Three different configurations existed. The straight (a) and coiled (c) configurations corresponding to unstable equilibria are shown in Figure 2.14. The bistability analysis was done for the presented morphing structure through a simple analytical model, predicting the positions of the stable and unstable states for different design parameters and material properties (Lachenal *et al.*, 2012). They found a good correlation between experimental results, finite element modelling.
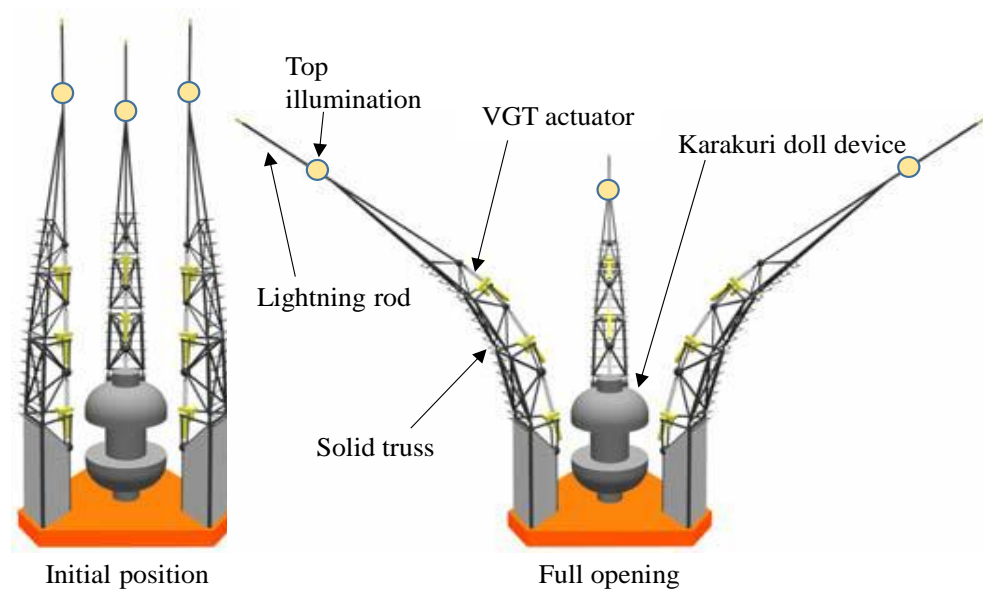
Figure 2.12: Scheme of the three morphing towers shown at the International Expo 2005, Aichi, Japan. Source: Inoue (2007).
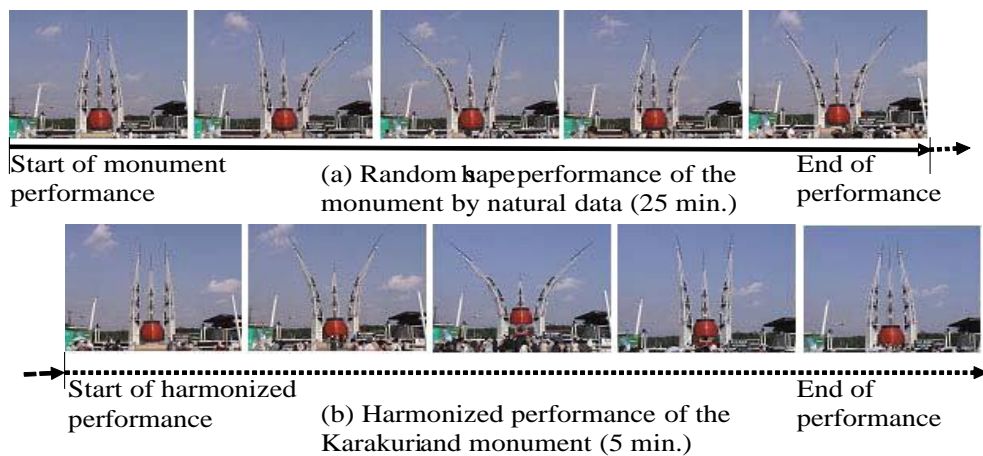
Figure 2.13: Shape changes of monument according to performance patterns. Source: Inoue *et al.* (2006).

(a)   (b)   (c)
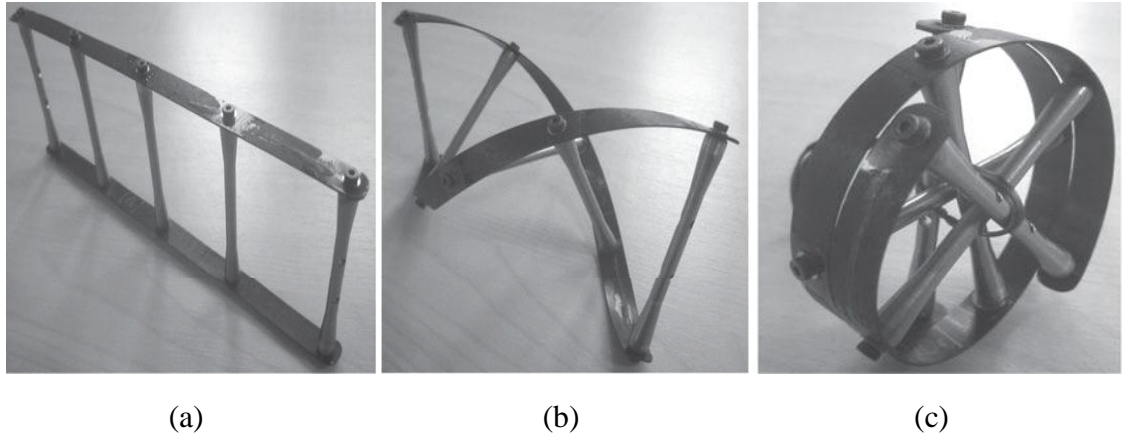
Figure 2.14: The prototype in (a) the straight, (b) the twisted and (c) the coiled configurations. Source: Lachenal *et al.* (2012).

2.7 Pantographic Structures

The base composition of morphing structure in this dissertation are pantographs, so we discuss the pantograph unit in detail. Pantograph elements are also called scissor-like elements. Different terms were used, *e.g.* pantographs (Pinero, 1961), scissor-like elements (SLE's) (Gantes, 2001), pivot-hinge structural unit (Gantes, 2001), in order to describe these units. Pantographs are defined by Glisic *et al.* (2013) as a specific type of deployable structures that are capable to deploy from a small compact state to a larger expanded state while carrying loads. The pantograph elements consist of two straight bars connected through a shear connector (revolute joint, scissor-hinge or pivotal connection) called the "intermediate hinge", typically near their centres while the ends remain free (De Temmerman, 2007; Maden *et al.*, 2011; Glisic *et al.*, 2013). The pivotal connections allow free rotation between two rods about the axis perpendicular to the common plane of the pantograph (Susam, 2013). By interconnecting such pantograph units at their end nodes using the revolute joint, a two-dimensional transformable linkage is formed (Merchan, 1987; De Temmerman, 2007). Through rotating the rods about the pin, the structure can be elongated or flattened in the plane of the rods to change shape (Wolfe, 2013) as shown in Figure 2.15. Some devices are constructed on the basis of this idea such as scissor lift and lazy tongs. Additional examples, *e.g.*, flat slab, beams, arches and domes, exist by connecting multiple pantographs elements together in two dimensions (Wolfe, 2013). A detailed review of pantographic structural mechanisms, geometric principles and design methods was done by Maden *et al.* (2011).
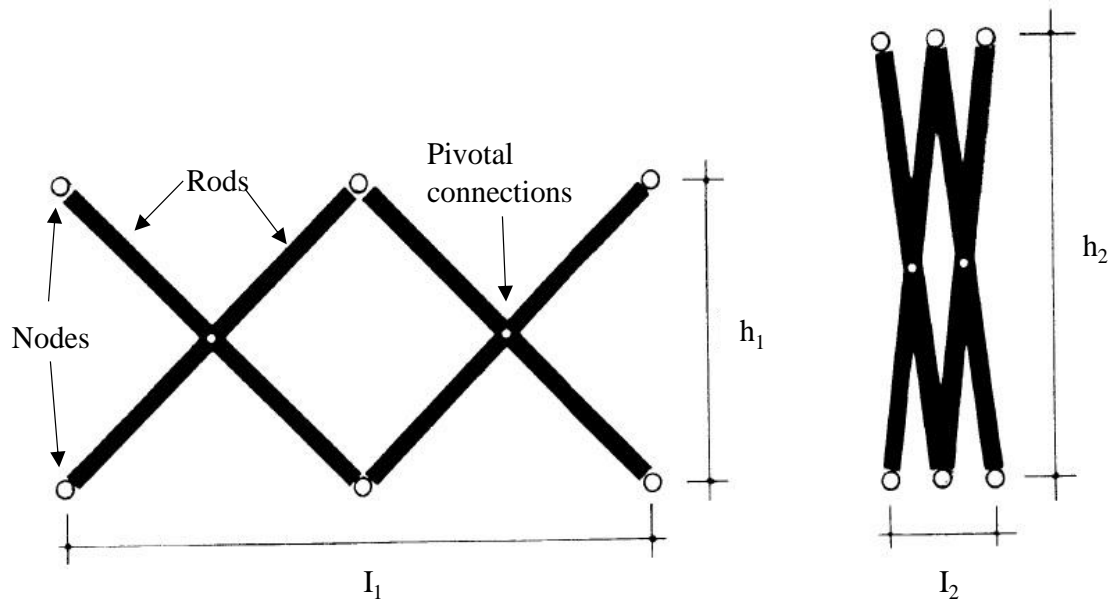
Figure 2.15: The concept of a pantograph. Adapted from Merchan (1987).

Rapid deployability with minimum labour is the main advantage of pantographic structures due to predetermined final shape of the structure by layout and orientation of the struts, thus simply pulling or pushing in a few locations automatically erects the structure (Wolfe, 2013). Further advantages of this structure are that there can be relatively little on site construction of the pantographic structure, high speed deployment and very compact storage, and deployment and contraction of all units can be carried out by one control force or mechanism (Chikahiro *et al.*, 2014). Deployable pantographic structures are used in a wide variety of applications, on both small and large scales, such as military, disaster relief, temporary structures, aerospace and roof structures (Wolfe, 2013).

Gantes (2001) defined deployable structures as structures that can be transformed from a closed compact configuration to a predetermined, expanded form, in which they are stable and can carry loads. Alternatively, morphing structure has a particular function in each steps of deploying, for instance morphing aerofoil gives a specific coefficient of lift and drag in each stage of morphing. Therefore, in this literature review we discuss both deployable and morphing structures that are built from the interconnecting of a series of pantographic units.

According to Gantes (2001) the first person who built a deployable structure in the modern sense was Emilio Perez Pinero, a Spanish architect, in 1961; thus, he is known as the pioneer of deployable structures. The first of his work was designing and constructing a real-size deployable theatre using the principle of pantograph as shown in Figure 2.16.
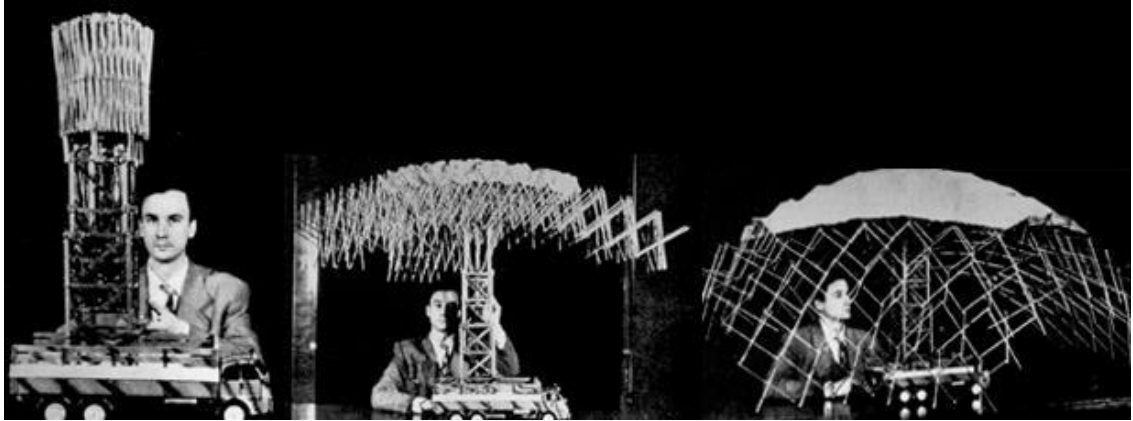
Figure 2.16: Pinero's deployable structure. Source: Akgün (2010).

After Pinero, other researchers worked on deployable structures on the basis of the pantograph concept. One of these researchers was Felix Escrig Pallares, who developed a deployable vault by incorporating rigid plates that overlap one another as shown in Figure 2.17. Moreover, Escrig has also developed several models on pantographs and designed a swimming pool in Seville by using one of his models (spherical lamella grids) on pantographs as shown in Figure 2.18. Numerical simulation and a physical prototype of a pantograph mast, activated and stiffened by a network of cable segments and active cables were presented by Kwan (1991).
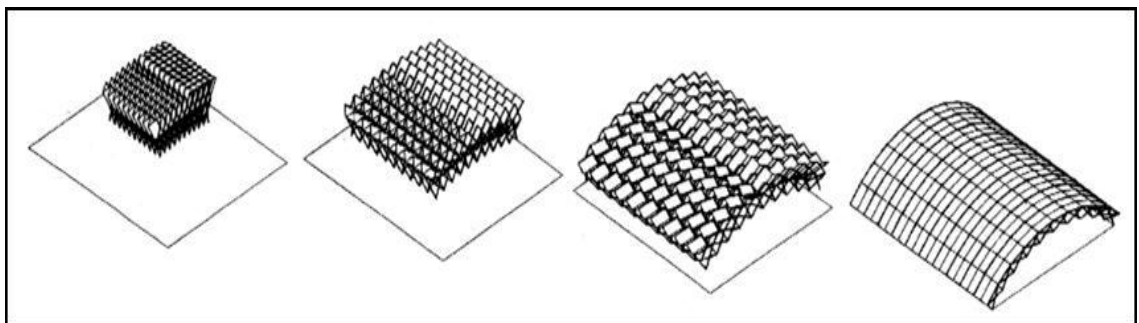
Figure 2.17: Escrig's deployable vault incorporating rigid panels. Source: Gantes (2001)
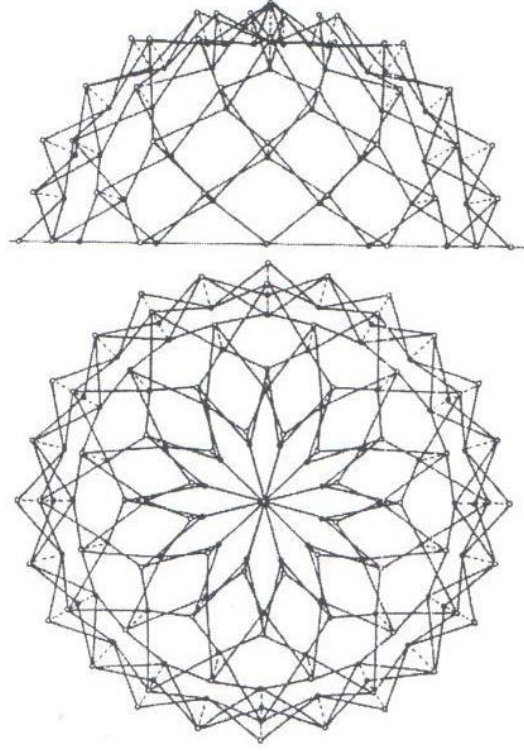
Figure 2.18: Escrig's spherical lamella grids. Source: Gantes (2001).

2.8   Pantographic Units

Different types of basic unit types for the pantographic structure can be produced through changing the location of the intermediate hinge or the shape of the bars such as translational, polar and angulated units (De Temmerman, 2007; Maden *et al.*, 2011).

2.8.1   Translational Units

In this type of pantographic unit, the unit lines, which connect the upper and lower end nodes of a pantograph unit are parallel and remain so during deployment. A plane and a curved translational unit are shown in Figure 2.19. An example for plane unit is a lazy-tong as shown in Figure 2.20, which is formed by linking a series of a plane pantographic elements at their ends to form two-dimensional linearly extendible structures (Jensen and Pellegrino, 2005). By linking a series of curved translational units at their ends, a curved linkage is formed as presented in Figure 2.21. In the curved translational unit, the lengths of the bars are different which produces a curved linkages, thus it is named as a curved

translational unit (De Temmerman, 2007; Maden *et al.*, 2011). This type of structure has just a single-degree-of-freedom mechanism characterised by the deployment angle θ (Alegria Mira, 2010). The structural thickness t, depends on the value of θ, which is measured between the lower and upper end points of the rods (Roovers and De Temmerman, 2014).
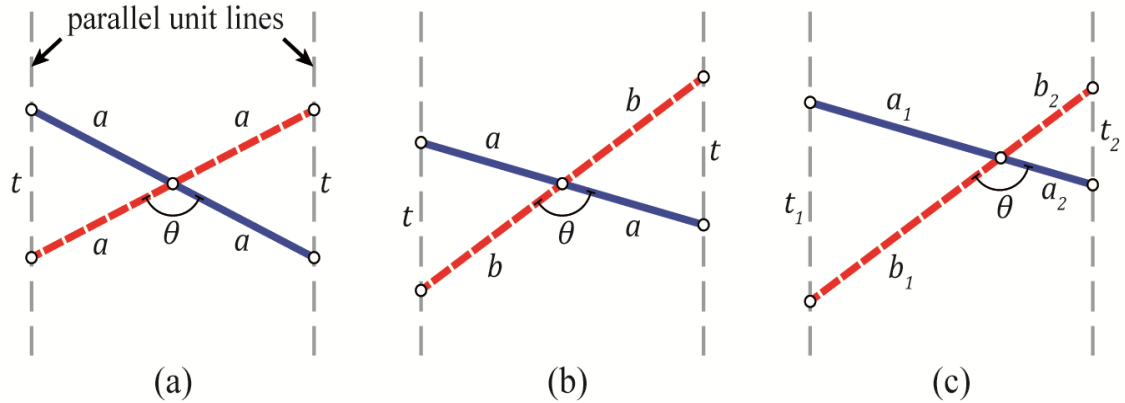
Figure 2.19: (a) A symmetrical plane-translational unit; (b) a symmetrical curved-translational unit; (c) a non-symmetrical curved-translational unit. Source: Roovers and De Temmerman (2014).
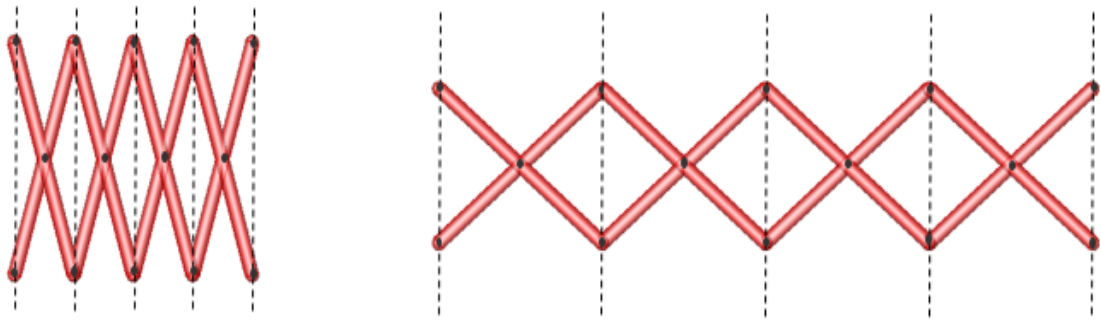
Figure 2.20: The simplest plane translational scissor linkage, called a "lazy-tong". Source: Alegria Mira (2010).
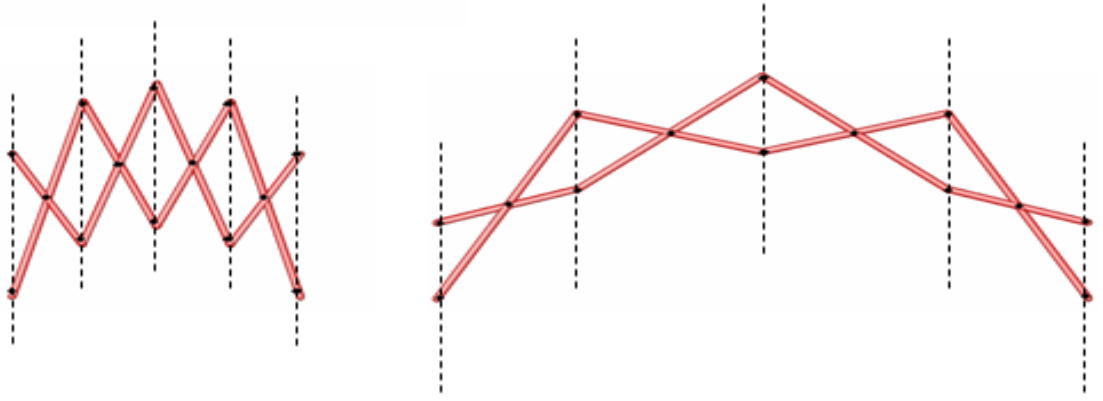
Figure 2.21: A curved translational linkage in its in two deployment stages. Source: Alegria Mira (2010).

2.8.2 Polar Units

This type of pantographic unit can be shaped by moving the intermediate hinge away from the centre of the bar with an eccentricity e' as shown in Figure 2.22. Hence a polar unit is formed with unequal semi-bars a and b see Figure 2.23. The unit lines intersect at an angle γ. When the unit deploys, the angle between lines varies, and varies more and more as the intersection point moves closer to the unit as the curvature increases as shown in Figure 2.24, which is a polar linkage in its undeployed and deployed configuration (De Temmerman, 2007; Alegria Mira, 2010).
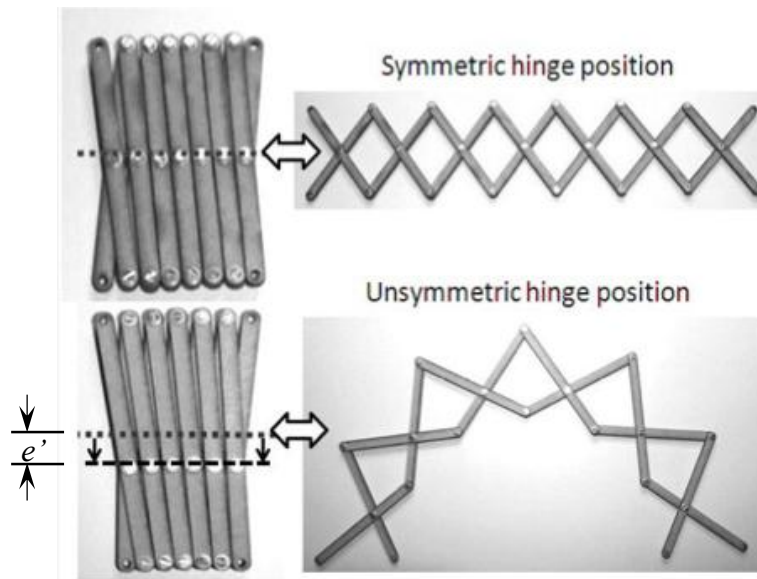
Figure 2.22: Effect of hinge moving on the shape of pantographic structure. Source: Alegria Mira (2010).
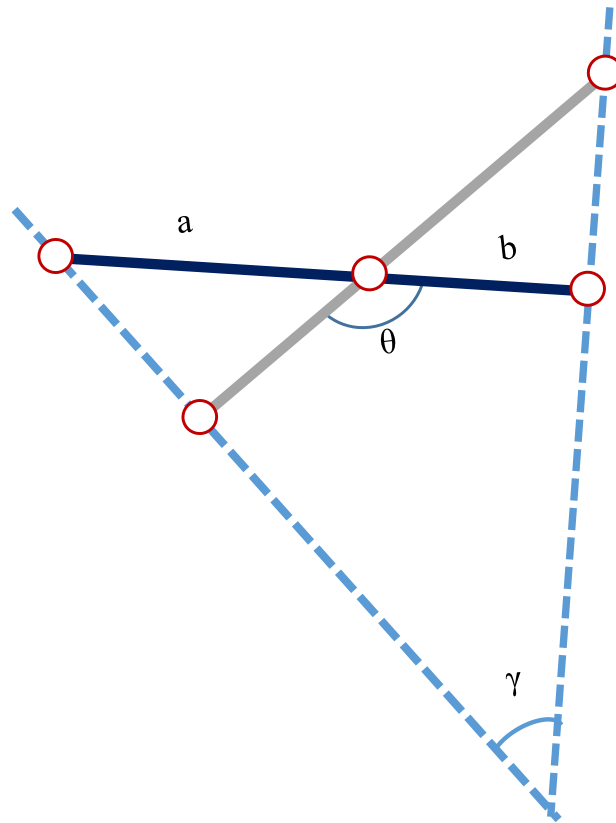
Figure 2.23: Polar unit.
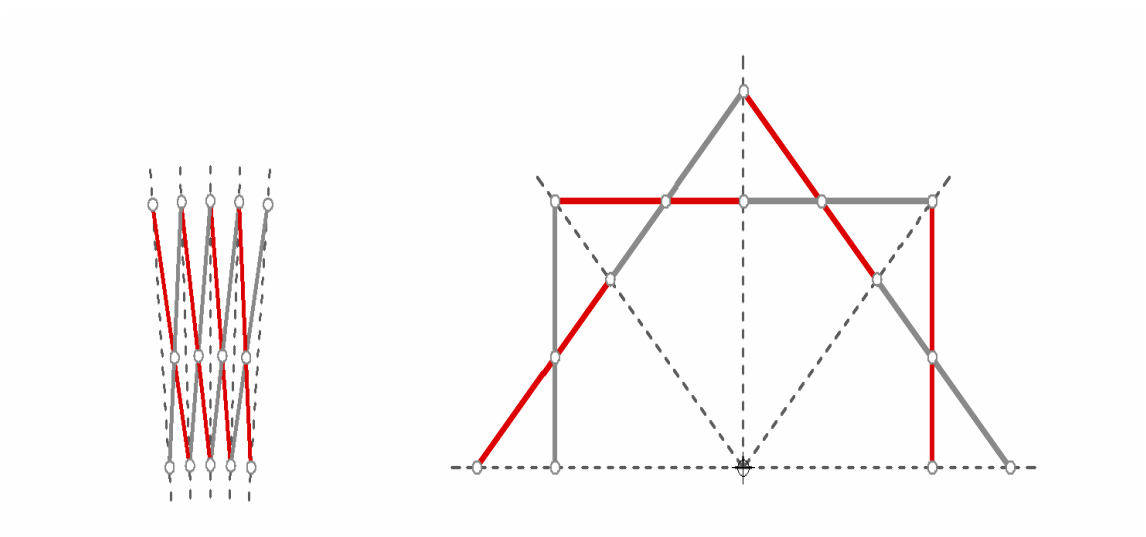
Figure 2.24: A polar linkage in its undeployed and deployed position. Source: De Temmerman (2007).

2.8.3 Angulated Units

The angulated pantograph unit normally called Hoberman's unit because it was first made popular by Hoberman (1990). This type of pantograph element consists of two identical angulated elements, each composed of two bars rigidly connected with a kink angle β as shown in Figure 2.25, unlike common pantograph units with straight bars (*i.e.* where β=180°). The angulated elements can be used to form expandable closed loop structures as shown in Figure 2.26. It is capable of retracting to their own perimeter, which is impossible to accomplish with translational or polar units. In Figure 2.26, a circular linkage is shown with angulated elements in its undeployed and deployed configuration, which is designed by two layers of identical angulated elements. Both layers are formed by angulated elements in opposite directions. During the deploying of the structure, each layer undergoes a rotation, with the same magnitude but opposite to each other.

The concept of the angulated pantograph element was extended by You and Pellegrino (1997) through their finding that a certain pantographic element with multiple kinks at the hinge positions (multi-angulated rod), as shown in Figure 2.27, has the same property and can be folded if the rods form a tessellation of parallelograms.
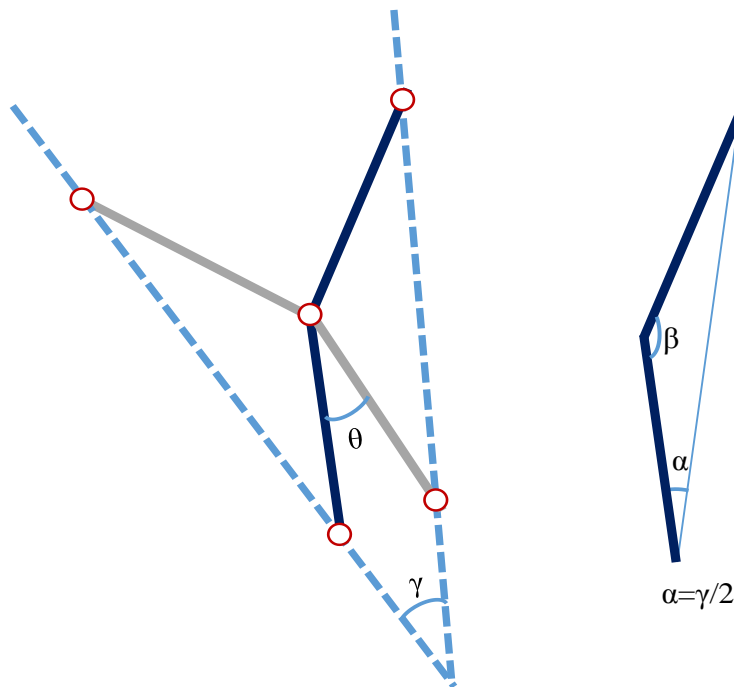
Figure 2.25: Angulated unit or Hoberman's unit.
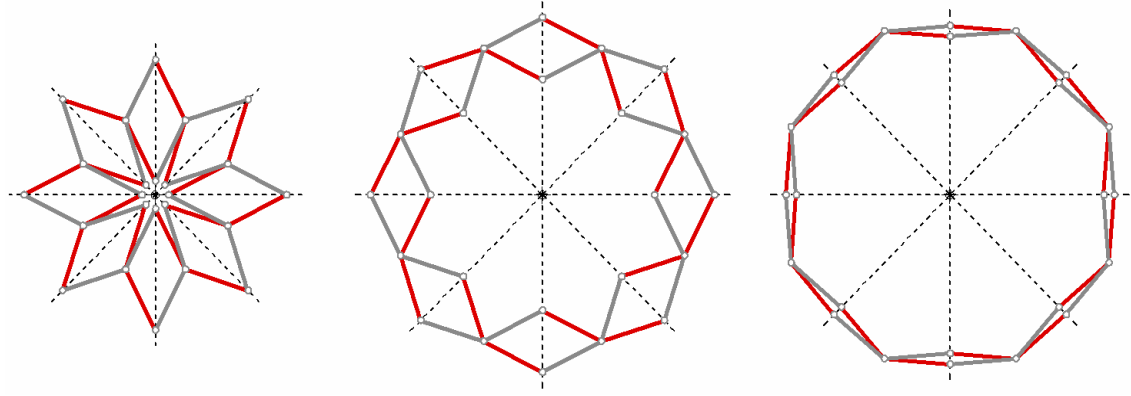
Figure 2.26: A radially deployable linkage consisting of angulated (or Hoberman's) units in three stages of the deployment. Source: De Temmerman (2007).
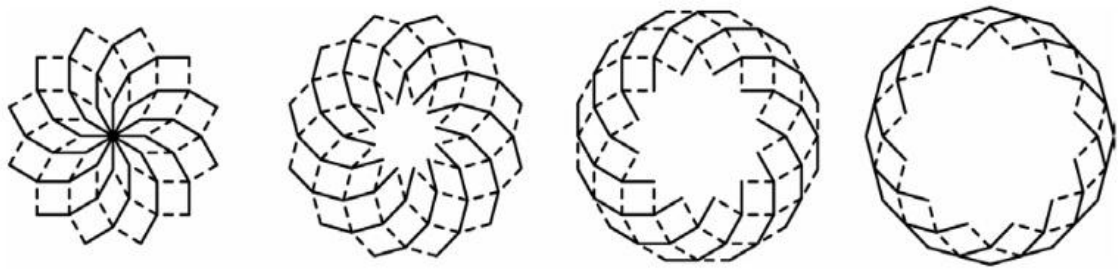
Figure 2.27: Retractable structure formed from multi-angulated elements. Source: You and Pellegrino (1997) and Jensen and Pellegrino (2005).

2.9   Modified Pantographic Unit

Akgün (2010) developed a new type of pantographic unit, called the modified pantographic unit, which can be distinguished from the normal pantographic unit by having additional revolute joints on various locations of the bars. These revolute joints increase not only the degrees of freedom of the unit, but also the transformation capacity of the whole system and increasing the possibilities of the number of structural forms (Akgün *et al.*, 2007; Akgün, 2010; Akgün *et al.*, 2010). Three different variations of the modified pantographic unit are shown in Figure 2.28. The modified pantographic unit in Figure 2.28a was obtained by the connection of four struts by three hinges on a common point, in this unit, compared to the structural pantograph unit, two additional degrees of freedom come from the revolute joint located at the point B (Akgün *et al.*, 2010).

Therefore, each of the four struts can rotate freely about their common point, without affecting the other three struts. In this modified pantographic unit, the number of degrees of freedoms is equal to three, while the number of degrees of freedom of the corresponding normal pantographic unit is equal to one. In Figure 2.28b, the additional revolute joints are located on the points D' and E'. The difference in this modified pantographic unit compared to a normal pantographic unit is the additional revolute joints on the bottom sides of the bars (points D' and E') (Akgün *et al.*, 2007). In the third shape of modified pantographic unit in Figure 2.28c, these additional revolute joints are located on the points D and E.
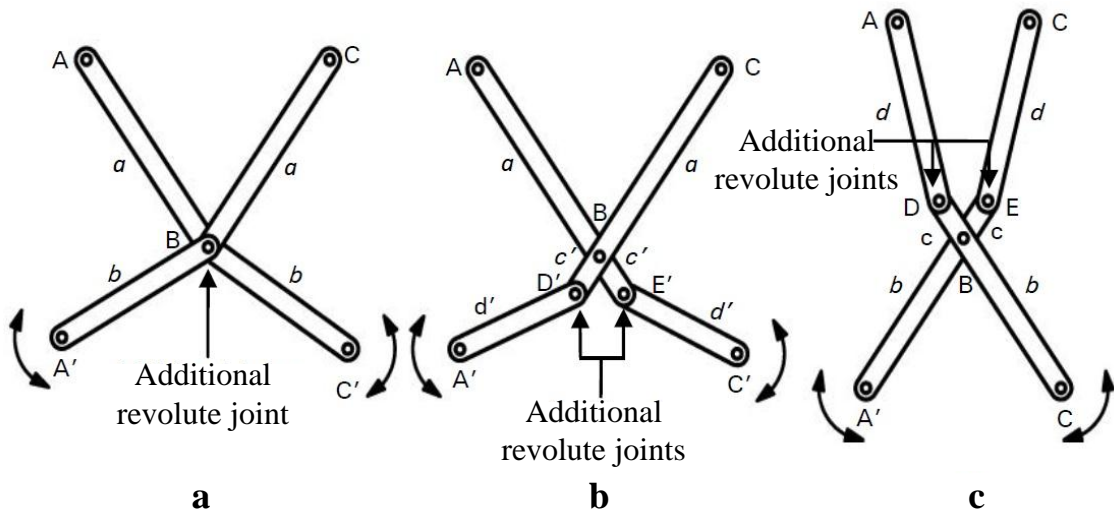
Figure 2.28: Variations of modified pantographic unit. Adapted: Akgün (2010).

On the basis of modified pantographic units, Akgün *et al.* (2010) designed a transformable planar pantographic roof structure. This adaptive structure can form various shapes without changing the size of the covered area because the modified pantographic units divide the entire system into sub-structures, acting as "isolators" of these sub-structures, so that each sub-structure can transform without directly affecting the other sub-structures. Hence, when a modified pantographic unit is used in a pantographic structure, it increases the number of degrees of freedoms of the whole system, thus enabling the system to change its shape, without changing the span length or the dimensions of the bars (Akgün, 2010; Akgün *et al.*, 2010). As an example for using

modified pantographic units in the system, Akgün (2010) presented the system shown in Figure 2.29 in his thesis. In the system, there are two modified pantographic units, dividing the whole structure into three "isolated" parts. Therefore, only the modified pantographic units in the same group follow any movement of one pantographic unit in the same group. Hence, it is possible to change the shape of the whole system without changing the dimensions of the struts or the span, since each sub-group has independency (Akgün, 2010).
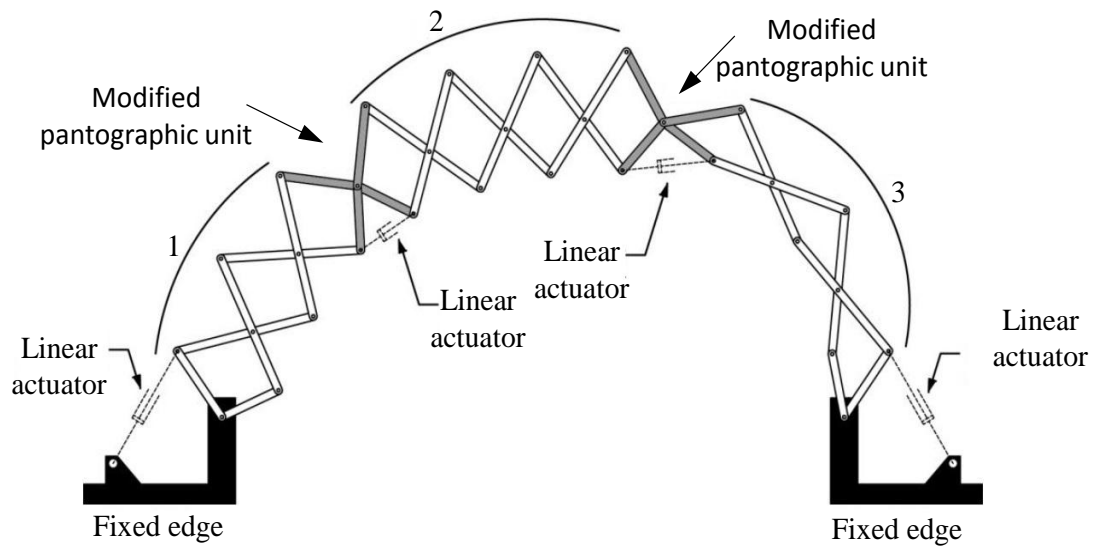
Figure 2.29: Location of modified pantographic unit on a scissor-hinge structure proposed by Akgün. Source: Akgün (2010).

2.10 Compact Folding Constraint

The introduction of kinematic degree of freedom is ensures mobility and transformation of the deployment of a structure. Crucial to the design of deployable morphing structures is the "deployability constraint" which is a simple formula derived by Escrig (1985), for instance for the linkage in Figure 2.30, as:

$$a + b = c + d$$

This equation means that for the system to fully close the sum of the semi-lengths a and b of a pantographic unit has to equal the sum of the semi-lengths c and d of the adjoining units.
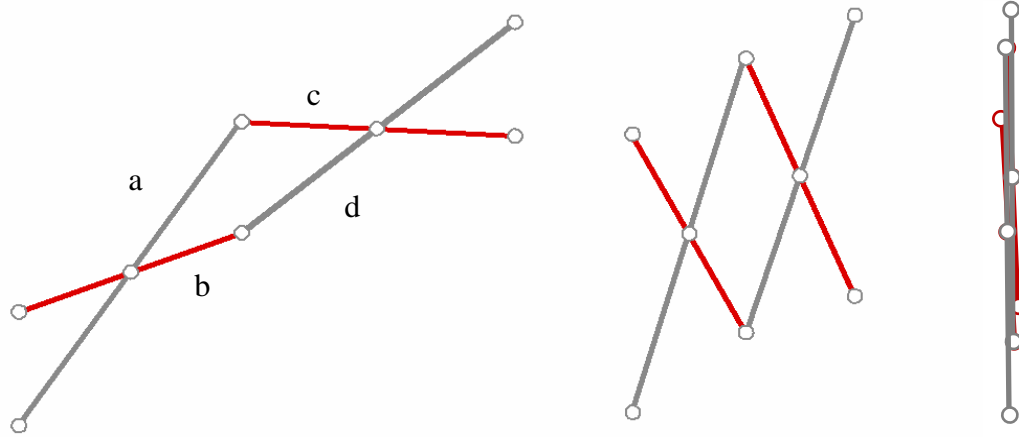
Figure 2.30: The deployability constraint in terms of the semi-lengths a, b, c and d of two adjoining pantograph units in three consecutive deployment stages. Adapted from De Temmerman (2007).

2.11 Analysis of Pantographic Structures

Morphing or deployable structures, consisting of only hinged pantographic units, usually have low structural stiffness, and high bending moment. Particularly for the large span grids, the structure can become inefficient (Wujun *et al.*, 2002). Therefore, researchers have concentrated on the methods for analysis for pantographic structures and have used numerous methods for formulating the structural matrix for a pantographic unit. Kwan (1991) used the force method, where the pantographic unit was discretised into four beam elements. The equilibrium, compatibility and flexibility matrices were derived for a typical beam element in a local coordinate system through using shear force and bending moment relationships. Subsequently, Pellegrino *et al.* (1992) reduced the equilibrium matrix in size by matrix partitioning and by setting the end moments to zero. In this method the number of self-stress states and the number of infinitesimal mechanisms of the given system could be evaluated by the singular value decomposition (SVD) of the equilibrium matrix (Pellegrino, 1993).

Using the same force method approach, Kwan and Pellegrino (1994), explored one particular class of deployable structures which consisted only of rods, hinged together to form a deployable backbone, some passive cables, and one or more active cables. "Passive cables" were slack when the backbone was fully or partially folded but become taut when fully deployed, while "active cables" activated deployment and setup suitable states of prestress once the structure was in its fully deployed configuration. Efficient methods of analysis for foldable pantographic structures have been developed by Kaveh and Davaran (1996). The authors have formulated the stiffness matrix a unit of such a structure into a standard stiffness method. The stiffness matrix of deployable pantograph masts with pantographic units was also obtained by Nagaraj *et al.* (2010) via an approach based on the constraint Jacobian matrix. They obtained the stiffness matrix in symbolic form and found a good match between their results and that obtained using the force method.

Chapter 3

Theoretical Analysis

This chapter deals with the general techniques of direct relationship between bar forces and/or bar length actuations and the external nodal displacements of a prestressable pin-jointed assembly, a beam and cable structure and a pantographic structure. These techniques will be used later in data analysis of a cable-stayed bridge (Chapter 4) and morphing pantographic structures (Chapter 6).

3.1 Introduction

Theoretical analysis using the Force Method of structural analysis can be applied to find the direct relationships among bar length actuations, the external nodal displacements and internal bar forces in order to identify the good/optimal locations for such actuators, and the amount of actuation to produce a prescribed shape or force change of structures under set of external loads. The set of equations are the equations for controlling external nodal displacements alone, controlling internal bar forces alone and simultaneously controlling both external nodal displacements and internal bar forces of the structures. The fundamental equations are linear (normal matrices and condensed matrices) for adjusting shape or force directly.

3.2   Linear Matrix Controlling Equations

3.2.1   The Force Method

The current technique is founded in the force method of structural analysis, principally because, unlike the displacement method, the force and displacement systems are not so "entangled" in the force method throughout the analysis, and thus allows "easy access" to the contributing parameters affecting the internal forces and the external displacements. Furthermore, the nature of the different effects are more clearly characterised, and thus there can be better handling of conflicting requirements of force and displacement. The Force Method is now briefly recapitulated.

Given an *i*-dimensional structural assembly with *b* bars and *j* joints, and a total of *c* degrees of freedom are constrained by external supports, the equilibrium balance between the vector of external loads **p** and internal bar forces **t** is expressed as

$$\mathbf{A}\mathbf{t} = \mathbf{p} \tag{3.1}$$

where **A** is the equilibrium matrix, and has size $(ij-c) \times b$. On the other hand, compatibility is the statement of general relationship between internal bar elongation **e** and external nodal displacements **d** and is expressed as

$$\mathbf{B}\mathbf{d} = \mathbf{e} \tag{3.2}$$

where **B** is the compatibility matrix, and has size $b \times (ij-c)$. Equilibrium is evidently entirely in the force realm, while compatibility concerns only structural displacements. Nonetheless, the two systems are clearly interdependent since they both relate to the same structure. The connection is that the equilibrium and compatibility matrices are transposes of each other, *i.e.* $\mathbf{B}^{\mathrm{T}} = \mathbf{A}$. This can be easily seen by expressing Eqn. 3.2 in incremental form, $\mathbf{B}\delta\mathbf{d} = \delta\mathbf{e}$ (or $\delta\mathbf{e}^{\mathrm{T}} = \delta\mathbf{d}^{\mathrm{T}}\mathbf{B}^{\mathrm{T}}$), with $\delta\mathbf{e}$ and $\delta\mathbf{d}$ as the virtual counterparts of **e** and **d**, and since the principle of virtual work (Livesley, 1975) provides $\delta\mathbf{e}^{\mathrm{T}}\mathbf{t} = \delta\mathbf{d}^{\mathrm{T}}\mathbf{p}$, then $\left[\delta\mathbf{d}^{\mathrm{T}}\mathbf{B}^{\mathrm{T}} \right]\mathbf{t} = \delta\mathbf{d}^{\mathrm{T}}\mathbf{p}$ and thus $\mathbf{B}^{\mathrm{T}}\mathbf{t} = \mathbf{p}$, *i.e.* $\mathbf{B}^{\mathrm{T}} = \mathbf{A}$.

The trio of relationships is completed by the flexibility relationship involving the individual member flexibilities, which, for a pin-jointed bar assembly, has a $b \times b$ diagonal flexibility matrix **F** such that

$$\mathbf{F}\,\mathbf{t} = \mathbf{e}\,. \tag{3.3}$$

where every bar has non-zero bar stiffness, $\mathbf{F}$ is of full rank and invertible. In this case, $\mathbf{t} = \mathbf{F}^{-1}\mathbf{e}$, and with Eqn. 3.1, $\mathbf{A}\left[\mathbf{F}^{-1}\mathbf{e}\right] = \mathbf{p}$, and with Eqn. 3.2, $\mathbf{A}\mathbf{F}^{-1}\left[\mathbf{B}\mathbf{d}\right] = \mathbf{p}$. Since the Displacement Method has $\mathbf{K}\mathbf{d} = \mathbf{p}$, then the stiffness matrix $\mathbf{K} = \mathbf{A}\mathbf{F}^{-1}\mathbf{B}$.

However, in the force method, the solution to the system is not via $\mathbf{K} = \mathbf{A}\mathbf{F}^{-1}\mathbf{B}$ but involves firstly expressing the general solution $\mathbf{t}$ to the equilibrium equations as the sum of a particular solution and the complementary homogeneous solution. The particular solution is *any* vector $\mathbf{t}$ that satisfies Eqn. 3.1, and one such vector $\mathbf{t}_{\mathrm{H}}$ can be obtained [There are other ways to obtain $\mathbf{t}_{\mathrm{H}}$, since $\mathbf{t}_{\mathrm{H}}$ is not unique] from $\mathbf{t}_{\mathrm{H}} = \mathbf{A}^{+}\mathbf{p}$ where $\mathbf{A}^{+}$ is the pseudo-inverse (or Moore-Penrose inverse) of $\mathbf{A}$. With the use of the pseudo-inverse $\mathbf{A}^{+}$, $\mathbf{t}_{\mathrm{H}}$ is actually not merely any particular solution to Eqn. 3.1, but it is in fact the least-squares solution, though this additional property is not necessary for our purpose.

The complementary homogenous solution is the set of solutions satisfying $\mathbf{A}\,\mathbf{t}=\mathbf{0}$, *i.e.* the sets of bar forces in equilibrium with zero external load. This is readily provided by the nullspace($\mathbf{A}$)=$\mathbf{S}$, which by definition satisfies $\mathbf{A}\mathbf{S} = \mathbf{0}$, and hence $\mathbf{S}$ is called the states of self-stress. There are *s* linearly independent vectors forming $\mathbf{S}$ and *s*=*b*-rank($\mathbf{A}$). The correct complementary homogeneous solution can be expressed as $\mathbf{S}\boldsymbol{\alpha}$, where $\boldsymbol{\alpha}$ is a set of *s* combinatorial constants for the vectors of $\mathbf{S}$ that has to be determined through satisfaction of compatibility. The total general solution for equilibrium, combining a particular solution and the complementary solution, is thus

$$\mathbf{t} = \mathbf{t}_{\mathrm{H}} + \mathbf{S}\boldsymbol{\alpha}\,. \tag{3.4}$$

At this point, we introduce a vector of elongation actuation to each bar called $\mathbf{e_o}$. In reality, since elongation actuation greatly complicates the physical makeup of a bar, we would have actuation only for a limited number of bars, and hence many elements of $\mathbf{e_o}$ will remain zero. Currently, we will allow any bar the capacity for actuation, and thus $\mathbf{e_o}$ is fully populated, and Eqn. 3.3 becomes

$$\mathbf{e} = \mathbf{e}_{\mathrm{o}} + \mathbf{F}\,\mathbf{t}\,, \tag{3.5}$$

i.e. the total elongation in each bar comprises of the sum of actuation for the bar and the elongation due to axial force. Substitution of Eqn. 3.4 into Eqn. 3.5 thus gives

$$\mathbf{e} = \mathbf{e}_o + \mathbf{F}\left(\mathbf{t}_H + \mathbf{S}\boldsymbol{\alpha}\right). \tag{3.6}$$

Whether a set of bar elongation satisfies compatibility or not can be assessed by whether it can be found in the set of compatibility elongations, *i.e.* in the columnspace($\mathbf{B}$), whereas the left-nullspace($\mathbf{B}$) contains the basis for all the incompatible elongations. The compatibility condition then is imposed through stating that the bar elongations $\mathbf{e}$ must be orthogonal to the left-nullspace($\mathbf{B}$), and that is actually identical to nullspace($\mathbf{A}$) (*i.e.* the states of self-stress $\mathbf{S}$) when $\mathbf{B}^T = \mathbf{A}$. The compatibility condition is thus $\mathbf{S}^T\mathbf{e} = \mathbf{0}$, *i.e.*

$$\mathbf{S}^T\mathbf{e}_o + \mathbf{S}^T\mathbf{F}\left(\mathbf{t}_H + \mathbf{S}\boldsymbol{\alpha}\right) = \mathbf{0} \tag{3.7}$$

and thus

$$-\boldsymbol{\alpha} = \left(\mathbf{S}^T\mathbf{F}\mathbf{S}\right)^{-1}\left[\mathbf{S}^T\mathbf{e}_o + \mathbf{S}^T\mathbf{F}\mathbf{t}_H\right]. \tag{3.8}$$

The expression for $\boldsymbol{\alpha}$ then reveals, by back-substitution, the structural vectors of $\mathbf{e}$ (Eqn. 3.6), $\mathbf{t}$ (Eqn. 3.4) and $\mathbf{d}$ (Eqn. 3.2).

3.2.2 *Displacement Control without Regard to Bar Forces*

The presentation in Section 3.2.1 is completely adequate for analysis of statically determinate and indeterminate structures under load, and even prestressed structures where the initial imperfection is entered via $\mathbf{e_o}$. The situation under consideration now is where some of the displacements of the structure resulting from loadings are considered too large (or too small) and need to be corrected by actuation in at least some of the bars. Such actuations will necessarily affect at least some of the bar forces, and possibly put some beyond tolerance, but we shall not in this section be concerned about changes in bar forces.

Equation 3.8 can be substituted into Eqn. 3.6 to give

$$\begin{aligned}
\mathbf{e} &= \mathbf{e}_o + \mathbf{F}\left(\mathbf{t}_H - \mathbf{S}\left(\mathbf{S}^T\mathbf{F}\mathbf{S}\right)^{-1}\left[\mathbf{S}^T\mathbf{e}_o + \mathbf{S}^T\mathbf{F}\mathbf{t}_H\right]\right) \\
&= \left[\mathbf{I} - \mathbf{F}\mathbf{S}\left(\mathbf{S}^T\mathbf{F}\mathbf{S}\right)^{-1}\mathbf{S}^T\right]\mathbf{e}_o + \left[\mathbf{F} - \mathbf{F}\mathbf{S}\left(\mathbf{S}^T\mathbf{F}\mathbf{S}\right)^{-1}\mathbf{S}^T\mathbf{F}\right]\mathbf{t}_H
\end{aligned} \tag{3.9}$$

and with Eqn. 3.2, we thus have

$$\mathbf{d} = \mathbf{Y}\mathbf{e}_o + \mathbf{d}_P \qquad (3.10)$$

where $\mathbf{Y} = \mathbf{B}^+ - \mathbf{B}^+ \mathbf{F} \mathbf{S}\left(\mathbf{S}^T \mathbf{F} \mathbf{S}\right)^{-1}\mathbf{S}^T$, and $\mathbf{d}_P = \left[\mathbf{B}^+\mathbf{F} - \mathbf{B}^+\mathbf{F}\mathbf{S}\left(\mathbf{S}^T\mathbf{F}\mathbf{S}\right)^{-1}\mathbf{S}^T\mathbf{F}\right]\mathbf{t}_H$ is the

vector of nodal displacements of the structure due only to load, vector $\mathbf{d}$ and is thus the resultant nodal displacements after some elongation actuation $\mathbf{e}_o$ has been applied. The vector $\mathbf{d}$, in whole or in part, can thus be used as the prescribed desired displacements and Eqn. 3.10 therefore provides the required corrective $\mathbf{e}_o$ to achieve that prescribed $\mathbf{d}$, despite the effects of load in $\mathbf{d}_P$. A form of Eqn. 3.10 (without the $\mathbf{d}_P$) has in fact been presented by You (1997), but his interest was in shape control of *unloaded* prestressed structures.

Clearly, $\mathbf{Y}$ is generally not a square matrix, and need not even be of full rank. Furthermore, it is likely that not every element of $\mathbf{d}$ needs to be prescribed a set value. For example, where the structure concerned is a truss supporting structure for a parabolic dish antenna, only the nodes in direct contact with the surface of the antenna need to be prescribed and carefully adjusted, while other nodes would be free to take any values due to the loading (and adjustment process). Furthermore, not all elements of $\mathbf{e}_o$ would typically have the ability to be actuated. The system of equations and unknowns in Eqn. 3.10 is thus normally likely to be only a (small) subset of the full set of equations. In view of all this, the solution for $\mathbf{e}_o$ is thus best obtained using the pseudoinverse of $\mathbf{Y}$:

$$\mathbf{e}_o = \mathbf{Y}^+ \left\{\mathbf{d} - \mathbf{d}_P\right\}. \qquad (3.11)$$

3.2.2.1 *An Illustrative Example of Displacement Control*

This procedure is now illustrated with the simple example shown in Figure 3.1, which has $EA = 4 \times 10^5$ for all bars. The structure has a single state of selfstress involving the left-hand half of the structure:

$$\mathbf{S} = \begin{bmatrix} 1 & 1 & -\sqrt{2} & -\sqrt{2} & 1 & 1 & 0 & 0 & 0 & 0 \end{bmatrix}^T. \qquad (3.12)$$
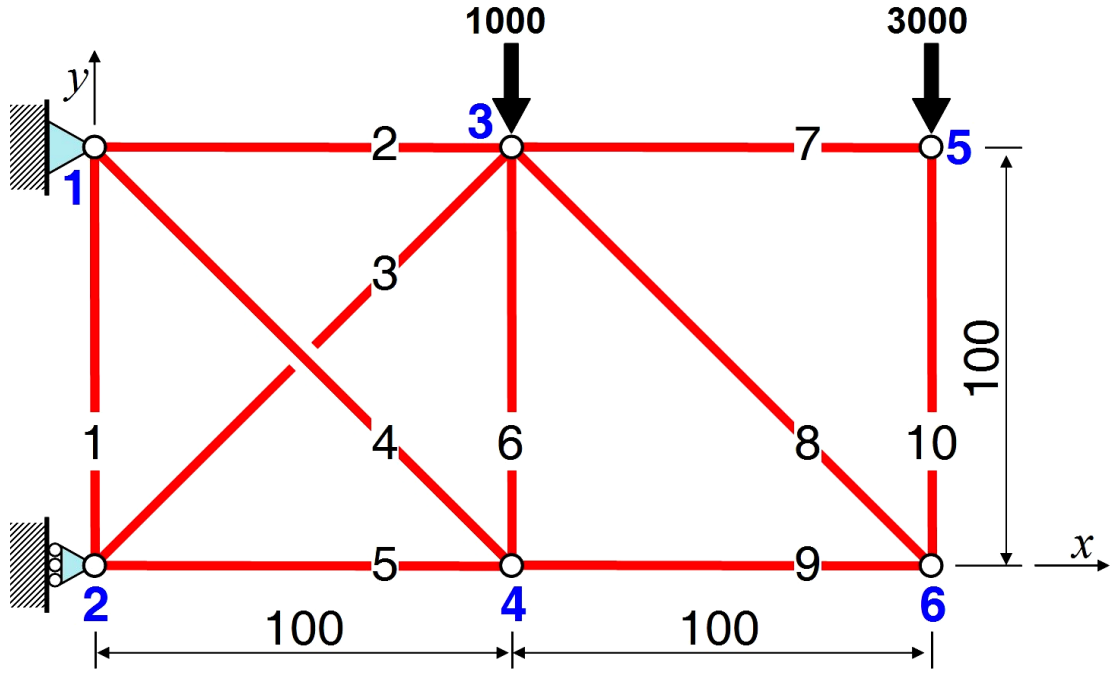
Figure 3.1: A simple cantilevered truss structure with one state of selfstress

The displacements under load $\mathbf{d}_P$ are as shown in Column 3 of Table 3.1, and the structure deforms primarily in the negative y-direction. It is supposed that the nodal displacements in $3y$ and $5y$ are too large and are to be limited to -2.000 each, while the remaining displacements are free to take any value. In prescribing both d_{3y} and d_{5y} to be -2.000, we have also prescribed a levelling condition; in some instances, the displacement control required would not be of absolute displacements, but of relative displacements between selected joints, *e.g.* to maintain a constant slope or specific shape of a surface.

Since we are prescribing only two displacements, Eqn. 3.10 has only two equations and becomes:

$$\begin{pmatrix} -2 \\ -2 \end{pmatrix} = \begin{pmatrix} -\frac{1}{2} & -\frac{1}{2} & \frac{1}{\sqrt{2}} & -\frac{1}{\sqrt{2}} & \frac{1}{2} & \frac{1}{2} & 0 & 0 & 0 & 0 \\ -\frac{1}{2} & -\frac{3}{2} & \frac{1}{\sqrt{2}} & -\frac{1}{\sqrt{2}} & \frac{3}{2} & \frac{1}{2} & 0 & -\sqrt{2} & 1 & 1 \end{pmatrix} \mathbf{e}_\mathrm{o} + \begin{pmatrix} -3.164 \\ -9.286 \end{pmatrix} \quad (3.13)$$

which clearly has many possible solutions. One possible solution is to simply use the pseudoinverse to solve Eqn. 3.13, where we thus obtain

$\mathbf{e}_\mathrm{o} = \{\text{-0.039} \quad \text{-1.046} \quad 0.056 \quad \text{-0.056} \quad +1.046 \quad +0.039 \quad 0 \quad \text{-1.424} \quad +1.007 \quad +1.007\}^\mathrm{T}$

which when entered in as a corrective $\mathbf{e}_\mathbf{o}$ does indeed produce a displacement of -2.000 in both d_{3y} and d_{5y} as required, see Column 4 of Table 3.1. As a beneficial side effect, the

other displacements have also been reduced, e.g. see d_{6y}. However, this set of $\mathbf{e_o}$ is not a particularly practical solution since it involves an elongation actuation in every bar except bar 7, and requires a total actuation of 5.721. A better set of $\mathbf{e_o}$ would be one that requires only a few non-zero actuations, and yet still produces the required displacements for d_{3y} and d_{5y}.

3.2.2.2 Best Location of Actuators

If the physical actuators were already in place, then the question of which bars could be actuated would not be an issue; what only remains to be decided is the amount of actuation for the actuators already in situ. However, at the design stage, while the location of actuators is still yet to be decided, the important question is where the actuators should be placed so that they could be of most effective in controlling the sort of displacements that will arise out of service loading. In this case, Eqn. 3.13 is now used to identify which are the best (*i.e.* most effective) bars to control d_{3y} and d_{5y} as well as what the associated actuations should be.

Table 3.1: Displacements of the structure in Figure 3.1 under different sets of $\mathbf{e_o}$ (MATLAB Program is shown in Appendix A.1).

(1)	(2)	(3)	(4)	(5)	(6)
Joint	Dir	Just $\mathbf{d_P}$, no $\mathbf{e_o}$	$\mathbf{Y^+e_o+d_P}$	4 elements in $\mathbf{e_o}$	2 elements in $\mathbf{e_o}$
1	*x*	0	0	0	0
	y	0	0	0	0
2	*x*	0	0	0	0
	y	-0.500	-0.461	-0.500	-0.741
3	*x*	+1.250	+0.204	-1.811	-4.630
	y	**-3.164**	-2.000	-2.000	-2.000
4	*x*	-1.250	-0.204	+1.811	-1.009
	y	-2.664	-1.539	-1.500	-1.741
5	*x*	+1.250	+0.204	-1.811	-4.630
	y	**-9.286**	-2.000	-2.000	-2.000
6	*x*	-2.000	+0.054	+1.061	-1.759
	y	-8.536	-2.257	-1.250	-1.250

The effectiveness of actuation in any bar in controlling a particular displacement is indicated by the associated coefficient in the **Y** matrix. For example, the null column in **Y** for bar 7 in Eqn. 3.13 shows that bar 7 is completely ineffectual in controlling both d_{3y} and d_{5y}. Conversely, the most effective bars are those with large coefficients in **Y**, *e.g.* bars 2 and 5 for d_{5y}, and bars 3 and 4 for d_{3y}. If there was a preference for elongation or shortening for the actuation, then the sign of the coefficient would also be relevant, otherwise, it is merely the size of the coefficient that matters. We shall now consider bars 2, 3, 4 and 5 as the four chosen bars for actuation since they have the largest coefficients in either row of **Y** and Eqn. 3.13 now becomes:

$$\begin{pmatrix} -2 \\ -2 \end{pmatrix} = \begin{pmatrix} -\frac{1}{2} & \frac{1}{\sqrt{2}} & -\frac{1}{\sqrt{2}} & \frac{1}{2} \\ -\frac{3}{2} & \frac{1}{\sqrt{2}} & -\frac{1}{\sqrt{2}} & \frac{3}{2} \end{pmatrix} \begin{Bmatrix} e_2 \\ e_3 \\ e_4 \\ e_5 \end{Bmatrix} + \begin{pmatrix} -3.164 \\ -9.286 \end{pmatrix}. \tag{3.14}$$

The use of the pseudoinverse gives

$$\mathbf{e}_o = \{0 \quad -3.061 \quad -1.341 \quad +1.341 \quad +3.061 \quad 0 \quad 0 \quad 0 \quad 0 \quad 0\}^{\mathrm{T}}.$$

Although this set of $\mathbf{e_o}$ has an increased total actuation of 8.803, it does have the advantage that only four bars are actuated, and the resultant nodal displacements still satisfy the condition that d_{3y} and d_{5y} equal -2.000, see Column 5 in Table 3.1.

Now, if only two bars are chosen for actuation instead of four, say bar 2 for d_{5y} and bar 3 for d_{3y}, Eqn. 3.13 is further reduced to

$$\begin{pmatrix} -2 \\ -2 \end{pmatrix} = \begin{pmatrix} -\frac{1}{2} & \frac{1}{\sqrt{2}} \\ -\frac{3}{2} & \frac{1}{\sqrt{2}} \end{pmatrix} \begin{Bmatrix} e_2 \\ e_3 \end{Bmatrix} + \begin{pmatrix} -3.164 \\ -9.286 \end{pmatrix} \tag{3.15}$$

and

$$\mathbf{e}_o = \{0 \quad -6.121 \quad -2.682 \quad 0 \quad 0 \quad 0 \quad 0 \quad 0 \quad 0 \quad 0\}^{\mathrm{T}}.$$

This reduced set of $\mathbf{e_o}$ is actually similar to the previous set since we can see bars 2 and 5 form a pair with similar effect and action, while bars 3 and 4 form another pair, and actuating one of the two in a pair is similar to half actuating both in the pair. The total actuation is still 8.803, but the distinct advantage is that the required displacements for d_{3y} and d_{5y} have been obtained with actuating only two bars.

The current approach not only determines the necessary amount of actuation to be applied to obtain specific prescribed displacements, it also identifies which are the most effective bars for a given set of displacement control, so that the minimum number of actuation can be used to deliver the required displacements. This is clearly an important tool in the design of shape sensitive structures with built-in shape control, and especially of those structures with variable loading (*e.g.* movable antenna or telescopes, or orbital structures under changing thermal loading).

3.2.3 *Bar Forces Control without Regard to Displacements*

For some structures under external loading, the internal forces in the structural members might require control more than that for the displacements. For example, under some loading conditions, a cable member could approach slack and thus needs to be retightened to remain structurally existent, or a slender strut could be approaching instability and thus needs its compressive force reduced. Length actuation thus has a function in the control of the internal forces in statically indeterminate structures. Kwan and Pellegrino (1993) have already discussed length actuation in the case of trying to achieve a specific prestress pattern before loading, as in the case of obtaining an even prestress throughout a cable-stayed bridge after construction, but the current concern is about controlling the axial force of some of the structural members which are over- or under-stressed as a result of loading, *e.g.* to avoid structural failure.

The equation for the required set of $\mathbf{e_0}$ to attain a given prescribed set of internal force comes from substituting Eqn. 3.8 into Eqn. 3.4 to give

$$
\begin{aligned}
\mathbf{t} &= \mathbf{t}_\mathrm{H} - \mathbf{S}\left(\mathbf{S}^\mathrm{T}\mathbf{F}\mathbf{S}\right)^{-1}\left[\mathbf{S}^\mathrm{T}\mathbf{e}_\mathrm{o} + \mathbf{S}^\mathrm{T}\mathbf{F}\mathbf{t}_\mathrm{H}\right] \\
&= \left\{\mathbf{t}_\mathrm{H} - \mathbf{S}\left(\mathbf{S}^\mathrm{T}\mathbf{F}\mathbf{S}\right)^{-1}\mathbf{S}^\mathrm{T}\mathbf{F}\mathbf{t}_\mathrm{H}\right\} - \left[\mathbf{S}\left(\mathbf{S}^\mathrm{T}\mathbf{F}\mathbf{S}\right)^{-1}\mathbf{S}^\mathrm{T}\right]\mathbf{e}_\mathrm{o} \\
&= \mathbf{t}_\mathrm{P} - \mathbf{Z}\mathbf{e}_\mathrm{o}
\end{aligned}
\tag{3.16}
$$

where $\mathbf{t}_\mathrm{P} = \mathbf{t}_\mathrm{H} - \mathbf{S}\left(\mathbf{S}^\mathrm{T}\mathbf{F}\mathbf{S}\right)^{-1}\mathbf{S}^\mathrm{T}\mathbf{F}\mathbf{t}_\mathrm{H}, \mathbf{Z} = \mathbf{S}\left(\mathbf{S}^\mathrm{T}\mathbf{F}\mathbf{S}\right)^{-1}\mathbf{S}^\mathrm{T}$. $\mathbf{t}_\mathrm{P}$ is the vector of internal force due to the applied load, and $\mathbf{t}$ is the resultant internal forces after some elongation actuation $\mathbf{e_0}$ has been applied. As in Section 3.2.2, the vector $\mathbf{t}$, or part of it, can be used as the prescribed internal force and thus Eqn. 3.16 provides the corrective $\mathbf{e_0}$ to achieve a prescribed $\mathbf{t}$, despite the effects of load found in $\mathbf{t}_\mathrm{P}$.

Although $\mathbf{Z}$ appears to be a square matrix in Eqn. 3.16, it is actually rank deficient (since $s < b$). Furthermore, as with $\mathbf{Y}$ in Section 3.2.2, not every bar will participate in $\mathbf{t}$ and $\mathbf{e_o}$ and thus $\mathbf{Z}$ is even unlikely to be square. Therefore, the most appropriate way of obtaining $\mathbf{e_o}$ is again through use of the pseudoinverse.

We shall illustrate the use of Eqn. 3.16 by again using the structure in Figure 3.1, and the bar forces due only to load, $\mathbf{t_P}$, is shown in Column 2 of Table 3.2. It is supposed that the three largest bar forces in bars 2, 5, and 8 need to be controlled. Given this, Eqn. 3.16 becomes:

$$\begin{Bmatrix} t_2 \\ t_5 \\ t_8 \end{Bmatrix} = \begin{Bmatrix} +5000 \\ -5000 \\ +4243 \end{Bmatrix} - 414.214 \begin{pmatrix} 1 & 1 & -\sqrt{2} & -\sqrt{2} & 1 & 1 & 0 & 0 & 0 & 0 \\ 1 & 1 & -\sqrt{2} & -\sqrt{2} & 1 & 1 & 0 & 0 & 0 & 0 \\ 0 & 0 & 0 & 0 & 0 & 0 & 0 & 0 & 0 & 0 \end{pmatrix} \mathbf{e}_o . \quad (3.17)$$

The first observation to make is that the third row of $\mathbf{Z}$, relating to t_8, contains only zero coefficients, and thus t_8 is completely unaffected by $\mathbf{e_o}$. This is because $\mathbf{S}$ affects only the doubly-braced left hand unit of the structure and bars 7 to 10 (on the right hand side) are un-prestressable, and hence they derive their bar force only from $\mathbf{t_P}$. Secondly, since bars 2 and 5 have the same coefficients in $\mathbf{S}$, and there is only a single state of selfstress, then any effect from $\mathbf{Ze_o}$ has to be uniform for both bars 2 and 5, $i.e.$ bar forces 2 and 5 could be both raised or decreased by the same amount, but they cannot be independently controlled. In this case, they can either both become more negative, in which case bar 5 has increased compression (but bar 2 has decreased tension) or they can both become more positive, in which case bar 2 has increased tension (and bar 5 correspondingly has decreased compression). We are thus unable to decrease the magnitude of both bar forces at the same time; this can also be noted by the fact that row 2 of $\mathbf{Z}$ is identical to row 5 and so the effect of $\mathbf{e_o}$ has to be the same for t_2 as for t_5.

Given the above limitations, we shall thus seek to reduce the compressive force in bar 5, but noting at the same time that any such reduction will be met with an equal magnitude increase in the tensile force of bar 2. We assume that the required t_5 is -4000, and thus the reduced Eqn. 3.16 is

$$\{-4000\} = \{-5000\} - 414.214\begin{pmatrix} 1 & 1 & -\sqrt{2} & -\sqrt{2} & 1 & 1 & 0 & 0 & 0 & 0 \end{pmatrix} \mathbf{e}_o . \quad (3.18)$$

If all possible bars are given an actuation, then the use of the pseudoinverse on Eqn. 3.18 gives

$$\mathbf{e}_o = -0.3018\{1 \quad 1 \quad -\sqrt{2} \quad -\sqrt{2} \quad 1 \quad 1 \quad 0 \quad 0 \quad 0 \quad 0\}^T$$

with a total actuation of 2.061, which gives the set of bar tensions including the required t_5 as shown in Column 4 of Table 3.2. Clearly, this set of $\mathbf{e}_o$ is excessively full of non-zeroes and only one bar length actuation is necessary to produce the prescribed tension. The most effective bar is either bar 3 or 4 (since they have the largest associated coefficient in $\mathbf{Z}$) and an actuation of 1.707 on either bar gives the final set of bar tensions shown in Column 5 of Table 3.2, which is actually the same result as achieved with six bars being actuated. (Since s=1, there can only be one $\mathbf{t}$ which has t_5=-4000, regardless of what $\mathbf{e}_o$ is actually set to.)

The ability of Eqn. 3.16 to control a specific prescribed bar force depends very much on $\mathbf{S}$, whether that particular bar has at least one non-zero coefficient in its corresponding row in $\mathbf{S}$, and whether there is enough flexibility in the different combinations of the columns of $\mathbf{S}$ to simultaneously satisfy all the (potentially conflicting) prescribed bar forces. If a bar has no non-zero entry in $\mathbf{S}$ then its bar force cannot be controlled by actuation at all. It is also possible that not all the prescribed bar forces can be achieved because s is too small (as in the example above), then only an approximate or least-squares solution is possible. Nonetheless, where s is large, and $\mathbf{S}$ is thus sufficiently expansive, Eqn. 3.16 gives the required $\mathbf{e}_o$ to control specific bar tensions.

Table 3.2: State of selfstress or bar forces of the structure in Figure 3.1 under different $\mathbf{e}_o$ (MATLAB program can be found in Appendix A.1).

(1)	(2)	(3)	(4)	(5)
Bar	Just $\mathbf{t}_P$, no $\mathbf{e}_o$	$\mathbf{S}$	All elements in $\mathbf{e}_o$	Only 1 element in $\mathbf{e}_o$
1	+2000	1	+3000	+3000
2	**+5000**	1	+6000	+6000
3	-2828	$-\sqrt{2}$	-4243	-4243
4	+2828	$-\sqrt{2}$	+1414	+1414
5	**-5000**	1	-4000	-4000
6	-2000	1	-1000	-1000
7	0	0	0	0
8	**+4243**	0	+4243	+4243
9	-3000	0	-3000	-3000
10	-3000	0	-3000	-3000

3.2.4 Simultaneous Displacement and Bar Force Control

Each of Section 3.2.2 or 3.2.3 provides a method to control either the displacements, or the bar forces, in a structure due to external load without regard of the other. In practice, it is highly likely that situations requiring control of one will also have some effects on the other. For example, while it is critical to restore the shape of an antenna to a prescribed profile via member length actuations, it is also necessary that the resultant set of $\mathbf{e_0}$ does not then increase some strut forces to dangerous levels, or reduce some cable forces to the point of making them slack. In many situations, there is thus a need to be able to simultaneously control both the external nodal displacements as well as the internal bar forces via the same set of $\mathbf{e_0}$.

The method we adopt for this is rather straightforward and it works well because in general, the total number of bars (and thus the total number of possible length actuations) outweighs the sum of the number of displacements and bar forces needing control. We can look for a solution in $\mathbf{e_0}$ that simultaneously satisfies displacement and bar force prescriptions by combining together Eqns. 3.10 and 3.16 to give:

$$\begin{bmatrix} \mathbf{Y} \\ \mathbf{Z} \end{bmatrix} \mathbf{e}_o = \begin{bmatrix} \mathbf{d} - \mathbf{d}_P \\ \mathbf{t}_P - \mathbf{t} \end{bmatrix}. \tag{3.19}$$

Since $\mathbf{e_0}$ is coupled to a single system involving both the $\mathbf{Y}$ and $\mathbf{Z}$ equations, then $\mathbf{e_0}$ is compelled to satisfy both the displacement and bar force prescriptions simultaneously, where it is possible to do so. Clearly, in the extreme, where there can be up to $ij - c$ equations in $\mathbf{Y}$ and b equations in $\mathbf{Z}$, and there are only b unknowns in $\mathbf{e_0}$, Eqn. 3.19 will be over-determinate and insoluble, and only a least-square "approximation" is possible for $\mathbf{e_0}$. However, this extreme situation is mainly only of academic interest, and typical situations are under-determinate and allow a choice in $\mathbf{e_0}$.

3.2.4.1 An Illustrative Example of Displacement and Force Control

We shall examine Eqn. 3.19 through the more complicated truss structure shown in Figure 3.2, which has $EA = 4 \times 10^5$ for all bars. Each of the three bays of the truss is doubly-braced, and adjacent pairs of bays are also further doubly-braced. The double-bracing

thus provides for us the states of selfstress, and there are seven in total, as shown in Figure 3.3.
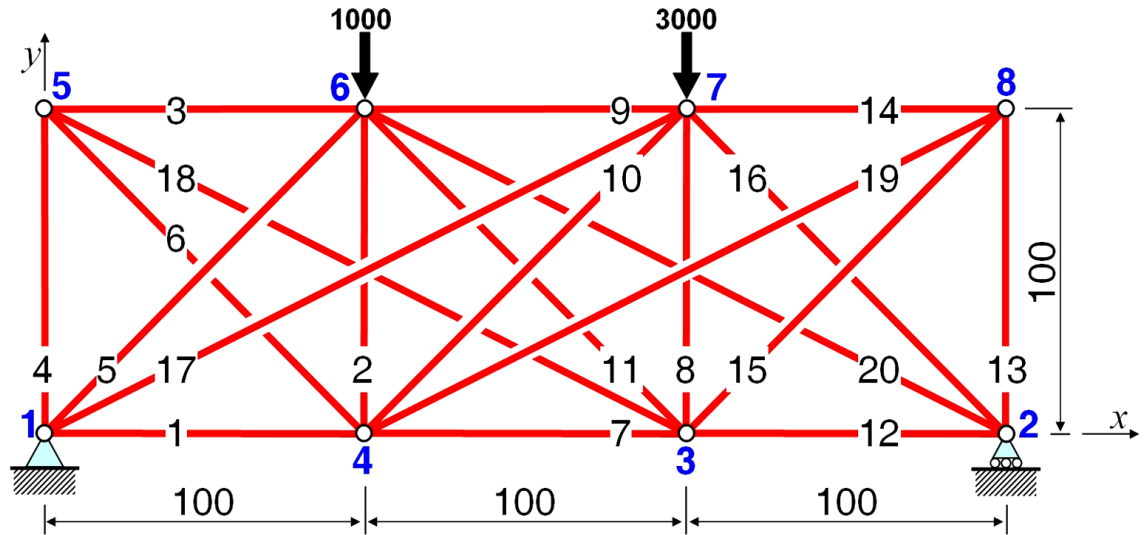
Figure 3.2: A 3-bay truss with seven degrees of statical indeterminacy.

(a) A single bay state of selfstress (only middle bay shown here); three states like this altogether.

(b) Double-bay states of Selfstress (only left-hand pair shown here); 2x2 states like this altogether.

(c)

tensile
compression
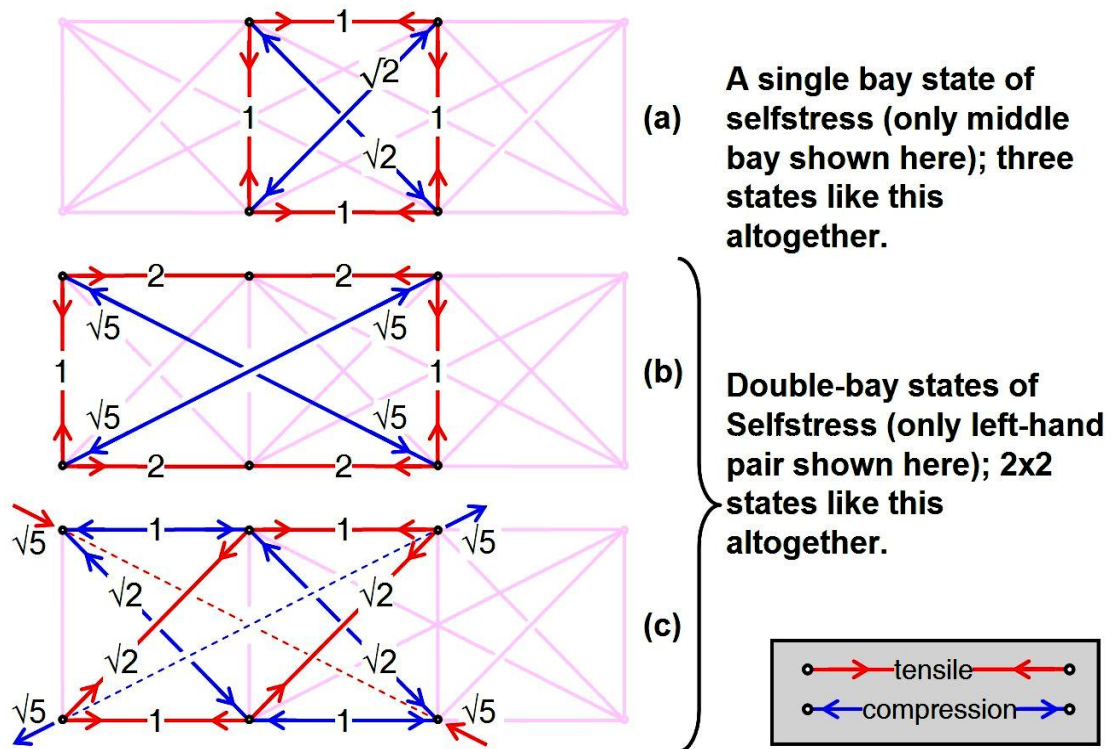
Figure 3.3: Illustration of the seven states of selfstress for the structure in Figure 3.2.

Each of the individual three bays has a state of selfstress as typified by Figure 3.3a (where only the middle bay is illustrated). This is similar to the state of selfstress on the left-hand half of the structure in Figure 3.1. Each of the two doubly-braced double-bays also has a similar state of selfstress, and the left-hand state is illustrated in Figure 3.3b. Furthermore, the doubly-braced double-bays have a second and less obvious state of selfstress as illustrated in Figure 3.3c, where the two main diagonals have opposite forces and the forces to equilibrate the diagonals are produced by leaning quadrilateral formations. Altogether, the presence of these seven states of selfstress means that each bar is spanned by at least two independent states of selfstress and thus there is a greater opportunity for bar force control that avoids two specific bars being immutably coupled (as in bars 2 and 5 of Section 3.2.3).

Table 3.3 shows the displacements and bar force for the structure under load, firstly without any corrective actuation $\mathbf{e_o}$ applied. As expected, the displacements are largely in the negative y-direction, and it is supposed that the top surface is required to remain horizontal, and thus all vertical displacements in joints 5 to 8 are to be the same amount. An approximate average value of these current vertical displacements under load is -8.00, and it is thus supposed that d_{5y}, d_{6y}, d_{7y}, and d_{8y} are all prescribed as -8.00. A set of four equations in twenty unknowns, based on Eqn. 3.11, gives a set of $\mathbf{e_o}$, labelled $(\mathbf{e_o})_1$ in Columns 3 and 4 of Table 3.3, which does result in the required displacements to maintain a horizontal top surface despite the applied load.

Table 3.3: Displacement and bar forces control of the structure in Figure 3.2 (MATLAB program can be found in Appendix A.2).

(*Displacements (shaded) and bar forces (unshaded) of the structure: with no e_o; with $(e_o)_1$ applied to adjust the controlled displacements shown in bold in Column 3; with $(e_o)_2$ applied to adjust the controlled displacements (Column 5) and bar forces (Column 6) shown in bold; with $(e_o)_3$ applied to adjust the controlled displacements (Column 7) and bar forces (Column 8) shown in bold, including t_9. Values exceeding prescribed limits are shown in bold*).

		(1)	(2)	(3)	(4)	(5)	(6)	(7)	(8)	
Jt	Dir.	no e_o		$(e_o)_1$		$(e_o)_2$		$(e_o)_3$		Bar
		d_p	t_p	d_p	t_p	d_p	t_p	d_p	t_p	
1	X	0	+1242		+1253		+1231		+1267	1
	Y	0	-240		-223		-302		-289	2
2	X	+11.38	-936	+4.84	-839	+4.93	-917	+4.87	-924	3
	Y	0	-701		-647		-661		-656	4
3	X	+7.40	-975	+3.08	-1112	+3.23	-1104	+3.18	-1065	5
	Y	-13.39	+658	-8.51	+643	-8.63	+573	-8.61	+549	6
4	x	+3.11	+1719	+1.93	**+1778**	+1.88	**+1500**	+1.81	**+1500**	7
	y	-11.87	-1046	-8.11	-1097	-8.14	-1372	-8.15	-1328	8
5	x	+9.93	-1380	+2.10	-1462	+2.07	**-1560**	+1.99	**-1500**	9
	y	**-1.75**	-621	**-8.00**	-556	**-8.00**	-484	**-8.00**	-501	10
6	x	+7.59	+147	+2.80	+258	+2.91	+428	+2.86	+370	11
	y	**-12.46**	+1589	**-8.00**	+1623	**-8.00**	**+1500**	**-8.00**	**+1500**	12
7	x	+4.14	-919	+2.01	-884	+2.08	-1053	+1.99	-1053	13
	y	**-16.00**	-1133	**-8.00**	-1045	**-8.00**	-1292	**-8.00**	-1308	14
8	x	+1.31	+998	+2.85	+1022	+3.11	+1151	+3.07	+1128	15
	y	**-2.30**	-1752	**-8.00**	**-1805**	**-8.00**	**-1500**	**-8.00**	**-1500**	16
			-618		-522		-503		-575	17
			+527		+430		+572		+599	18
			+477		+361		+534		+570	19
			-391		-387		-491		-491	20

It is now supposed that the bar forces are not to exceed 1500 in both tension and compression and thus bar forces t_7, t_{12}, and t_{16} need to be controlled with a new set of $\mathbf{e_o}$, while the control on the displacements is at the same time retained. Equation 3.19 is now employed as a system of seven equations in twenty elongation unknowns:

$$
\begin{bmatrix} \mathbf{Y}_{\text{[rows 7 9 11 13, all 20 columns]}} \\ \hline \mathbf{Z}_{\text{[rows 7 12 16, all 20 columns]}} \end{bmatrix} \mathbf{e_o} = \begin{bmatrix} -6.25 \\ +4.46 \\ +8.00 \\ -5.70 \\ \hline 219 \\ 89 \\ -252 \end{bmatrix} \tag{3.20}
$$

and through use of the pseudoinverse on the 7×20 compound matrix $[\ \mathbf{Y} \mid \mathbf{Z}\ ]^{\mathrm{T}}$, we get a second fully populated set of actuation, labelled $(\mathbf{e_o})_2$ in Table 3.3, $(\mathbf{e_o})_2$ = [-1.20 0.89 3.13 -6.35 0.30 -2.06 -2.40 4.06 3.07 1.95 -0.84 -2.05 -5.37 4.26 -3.71 1.66 1.10 -1.87 -1.82 0.98]. Table 3.3 shows that $(\mathbf{e_o})_2$ does enable all the required displacement Column 5 and bar force Column 6 controls to be simultaneously achieved, but $(\mathbf{e_o})_2$ has also caused bar 9 to now carry a force greater than the 1500 limit. Since length actuation does not merely *restrict* displacements and bar forces, but should be more accurately viewed as a redistribution of displacements and bar forces, we should be prepared for this eventuality that actuations actually can cause limits to be exceeded in some areas while we try to control some other areas.

In general, we will have prior knowledge of which specific displacements are to be critically controlled, and the remaining displacements will typically be free to take on any values within reason. Any increase of displacements in the uncontrolled joints is likely to cause no concern. On the other hand, all bars will have limits for both compression and tension regardless of whether they are in the set of controlled bar forces or not, and so it is likely that new violations in bar force limits are possible in hitherto uncontrolled bars as a result of some length actuation. The bar force control should thus be viewed as an iterative procedure where any limit-violation in one round of actuation then causes that bar to be included in the set of bar force for control in the next. In the current example, a new violation of t_9 has caused bar 9 to be added into the Eqn. 3.20 and a new 8×20 compound matrix then produces $(\mathbf{e_o})_3$ and a corresponding deflected shape which has the

required horizontal top surface as well as no bar carrying a force larger than 1500 in either tension or compression (see Columns 7 and 8 in Table 3.3).

3.2.4.2 *Controlling Displacement and Force with Minimal Actuation*

The eventual set of $(e_o)_3$ which allowed simultaneous displacements and bar force control had a sum of absolute actuations of 49.19. More pertinent is the fact that all twenty bars were involved in the actuation, and this could practically be a prohibitively high number. Every length actuation requires some electro-mechanical turnbuckle device embedded in the bar which can be remotely controlled and monitored, and this can be an expensive and difficult provision. Preferably, only some of the bars should be fitted with actuation capability, and ideally, only the most effective bars for this particular set of control parameters should be actuated, thus securing both the minimum number of actuators as well as minimum actuation. The process for this involves examination of the size of the coefficients in the 8×20 [$\mathbf{Y} \mid \mathbf{Z}$]^T compound matrix of Eqn. 3.19, which we know has at least one solution, *i.e.* $(e_o)_3$, but should also have the potential for many solutions involving only eight bars since there are only eight equations. Simple Gauss-Jordan row operations would produce viable solutions involving only eight non-zero coefficients in e_o. Additionally, an e_o with eight *minimal* non-zero coefficients would come by choosing columns [$\mathbf{Y} \mid \mathbf{Z}$]^T with large coefficients for the pivots. In the current work, Gauss-Jordan operations have been carried out with column exchanges on [$\mathbf{Y} \mid \mathbf{Z}$]^T to enable the largest coefficients to be selected as pivots, and the eventual pivotal columns therefore identify the best bars for actuation.

It should be noted that use of the Gauss-Jordan operations with column exchange does not immediately provide a completely satisfactory set of e_o. Only the prescribed parameters are part of the control set, and since Eqn. 3.19 knows nothing of the displacements and (especially) bar forces which are not in the control set, the resultant e_o can easily cause some of those bars to have bar force exceeding their limits. There are three approaches to this problem.

3.2.4.2.1 Increasing the Control Set

Given that one or more bars have now additionally exceeded their force limits, they could be appended into the set of controlled parameters and a new $\mathbf{e_o}$ be calculated with this larger control set, as seen in Section 3.2.4.1. However, this is not the method of choice because increasing the control set means also increasing the number of actuators. It may also be unnecessary to continually increase the number of actuators to increasingly restrain bar forces at their prescribed limit, because as new actuations are introduced, some bars which have previously exceeded their limit (and are now included in the control set) might have their bar forces drop once again below the limit, but are no longer able to do just that because they are in the control set and thus have their bar force non-negotiably set at the limit. The bar force controls concurrently prescribe both a maximum and a minimum on bar forces, and thus actuation might inadvertently be used to actually keep a bar force high, rather than low. Retaining these bar forces at the point of limit through actuations, rather than allowing them to drop, would be counter-productive. Nonetheless, increasing the control set may be a necessary approach in some instances, and we will return to this discussion.

3.2.4.2.2 Quadratic Programming

Bar forces can be artificially held high by actuations through injudicious selection of bars for actuation because the bar force limits in $\mathbf{Z}$ are set as equalities, whereas they should really be inequalities. The use of inequalities for $\mathbf{Z}$ means that bar forces are only controlled when they have to be controlled, and the control set can be increased or decreased from one iteration to the next. Therefore, the bar forces should ideally be restricted with inequalities, so that Eqn. 3.19 might be restated in the form of quadratic programming, *i.e.*

$$\min \sum_{i=1}^{b} \left(e_o \right)_i^2 \tag{3.21}$$

subject to

$$
\begin{aligned}
\mathbf{Y}\mathbf{e}_o &= \mathbf{d} - \mathbf{d}_P \\
\mathbf{Z}\mathbf{e}_o &\leq \mathbf{t}_P - \mathbf{t}
\end{aligned}
\tag{3.22}
$$

Although algorithms for quadratic programming are readily available, Eqn. 3.21 is interpreted as minimizing the norm of $\mathbf{e_o}$, rather than minimising the number of non-zero elements in $\mathbf{e_o}$, as well as their size. This crucial detail means that while quadratic programming allows "slack" in (a potentially larger set of) bar force control, the resultant $\mathbf{e_o}$ also tends to be fully populated, which is not much of an advantage over the $\mathbf{e_o}$ obtained with the pseudoinverse. Standard quadratic programming is thus of limited use for our purpose.

3.2.4.2.3 Reselection of Bars

The problem we still face is that by limiting the number of non-zero elements in $\mathbf{e_o}$, force redistribution could violate bar force limits in hitherto uncontrolled bars. However, there are potentially many other possible set of bars (with the same number of non-zero elements in $\mathbf{e_o}$) that could be chosen, albeit with larger norms in their $\mathbf{e_o}$. Among these other possible solutions with larger norms, there can be one or more which would not only satisfy the controlled parameters, but also *not* introduce new violations of bar force limits in the uncontrolled bars. Therefore, instead of dealing with a new violation of bar force by merely increasing the control set, or by using quadratic programming to allow inequalities in the bar force prescription, a simpler technique is to seek an alternative set of actuators which would not raise any uncontrolled bar force to beyond their limits. This can be effected by selecting columns in the compound matrix $[\ \mathbf{Y} \mid \mathbf{Z}\ ]^T$ in a different order, or selecting different columns. For example, a column relating to an uncontrolled bar force which has exceeded its bar force limit in the current iteration can be the first column to be selected in the next iteration, or alternatively, the second largest rather than the absolute largest coefficients can be selected as pivots.

Nonetheless, even though the first strategy is to look for a different set of actuators with the same number of bars, it is entirely possible that there is no solution to be found that satisfies all bar force and displacement limits without increasing the number of actuators. The displacement or bar force limits set could be too stringent to allow a solution with the current number of actuators. Where the search is proving unfruitful, then one of the bar forces (*e.g.* the one with the largest violation, or the one that most

consistently exceed the limit) should be added to the list of controlled bar force, and a solution with one more non-zero element in $\mathbf{e_o}$ be sought.

3.2.4.2.4 Illustrative Example in Minimising Non-Zero Elements in $\mathbf{e_o}$

The use of twenty actuators with $(\mathbf{e_o})_3$ in Table 3.3 produced the required displacements for the four top joints, and kept all bar forces within the limit of $\left|1500\right|$, and four bars are controlled.   There are thus eight controlled parameters, and eight equations in the compound matrix $[\ \mathbf{Y}\ |\ \mathbf{Z}\ ]^T$, and thus there should be a solution with only eight non-zero elements in $\mathbf{e_o}$. The Gauss-Jordan operation with column exchange to exploit the most effective pivots produces the actuation $(\mathbf{e_o})_4$ (Column 3 in Table 3.4) and the resultant displacements and bar forces as shown in Columns 1 and 2 of Table 3.4. Clearly, the required eight control parameters are satisfied, but two further bar force violations are now also found in bars 1 and 8.

Although the first strategy is to look for another eight bars (Section 3.2.4.2.3) which would satisfy all controlled displacements and produce no bar force violations, no solution with eight bars was found, and thus a further bar was added into the control list (Section 3.2.4.2.1). Only one further bar (Bar 1) was added to the controlled list even though two bar forces exceeded their limits, because it is entirely possible the new force redistribution can bring both bar forces to, or below, the limit. The Gauss-Jordan operation was carried out and a new set of actuation with nine non-zero elements $(\mathbf{e_o})_5$ and the resultant displacements and bar forces are shown in Columns 4 and 5 of Table 3.4, where it can be seen that there is now no bar force violation. Furthermore, the total actuation has also slightly decreased from 55.44 to 45.17, even though the total number of actuations has now gone up to nine.

Table 3.4: Displacements (shaded) and bar forces/elongation of the structure in Figure 3.2, with increasing number of actuations in $\mathbf{e_o}$. Values exceeding limit are shown in bold (MATLAB program is shown in Appendix A.2).

		(1)	(2)	(3)	(4)	(5)	(6)	(7)	(8)	(9)	
Jt	Dir	d_p	t_p	$(e_o)_4$	d_p	t_p	$(e_o)_5$	d_p	t_p	$(e_o)_6$	Bar
1	x	0	**+1985**	0	0	1500	0	0	+1500	0	1
	y	0	-594	0	0	-175	0	0	-139	0	2
2	x	+6.97	-391	0	8.12	-543	0	+1.81	-567	0.73	3
	y	0	-240	-7.40	0	-416	-6.96	0	-413	-6.97	4
3	x	+3.22	-1227	0	4.37	-1416	0	+3.97	-1424	0	5
	y	-11.46	+127	0	-7.34	409	-0.71	-7.49	+367	0	6
4	x	+4.96	+1500	-5.50	3.75	1500	-3.13	+3.75	1500	-3.53	7
	y	-6.52	**-1813**	+8.00	-7.56	-1171	-2.27	-7.65	-1192	+2.47	8
5	x	+2.84	-1500	+11.39	2.28	-1500	-3.34	+1.57	-1500	+3.43	9
	y	-8.00	-612	0	-8.00	-734	0	-8.00	-708	0	10
6	x	+1.87	+963	0	0.92	559	0	+0.88	+517	0	11
	y	-8.00	+1500	0	-8.00	1500	0	-8.00	+1500	-5.91	12
7	x	+9.51	-1053	-5.37	0.51	-1053	-5.38	+0.56	-1053	-5.37	13
	y	-8.00	-1124	0	-8.00	-1457	+12.75	-8.00	-1433	+12.26	14
8	x	+6.70	+1389	0	9.62	917	0	+9.24	+952	0	15
	y	-8.00	-1500	-2.15	-8.00	-1500	+5.03	-8.00	-1500	+0.53	16
			-1249	+11.91		-558	0		-551	0	17
			+337	0		283	0		+344	0	18
			+159	0		904	0		+850	0	19
			-491	3.73		-491	+5.61		-491	0	20
	total actuation →		55.44			45.17			41.20		

It should be pointed out that the proposed Gauss-Jordan technique with column exchanges, and gradual increase of control set is not guaranteed to produce the solution with absolute minimum actuation. This is because selection of the largest available pivots in sequence does not actually guarantee that the absolute best bars (in terms of minimum actuation) will be selected. Nonetheless, the technique will produce solutions which not only satisfy the design requirements, but are also near-minimal. By way of comparison, and exhaustive search was carried out examining the $_{20}C_9=167960$ solutions and the results for the solution for minimal actuation $(\mathbf{e_o})_6$ is shown in Table 3.4. It can be seen that the total actuation of 41.20 is only 9% smaller than the solution obtained by the Gauss-Jordan operations.

3.2.4.3 Control Where Actuator Locations Are Already Fixed

The discussion so far has focussed on the design stage, where it is supposed that the location of actuators is part of the design variables, and the quest is for the locations of those actuators, as well as the amount of actuation, for a given set of control parameters. Once the structure is assembled, and the actuators are in place, their location will remain fixed. Whether a pre-fixed set of actuators will be any good in achieving a given set of control parameters will depend on whether the columns of the compound matrix $\begin{bmatrix} \mathbf{Y} \mid \mathbf{Z} \end{bmatrix}^{\mathbf{T}}$ formed with only columns relating the bars with actuators.

3.2.5 Adjusting Assembly Imperfections

Throughout this thesis, the focus has been on adjusting the structural shape or the internal forces of a pin-jointed assembly due to load, but the techniques presented here are not confined to rectifying effects of load. Equations 3.10 and 3.16 (and therefore 3.19) have been derived for a loaded structure, but the form of the final equations specifically isolate the effects due to $\mathbf{e_o}$ from any other effects. Although these other effects so far have been explicitly due to load, there is no reason to restrict to any the effects to load, so Eqn. 3.19 (or 3.10 and 3.16) can be re-written as

$$\begin{bmatrix} \mathbf{Y} \\ \mathbf{Z} \end{bmatrix} \mathbf{e}_o = \begin{bmatrix} \mathbf{d}_n - \mathbf{d}_c \\ \mathbf{t}_c - \mathbf{t}_n \end{bmatrix}. \tag{3.23}$$

where $\mathbf{d}_c$ and $\mathbf{t}_c$ are the current displacements and bar forces (due to whatever cause) and $\mathbf{d}_n$ and $\mathbf{t}_n$ are the new resultant displacements and bar forces after the application of $\mathbf{e}_o$.

In this way, Eqn. 3.23 can be used to correct manufacture or assembly imperfection, or restore structural shape or internal force due to environmental effects (*e.g.* thermal distortion) or structural movements (*e.g.* foundation settlement, or the structure moving, as in a mobile support structure). The necessary information is simply the displacements and bars forces to be controlled (*i.e.* not all the displacements or forces) as they stand, and what values they should become.

3.2.6 *Comparison of Linear Shape Control Technique*

The present technique is now compared with results previously published by You (1997), Shen *et al.* (2006) as cited by Xu and Luo (2008) and Xu and Luo (2008) who worked on displacement control of a prestressed 9-cable network structure as shown in Figure 3.4, where all cables have axial stiffness of 43.16kN. The prestress of the structure (as given by You, 1997) is shown in Column 4 of Table 3.5, which is produced by changing the length of the cables vii, viii, ix by the amounts of -5.02mm, +4.49mm and -5.52mm respectively. The consequent displacements for these actuations are shown in Column 3. You (1997) set the target displacement for control as negation of the displacement of node 6, which has pre-adjustment displacements of $[2.56, -4.31]^T$, and this was to be changed to $[0, 0]^T$. Furthermore, the condition was also given that the internal force of the cables had to be kept above their initial values *i.e.* $\mathbf{t} \geq \mathbf{t_o}$.

The set of results are achieved via two alternative sets of actuator. The first set assumed that only the cables 5 to 9 are adjustable, while in the second set, all cables were allowed to participate in the adjustment process for achieving the required target.

Firstly, following You's original work in allowing only cables 5 to 9, the displacements and internal bar forces after adjustment from using the present method, are shown in Columns 8 and 9 of Table 3.5. The set of actuation calculated (Column 10) is slightly different to that given by You (Column 7) and Shen *et al.* (Column 11), and a

slightly smaller total actuation than both previous methods have also been achieved. All three methods attained the target of both eliminating displacements of node 6 (Columns 5 and 8) without any decrease in any of the cable forces.

Secondly, when Shen *et al.* (2006) studied this example, they also allowed all cables to be actuated, and the post-adjustment displacement and cable force results from the present method, are shown in Columns 12 and 13 of Table 3.5, which shows again that the target control was achieved. In actual fact, the present technique found the same set of actuation found by Shen *et al.* (2006) (Column 15) while Xu and Luo (2008) found a slightly different set of actuator (Column 16) which had a slightly smaller total actuation.
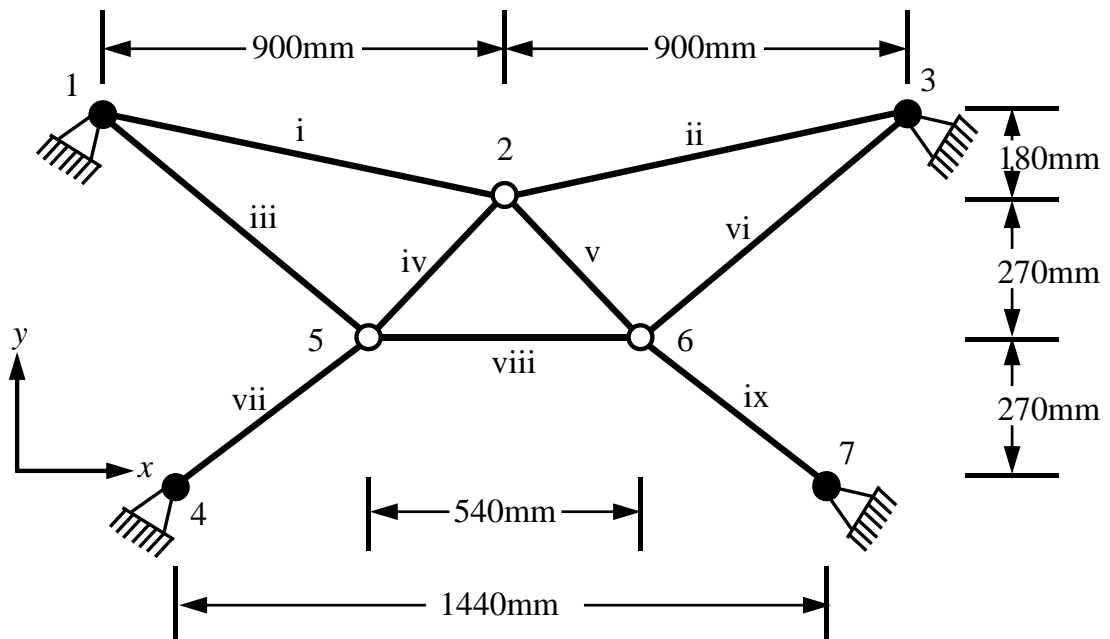
Figure 3.4: A plane cable net structure. Source: You (1997).

Table 3.5: Comparison the present technique of linear shape control with You, Shen and Xu techniques for linear shape control of cable net structure in Figure 3.4.

(1)	(2)	(3)	(4)	(5)	(6)	(7)	(8)	(9)	(10)	(11)	(12)	(13)	(14)	(15)	(16)	(17)
		Before shape adjustment		After shape adjustment (Theoretical)												
Joint	Dir	Theoretical		You *			Present study*			Shen*	Present study			Shen	Xu	Member
		d_o(mm)	t_o (N)	d(mm)	t(N)	e_o(mm)	d(mm)	t(N)	e_o(mm)	e_o(mm)	d(mm)	t(N)	e_o(mm)	e_o(mm)	e_o(mm)	
2	x	0.00	61.38	0.29	141.8	0.00	-0.02	117.48	0.00	0.00	-1.05	61.38	-1.72	-1.72	-2.56	1
	y	-6.66[+]	61.38	-0.60	115.0	0.00	-12.82	118.84	0.00	0.00	-3.13	61.38	0.34	0.34	0.00	2
5	x	-2.56[+]	23.55	-0.21	33.3	0.00	-5.22	23.55	0.00	0.00	-3.24	23.55	-1.38	-1.38	0.00	3
	y	-4.31	17.02	-8.50	17.0	0.00	-8.03	33.71	0.00	0.00	-2.90	17.02	1.24	1.24	0.02	4
6	x	2.56	17.02	0.00	54.1	-10.53	0.00	31.83	-9.33	-8.90	0.00	17.02	-1.62	-1.62	-2.44	5
	y	-4.31	23.55	0.00	23.5	-0.42	0.00	24.05	-0.43	-0.57	0.00	23.55	-0.42	-0.42	-0.63	6
			50.00		61.1	-4.67		72.94	-4.47	-4.83		50.00	0.14	0.14	-0.01	7
			50.00		67.5	0.00		57.87	0.00	0.00		50.00	-1.88	-1.88	-3.09	8
			50.00		101.1	3.79		70.91	4.16	4.30		50.00	4.41	4.41	4.21	9
		total actuation (mm)		19.41			18.39			18.60		13.15		13.15	12.96	

*These three solutions have assumed that only the cables no. 5-9 are adjustable.

+These numbers have been corrected due to a sign omission in the original.

3.3 Linear Condensed Matrix Controlling Equations

The preceding section has described shape adjustment for a structure made of simple elements. The examples given in Section 3.2 concern only pin-jointed trusses with bar elements, but the same equations and techniques apply also to other structures with elementary elements (*e.g.* rigidly jointed frames, or plated structures). Structures made up of more complicated structural components (*i.e.* those with "macro-elements", *e.g.* the pantographic element in Section 3.3.5 have their structural matrices built up from matrices of elementary elements, but the building also involves "matrix condensation" in the process. The governing equations for shape adjustment are thus re-derived in this section, for structures with macro-elements.

3.3.1 Matrix Condensation

Matrix condensation is a technique of reducing the size and simplification of the structural matrices (equilibrium, compatibility and flexibility matrices) in the force method equations of structural analysis by condensing out unloaded degrees of freedom (Pellegrino *et al.*, 1992). This condensation facility allows "macro-elements" to be built up from elementary elements, where the connectivity between the elementary elements form unloaded "internal joints" within the macro-elements which can then be "condensed out" (Kwan and Pellegrino, 1994). The system of equilibrium, compatibility and flexibility should be in the form of Figure 3.5.

$$m\left\{\begin{array}{c} \\ \\ \end{array}\right. p\left\{\begin{array}{c} \\ \\ \end{array}\right. \overbrace{\begin{bmatrix} \mathbf{A}_{mn} & \mathbf{A}_{mp} \\ \hline \mathbf{A}_{pn} & \mathbf{A}_{pp} \end{bmatrix}}^{n \quad p} \begin{bmatrix} \mathbf{t}_n \\ \hline \mathbf{t}_p \end{bmatrix} = \begin{bmatrix} \mathbf{p}_m \\ \hline \mathbf{p}_p=0 \end{bmatrix}$$

$$n\left\{\begin{array}{c} \\ \\ \end{array}\right. p\left\{\begin{array}{c} \\ \\ \end{array}\right. \overbrace{\begin{bmatrix} \mathbf{B}_{nm} & \mathbf{B}_{np} \\ \hline \mathbf{B}_{pm} & \mathbf{B}_{pp} \end{bmatrix}}^{m \quad p} \begin{bmatrix} \mathbf{d}_m \\ \hline \mathbf{d}_p \end{bmatrix} = \begin{bmatrix} \mathbf{e}_n \\ \hline \mathbf{e}_p \end{bmatrix}$$

$$n\left\{\begin{array}{c} \\ \\ \end{array}\right. p\left\{\begin{array}{c} \\ \\ \end{array}\right. \overbrace{\begin{bmatrix} \mathbf{F}_{nn} & \mathbf{F}_{np} \\ \hline \mathbf{F}_{pn} & \mathbf{F}_{pp} \end{bmatrix}}^{n \quad p} \begin{bmatrix} \mathbf{t}_n \\ \hline \mathbf{t}_p \end{bmatrix} = \begin{bmatrix} \mathbf{e}_n \\ \hline \mathbf{e}_p \end{bmatrix}$$

(a)   (b)   (c)

Figure 3.5: Partitioned forms of the systems of (a) equilibrium, (b) compatibility and (c) flexibility equations. Adapted from Pellegrino *et al.* (1992).

In the Force Method, the relation between the generalized internal bar force $\mathbf{t}$ and the generalized external nodal load $\mathbf{p}$ is the equilibrium matrix $\mathbf{A}$ as shown in linear equilibrium equation Eqn. 3.1. In addition, the generalized internal bar elongation $\mathbf{e}$ due to $\mathbf{t}$ are related to the generalized external nodal displacements $\mathbf{d}$ (due to $\mathbf{p}$) by compatibility matrix $\mathbf{B}$, because of the linear equations of compatibility as presented in Eqn. 3.2. Lastly, the flexibility relationships involving the flexibility matrix $\mathbf{F}$ are as given in Eqn. 3.3.

For an i-dimensional structural assembly with b bar and j joints, it is likely that some of the nodal forces are always equal to zero. The equilibrium equations relating to these zero load components can be condensed out from immediate consideration, and similarly the corresponding displacement components and compatibility equations can also be condensed out as well, thus leaving a smaller set of equations. Similarly, when "macro-elements" are built up from elementary elements, the unloaded "internal" joints within the macro-elements present equations for condensation. Consider $(m + p)$-dimensional vectors of external joint load $\mathbf{p}$ and displacement $\mathbf{d}$, and $(n + p)$-dimensional vectors of internal bar force $\mathbf{t}$ and bar elongation $\mathbf{e}$, where the load vector $\mathbf{p}$ is partitioned into the two sub-vectors $\mathbf{p_m}$ with m non-zero components and the remaining $\mathbf{p_p}$ with p zero components. Similarly, the vector of displacements $\mathbf{d}$ can also be partitioned into $\mathbf{d_m}$ and $\mathbf{d_p}$ sub-vectors where $\mathbf{d_m}$ and $\mathbf{d_p}$ correspond directly to $\mathbf{p_m}$ and $\mathbf{p_p}$ respectively, as shown in Figures 3.5a and 3.5b.

The equilibrium matrix can be re-arranged with simple row-exchange so that the equations corresponding to zero loads appear in the lower p equations, and hence $\mathbf{p_m}$ and $\mathbf{p_p}$ contain only (non-zero) and (zero) load components respectively. Partitioning can then be carried on the equilibrium matrix as shown in Figure 3.5a. Due to the correspondence between components of load and displacement, the compatibility matrix can also be re-arranged in a similar way with column-exchanges corresponding exactly to the row-exchanges of the equilibrium matrix. In this way, the $\mathbf{B_{nm}}$ sub-matrix in Figure 3.5b is still the transpose of the equilibrium sub-matrix $\mathbf{A_{mn}}$ in Figure 3.5a. Furthermore, the same row- and column exchanges must also be carried out in the flexibility matrix so that the $\mathbf{t_n}$, $\mathbf{e_n}$, *etc.* in Figure 3.5c correspond to the internal forces and displacements in the equilibrium and compatibility relationships in Figures 3.5a and 3.5b.

The reduced matrices can be obtained from the following process (Pellegrino *et al.*, 1992). Firstly, the system of equilibrium equations after reduction of the equilibrium matrix by condensing out *p* rows with corresponding *p* load components is:

$$\mathbf{A}^* \mathbf{t}^* = \mathbf{p}^*. \tag{3.24}$$

where $\mathbf{A}^*$ is the reduced equilibrium matrix which relates the *m* non-vanishing (non-zero) load components to *n* (almost) arbitrary chosen condensed generalized internal bar forces. Since the lower *p* equation of $\mathbf{A}$ are homogeneous, $\mathbf{A_{pn}}\ \mathbf{t_n}\ +\ \mathbf{A_{pp}}\ \mathbf{t_p}\ =\ \mathbf{0}$, *i.e.* $\mathbf{t_p} = \mathbf{-A_{pp}^{-1}A_{pn}}\ \mathbf{t_n}$, which can be used as substitution for $\mathbf{t_p}$ in $\mathbf{A_{mn}}\ \mathbf{t_n} - \mathbf{A_{mp}}\ \mathbf{t_p} = \mathbf{p_m}$, to give $\mathbf{A_{mn}}\ \mathbf{t_n} - \mathbf{A_{mp}}\ \mathbf{A_{pp}^{-1}}\ \mathbf{A_{pn}}\ \mathbf{t_n} = \mathbf{p_m}$, *i.e.* $(\mathbf{A_{mn}} - \mathbf{A_{mp}}\ \mathbf{A_{pp}^{-1}}\ \mathbf{A_{pn}})\ \mathbf{t_n} = \mathbf{p_m}$ and hence

$$\mathbf{A}^* = \mathbf{A_{mn}} - \mathbf{A_{mp}}\ \mathbf{A_{pp}^{-1}}\ \mathbf{A_{pn}} \tag{3.25}$$

$\mathbf{t}^*$ is the generalized internal bar forces and is equal to $\mathbf{t_n}$, and

$\mathbf{p}^*$ is the generalized external (non-zero) load and equal to $\mathbf{p_m}$.

The size of reduced equilibrium matrix $\mathbf{A}^*$ is *m* by *n*.

Secondly, the system of compatibility equations "mirrors" the reduction in equilibrium equations, by condensing out *p* columns corresponding to the *p* displacements components and *p* rows corresponding to *p* generalized internal bar elongation, resulting in:

$$\mathbf{B}^* \mathbf{d}^* = \mathbf{e}^*. \tag{3.26}$$

where $\mathbf{d}^*$ is the generalized external nodal displacement (and equal to $\mathbf{d_m}$) and $\mathbf{B}^*$ is the reduced compatibility matrix relating the *m* joint displacements (corresponding to the *m* non-zero load components) to the *n* chosen condensed generalized internal bar elongation (corresponding to the chosen generalized internal bar force):

$$\mathbf{B}^* = \mathbf{A_{mn}^T} - \mathbf{A_{pn}^T}\ (\mathbf{A_{pp}^T})^{-1}\ \mathbf{A_{mp}^T} \tag{3.27}$$

The matrix $\mathbf{B}^*$ thus has size *n* by *m*. From Eqns. 3.25 and 3.27

$$\mathbf{B}^* = (\mathbf{A}^*)^\mathbf{T} \tag{3.28}$$

The vector $\mathbf{e}^*$ is the condensed generalized internal bar elongation corresponding to the chosen generalized internal bar force

$$\mathbf{e}^* = \mathbf{e_n} - \mathbf{A_{pn}^T} \, (\mathbf{A_{pp}^T})^{-1} \, \mathbf{e_p}.$$

(3.29)

where $\mathbf{e_p}$ is the generalized internal bar elongation corresponding to the generalized internal bar force $\mathbf{t_p}$.

$$\mathbf{t_p} = - (\mathbf{A_{pp}})^{-1} \, \mathbf{A_{pn}} \, \mathbf{t_n}.$$

(3.30)

Substituting Eqn. 3.27 into Eqn. 3.26 yields:

$$\mathbf{B}^* \mathbf{d_m} = \mathbf{e}^*.$$

(3.31)

Pellegrino *et al.* (1992) also found the components of external displacement $\mathbf{d_p}$, which are the displacements corresponding to the zero load components $\mathbf{p_p}$ (=**0**):

$$\mathbf{d_p} = (\mathbf{A_{pp}^T})^{-1} \mathbf{e_p} - \left(\mathbf{A_{pp}^T}\right)^{-1} \mathbf{A_{mp}^T} \mathbf{d_m}.$$

(3.32)

Finally, the condensed system of flexibility equations is

$$\mathbf{F}^* \mathbf{t}^* = \mathbf{e}^*$$

(3.33)

where $\mathbf{F}^*$ the reduced flexibility matrix is given by

$$\mathbf{F}^* = \mathbf{F_{nn}} - \mathbf{F_{np}} \, \mathbf{A_{pp}^{-1}} \, \mathbf{A_{pn}} - \mathbf{A_{pn}^T} \left(\mathbf{A_{pp}^T}\right)^{-1} \mathbf{F_{pn}} + \mathbf{A_{pn}^T} \left(\mathbf{A_{pp}^T}\right)^{-1} \mathbf{F_{pp}} \, \mathbf{A_{pp}^{-1}} \, \mathbf{A_{pn}}$$

(3.34)

and $\mathbf{t}^*$ is the internal bar forces (and equal to $\mathbf{t_n}$).

Moreover $\mathbf{e_n}$ and $\mathbf{e_p}$ can be calculated separately through the following equations respectively:

$$\mathbf{e_n} = \left(\mathbf{F_{nn}} - \mathbf{F_{np}} \, \mathbf{A_{pp}^{-1}} \, \mathbf{A_{pn}} \right)\mathbf{t_n},$$

(3.35)

$$\mathbf{e_p} = \left(\mathbf{F_{pn}} - \mathbf{F_{pp}} \, \mathbf{A_{pp}^{-1}} \, \mathbf{A_{pn}} \right)\mathbf{t_n}.$$

(3.36)

As discussed in Section 3.2.1, the general solution of the reduced internal bar force $\mathbf{t_n}$ in the condensed equilibrium equations is the summation of a particular solution

(which is a set of bar forces in equilibrium with the load, but not necessarily satisfying compatibility) and the complementary homogeneous solution. The particular solution is *any* vector $\mathbf{t_n}$ that satisfies Eqn. 3.24, and one such vector is $\mathbf{t_{nH}}$ obtained from

$\mathbf{t_{nH}} = \left(\mathbf{A}^*\right)^+ \mathbf{p_m}$ where $\left(\mathbf{A}^*\right)^+$ is the pseudo-inverse of reduced equilibrium matrix.

The complementary homogenous solution is the set of reduced bar forces solutions that satisfies $\mathbf{A}^* \mathbf{t_n} = \mathbf{0}$, *i.e.* the set of non-vanishing bar forces in equilibrium with zero external load. This is readily calculated by the nullspace $(\mathbf{A}^*) = \mathbf{S}^*$, and $\mathbf{s}^*$ is the condensed states of self-stress. The number of such condensed states of self-stress depends on the statical redundancy s^* of the indeterminate structure (*note:* the determinate structure there has no states of self-stress). The expression of $\mathbf{S}^* \boldsymbol{\alpha}^*$ is thus the complementary homogeneous solution, where $\boldsymbol{\alpha}^*$ is a vector of s^* coefficients reflecting a set of combinatorial constants (that has to be determined through satisfaction of compatibility). The total general solution for condensed equilibrium equation is thus combining a particular solution and the complementary solution, consequently

$$\mathbf{t_n} = \mathbf{t_{nH}} + \mathbf{S}^* \boldsymbol{\alpha}^*, \tag{3.37}$$

A structure can in general have lack of fit due to initial construction imperfection, or temperature change, or, as in our purpose, deliberate extensional changes to control the displacement or/and internal bar force of the structure. A bar can have axial force due to external load or any of these other "lack of fit" effects. Therefore, the total elongation of the bar is made up of two parts, one part due to axial force of the bar, *i.e.* $\mathbf{F}^* \mathbf{t_n}$, while the other part $\mathbf{e}_0^*$ comes from lack of fit (or which can be deliberately introduced to adjust the structure's shape or force distribution):

$$\mathbf{e}^* = \mathbf{e}_0^* + \mathbf{F}^* \mathbf{t_n}, \tag{3.38}$$

In the current context, $\mathbf{e}_0^*$, is principally the vector of elongation actuation introduced to each bar for the purpose of adjustment.

In the same fashion as Eqn. 3.38, Eqns. 3.35 and 3.36 can be re-written to include the lack of fit, and they thus take the following form:

$$\mathbf{e_n} = \mathbf{e_{no}} + \left(\mathbf{F_{nn}} - \mathbf{F_{np}} \, \mathbf{A_{pp}^{-1}} \, \mathbf{A_{pn}} \right) \mathbf{t_n} \text{, and} \tag{3.39}$$

$$\mathbf{e_p} = \mathbf{e_{po}} + \left(\mathbf{F_{pn}} - \mathbf{F_{pp}} \, \mathbf{A_{pp}^{-1}} \, \mathbf{A_{pn}} \right) \mathbf{t_n} \text{,} \tag{3.40}$$

i.e. the total condensed elongation in each condensed bar is the sum of actuation of the condensed bar, and the elongation of the same bar due to axial force. Substitution of Eqn. 3.37 into Eqn. 3.38 thus gives

$$\mathbf{e}^* = \mathbf{e_o^*} + \mathbf{F}^* \, (\mathbf{t_{nH}} + \mathbf{S}^* \, \boldsymbol{\alpha}^*) \text{.} \tag{3.41}$$

Compatibility for the set of condensed bar elongations can be assured by it being found in the set of compatible elongations, *i.e.* in columnspace($\mathbf{B}^*$), whereas left-nullspace($\mathbf{B}^*$) contains the basis for all the incompatible condensed bar elongations. Subsequently, the compatibility condition can be imposed by stating that the condensed bar elongations $\mathbf{e}^*$ must be orthogonal to the left-nullspace($\mathbf{B}^*$) (*i.e.* by stating that the elongations cannot have any component among the incompatible elongations as found in the left-nullspace). By virtue of $(\mathbf{B}^*)^{\mathbf{T}} = \mathbf{A}^*$, left-nullspace($\mathbf{B}^*$) = nullspace($\mathbf{A}^*$), and since nullspace($\mathbf{A}^*$) are the states of selfstress, then the compatibility condition is thus that the states of selfstress must be orthogonal to the elongations, *i.e.* $\left(\mathbf{S}^* \right)^{\mathbf{T}} \mathbf{e}^* = \mathbf{0}$, and

$$\mathbf{S^{*T}e_o^*} + \mathbf{S^{*T}} \mathbf{F}^* \, (\mathbf{t_{nH}} + \mathbf{S}^* \, \boldsymbol{\alpha}^*) = 0 \tag{3.42}$$

and thus

$$-\boldsymbol{\alpha}^* = \left(\mathbf{S^{*T}} \mathbf{F}^* \mathbf{S}^* \right)^{-1} [\mathbf{S^{*T}e_o^*} + \mathbf{S^{*T}} \mathbf{F}^* \mathbf{t_{nH}}] \text{.} \tag{3.43}$$

Through back-substitution with $\boldsymbol{\alpha}^*$, we can thus find the structural vectors of $\mathbf{e}^*$ (Eqn.3.41), $\mathbf{t_n}$ (Eqn.3.37) and $\mathbf{d_m}$ (Eqn.3.31).

3.3.2 Displacement Control without Regard to Bar Forces

In Section 3.3.1, structural analysis was presented utilizing a matrix reduction technique, for structures prestressed with an initial $\mathbf{e_o}$. This reduced matrix technique in the Force Method can now be applied to the process of controlling (imperfect) structural shape as was carried out for the non-condensed matrices in Section 3.2.2. We shall initially be concerned with only displacement control without any concern of associated internal force change in the structure.

For controlling displacements $\mathbf{d_m}$ which are not associated with zero loads, we start with substituting Eqn. 3.43 into Eqn. 3.41 to give

$$\mathbf{e}^* = \mathbf{e}_o^* + \mathbf{F}^* \left(\mathbf{t_{nH}} - \mathbf{S}^* \left(\mathbf{S}^{*T} \mathbf{F}^* \mathbf{S}^* \right)^{-1} [\mathbf{S}^{*T} \mathbf{e}_o^* + \mathbf{S}^{*T} \mathbf{F}^* \mathbf{t_{nH}}] \right). \tag{3.44}$$

and also by substituting Eqn. 3.44 into Eqn. 3.31. to give

$$\mathbf{d_m} = \mathbf{B}^{*+} \left[\mathbf{e}_o^* + \mathbf{F}^* \left(\mathbf{t_{nH}} - \mathbf{S}^* \left(\mathbf{S}^{*T} \mathbf{F}^* \mathbf{S}^* \right)^{-1} [\mathbf{S}^{*T} \mathbf{e}_o^* + \mathbf{S}^{*T} \mathbf{F}^* \mathbf{t_{nH}}] \right) \right], \tag{3.45}$$

Equation 3.29 showed that $\mathbf{e}^* = \mathbf{e_n} - \mathbf{A_{pn}^T} (\mathbf{A_{pp}^T})^{-1} \mathbf{e_p}$ and hence, similarly,

$$\mathbf{e}_o^* = \mathbf{e_{no}} - \mathbf{A_{pn}^T} (\mathbf{A_{pp}^T})^{-1} \mathbf{e_{po}}. \tag{3.46}$$

where $\mathbf{e}_o^*$ is the condensed generalized internal bar actuation of bar force. Substitution of Eqn. 3.46 into Eqn. 3.45 gives

$$\mathbf{d_m} = \mathbf{B}^{*+} \left[(\mathbf{e_{no}} - \mathbf{A_{pn}^T} (\mathbf{A_{pp}^T})^{-1} \mathbf{e_{po}}) + \mathbf{F}^* \left(\mathbf{t_{nH}} - \mathbf{S}^* \left(\mathbf{S}^{*T} \mathbf{F}^* \mathbf{S}^* \right)^{-1} [\mathbf{S}^{*T}(\mathbf{e_{no}} - \mathbf{A_{pn}^T} (\mathbf{A_{pp}^T})^{-1} \mathbf{e_{po}}) + \mathbf{S}^{*T} \mathbf{F}^* \mathbf{t_{nH}}] \right) \right]$$

and

$$\mathbf{d_m} = \mathbf{B}^{*+} \mathbf{F}^* \left[\left(\mathbf{t_{nH}} - \mathbf{S}^* \left(\mathbf{S}^{*T} \mathbf{F}^* \mathbf{S}^* \right)^{-1} \mathbf{S}^{*T} \mathbf{F}^* \mathbf{t_{nH}} \right) \right] + \mathbf{B}^{*+} \mathbf{e_{no}} - \mathbf{B}^{*+} \mathbf{F}^* \mathbf{S}^* \left(\mathbf{S}^{*T} \mathbf{F}^* \mathbf{S}^* \right)^{-1} \mathbf{S}^{*T} \mathbf{e_{no}}$$
$$- \mathbf{B}^{*+} \mathbf{A_{pn}^T} (\mathbf{A_{pp}^T})^{-1} \mathbf{e_{po}} + \mathbf{B}^{*+} \mathbf{F}^* \mathbf{S}^* \left(\mathbf{S}^{*T} \mathbf{F}^* \mathbf{S}^* \right)^{-1} \mathbf{S}^{*T} \mathbf{A_{pn}^T} (\mathbf{A_{pp}^T})^{-1} \mathbf{e_{po}}) \tag{3.47}$$

$$\mathbf{d_m} = \left[\mathbf{B}^{*+} \mathbf{F}^* - \mathbf{B}^{*+} \mathbf{F}^* \mathbf{S}^* \left(\mathbf{S}^{*T} \mathbf{F}^* \mathbf{S}^* \right)^{-1} \mathbf{S}^{*T} \mathbf{F}^* \right] \mathbf{t_{nH}}$$
$$+ \left[\mathbf{B}^{*+} - \mathbf{B}^{*+} \mathbf{F}^* \mathbf{S}^* \left(\mathbf{S}^{*T} \mathbf{F}^* \mathbf{S}^* \right)^{-1} \mathbf{S}^{*T} \right] \mathbf{e_{no}}$$
$$- \left[\mathbf{B}^{*+} \mathbf{A_{pn}^T} (\mathbf{A_{pp}^T})^{-1} - \mathbf{B}^{*+} \mathbf{F}^* \mathbf{S}^* \left(\mathbf{S}^{*T} \mathbf{F}^* \mathbf{S}^* \right)^{-1} \mathbf{S}^{*T} \mathbf{A_{pn}^T} (\mathbf{A_{pp}^T})^{-1} \right] \mathbf{e_{po}}$$

Equation 3.48 can be written in the simpler form

$$\mathbf{d_m} = \mathbf{C_1} \mathbf{t_{nH}} + \mathbf{C_2} \mathbf{e_{no}} + \mathbf{C_3} \mathbf{e_{po}}. \tag{3.48}$$

where

$$\mathbf{C_1} = \mathbf{C} \mathbf{F}^*$$

$$\mathbf{C_2} = \mathbf{C}$$

$$\mathbf{C_3} = \mathbf{C} \mathbf{r}$$

$$\mathbf{C} = (\mathbf{B}^{*+} - \mathbf{B}^{*+} \mathbf{F}^* \mathbf{S}^* \left(\mathbf{S}^{*T} \mathbf{F}^* \mathbf{S}^* \right)^{-1} \mathbf{S}^{*T})$$

$$\mathbf{r} = -\mathbf{A}_{pn}^{T} \ (\mathbf{A}_{pp}^{T})^{-1}$$

To calculate $\mathbf{d}_p$, we substitute Eqns. 3.40 and 3.48 into Eqn. 3.32 to give

$$\mathbf{d}_p = (\mathbf{A}_{pp}^{T})^{-1}\left[\mathbf{e}_{po} + \left(\mathbf{F}_{pn} - \mathbf{F}_{pp} \ \mathbf{A}_{pp}^{-1} \mathbf{A}_{pn}\right)\mathbf{t}_n\right] - \left(\mathbf{A}_{pp}^{T}\right)^{-1}\mathbf{A}_{mp}^{T}\left[\mathbf{C}_1 \mathbf{t}_{nH} + \mathbf{C}_2 \ \mathbf{e}_{no} + \mathbf{C}_3 \ \mathbf{e}_{po}\right], \quad (3.49)$$

For ease of presentation, we adapt $\mathbf{v} = \mathbf{F}_{pn} - \mathbf{F}_{pp} \ \mathbf{A}_{pp}^{-1} \mathbf{A}_{pn}$ and then substitute Eqn. 3.37 and 3.43 into 3.49 to give

$$\mathbf{d}_p = (\mathbf{A}_{pp}^{T})^{-1}\left[\mathbf{e}_{po} + \mathbf{v}\left\{\mathbf{t}_{nH} - \mathbf{S}^* \left(\mathbf{S}^{*T} \mathbf{F}^* \mathbf{S}^*\right)^{-1} [\mathbf{S}^{*T}\mathbf{e}_o^* + \mathbf{S}^{*T} \mathbf{F}^* \mathbf{t}_{nH}]\right\}\right] \\ - \left(\mathbf{A}_{pp}^{T}\right)^{-1} \mathbf{A}_{mp}^{T}\left[\mathbf{C}_1 \ \mathbf{t}_{nH} + \mathbf{C}_2 \ \mathbf{e}_{no} + \mathbf{C}_3 \ \mathbf{e}_{po}\right], \tag{3.50}$$

Substituting Eqn. 3.46 into Eqn. 3.50, we obtain the condensed displacements $\mathbf{d}_p$, which are the displacements corresponding to the zero load components $\mathbf{p}_p$ (=0) as

$$\mathbf{d}_p = (\mathbf{A}_{pp}^{T})^{-1}\left[\mathbf{e}_{po} + \mathbf{v}\left\{\mathbf{t}_{nH} - \mathbf{S}^* \left(\mathbf{S}^{*T} \mathbf{F}^* \mathbf{S}^*\right)^{-1} [\mathbf{S}^{*T}\left(\mathbf{e}_{no} - \mathbf{A}_{pn}^{T} \ (\mathbf{A}_{pp}^{T})^{-1}\mathbf{e}_{po}\right) + \mathbf{S}^{*T} \mathbf{F}^* \mathbf{t}_{nH}]\right\}\right] \\ - \left(\mathbf{A}_{pp}^{T}\right)^{-1} \mathbf{A}_{mp}^{T}\left[\mathbf{C}_1 \ \mathbf{t}_{nH} + \mathbf{C}_2 \ \mathbf{e}_{no} + \mathbf{C}_3 \ \mathbf{e}_{po}\right], \tag{3.51}$$

$$\mathbf{d}_p = (\mathbf{A}_{pp}^{T})^{-1}\left[\mathbf{e}_{po} + \mathbf{v}\left\{\mathbf{t}_{nH} - \mathbf{S}^* \left(\mathbf{S}^{*T} \mathbf{F}^* \mathbf{S}^*\right)^{-1} [\mathbf{S}^{*T}\left(\mathbf{e}_{no} + \mathbf{r}\,\mathbf{e}_{po}\right) + \mathbf{S}^{*T} \mathbf{F}^* \mathbf{t}_{nH}]\right\}\right] \\ - \left(\mathbf{A}_{pp}^{T}\right)^{-1} \mathbf{A}_{mp}^{T}\left[\mathbf{C}_1 \ \mathbf{t}_{nH} + \mathbf{C}_2 \ \mathbf{e}_{no} + \mathbf{C}_3 \ \mathbf{e}_{po}\right], \tag{3.52}$$

$$\mathbf{d}_p = (\mathbf{A}_{pp}^{T})^{-1}\mathbf{v}\left(\mathbf{t}_{nH} - \mathbf{S}^* \left(\mathbf{S}^{*T} \mathbf{F}^* \mathbf{S}^*\right)^{-1} \mathbf{S}^{*T}\left(\mathbf{e}_{no} + \mathbf{r}\,\mathbf{e}_{po}\right) - \mathbf{S}^* \left(\mathbf{S}^{*T} \mathbf{F}^* \mathbf{S}^*\right)^{-1} \mathbf{S}^{*T} \mathbf{F}^* \mathbf{t}_{nH}\right) \\ + (\mathbf{A}_{pp}^{T})^{-1}\mathbf{e}_{po} - \left(\mathbf{A}_{pp}^{T}\right)^{-1} \mathbf{A}_{mp}^{T}\left(\mathbf{C}\mathbf{F}^* \mathbf{t}_{nH} + \mathbf{C}\mathbf{e}_{no} + \mathbf{C}\mathbf{r}\,\mathbf{e}_{po}\right)$$

$$\mathbf{d}_p = \left[\left(\mathbf{A}_{pp}^{T}\right)^{-1} \mathbf{v} - \left(\mathbf{A}_{pp}^{T}\right)^{-1} \mathbf{v} \ \mathbf{S}^* \left(\mathbf{S}^{*T} \mathbf{F}^* \mathbf{S}^*\right)^{-1} \mathbf{S}^{*T} \mathbf{F}^*\right]\mathbf{t}_{nH} - (\mathbf{A}_{pp}^{T})^{-1}\mathbf{v}\mathbf{S}^* \left(\mathbf{S}^{*T} \mathbf{F}^* \mathbf{S}^*\right)^{-1} \mathbf{S}^{*T}\left(\mathbf{e}_{no} + \mathbf{r}\,\mathbf{e}_{po}\right) \\ + (\mathbf{A}_{pp}^{T})^{-1}\mathbf{e}_{po} - \left(\mathbf{A}_{pp}^{T}\right)^{-1} \mathbf{A}_{mp}^{T}\left(\mathbf{C}\mathbf{F}^* \mathbf{t}_{nH} + \mathbf{C}\mathbf{e}_{no} + \mathbf{C}\mathbf{r}\,\mathbf{e}_{po}\right)$$

$$\mathbf{d}_p = \left[\left(\mathbf{A}_{pp}^{T}\right)^{-1} \mathbf{v} - \left(\mathbf{A}_{pp}^{T}\right)^{-1} \mathbf{v} \ \mathbf{S}^* \left(\mathbf{S}^{*T} \mathbf{F}^* \mathbf{S}^*\right)^{-1} \mathbf{S}^{*T} \mathbf{F}^*\right]\mathbf{t}_{nH} \\ - (\mathbf{A}_{pp}^{T})^{-1}\mathbf{v}\mathbf{S}^* \left(\mathbf{S}^{*T} \mathbf{F}^* \mathbf{S}^*\right)^{-1} \mathbf{S}^{*T} \mathbf{e}_{no} - (\mathbf{A}_{pp}^{T})^{-1}\mathbf{v}\mathbf{S}^* \left(\mathbf{S}^{*T} \mathbf{F}^* \mathbf{S}^*\right)^{-1} \mathbf{S}^{*T} \mathbf{r}\,\mathbf{e}_{po} \\ + (\mathbf{A}_{pp}^{T})^{-1}\mathbf{e}_{po} - \left(\mathbf{A}_{pp}^{T}\right)^{-1} \mathbf{A}_{mp}^{T} \mathbf{C}\mathbf{F}^* \mathbf{t}_{nH} - \left(\mathbf{A}_{pp}^{T}\right)^{-1} \mathbf{A}_{mp}^{T} \ \mathbf{C}\mathbf{e}_{no} - \left(\mathbf{A}_{pp}^{T}\right)^{-1} \mathbf{A}_{mp}^{T} \mathbf{C}\mathbf{r}\,\mathbf{e}_{po}$$

$$\mathbf{d_p} = \left[\left(\mathbf{A_{pp}^T}\right)^{-1}\mathbf{v} - \left(\mathbf{A_{pp}^T}\right)^{-1}\mathbf{v}\,\mathbf{S^*}\left(\mathbf{S^{*T}}\,\mathbf{F^*}\,\mathbf{S^*}\right)^{-1}\mathbf{S^{*T}}\,\mathbf{F^*} - \left(\mathbf{A_{pp}^T}\right)^{-1}\mathbf{A_{mp}^T}\,\mathbf{CF^*}\right]\mathbf{t_{nH}}$$
$$- \left[(\mathbf{A_{pp}^T})^{-1}\mathbf{vS^*}\left(\mathbf{S^{*T}}\,\mathbf{F^*}\,\mathbf{S^*}\right)^{-1}\mathbf{S^{*T}} + \left(\mathbf{A_{pp}^T}\right)^{-1}\mathbf{A_{mp}^T}\,\mathbf{C}\right]\mathbf{e_{no}}$$
$$- \left[(\mathbf{A_{pp}^T})^{-1}\mathbf{vS^*}\left(\mathbf{S^{*T}}\,\mathbf{F^*}\,\mathbf{S^*}\right)^{-1}\mathbf{S^{*T}}\,\mathbf{r} - (\mathbf{A_{pp}^T})^{-1} + \left(\mathbf{A_{pp}^T}\right)^{-1}\mathbf{A_{mp}^T}\,\mathbf{Cr}\right]\mathbf{e_{po}}$$

Which can be presented in a simplified form as

$$\mathbf{d_p} = \mathbf{Q_1}\,\mathbf{t_{nH}} + \mathbf{Q_2}\,\mathbf{e_{no}} + \mathbf{Q_3}\,\mathbf{e_{po}}, \tag{3.53}$$

where

$$\mathbf{Q_1} = \left[\left(\mathbf{A_{pp}^T}\right)^{-1}\mathbf{v} - \left(\mathbf{A_{pp}^T}\right)^{-1}\mathbf{v}\,\mathbf{k}\,\mathbf{F^*} - \left(\mathbf{A_{pp}^T}\right)^{-1}\mathbf{A_{mp}^T}\,\mathbf{CF^*}\right]$$

$$\mathbf{Q_2} = -\left[(\mathbf{A_{pp}^T})^{-1}\mathbf{vk} + \left(\mathbf{A_{pp}^T}\right)^{-1}\mathbf{A_{mp}^T}\,\mathbf{C}\right]$$

$$\mathbf{Q_3} = -\left[(\mathbf{A_{pp}^T})^{-1}\mathbf{vk}\,\mathbf{r} - (\mathbf{A_{pp}^T})^{-1} + \left(\mathbf{A_{pp}^T}\right)^{-1}\mathbf{A_{mp}^T}\,\mathbf{Cr}\right]$$

$$\mathbf{Q} = \mathbf{S^*}\left(\mathbf{S^{*T}}\,\mathbf{F^*}\,\mathbf{S^*}\right)^{-1}\mathbf{S^{*T}}$$

$$\mathbf{v} = \mathbf{F_{pn}} - \mathbf{F_{pp}}\left(\mathbf{A_{pp}}\right)^{-1}\mathbf{A_{pn}}$$

Equations 3.48 and 3.53 provide the non-vanishing and vanishing displacements of the structure respectively, without regard to each other through using the condensed matrix method, due to $\mathbf{t_{nH}}$ and the actuation $\mathbf{e_{no}}$ and $\mathbf{e_{po}}$. Both equations have a great role in calculating displacement of a morphing structure through adjusting bar actuation (rotation), especially Eqn. 3.48 which can be used to provide displacement of non-vanishing displacements of a pantographic morphing aerofoil structure since in the morphing aerofoil structure, only the outer face shape of the aerofoil is significant.

Combining together Eqns. 3.48 and 3.53, we get:

$$\mathbf{d_c} = \mathbf{d_{pc}} + \mathbf{Y_c}\,\mathbf{e_{oc}}. \tag{3.54}$$

where

$\mathbf{d_{pc}} = [\mathbf{C_1}\ \mathbf{Q_1}]^T\,\mathbf{t_{nH}}$ is the vector of nodal displacements of the structure due only to non-vanishing load component.

$$\mathbf{Y_c} = \begin{bmatrix} \mathbf{Y_n} & \mathbf{Y_p} \end{bmatrix}$$

$$\mathbf{Y_n} = [\mathbf{C_2} \ \mathbf{Q_2}]^{\mathbf{T}}$$

$$\mathbf{Y_p} = [\mathbf{C_3} \ \mathbf{Q_3}]^{\mathbf{T}}$$

$$\mathbf{e_{oc}} = [\mathbf{e_{no}} \ \mathbf{e_{po}}]^{\mathbf{T}}$$

$\mathbf{d_c}$ is the resultant nodal displacements after some elongation actuation $\mathbf{e_{oc}}$ has been applied in the condensed matrix method.

3.3.3 Bar Forces Control without Regard to Displacements

As discussed in Section 3.2.3, controlling of internal member force of some structures and/or some members are more important than the controlling displacements particularly if the structures have cable members in order to avoid slack of the cables so that the cable must be tightened. Furthermore slender members of the structures are exposed to buckling with extra load, and in this case the compressive force of those type of member must be reduced. The process of force control can be done only in statically indeterminate structures.

For the equation of non-vanishing bar forces control without regard to displacements, we can start by substituting Eqn. 3.46 into Eqn. 3.37 to give

$$\mathbf{t_n} = \mathbf{t_{nH}} - \mathbf{S^*}\left(\mathbf{S^{*T}} \mathbf{F^*} \mathbf{S^*}\right)^{-1} [\mathbf{S^{*T}}\left(\mathbf{e_{no}} - \mathbf{A_{pn}^T} \ (\mathbf{A_{pp}^T})^{-1} \mathbf{e_{po}}\right) + \mathbf{S^{*T}} \mathbf{F^*} \mathbf{t_{nH}}]. \tag{3.55}$$

With previously defined substitutions $\mathbf{r} = -\mathbf{A_{pn}^T} \ (\mathbf{A_{pp}^T})^{-1}$ and $\mathbf{Q} = \mathbf{S^*}\left(\mathbf{S^{*T}} \mathbf{F^*} \mathbf{S^*}\right)^{-1} \mathbf{S^{*T}}$ (Eqns. 3.48 and 3.53) Eqn. 3.55 can be re-written as

$$\mathbf{t_n} = \mathbf{t_{nH}} - \mathbf{Q} \ \mathbf{F^*} \mathbf{t_{nH}} - \mathbf{Q}\mathbf{e_{no}} - \mathbf{Q}\mathbf{r} \mathbf{e_{po}}. \tag{3.56}$$

For controlling $\mathbf{t_p}$ without any regard to displacements, Eqn. 3.56 is substituted into Eqn. 3.30 to give

$$\mathbf{t_p} = \mathbf{J}\mathbf{t_{nH}} - \mathbf{J}\mathbf{Q} \ \mathbf{F^*} \mathbf{t_{nH}} - \mathbf{J}\mathbf{Q}\mathbf{e_{no}} - \mathbf{J}\mathbf{Q}\mathbf{r} \mathbf{e_{po}}. \tag{3.57}$$

where

$\mathbf{J} = -(\mathbf{A}_{pp})^{-1}\mathbf{A}_{pn}$ for ease of viewing

Combination of Eqns. 3.56 and 3.57 gives

$$\mathbf{t}_c = \mathbf{t}_{pc} + \mathbf{Z}_c\,\mathbf{e}_{oc} \tag{3.58}$$

where $\quad \mathbf{t}_{pc} = \begin{bmatrix} \mathbf{t}_{nH} - \mathbf{Q}\mathbf{F}^*\mathbf{t}_{nH} \\ \mathbf{J}\mathbf{t}_{nH} - \mathbf{J}\mathbf{Q}\mathbf{F}^*\mathbf{t}_{nH} \end{bmatrix}$ is the vector of bar forces of the structure due only to

non-vanishing load components, and

$\mathbf{Z}_c = \begin{bmatrix} \mathbf{Z}_n & \mathbf{Z}_p \end{bmatrix}$

$\mathbf{Z}_n = [-\mathbf{Q} \quad -\mathbf{J}\mathbf{Q}]^{\mathbf{T}}$

$\mathbf{Z}_p = [\mathbf{Q}\mathbf{r} \quad \mathbf{J}\mathbf{Q}\mathbf{r}]^{\mathbf{T}}$

$\mathbf{e}_{oc} = [\mathbf{e}_{no}\,\mathbf{e}_{po}]^{\mathbf{T}}$

$\mathbf{t}_c$ is the resultant bar forces after some elongation actuation $\mathbf{e}_{oc}$ has been applied in the condensed matrix method.

3.3.4 Simultaneous Displacement and Bar Force Control

Controls of either joint displacement or the bar force due to the external load without consideration of the other, through using the condensed matrix method are discussed in Sections 3.3.2 and 3.3.3 respectively. Practically and theoretically, control of one will also have some requirements on the other, or at least monitoring on the other to ensure present limits are not breached. For instance, in a structure with cables, these might have a lower limit on axial force to prevent slack, while other slender strut members will have upper limits to prevent buckling. So while controlling the external nodal displacements of such a structure, it may be necessary to also control the internal bar forces simultaneously via the same set of $\mathbf{e}_{oc}$. For the purpose of adoption this method, Eqns. 3.54 and 3.58 are combined together, to enforce displacement and bar force are satisfied simultaneously

$$\begin{bmatrix} \mathbf{Y}_c \\ \mathbf{Z}_c \end{bmatrix}\mathbf{e}_{oc} = \begin{bmatrix} \mathbf{d}_c - \mathbf{d}_{pc} \\ \mathbf{t}_c - \mathbf{t}_{pc} \end{bmatrix}. \tag{3.59}$$

In this method, because of the typically high number of equations ($ij - c$ in $\mathbf{Y}_c$ and b in $\mathbf{Z}_c$) while there are only b unknowns in $\mathbf{e_{oc}}$, then Eqn. 3.59 will be over-determinate by many degrees and insoluble. Therefore, only a least-squares "approximation" is possible for $\mathbf{e_{oc}}$. This is mainly only of academic interest, and typical situations are under-determinate and allow a choice in $\mathbf{e_{oc}}$ because in most typical structures the displacements of only some joints are expected to be controlled, and the remaining displacements will typically be free to take on any values, and similarly, the number of bar forces that exceed specified limits are also not typically large.

3.3.5 *An Illustrative Example of Using Condensed Matrix in Control*

The procedure of displacement control without regard to bar forces, bar forces control without regard to displacements, and simultaneous displacement and bar force control by using condensed matrices in equations of control are now illustrated with the simple example pantographic structure as shown in Figure 3.6. The structure has $EA = 3.6 \times 10^5$ N and $EI = 10.8 \times 10^5$ N.mm^2 .

The example consists of a two-dimensional single unit pantograph which is formed from two coplanar beams of equal length connected at their mid-point by frictionless shear connector which is perpendicular to both beams. Four bars connect between adjacent ends of the pantograph. The structure has three states of selfstress as shown in Figure 3.7 .The technique of the reduced matrix is now applied to this example to find $\mathbf{A}^*$, $\mathbf{B}^*$ and $\mathbf{F}^*$. The original size of the equilibrium matrix is 18×24, and through using the condensation process (Kwan, 1991; Pellegrino *et al.*, 1992) the size of the given example reduces to 5×8 as shown below

$$
\overbrace{
\begin{bmatrix}
-\dfrac{1}{\sqrt{2}} & 0 & -\dfrac{1}{2\sqrt{2}} & \dfrac{1}{2\sqrt{2}} & 0 & -1 & 0 & 0 \\[2.5ex]
0 & \dfrac{1}{\sqrt{2}} & \dfrac{1}{2\sqrt{2}} & -\dfrac{1}{2\sqrt{2}} & 1 & 0 & 0 & 0 \\[2.5ex]
0 & \dfrac{1}{\sqrt{2}} & -\dfrac{1}{2\sqrt{2}} & \dfrac{1}{2\sqrt{2}} & 0 & 0 & 0 & 1 \\[2.5ex]
\dfrac{1}{2\sqrt{2}} & -\dfrac{1}{2\sqrt{2}} & 0 & \dfrac{1}{\sqrt{2}} & 0 & 0 & 1 & 0 \\[2.5ex]
\dfrac{1}{2\sqrt{2}} & -\dfrac{1}{2\sqrt{2}} & 0 & -\dfrac{1}{\sqrt{2}} & 0 & 0 & 0 & -1
\end{bmatrix}
}^{\mathbf{A}}
\overbrace{
\begin{bmatrix}
t_1 \\ t_2 \\ t_3 \\ t_4 \\ t_5 \\ t_6 \\ t_7 \\ t_8
\end{bmatrix}
}^{\mathbf{t^*=t}}
=
\overbrace{
\begin{bmatrix}
P_{2y} \\ P_{3x} \\ P_{3y} \\ P_{4x} \\ P_{4y}
\end{bmatrix}
}^{\mathbf{p^*=p}}
\qquad (3.60)
$$
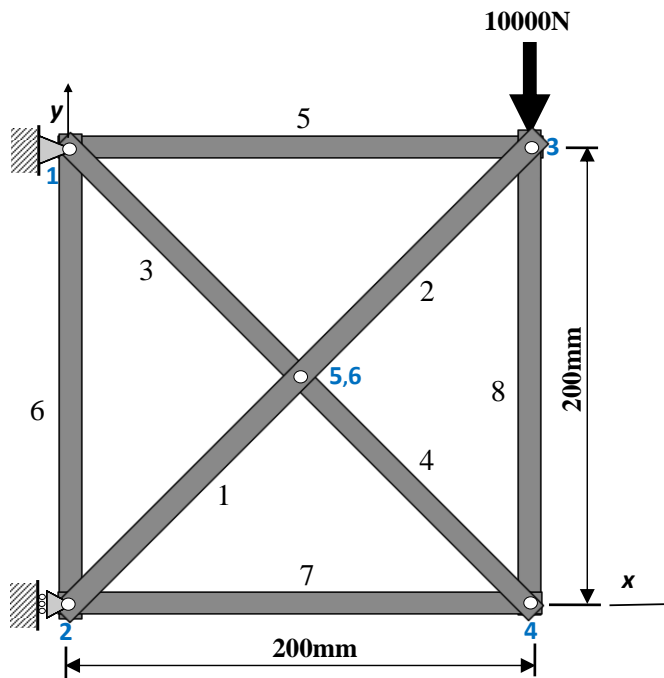
Figure 3.6: A simple pantographic structure with three degrees of statical indeterminacy.
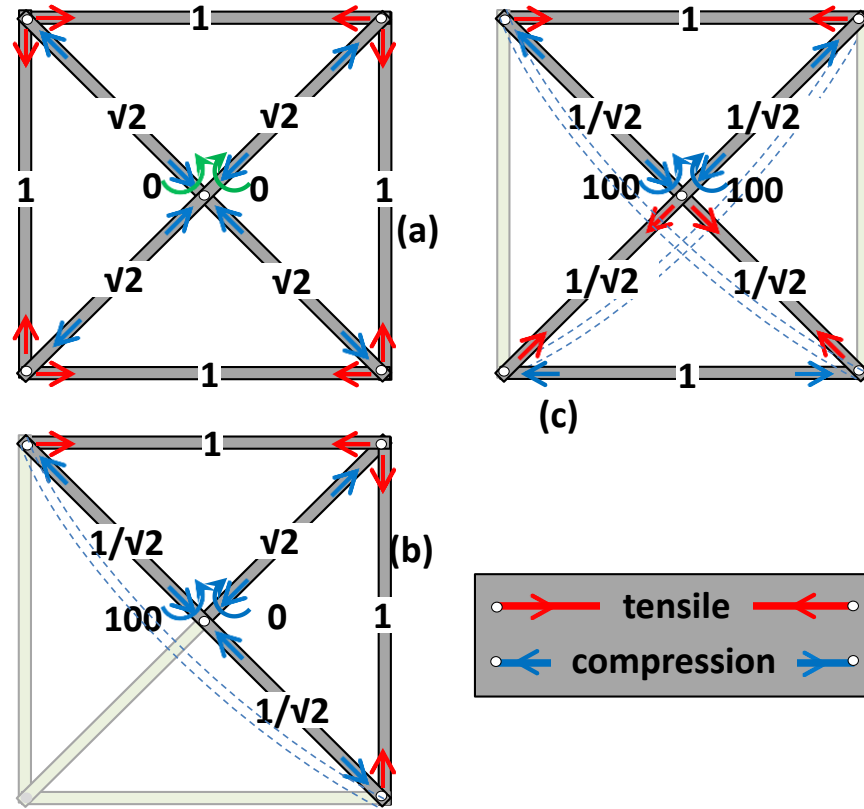
Figure 3.7: Illustration of the three states of selfstress for the structure in Figure 3.6 with exaggerated bending (-------) in the pantograph to show involvement by bending in the selfstress.

So the compatibility matrix satisfies Eqn. 3.28 and the size of the matrix reduces from 24×18 to 8×5 as shown here.

$$
\overbrace{
\begin{bmatrix}
-\dfrac{1}{\sqrt{2}} & 0 & 0 & \dfrac{1}{2\sqrt{2}} & \dfrac{1}{2\sqrt{2}} \\[2mm]
0 & \dfrac{1}{\sqrt{2}} & \dfrac{1}{2\sqrt{2}} & -\dfrac{1}{2\sqrt{2}} & -\dfrac{1}{2\sqrt{2}} \\[2mm]
-\dfrac{1}{2\sqrt{2}} & \dfrac{1}{2\sqrt{2}} & -\dfrac{1}{2\sqrt{2}} & 0 & 0 \\[2mm]
\dfrac{1}{2\sqrt{2}} & -\dfrac{1}{2\sqrt{2}} & \dfrac{1}{2\sqrt{2}} & \dfrac{1}{\sqrt{2}} & -\dfrac{1}{\sqrt{2}} \\[2mm]
0 & 1 & 0 & 0 & 0 \\[1mm]
-1 & 0 & 0 & 0 & 0 \\[1mm]
0 & 0 & 0 & 1 & 0 \\[1mm]
0 & 0 & 1 & 0 & -1
\end{bmatrix}
}^{\mathbf{B}^*}
\overbrace{
\begin{bmatrix}
d_{2y} \\[1mm]
d_{3x} \\[1mm]
d_{3y} \\[1mm]
d_{4x} \\[1mm]
d_{4y}
\end{bmatrix}
}^{\mathbf{d}^*=\mathbf{d_m}}
=
\overbrace{
\begin{bmatrix}
e_{o1}^* \\[1mm]
e_{o2}^* \\[1mm]
e_{o3}^* \\[1mm]
e_{o4}^* \\[1mm]
e_{o5}^* \\[1mm]
e_{o6}^* \\[1mm]
e_{o7}^* \\[1mm]
e_{o8}^*
\end{bmatrix}
}^{\mathbf{e}^*}
\qquad (3.61)
$$

Correspondingly, the flexible matrix reduces from 24×24 to 8×8:

$$
10^{-3} \times
\underbrace{
\begin{bmatrix}
436.87 & -436.49 & 0 & 0 & 0 & 0 & 0 & 0 \\
-436.49 & 436.87 & 0 & 0 & 0 & 0 & 0 & 0 \\
0 & 0 & 436.87 & -436.49 & 0 & 0 & 0 & 0 \\
0 & 0 & -436.49 & 436.87 & 0 & 0 & 0 & 0 \\
0 & 0 & 0 & 0 & 0.56 & 0 & 0 & 0 \\
0 & 0 & 0 & 0 & 0 & 0.56 & 0 & 0 \\
0 & 0 & 0 & 0 & 0 & 0 & 0.56 & 0 \\
0 & 0 & 0 & 0 & 0 & 0 & 0 & 0.56
\end{bmatrix}
}_{\mathbf{F}^*}
\overbrace{
\begin{Bmatrix}
t_1 \\ t_2 \\ t_3 \\ t_4 \\ t_5 \\ t_6 \\ t_7 \\ t_8
\end{Bmatrix}
}^{\mathbf{t}^* = \mathbf{t_n}}
=
\overbrace{
\begin{Bmatrix}
e^*_{o1} \\ e^*_{o2} \\ e^*_{o3} \\ e^*_{o4} \\ e^*_{o5} \\ e^*_{o6} \\ e^*_{o7} \\ e^*_{o8}
\end{Bmatrix}
}^{\mathbf{e}^*}
\tag{3.62}
$$

3.3.5.1 Controlling Joint Displacements Only

The condensed displacements under non-zero load $\mathbf{d_{pc}}$ are as shown in Table 3.6 Column 4, and the structure deforms in such a way that the non-foundation joints 3 and 4 move to the right and downwards. For the controlling purpose, it is assumed that the nodal displacements in d_{3y} is to be restored to its original position zero displacement, *i.e.* we prescribe a levelling condition of the top of the structure, whilst the remaining displacement are free to take any value. All non-vanishing (*i.e.* uncondensed) e_{no} were chosen for actuation, since these bar elongations are actually possible and easy to effect (On the other hand, the condensed bar curvature would be a difficult actuation to practically effect). Since we are prescribing only one displacement, Eqn. 3.54 has only one equation and becomes:

$$
\{0\} = \left\{ +\frac{1}{\sqrt{2}} \quad +\frac{1}{\sqrt{2}} \quad -\frac{1}{\sqrt{2}} \quad -\frac{1}{\sqrt{2}} \quad -\frac{1}{2} \quad -\frac{1}{2} \quad +\frac{1}{2} \quad +\frac{1}{2} \quad 0 \quad 0 \right\} \mathbf{e_{oc}} + \{-13.409\} \tag{3.63}
$$

which clearly has many possible solutions. One possible solution is to simply use the pseudoinverse to solve Eqn. 3.63, where we thus obtain

$$\mathbf{e}_{oc} = \{ +3.162 \quad +3.162 \quad -3.164 \quad -3.160 \quad -2.234 \quad -2.234 \quad +2.234 \quad +2.234 \quad 0 \quad 0 \}^{T}$$

Since the desired control displacement d_{3y} is one of the non-vanishing displacements and the actuation set of bars to control are non-vanished bar elongations $\mathbf{e}_{no}$, then Eqn. 3.48, can also be used in this case, to give the same as, $i.e.$

$$\mathbf{e}_{no} = \{ +3.162 \quad +3.162 \quad -3.164 \quad -3.160 \quad -2.234 \quad -2.234 \quad +2.234 \quad +2.234 \}^{T},$$

when this $\mathbf{e}_{no}$ is used as the corrective $\mathbf{e}_{oc}$, a displacement of 0.000 in d_{3y} as required does result, see Table 3.6 Column 5. Another useful impact is that all other displacements have also been reduced, in both x and y directions. However, the total elongation actuation of the non-vanished bar elongations is 21.59mm, with eight separate actuations being used. Practically this is not a particular solution due to high member and amount of control in the non-vanishing bar elongations. For this purpose, we have to look for another set of $\mathbf{e}_{oc}$ which contains a fewer non-zero actuations, while still providing the target d_{3y}.

Table 3.6: Displacements of the structure in Figure 3.6 under different sets of $\mathbf{e}_{no}$ (MATLAB program can be found in Appendix A.3).

(1)	(2)	(3)	(4)	(5)	(6)	(7)	(8)	(9)
Joint	Cond. Disp.	Dir.	Just $\mathbf{d}_{pc}$, no $\mathbf{e}_{oc}$	$\mathbf{Y}_c^+\mathbf{e}_{no}+\mathbf{d}_{pc}$	Control with only $\mathbf{e}_{n1}$	Control with only $\mathbf{e}_{n2}$	Control with only $\mathbf{e}_{n3}$	Control with only $\mathbf{e}_{n4}$
1		x	0	0	0	0	0	0
		y	0	0	0	0	0	0
2		x	0	0	0	0	0	0
	$\mathbf{d_m}$	y	-2.776	-0.543	-5.557	-5.549	+0.004	-0.002
3		x	+2.776	+0.543	+5.549	+5.557	-0.004	+0.002
		y	**-13.409**	**0.000**	**0.000**	**0.000**	**0.000**	**0.000**
4		x	-2.776	-0.543	+0.005	-0.003	-5.547	-5.559
		y	-10.633	+0.543	+0.003	-0.005	+5.547	+5.559
5,6	$\mathbf{d_p}$	x	-1.387	-0.273	+6.701	-6.698	-9.469	+3.927
		y	-5.318	+0.273	+6.698	-6.701	+9.469	-3.927

As explained in Section 3.2.2.2 the best location of actuators should be decided at the design stage, so that structures can have actuators embedded for effective control of displacements under service loading. For recognition of which are the most effective bars to control d_{3y}, and the amount of required actuation, Eqn. 3.63 must be used.

The effectiveness of actuation in any bar is indicated by the size of the associated coefficient in the $\mathbf{Y_c}$ matrix in Eqn. 3.63. Here, there two groups for effectual control of d_{3y}: firstly bars 1 to 4, and secondly, bars 5 to 8. The most effective actuation bars are those in the first group with the larger coefficients in $\mathbf{Y_c}$. The two elements of $\mathbf{Y_c}$ which vanish are the curvature of beam-pairs 1-5-3 and 2-6-4. For providing minimum actuation, we shall choose one of the four bars 1, 2, 3 and 4 for actuation since they have the largest coefficients in $\mathbf{Y_c}$ of Eqn. 3.63. Even though each of the four bars, all with the large coefficients of $\mathbf{Y_c}$ in Eqn. 3.63 has ability to control displacement of d_{3y} alone, the calculation was repeated for each of them in turn, with the results for each calculation shown Columns 6 to 9 in Table 3.6. This was to check the displacement of all joints in both x and y directions after applying required amount of actuation for each bar separately. For example, for bar 1, Eqn. 3.63 becomes:

$$\{0\} = \left\{ \frac{1}{\sqrt{2}} \quad 0 \quad 0 \quad 0 \quad 0 \quad 0 \quad 0 \quad 0 \quad 0 \right\} \mathbf{e_{oc}} + \{-13.409\} \cdot \qquad (3.64)$$

The use of the pseudoinverse on $\mathbf{Y_c}$ gives

$$\mathbf{e_{oc}} = \left\{ 18.963 \quad 0 \quad 0 \quad 0 \quad 0 \quad 0 \quad 0 \quad 0 \quad 0 \right\}^{\mathrm{T}}.$$

Similarly, the other calculations yields 18.963 for bar 2, -18.951 for bar 3, and -18.975 for bar 4.

As a result, comparison of the required amount of actuation in each of the four bars shows they are almost the same, and they all produce the target zero displacement of $dy3$. However, actuation in bar 4 does have advantage over other bars because, while all the other actuations produce similar displacements in joints 1 to 4, actuation in bar 4 does produce the least displacement in joint 5-6. This is principally because bar 4 is further remote from joint 5-6 to the support in joints 1 and 2, and hence shortening of bar 4 is not immediately displacing joint 5-6.

In this way, as explained in Section 3.2.2.2, the current approach can actually determine not only the necessary amount of actuation to be applied, but can also indicate the most effective bar(s) for a given set of displacement control.

3.3.5.2 Controlling Bar Forces Only

For the purpose of controlling bar force without regarding to the joint displacements, firstly the bar forces $\mathbf{t_{pc}}$ under load are as shown in Table 3.7, Column 3. Structural members have a greater tendency for failure in compression than the tension, due to buckling in slender members, so it is presumed the need to control compression force in all members to a limit of -6000, whilst the tensile forces are free to take any value. Under the loading shown in Figure 3.6, the given example has axial force in bars 1 and 2 ($\mathbf{t_{n1}}$ and $\mathbf{t_{n2}}$) exceeding the compression limit (see Column 3 in Table 3.7) with values of 7071.1.

In the first trial, all non-vanishing bar $\mathbf{e_{no}}$ were chosen for actuation since they are easily accessible for the actuation process (being bar length actuations rather than curvature). Only two bar forces are prescribed for control, which are those for bars 1 and 2 (t_{n1} and t_{n2}), thus Eqn. 3.58 has only two equations, and becomes:

$$\begin{bmatrix} -6000 \\ -6000 \end{bmatrix} = \begin{bmatrix} \text{-}373.4 & \text{-}372.2 & \text{-}372.8 & \text{-}372.8 & 263.2 & 264.0 & 264.0 & 263.2 & 0 & 0 \\ \text{-}372.2 & \text{-}373.4 & \text{-}372.8 & \text{-}372.8 & 264.0 & 263.2 & 263.2 & 264.0 & 0 & 0 \end{bmatrix} \mathbf{e_{oc}} + \begin{bmatrix} -7071.1 \\ -7071.1 \end{bmatrix} \quad (3.65)$$

This system of course has many possible solutions. One possible solution process is to simply use the pseudoinverse to solve Eqn. 3.65, which gives:

$$\mathbf{e_{oc}} = \left\{ -0.479 \quad -0.479 \quad -0.479 \quad -0.479 \quad +0.339 \quad +0.339 \quad +0.339 \quad +0.339 \quad 0 \quad 0 \right\}^T$$

Alternatively (and as also mentioned in Section 3.3.5.1), since t_{n1} and t_{n2} are among the non-vanishing $\mathbf{t_n}$ in this example, and the actuation is also among the non-vanishing bar elongations $\mathbf{e_{no}}$, then Eqn. 3.56 can equally be used, giving the same results of

$$\mathbf{e_{no}} = \left\{ -0.479 \quad -0.479 \quad -0.479 \quad -0.479 \quad +0.339 \quad +0.339 \quad +0.339 \quad +0.339 \right\}^T$$

After using the corrective $\mathbf{e}_{oc}$ the force in bars 1 and 2 are reduced to -6000 as required, (see Table 3.7, Column 4) and at the same time, none of the other bars have compression force greater than 6000 and so, the objective condition is satisfied, and with a total actuation of $\mathbf{e}_{no}$ of 3.27mm.

Table 3.7: Bar forces of the structure in Figure 3.6 under different sets of $\mathbf{e}_{no}$ (MATLAB program is shown in Appendix A.3).

(1)	(2)	(3)	(4)	(5)	(6)	(7)
Bar	Cond. Force	Just $\mathbf{t}_{pc}$, no $\mathbf{e}_{oc}$	All elements in $\mathbf{e}_{no}$	Control with only $\mathbf{e}_{n1}$ & $\mathbf{e}_{n2}$	Control with only $\mathbf{e}_{n1}$	Control with only $\mathbf{e}_{n2}$
1		-7071.1	-6000.0	-6000.0	-5998.4	-6001.6
2		-7071.1	-6000.0	-6000.0	-6001.6	-5998.4
3		+7075.6	+8146.6	+8146.6	+8146.6	+8146.6
4	$\mathbf{t}_n$	+7066.6	+8137.6	+8137.6	+ 8137.6	+ 8137.6
5		+4996.8	+4239.5	+4239.5	+4240.6	++4238.3
6		+4996.8	+4239.5	+4239.5	+4238.3	+4240.6
7		-4996.8	-5754.2	-5754.2	-5755.3	-5753.0
8		-4996.8	-5754.2	-5754.2	-5753.0	-5755.3
m(1,2)	$\mathbf{t}_p$	-635.7	-635.7	-635.7	-635.7	-635.7
m(3,4)		0.0	0.0	0.0	+232.5	-232.5

Observation of Eqn. 3.65 shows that bars 1 to 4 have almost the same coefficients in $\mathbf{Z}_c$ in the two rows. Therefore, any effect $\mathbf{Z}_c\mathbf{e}_{oc}$ has on each of bars 1 to 4 is the same for bars 1 and 2. In other words, the force in bars 1 and 2 can (only) be raised or lowered by the same amount, with actuation in any of bars 1 to 4. In this case, we can reduce the number of actuators from eight to two, thus we restrict the length actuators to just bars 1 and 2 (*i.e.* the same bars with force requiring control). As before, we shall seek to reduce the compressive force in bars 1 and 2 to -6000 for all bars. With the required $\mathbf{t}_n$ as -6000, the reduced Eqn. 3.65 is

$$\begin{bmatrix} -6000 \\ -6000 \end{bmatrix} = \begin{bmatrix} -373.4 & -372.2 & 0 & 0 & 0 & 0 & 0 & 0 & 0 & 0 \\ -372.2 & -373.4 & 0 & 0 & 0 & 0 & 0 & 0 & 0 & 0 \end{bmatrix} \mathbf{e}_{oc} + \begin{bmatrix} -7071.1 \\ -7071.1 \end{bmatrix} \quad (3.66)$$

which (through use of pseudoinverse) gives

$$\mathbf{e}_{oc} = \{-1.437 \quad -1.437 \quad 0 \quad 0 \quad 0 \quad 0 \quad 0 \quad 0 \quad 0 \quad 0\}^T$$

This corrective $\mathbf{e}_{oc}$ is different to, and simpler than $\mathbf{e}_{no}$ above, but, when applied, gives the same set of bar forces and also limits the force of bars 1 and 2 to -6000 as required, without any other bar force consequently exceeding the limit, see Table 3.7, Column 5. This time, the control is achieved with only 2.874mm as the total actuation of $\mathbf{e}_{no}$.

Actually, a further reduction in the number of actuators is possible this example by controlling the chosen bar forces $\mathbf{t}_{n1}$ and $\mathbf{t}_{n2}$ with only one actuator, since Eqn. 3.65 shows that bars 1 to 4 have nearly the same coefficients in $\mathbf{Z}_c$. Therefore, any effect resulting from actuation in any of bars 1 to 4 has to be the nearly identical for both $\mathbf{t}_{n1}$ and $\mathbf{t}_{n2}$. If we choose bar 1 alone for actuation, then Eqn. 3.65 becomes

$$\begin{bmatrix} -6000 \\ -6000 \end{bmatrix} = \begin{bmatrix} -373.4 & 0 & 0 & 0 & 0 & 0 & 0 & 0 & 0 & 0 \\ -372.2 & 0 & 0 & 0 & 0 & 0 & 0 & 0 & 0 & 0 \end{bmatrix} \mathbf{e}_{oc} + \begin{bmatrix} -7071.1 \\ -7071.1 \end{bmatrix} \tag{3.67}$$

and

$$\mathbf{e}_{oc} = \{-2.873 \quad 0 \quad 0 \quad 0 \quad 0 \quad 0 \quad 0 \quad 0 \quad 0 \quad 0\}^T$$

Similarly, if we choose bar 2 for actuation, then reduced Eqn. 3.65 becomes

$$\begin{bmatrix} -6000 \\ -6000 \end{bmatrix} = \begin{bmatrix} 0 & -372.2 & 0 & 0 & 0 & 0 & 0 & 0 & 0 & 0 \\ 0 & -373.4 & 0 & 0 & 0 & 0 & 0 & 0 & 0 & 0 \end{bmatrix} \mathbf{e}_{oc} + \begin{bmatrix} -7071.1 \\ -7071.1 \end{bmatrix} \tag{3.68}$$

which again gives a similar

$$\mathbf{e}_{oc} = \{0 \quad -2.873 \quad 0 \quad 0 \quad 0 \quad 0 \quad 0 \quad 0 \quad 0 \quad 0\}^T$$

The resultant bar forces from applying these two $\mathbf{e}_{oc}$ are calculated and collected in Columns 6 and 7 of the Table 3.7. Both columns show (near) identical results, so the force in bars 1 and 2 can actually be controlled via only one actuator. The principal difference in the two sets of resultant forces is in the moment of beam-pair 1-6-4 (i.e. m(3,4)) which have values of -232.1 and +232.1. The difference results from $\mathbf{e}_{oc}$ having a shortening each time, in either bar 1 or in bar 2, but a shortening in bar 1 (which is "below" beam-pair 1-6-4) would bend that beam-pair in the opposite direction to a shortening in bar 2 (which is "above" that beam-pair). However, whether the beam-pair bends one way or the other, so long as the amount of bending is the same, then the effect at its pinned-ends

(i.e. overall shortening) is the same, and hence the controlling effect on the rest of the structure is the same. This is why either Eqn. 3.67 or Eqn. 3.68 produces the same overall bar force effect (except for the moment m(3,4)).

3.3.5.3 Simultaneously Controlling Joint Displacement and Bar Force

The joint displacements and bar forces of the structure under load without any corrective actuation e_{oc} applied are shown together in Columns 4 and 5 of Table 3.8 respectively. We shall now impose both the controlling conditions introduced in the Subsections 3.3.5.1 and 3.3.5.2 simultaneously; so the nodal displacement in d_{3y} is to be zero (in order to keep the top of the structure level), and compression force in members are limited to -6000. Control is to be achieved through actuation in non-vanishing bar elongation e_{no}, which we choose to be t_{n1} and t_{n2}. Equation 3.59 is now employed as a system of two equations in eight non-vanishing elongation unknowns:

$$
\begin{Bmatrix} 0 \\ -6000 \\ -6000 \end{Bmatrix} = \left\{ \frac{\mathbf{Y_c}_{[\text{row 3, columns}[1-8]]}}{\mathbf{Z_c}_{[\text{rows 1 and 2, columns}[1-8]]}} \right\} \mathbf{e_{oc}} + \begin{Bmatrix} -13.41 \\ -7071 \\ -7071 \end{Bmatrix} \tag{3.69}
$$

Thus, Eqn. 3.69 becomes:

$$
\begin{Bmatrix} 0 \\ -6000 \\ -6000 \end{Bmatrix} = \begin{Bmatrix} +0.707 & +0.707 & -0.707 & -0.707 & -0.500 & -0.500 & +0.500 & +0.500 & 0 & 0 \\ -373.4 & -372.2 & -372.8 & -372.8 & +263.2 & +264.0 & +264.0 & +263.2 & 0 & 0 \\ -372.2 & -373.4 & -372.8 & -372.8 & +264.0 & +263.2 & +263.2 & +264.0 & 0 & 0 \end{Bmatrix} \mathbf{e_{oc}} + \begin{Bmatrix} -13.41 \\ -7071 \\ -7071 \end{Bmatrix} \tag{3.70}
$$

Simply through the pseudoinverse of the 3×8 compound matrix $\left[\mathbf{Y_c} \mid \mathbf{Z_c} \right]^{\mathrm{T}}$ a set of actuation obtained as:

$$
(\mathbf{e_{oc}})_1 = \begin{Bmatrix} 2.683 & 2.683 & -3.643 & -3.638 & -1.896 & -1.896 & 2.573 & 2.573 & 0 & 0 \end{Bmatrix}^{\mathrm{T}}
$$

Table 3.8: Displacement and bar forces control of of the structure in Figure 3.6 (MATLAB program is shown in Appendix A.3).

(Displacements (shaded) and bar forces (unshaded) of the structure: with no e_{oc}; with $(e_{oc})_1$ and $(e_{oc})_2$ applied to adjust the controlled displacements (Column 4) and bar forces (Column 5) shown in bold).

(1)	(2)	(3)	(4)	(5)	(6)	(7)	(8)	(9)	(10)	(11)
Jt	Cond. Disp.	Dir.	no e_{oc}		$(e_{oc})_1$		$(e_{oc})_2$		Cond. Force	Bar
			d_{pc}	t_{pc}	d_{pc}	t_{pc}	d_{pc}	t_{pc}		
1		x	0	**-7071**	0	**-6000**	0	**-6000**		1
		y	0	**-7071**	0	**-6000**	0	**-6000**		2
2		x	0	+7076	0	+8143	0	+8140		3
	d_m	y	-2.78	+7067	-0.46	+8141	-2.36	+8144	t_n	4
3		x	+2.78	+4997	0.46	+4242	+2.36	+4244		5
		y	**-13.41**	+4997	**0.00**	+4242	**0.00**	+4244		6
4		x	-2.78	-4997	-0.63	-5757	-3.20	-5759		7
		y	-10.63	-4997	+0.63	-5757	+3.20	-5759		8
5,6	d_p	x	-1.39	-636	-0.31	-125	+2.26	+248	t_p	m(1,2)
		y	-5.32	0	+0.31	0	-2.26	0		m(3,4)

Table 3.8 shows the effects of $(e_{oc})_1$ in Columns 6 and 7, and that all the required controls are achieved, without any introduction of a new bar force compression violation. The total amount of actuation required by $(e_{oc})_1$ is 21.585mm.

The coefficients in Eqn. 3.70 also identify which are the most effective bars for a given set of simultaneous displacement and bar force control. The minimum number of actuations to deliver the required displacements and bar forces can obtained by choosing the bars corresponding to the biggest coefficients of $\left[\mathbf{Y_c} \mid \mathbf{Z_c}\right]^{\mathrm{T}}$. In this example, we thus choose the three most effective bars, instead of all eight, for actuation, and these are bars 1, 2 and 4. Bar 4 was chosen for control of d_{3y} (following the large coefficients for $\mathbf{Y_c}$) and bars 1 and 2 were chosen for $\mathbf{t_{n1}}$ and $\mathbf{t_{n2}}$ respectively (following the large coefficients for $\mathbf{Z_c}$). Therefore. Therefore, Eqn. 3.70 simplified to

$$\begin{Bmatrix} 0 \\ -6000 \\ -6000 \end{Bmatrix} = \begin{Bmatrix} 0.7071 & +0.7071 & 0 & -0.7067 & 0 & 0 & 0 & 0 & 0 & 0 \\ -373.4 & -372.2 & 0 & -372.8 & 0 & 0 & 0 & 0 & 0 & 0 \\ -372.2 & -373.4 & 0 & -372.8 & 0 & 0 & 0 & 0 & 0 & 0 \end{Bmatrix} \mathbf{e}_{oc} + \begin{Bmatrix} -13.41 \\ -7071 \\ -7071 \end{Bmatrix} \quad (3.71)$$

and

$$(\mathbf{e}_{oc})_2 = \{ \begin{matrix} +4.024 & +4.024 & 0 & -10.921 & 0 & 0 & 0 & 0 & 0 & 0 \end{matrix} \}^{\mathrm{T}}$$

This reduced set of $\mathbf{e}_{oc}$ satisfies both displacement and bar force condition without any bar violations, as shown in Columns 8 and 9 of Table 3.8. At the same time, not only is the total number of actuators reduced from eight to three, but the total amount of actuation has also reduced, from $(\mathbf{e}_{oc})_1 = 21.585$mm to $(\mathbf{e}_{oc})_2 = 18.970$mm. There has thus been a double advantage in using Eqn. 3.71.

As a result, it is proven in this Section that linear controlling equations using condensed matrix is as powerful as using non-condensed matrix for control or adjustments of structural shape and/or force. Moreover, these equations can be used in finding controlling displacement and bar force with minimum actuation in the same way as in Section 3.2.4.2, as well as in cases where the actuator locations are already fixed. The same set of equations derived in this Section are also applicable for shape adjustment of structures containing macro-elements (i.e. elements built up from one or more fundamental elements), of which the pantograph element used in Figure 3.6 is only one example.

3.4   Computer Programing

The MATLAB R2012a software has been used for calculation of the techniques described in this chapter. In general, the program contains a number of processes as presented in the form of flowchart in Figure 3.8. The main body of the program can be divided into two parts. The first part is just the analysis of a given structure and the second part is preparation and calculation for the control of joint displacements and/or bar forces of the given structure. In the beginning of the MATLAB program the joint coordinates of the chosen structure, the bar/beam connectivity between the joints, support conditions and the external loads are read. Furthermore, the material and geometric properties of the each member of the structure must be specified, *e.g.* like cross-sectional area, second moment

of area and Young's Modulus of each bar. The program then assembles the global equilibrium matrix and flexibility matrix through a looping process, cycling through each bar in twin. For the reduced matrix method, another process is required in order to condensing out the equilibrium, compatibility and flexibility matrix. The analysis of the states of the states of the self-stress and mechanisms is done through the nullspace of the equilibrium matrix and compatibility matrix respectively. The MATLAB program then calculates the internal bar forces of the structure with the external joint displacements, due to external loads or any "lack of fit" *i.e.* prestressing elongations.

The controlling part of the program starts with calculating either $\mathbf{Y}$ and $\mathbf{Z}$ in Eqns. 3.10 and 3.16 respectively, or in the case of condensed matrices $\mathbf{Y_c}$ and $\mathbf{Z_c}$ in Eqns. 3.54 and 3.58 respectively. Then the required condition for joint displacement and/or bar force must be specified in the program, as well as the most effective bars for actuation, (which depend on the size of the coefficients in $\mathbf{Y}$ and $\mathbf{Z}$). Following this, $\mathbf{e_0}$ from each of the selected active bars are calculated in the program, and through back substituting $\mathbf{e_0}$ into the Eqns. 3.10 and 3.16 the post-adjustment joint displacements and bar forces can be calculated respectively. Sometimes after using the corrective $\mathbf{e_0}$, it is impossible to achieve the required conditions, or possibly, new violations in the joint displacements or bar forces have come about. In this case, the solution process requires increasing the control set of the bars of actuation, or changing the actuation bar set.
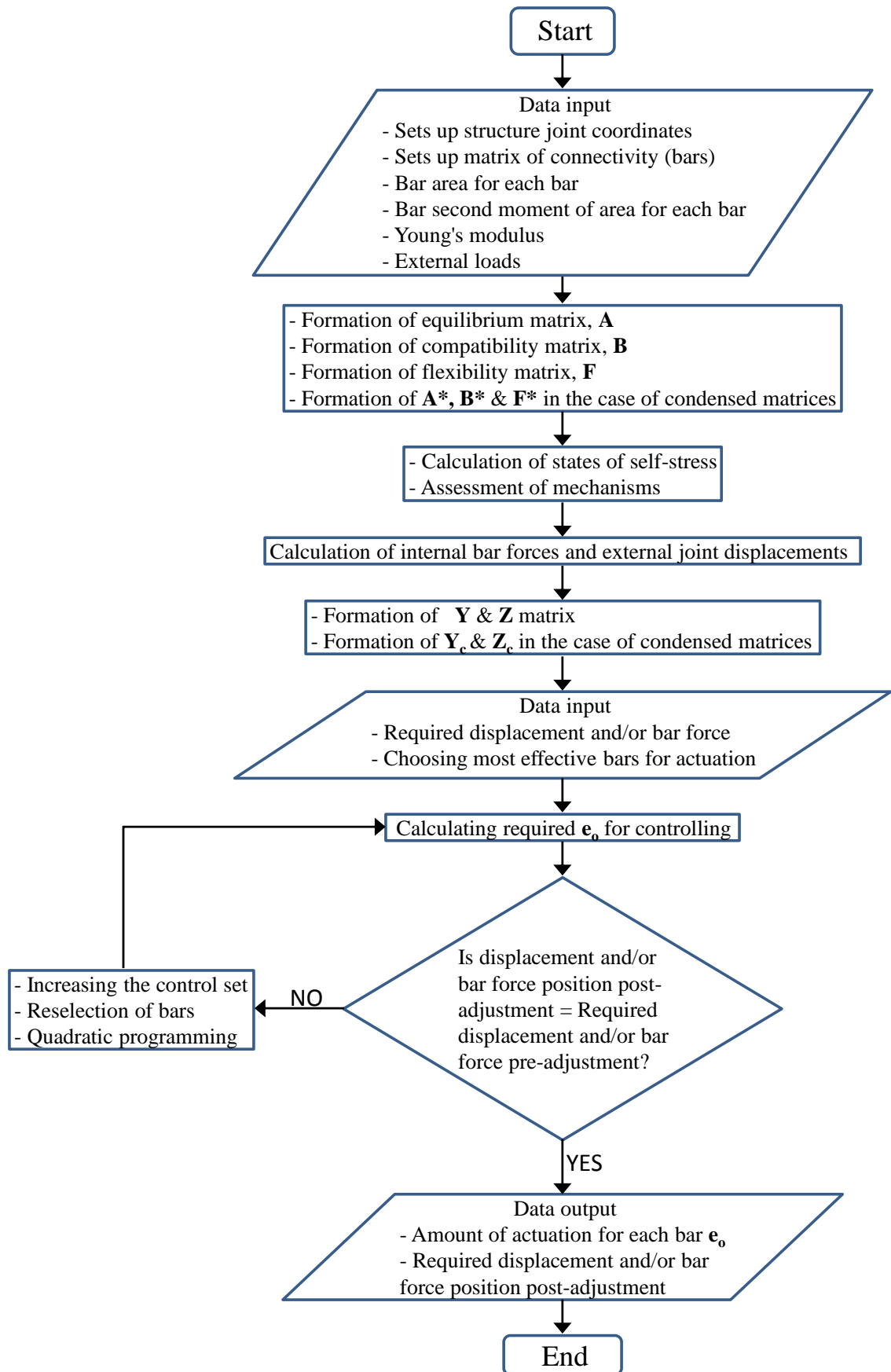
Figure 3.8: Flowchart of the MATLAB computer program

Chapter 4

Shape Adjustment on a Cable Stayed Bridge Structure

4.1 Introduction

This Chapter details an experimental model constructed and tested in Structures Laboratory of School of Engineering of Cardiff University for verification of theoretical results from equations of linear adjustment of bar and beam structure in Chapter 3. This chapter begins with a discussion of the design and constructing of the model, part by part, and the system of measurement with instruments used for that specific purpose. In addition, testing procedure and comparison of experimental and theoretical results are also explained and discussed in this chapter.

4.2 Cable Stayed Bridge Structure

A cable stayed bridge structure as shown in Figure 4.1 has been built for the experimental results of the linear shape adjustment. This structure consists of eight cables originally (*i.e.* some cables were later removed in some tests), two beams and one continuous column (tower). The total height and length of the model are 980mm and 2806mm respectively.

The cables are connected to the top of the column in the "fan arrangement" in which all the stay cables are attached to a single point at top of column (Zadeh, 2012) for reducing the moment applied to the towers to the minimum. The column is the load-bearing structures, which transmits the total bridge loads to the support. The beams on both sides of the column cantilever outwards and are welded to the central column, and are supported by cable stays every 350mm, except for the first bay which was 353mm.

4.2.1 Column

A square shaped solid steel section was chosen for the column of the model of the cable-stayed bridge. The section was chosen due to the need for the column to have sufficiently high stiffness for preventing significant bending of the column when exposed to differential side loading, either from uneven loading one side of the model, or uneven shortening on one side of the cable stays.

The column of the model carries the whole bridge. Loads applied to the relatively flexible bridge deck are quickly taken up by the cable stays to the top of the column as displayed in Figure 4.2. The load then becomes principally a compression force in the column, with some moment from unbalanced load from of the side beams. The connection to the beam presents also both a horizontal load from the horizontal component of the cable forces, and a vertical load directly from the beams. Furthermore, since the beams are fixed to the column at a height of 190mm from the base, there is additionally a moment force at the base.

4.2.2 Beams

For the beams, a suitably sized and flexible solid round mild steel section has been selected for the model. The beams had spans equal to 1403mm. that is a good allowable to the beam to be flexible and tends to high deflection, this high deflection is a good help for making adjustment test since a very big part of loadings are carried by cables.
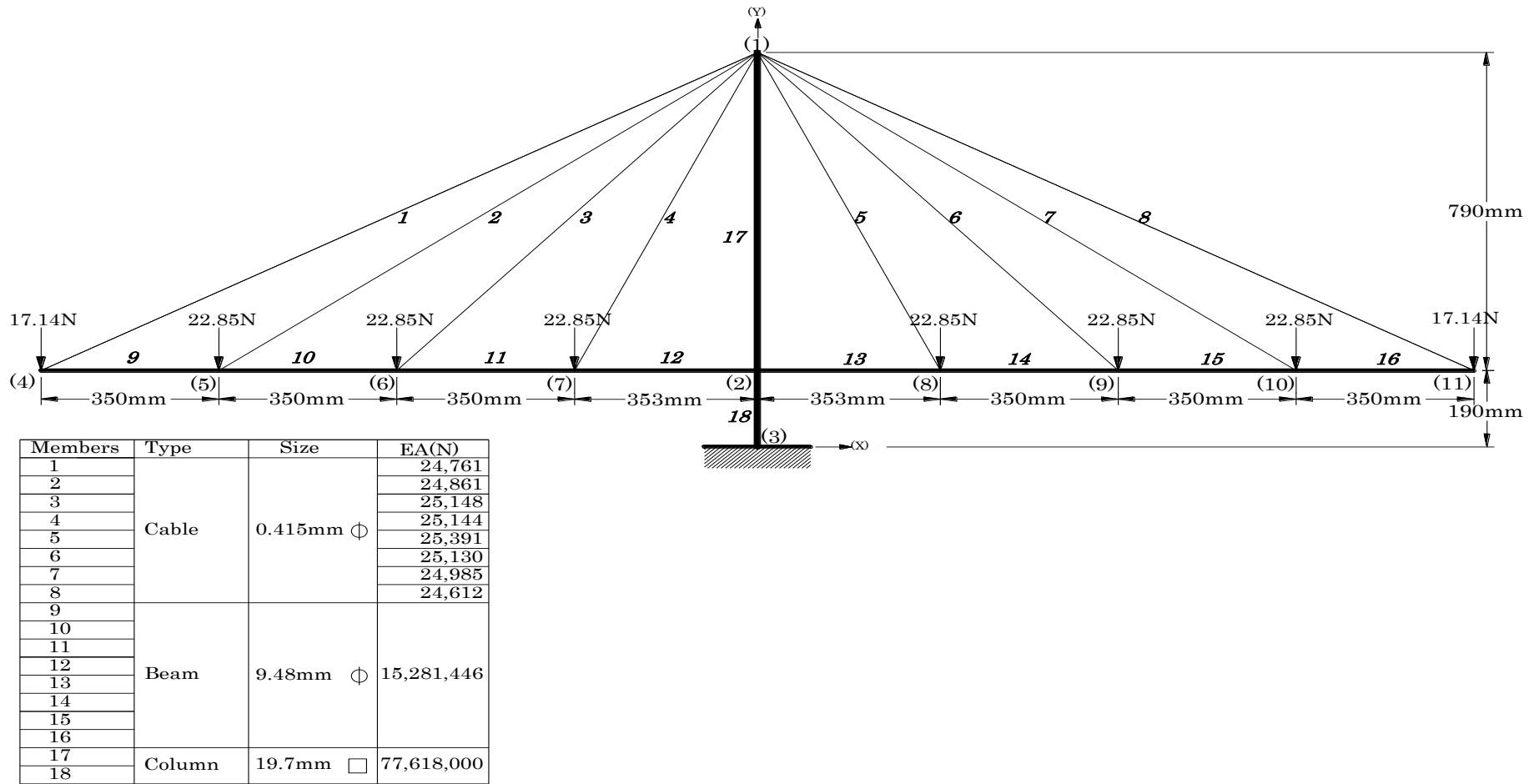
Figure 4.1: Cable-stayed bridge with eight cables.

Members	Type	Size	EA(N)
1			24,761
2			24,861
3			25,148
4	Cable	0.415mm ◍	25,144
5			25,391
6			25,130
7			24,985
8			24,612
9			
10			
11			
12	Beam	9.48mm ◍	15,281,446
13			
14			
15			
16			
17	Column	19.7mm ▢	77,618,000
18			

The sizing and spans were chosen, together with the cable stays, to result in a flexibility that enables a reasonably large (a few millimetres) deflection under the loadings to be used. This was desirable, so that subsequent control of the sizeable deflection could be verified. In the model, the cantilevered beams are fully fixed to the central column by welded joints, as shown in Figure 4.2 each beam is carried by four cables in the original model.
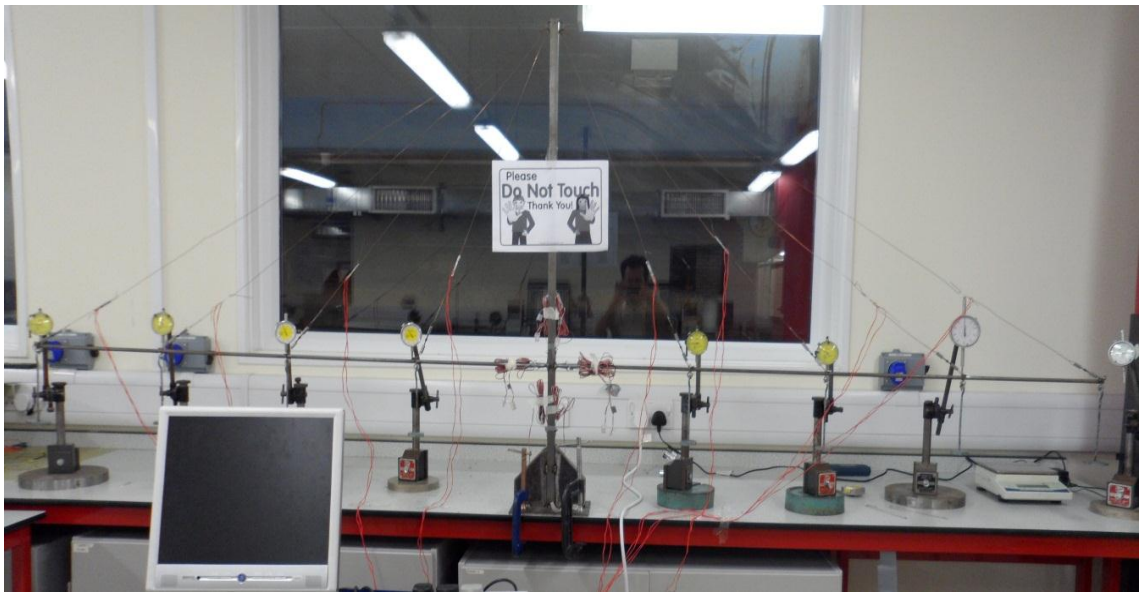
Figure 4.2: The photograph of the model of cable stayed bridge.

4.2.3   Cables

The cable-stays, or tension-ties, transfer loads from the beam to the top of the column directly. Since they are cables made from stainless steel wire approximately (0.4mmΦ) they also need to be kept taut to be structurally effective. The factors governing the selection of the section of this wire were its low flexibility and sufficiently high strength (about 200N). The choice of this wire helps in the testing since it allows appreciably large deflection in the beam under load, and structural shape adjustment can be carried out with practically applicable length actuation. An alternative wire with much higher strength was tested, but its associated high axial stiffness also did not let the beam deflect noticeably which consequently rendered adjustment redundant. Furthermore, each cable has a turnbuckle (see Section 4.2.5) and a strain gauged plate (see Section 4.2.7.2) attached to it.

4.2.4 Joints

Various different types of connections were employed in the model. The first type of joint involves the side beams and the column, which is by all round welding so both beams are fixed perpendicularly to the column, as shown in Figure 4.3.
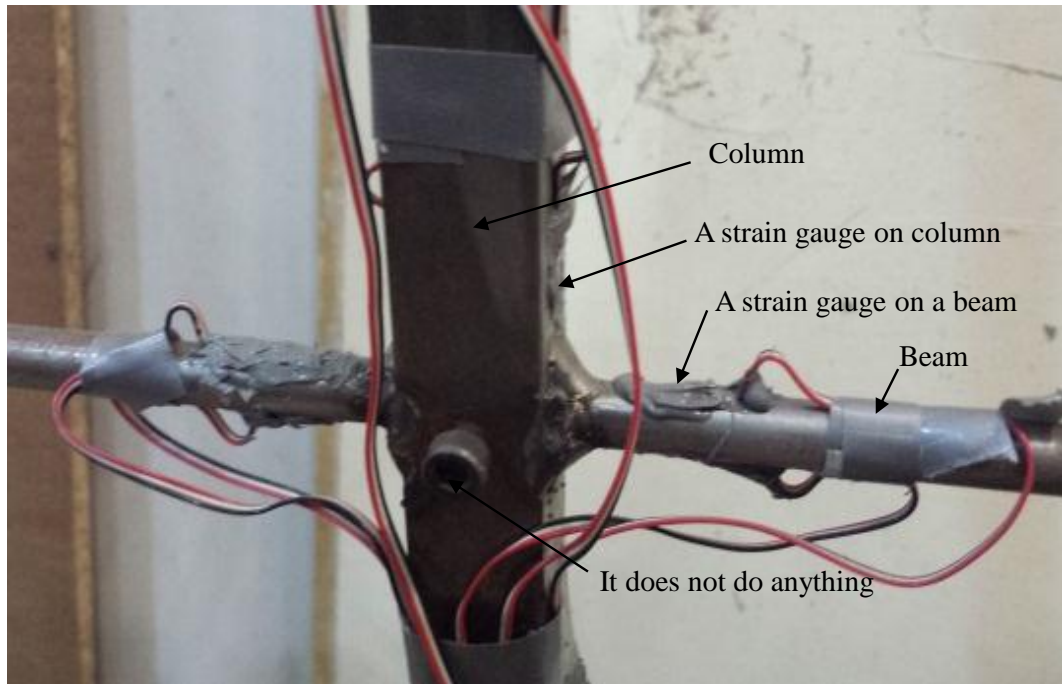
Figure 4.3: Photograph of the joint between column and beams of the model.

Figure 4.4 shows the second type of joint, which is actually a hinge joint in the top of the column, via two steel half-ring hangers welded onto each side of the column for attaching cables to. The end of each cable is looped around a semi-circular aluminium tube, which is then inserted into the half-ring of the column. The semi-circular aluminium tube prevents a tight bending radius which can lead to a breaking of the cable. Beyond the looping, the cables are terminated with crimps in conjunction with a high strength glue, to avoid any slack or looseness in the joint. The choice of crimping as opposed to soldering was made because the cables are made of stainless steel material, and only "silver solder" is suitable for this. However, the high temperature of the silver solder would also lead to melting of the thin wire, and hence a mechanical connection was the chosen method.

The last type of the joint in the model is the hinge joint between beams and cables. This joint is constructed by drilling a small hole from the side to side of the beam cross-section, see Figure 4.5, and the cable is passed through this hole before termination. At the same place a ring (for attaching load hangers to) and a flat plate (for resting the plunger of a dial gauge on) are also fixed onto the beam of each of these joints.

4.2.5 Turnbuckles

The cable length need to be adjusted by prescribed amounts to progress the shape adjustment of the structure. For this purpose, a small turnbuckle is attached to each cable. Figure 4.6 shows a longitudinal-section of a turnbuckle, which is connected to the cable at both its ends. The middle segment of the turnbuckle is a hexagonal shaped boss, which can be turned by small spanner. Both sides of the hexagonal shaped boss are fixed to the left-and right-handed threaded bar. Each end of this middle piece can rotate inside a 6mm square cross-sectional aluminium cap, to bring about simultaneous moving apart or closer together, of these end caps. The length of the turnbuckle is thus increased or decreased evenly and gradually, at a rate of 1mm length variation for every rotation of the turnbuckle. In this way, a fairly accurate (to 0.2mm) length adjustment is possible. The aluminium caps have a small hole at their ends for connecting to the cable.
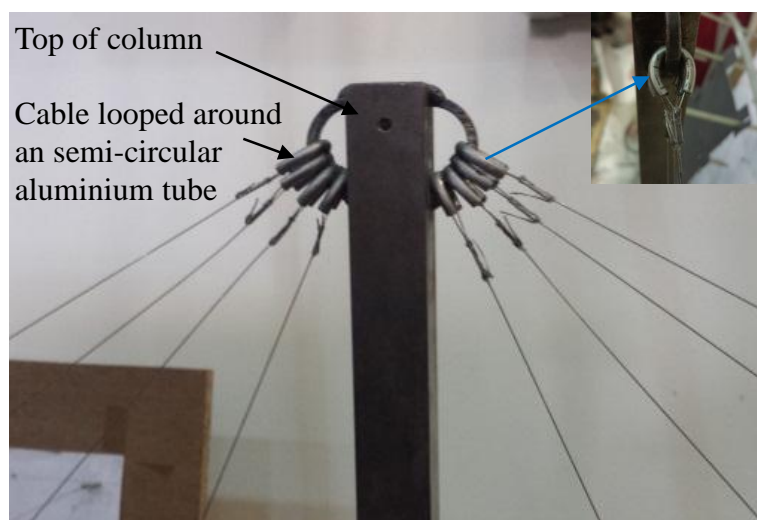
Figure 4.4: Photograph of the joint between the top of the column and the cables in the model.
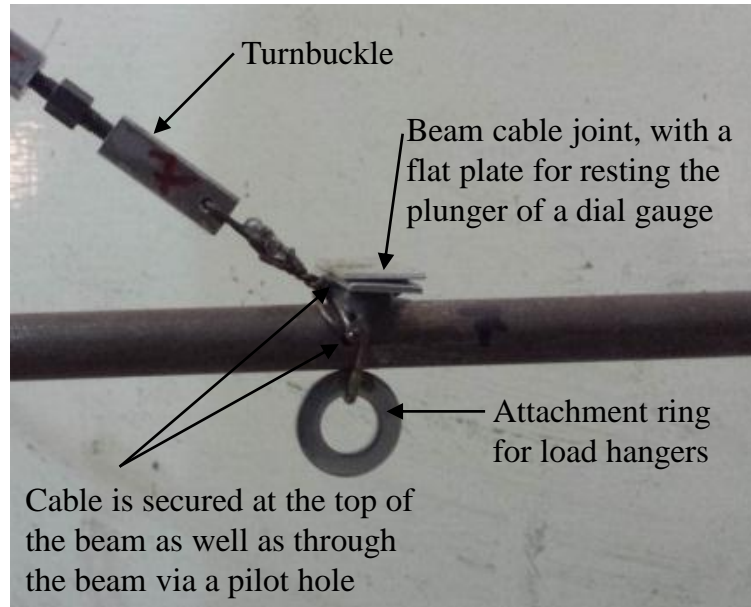
Figure 4.5: Photograph of a beam and cable joint.
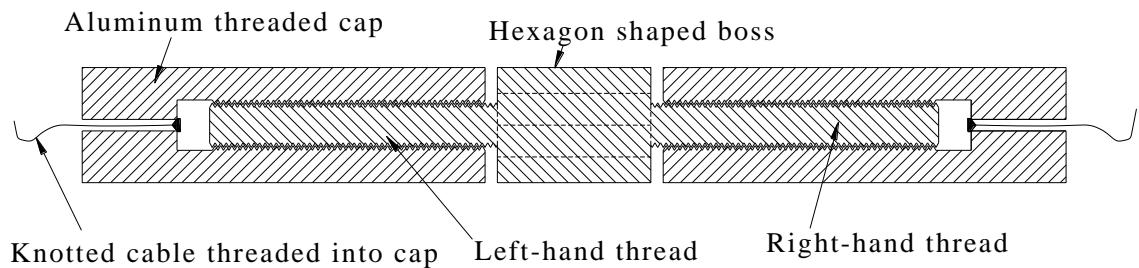
Figure 4.6: Longitudinal-section of the turnbuckle.

4.2.6 Model Support

The cable stayed bridge model has a very simple support as shown in Figure 4.7, which is used for supporting the whole model structure during the tests. The support is constructed from 5mm thick horizontal steel base plate welded to the bottom of the column. Moreover, two vertical 15mm steel plates are welded to the column and base plate as buttresses for further rigidity of the support. During testing the base plate area is held firmly to the test bench by four G-clamps.
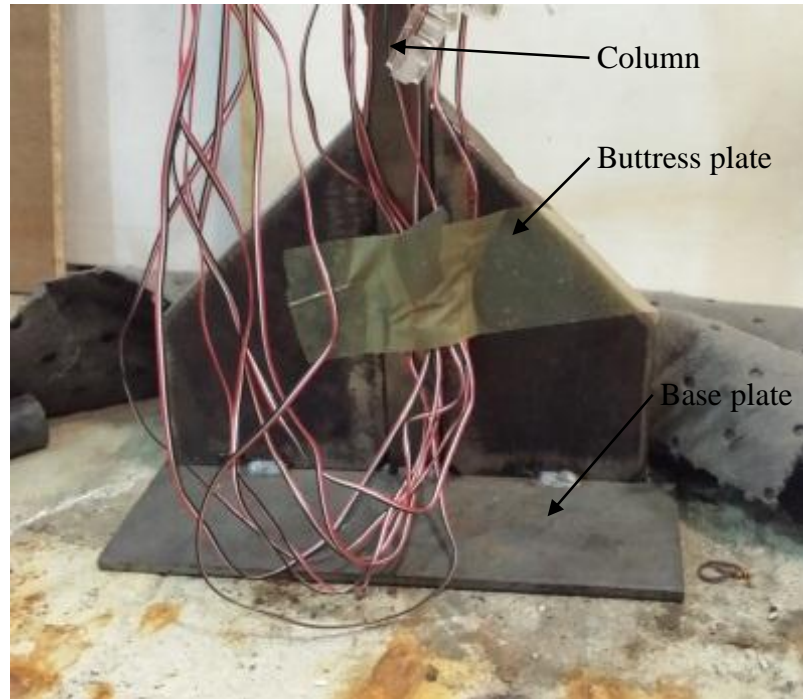
Figure 4.7: Photograph of the model support.

4.2.7   System of Measurement and Instruments

In the course of the experiments on the model of the cable-stayed bridge, three kinds of measurements have been recorded, *i.e.* joint displacements, cable forces and beam forces as detailed below.

4.2.7.1 Displacement of Joints

The vertical deflections of the beams at joints and horizontal deflection of the top of the column were measured. For this purpose the dial gauges (Mohn bull, Maty, Mercer and Mitutoyo) of 0.01mm accuracy with variable maximum range of 15mm to 50mm were used. Eight dial-gauges were used for measuring vertical deflection at the eight joints on both beams. The dial-gauges were attached onto horizontal aluminium plates glued to the beam. Moreover, a dial-gauge was also applied to measure horizontal deflection of the top joint of the column.

4.2.7.2 Cable Forces

For measuring axial force in the cables, strain gauges have been provided. For each single cable, strain gauges were glued to both sides of a 0.5mm thick aluminium plate of approximate length and width 45mm and 6mm respectively. This plate was then inserted into, and became part of the cable, such that the cable force went through the plate. Two strain gauges were used for measuring of cable force in order to remove errors occurring due to bending of plates since bending strains at the top and bottom surface could be averaged out to provide only the extension strain. The cable is terminated at both ends of the aluminium plate as shown in Figure 4.8. An aluminium plate was chosen such that its elastic extension stiffness (EA) still allowed significant strains to be measured, but its EA was still significantly higher than the cable EA so as to not change the combined EA too much. Stain gauges are connected to a computer data logger through a 16-channel Vishay Micro-Measurements System 7000 apparatus. The measurement accuracy of this system was ±0.05% with measurement resolution of 0.5 micro-strain which corresponding to ±0.216N in a typical cable.

Each plate had slightly different dimensions and construction, and so each plate was individually labelled and calibrated before use. Nevertheless, it was found that the behaviour of all cable strain gauges were approximately the same as each other, and a sample strain gauge calibration curve for cable 7 is presented in Figure 4.9. The cable strain gauges are calibrated for the entire expected working range, according to the preliminary design cable tensile forces from theoretical analysis, with some extra factor of safety. In general, the relationship is very linear, with a constant slope from the beginning to the end of the curve.

4.2.7.3 Beam Forces

The beam forces are varying along their length and these include both axial force and flexural bending moment. In this experiment, only bending moment near the fixed joint with the column is measured, on both sides. The bending moments are measured by fixing two strain gauges on top and bottom of each beam, as shown in Figure 4.3, and the data recorded by using same apparatus and software mentioned in Section 4.2.7.2.
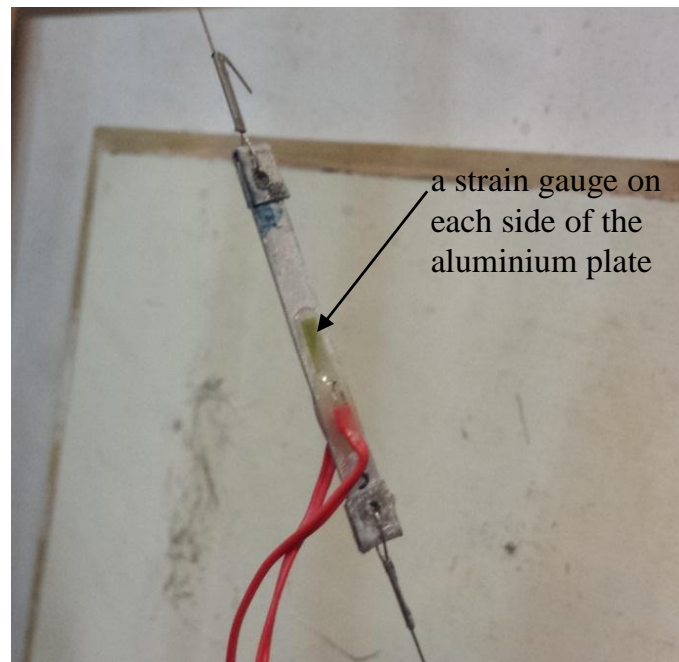
Figure 4.8: Photograph of the strain gauges on an aluminium plate for measuring cable forces.
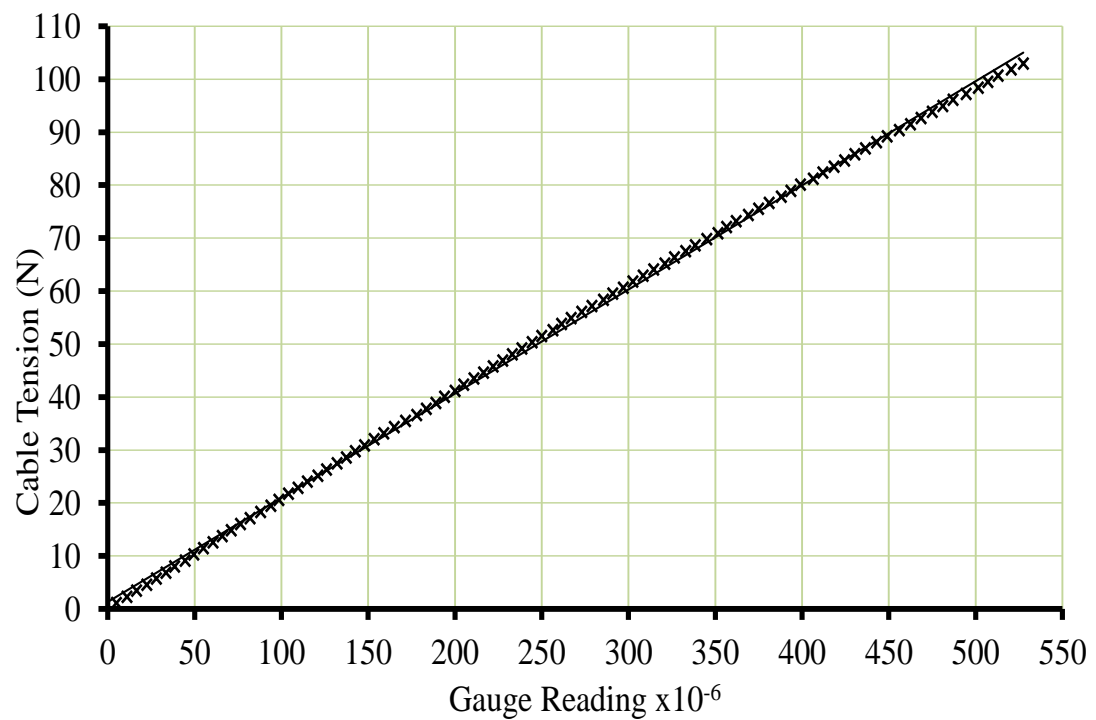
Figure 4.9: Strain gauge calibration curve for measuring cable tension versus gauge reading for cable 7.

4.2.8 Properties of Materials

The materials used in constructing cable stayed bridge model are square cross-section solid steel for the column, a solid round mild steel section for the beams, stainless steel wire for cables and small aluminium plates for measuring cable force. In spite of having material properties provided by the manufactures (*e.g.* Young's Modulus and cross-sectional dimensions), these were all measured again in the Structural Laboratory of Cardiff University School of Engineering.

The same procedure has been used for calculating the Young's Modulus of the column and beam. They were tested by applying a point load at the free end of a cantilever beam and deflection of the free end was measured. The flexural stiffness of the beam is linked to the slope and deflection of the bent loaded beam. Young's Modulus of the beam was $E=210kN/mm^2$, and correspondingly, $EA=14.82MN$ and $EI=83.25N.m^2$ while the Young's Modulus of the column used was $E=200kN/mm^2$. Furthermore, $EA=77.62MN$ and $EI=2.51kN.m^2$.

The Young's Modulus of cables and the small aluminium plates for strain gauges for measuring cable force were tested on a tensile testing machine (Shimadzu AG-I 20KN). The test specimens were gripped at their ends in the top and bottom jaws of the testing machine. The ends of the cable specimens were protected by additional aluminium plates in order to prevent damaging of the cable, which would then ensure measuring the stiffness and strength of the cables accurately. An extensometer held by small clamps in the middle of the specimens provided extension data which were recorded and displayed on an attached screen. The load-extension of the stainless steel cables was found to be linear in the full range of loading until breaking at a load of 190N. The cables EA was measured as 24.14kN. However, since aluminium plates for strain gauges for measuring cable forces form part of the cable length, the EA of the plates must be taken into consideration, and an "effective" EA be calculated for the control, as shown in

Table 4.1. The EA of the aluminium plates are each slightly different because of having slightly different cross-sectional areas and hence the effective $EA_{combined}$ should be calculate for each cable following equation 4.1.

$$EA_{combined=}Length_{combined} / (Length_{plate} / EA_{plate} + Length_{cable} / EA_{cable}) \qquad (4.1)$$

Table 4.1: Cables stayed bridge model cables EA values

Cable	EA_{plate} (N)	EA_{cable} (N)	Combined Length (mm)	$EA_{combined}$ (N)
1	192,100	24,144.8	1,616.23	24,761
2	192,200	24,144.8	1,322.01	24,861
3	196,500	24,144.8	1,062.17	25,148
4	215,800	24,144.8	868.16	25,144
5	183,000	24,144.8	868.16	25,391
6	184,700	24,144.8	1,062.17	25,130
7	201,600	24,144.8	1,322.01	24,985
8	168,500	24,144.8	1,616.23	24,612

4.3 Procedure of Testing

After preparation of the cable stayed bridge model, the structure was tested for different load cases and structural arrangements. At the beginning the model was firmly fixed to the test bench through using four G-clamps, and equally, a networked of dial gauges were also fixed properly for measuring vertical displacements of eight beam joints and horizontal movement of the top joint of the column. Loads were applied as weights added to a load hanger and all weights were checked by a sensitive electronic balance before use. Furthermore, all strain gauges are "adapted" and checked.

For a given experiment, some steps were routinely carried out. Firstly, all initial dial gauge and strain gauge readings without applying any load were recorded. Secondly, loads were then gently applied to the structure via load hangers. A visual inspection on the deflection in joints and force in members was carried out, especially in cables to see if any had become or were approaching becoming slack. Thirdly, all dial gauge and strain gauge readings were recorded again, and compared against expected values from computation by MATLAB. This is the initial loaded state and the joint displacements and member forces in this state were entered into the algorithm for shape adjustment control. Fourthly, following decision of which joint displacements or member forces were to be controlled then which actuator (and by how much) is calculated. In the fifth stage, the calculated amount of actuation (e_0) is then carefully applied to the cables by rotation in their turnbuckles while taking care to otherwise "disturb" the structure as little as possible. In the last stage of the experiment, all readings were recorded and used in the adjustment program. The results achieved are compared with the theoretical results as discussed in Section 4.4.

4.4 Experimental and Theoretical Result Comparison and Discussion

The direct method for controlling nodal displacements, or internal bar forces, and then simultaneously both nodal displacements and internal bar forces was verified by a set of experimented studies on the eight- and four-cable cable-stayed bridge structure model. The process of linear adjustment was applied for adjustment and controlling of the joint displacement and bar forces of the model.

4.4.1 Linear Structure

The overall static behaviour of many structures can be characterized by its load-deflection response. The linearity or nonlinearity of materials and members depends on how the strain of materials and deformation of members evolve with increasing corresponding stress and force. Nonlinearity of the load-deflection response can also result from deformation that is too large such that the overall geometry of the deformed structure (and its stiffness) is no longer essentially that same as that of the original structure.

Therefore, before using the linear techniques of controlling nodal displacement, *etc* introduced in Chapter 3 for shape adjustment of the physical model, evaluation was made to check whether this structure's response to load is linear or nonlinear. The cable-stayed bridge model would be used in two different configurations (with eight cables as shown in Figure 4.1 and with four cables as shown in Figure 4.14), so both configurations would be tested for presence of geometical nonlinearity.

The eight-cable bridge was tested under two point loads in each side of the model on joints 4, 6, 9 and 11 until 34.3N per joint as maximum load. The results for all tested joints are as shown in Figures 4.10 and 4.11, and load-cable tension diagrams are shown in Figures 4.12 and 4.13. Similarly, the bridge model with four cables (see Figure 4.14) was tested under two point loads in each beam on joints 4, 6, 9 and 11, until the maximum total load reached 41.13N per joint. Figures 4.14 and 4.15 show the load-deflection plots of the loaded joints and the load-cable tension diagrams are in Figures 4.16 and 4.17.

Although the size of the deflections were of the same order of magnitude as the depth of the beam, the results mostly indicate that the behaviour of the physical model in

both configurations is linear. Therefore, an attempt will be made to verify the linear control techniques as detailed in Chapter 3.
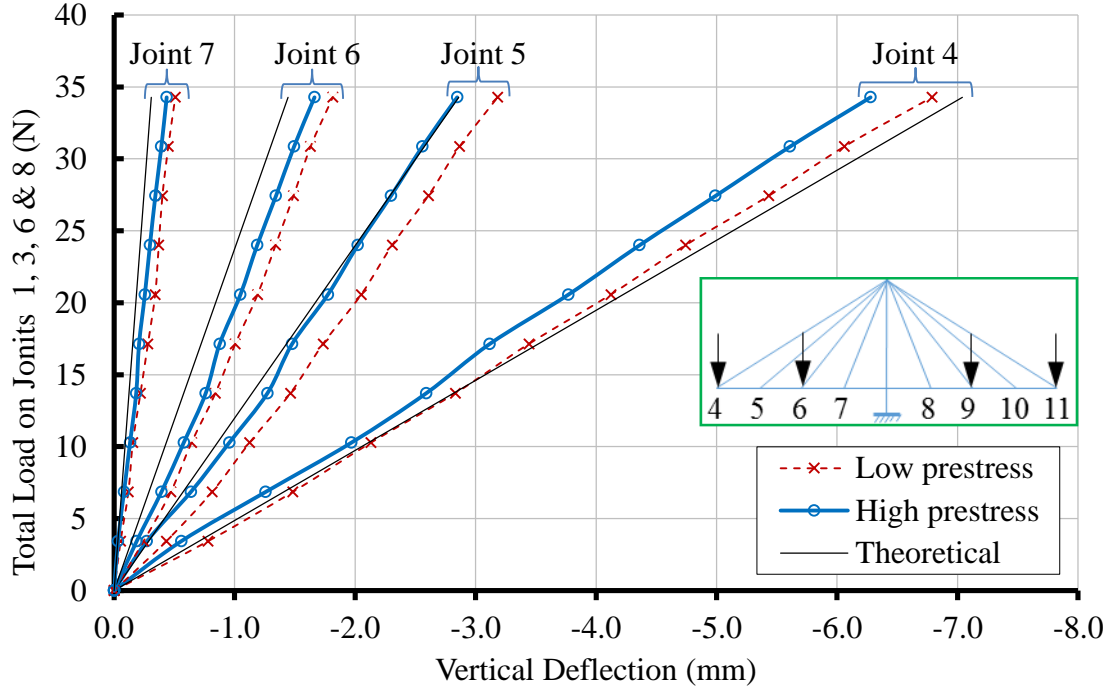
Figure 4.10: Load-deflection diagram of left-side joints of the structure in Figure 4.1.
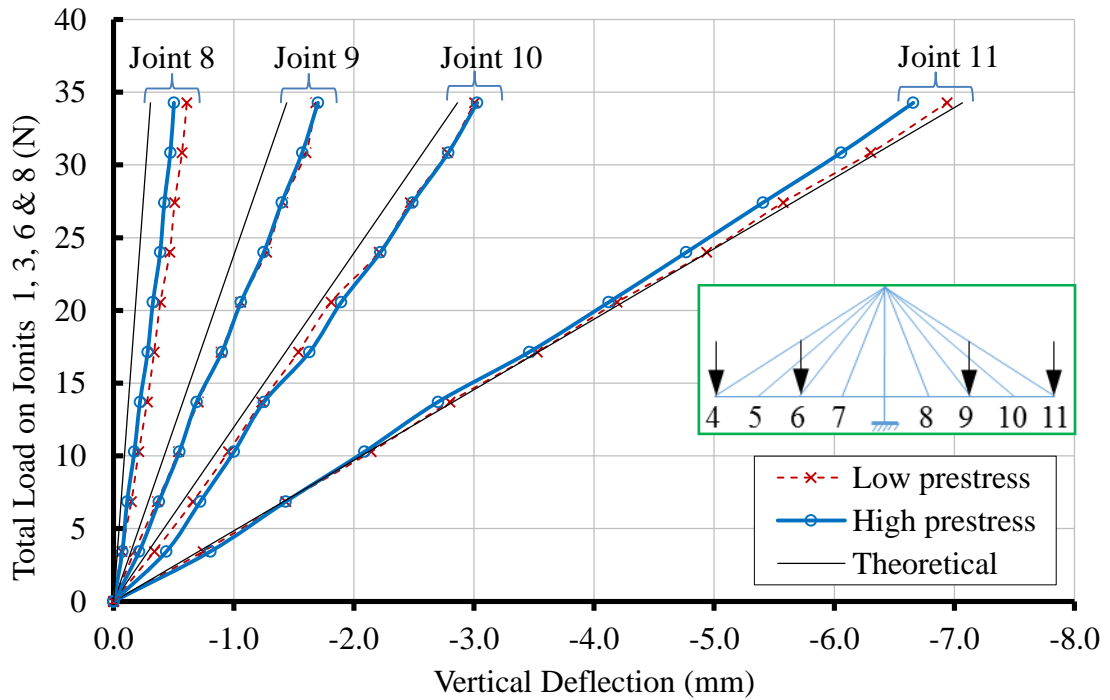
Figure 4.11: Load-deflection diagram of right-side joints of the structure in Figure 4.1.
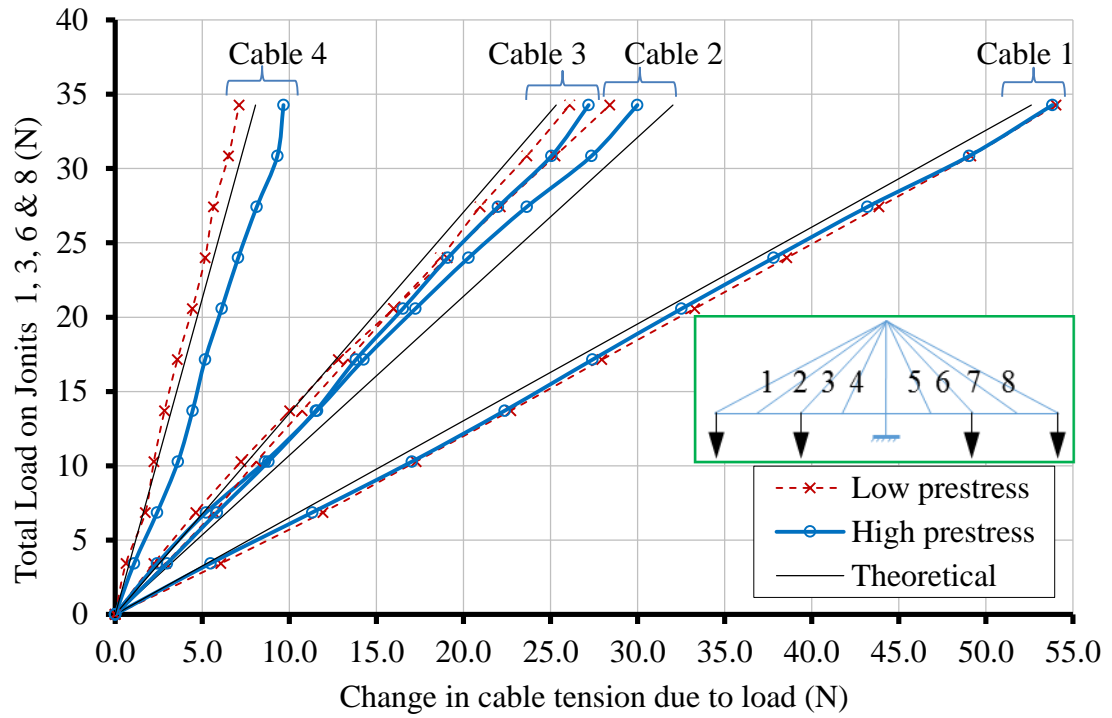
Figure 4.12: Load-cable tension diagram of the left-side cables of the structure in Figure 4.1.
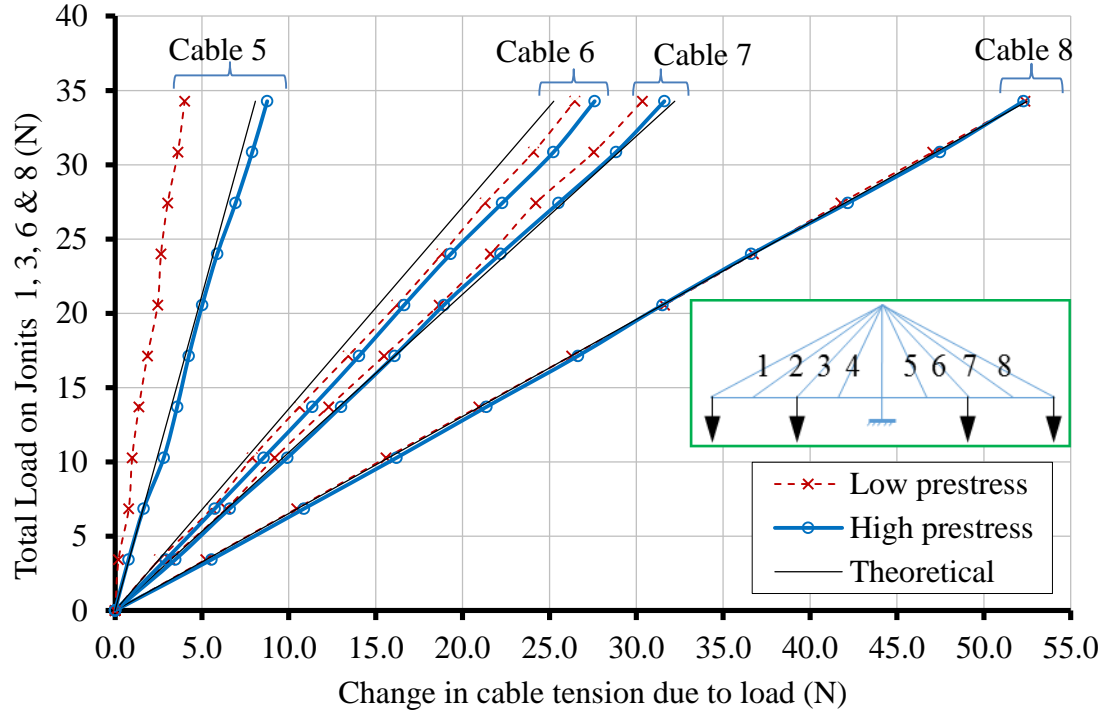
Figure 4.13: Load-cable tension diagram of the right-side cables of the structure in Figure 4.1.
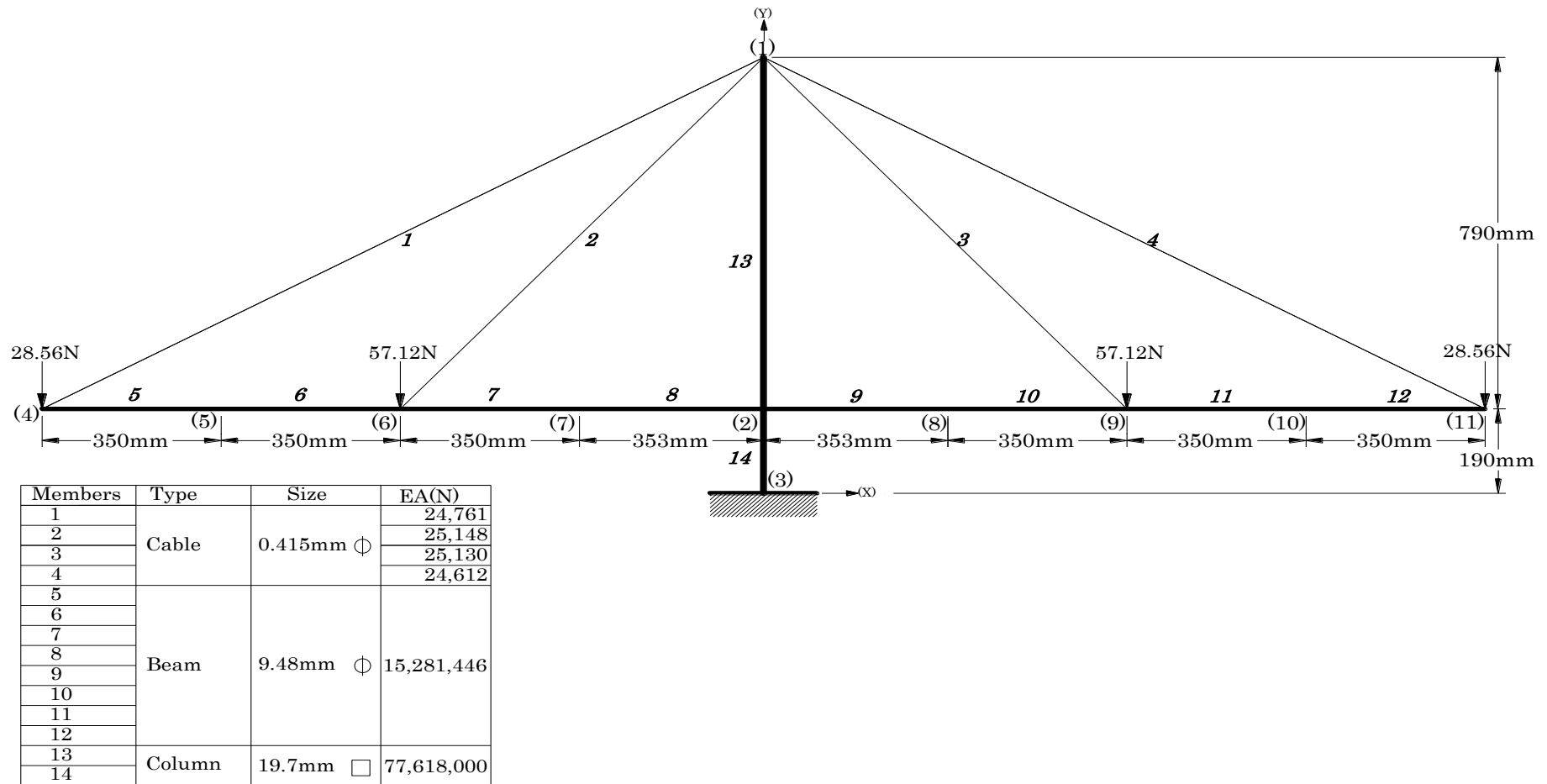
Figure 4.14: Cable-stayed bridge with four cables.

Members	Type	Size	EA(N)
1	Cable	0.415mm ⌀	24,761
2			25,148
3			25,130
4			24,612
5	Beam	9.48mm ⌀	15,281,446
6			
7			
8			
9			
10			
11			
12			
13	Column	19.7mm □	77,618,000
14			
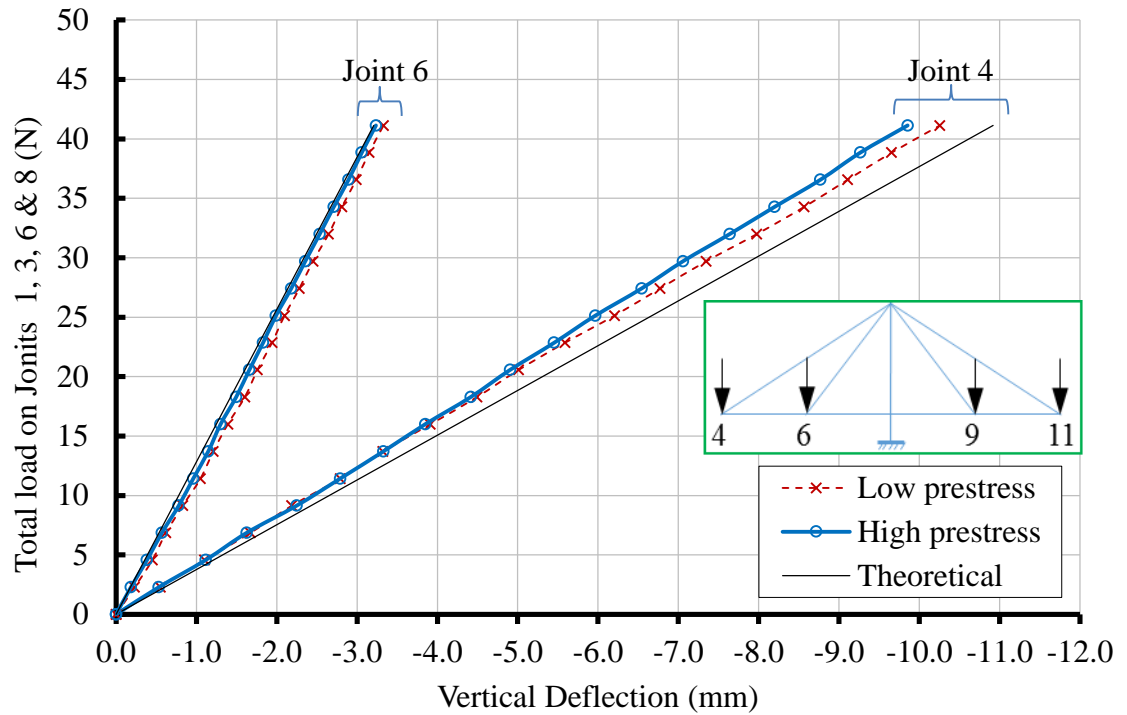
Figure 4.15: Load-deflection diagram of the joints 1 and 3 of the structure in Figure 4.14.
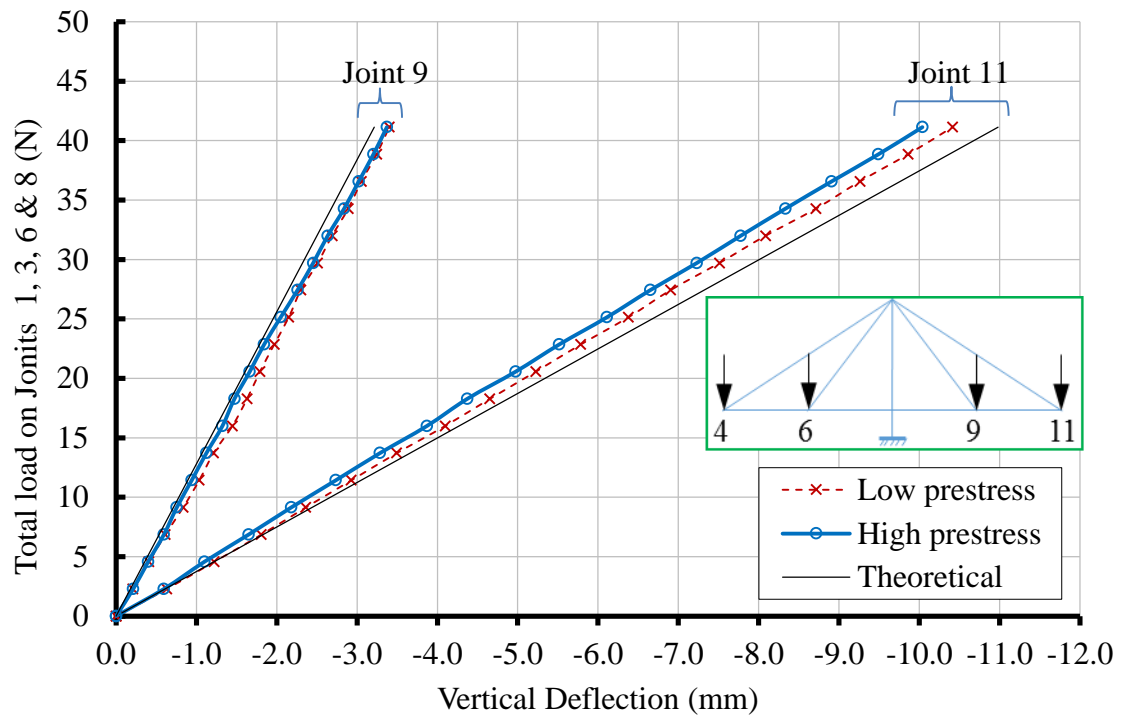
Figure 4.16: Load-deflection diagram of the joints 6 and 8 of the structure in Figure 4.14.
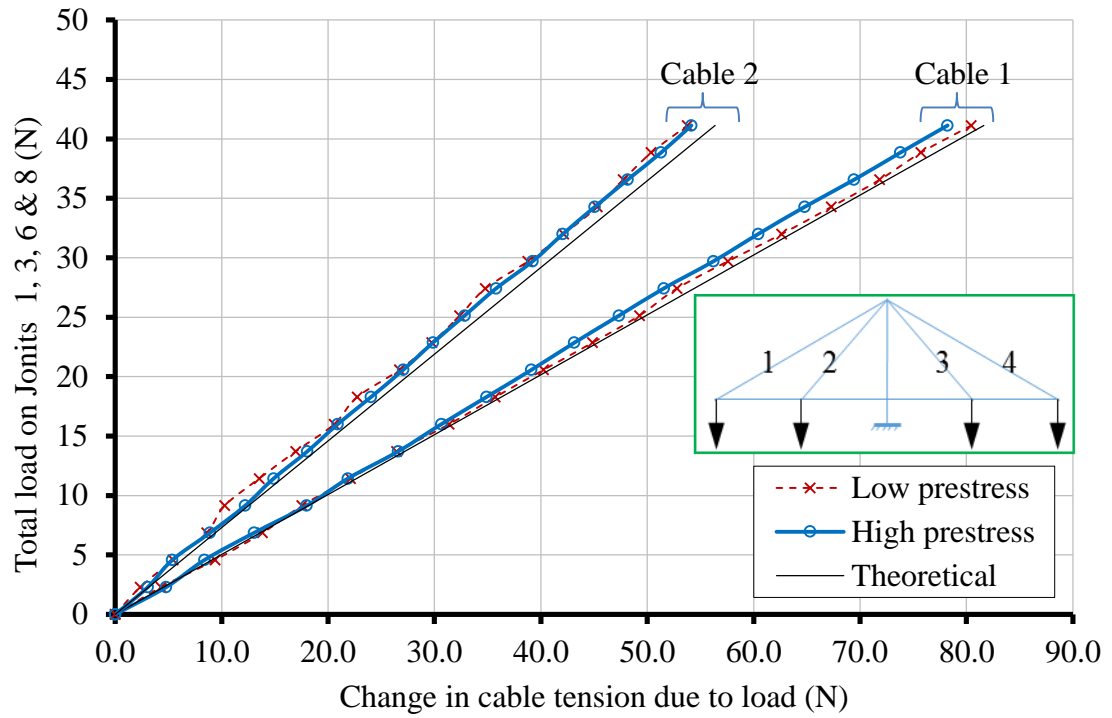
Figure 4.17: Load-cable tension diagram of the left-side cables of the structure in Figure 4.14.
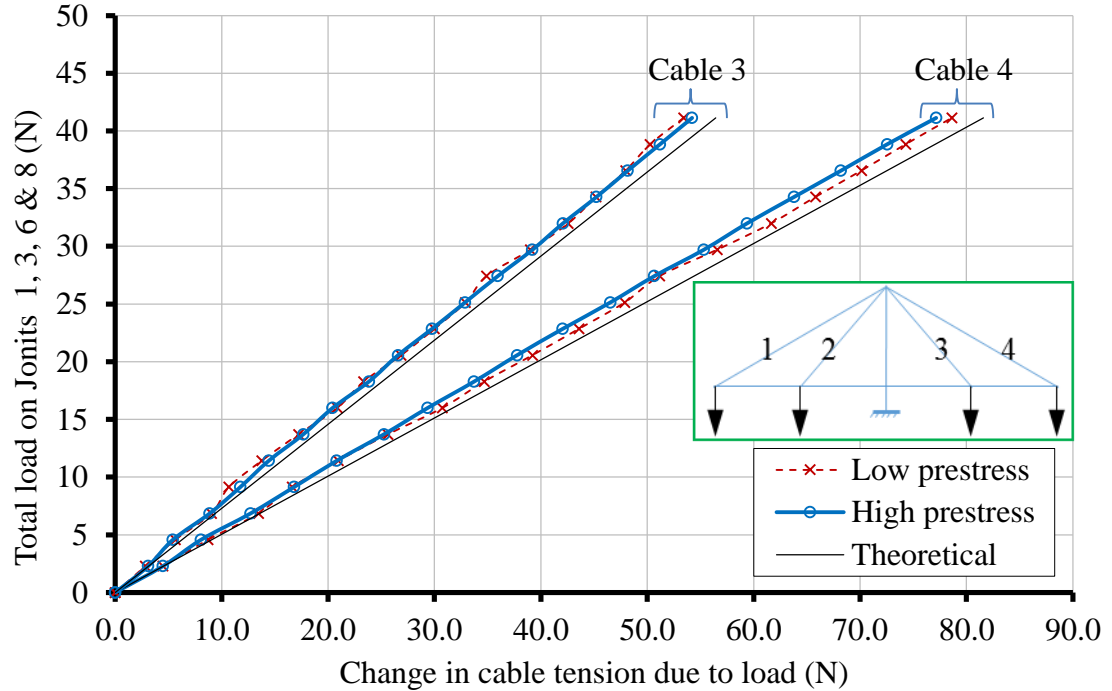
Figure 4.18: Load-cable tension diagram of the right-side cables of the structure in Figure 4.14.

4.4.2   Linear Adjustment

Linear adjustment in controlling joint displacement and bar force of the structure means finding a required set of e_0 in one cycle of the direct method then applying the obtained set of e_0 to the structure to reach the target shape. The success or otherwise of this can be verified by measurement of the resultant shape. This technique was applied to the model bridge structure in both configurations.

4.4.2.1 Eight Cables Model of Cable Stayed Bridge

In this load case the bridge model has eight cables to carry side beams at eight joints. The model was tested under six vertical downward of point loads 22.85N each applied at joints 5 to 10 and two vertical point loads 17.14N applied at joints 4 and 11. Two different sets of experiments were carried out on the model. In the first set of experiments (Experiments 1, 3 and 5), adjustment was carried out on all eight cables with results shown in Tables 4.2, 4.4 and 4.6. Additionally in the second set of experiments (Experiments 2, 4 and 6), although the structure still had eight cables, adjustment was done only on just four cables (Cables 1, 3, 6, and 8), and these results are presented in Tables 4.3, 4.5 and 4.7.

4.4.2.1.1 Experimental Displacement Control Regardless of Bar/Beam Forces

Tables 4.2 and 4.3 (Experiments 1 and 2) show the displacement control without regard to bar forces, due to the actuation in eight and four cables respectively as an application of Eqn. 3.10 in Section 3.2.2. Initially, after loading, the structure has measured displacements as shown in Column 3. For the case of eight actuators, the chosen target was fixed at -1mm deflection in all beam joints, *i.e.* Column 4 in Table 4.2. A set of e_0 is calculated to achieve the desired target shape, which is shown in Column 5. After application of this set of e_0 the theoretical outcome (Column 6) is exactly the desired target shape. However, experimental results in column 7 show very close (though not perfect) correlation to the target shape, as seen in Figure 4.19.

Unlike the case with eight actuators, when there are only four actuators, it is impossible to get (even theoretical) results which is the same as the target of having all

nodes with -1mm deflection, because in this structure, every single cable has a high direct effect on the one node to which it is connected, but also little effect on the other joints. The set of only four components in $\mathbf{e_o}$ is thus not sufficient for controlling eight displacements. In this case, the MATLAB software output gives the best (*i.e.* least-square) set of result as shown in Column 5 of Table 4.3. After adjustment with this set of $\mathbf{e_o}$, the theoretical and experimentally measured results are very close to each other (*i.e.* Columns 6 and 7) but not close to the target shape (*i.e.* Column 4) as also shown in Figure 4.20.

For understanding how each cable has a direct effect on meeting nodes, a theoretical calculation was done, where for each actuator individually applied, in turn, with the results in Figure 4.21. The "no $\mathbf{e_o}$"-line shows the position of all nodes from the loading before any adjustment, and the "$\mathbf{e_o}$ all"-line shows the position of those nodes when the full $\mathbf{e_o}$ for all four actuators have been applied. All other lines show the effect of a single actuator the on displacements of all joints. For example, "$\mathbf{e_o}1$" shows the effect of shortening only cable1 by 2.43mm, whereby node 4 goes up from deflection of -4.52mm to -0.74mm, while node 5 rises from -3.52mm to -2.48mm. However, its effect decreases so that the last joint (joint 8) has no observed change. Similarly, the effect of other actuators are also the same.

Table 4.2: Displacement control of the structure in Figure 4.1 with eight elements of **e₀** (MATLAB program can be found in Appendix A.4).

(1)	(2)	(3)	(4)	(5)	(6)	(7)	(8)
		Exp1 (8-Cable model, adjustment in only 8 elements in					
Joint	Dir	Just **d**$_P$, no **e₀** (mm)	target disp (mm)	**e₀** (mm)	8 elements in **e₀** (mm) Theo. results	8 elements in **e₀** (mm) Exp. results	Bar actuation
1	x	-0.01		**-1.68**	0	0.09	1e
	y	0.00		**-1.63**	0.00		2e
	θ	0.00		**-1.17**	0.00		3e
2	x	0.00		**0.45**	0.00		4e
	y	0.00		**0.47**	0.00		5e
	θ	0.00		**-1.22**	0.00		6e
3	x	0		**-1.34**	0	0	7e
(Fixed)	y	0		**-1.72**	0	0	8e
	θ	0		0	0	0	9e
4	x	0.01		0	0.01		9ψ1
	y	**-4.62**	**-1.00**	0	**-1.00**	**-1.11**	9ψ2
	θ	4.10e-03		0	1.20e-03		10e
5	x	0.01		0	0.01		10ψ1
	y	**-3.57**	**-1.00**	0	**-1.00**	**-1.03**	10ψ2
	θ	4.10e-03		0	0.70e-03		11e
6	x	0.00		0	0.00		11ψ1
	y	**-2.21**	**-1.00**	0	**-1.00**	**-1.00**	11ψ2
	θ	3.60e-03		0	-0.80e-03		12e
7	x	0.00		0	0.00		12ψ1
	y	**-0.98**	**-1.00**	0	**-1.00**	**-0.99**	12ψ2
	θ	3.10e-03		0	1.50e-03		13e
8	x	-0.00		0	-0.00		13ψ1
	y	**-0.97**	**-1.00**	0	**-1.00**	**-0.97**	13ψ2
	θ	-3.10e-03		0	-1.60e-03		14e
9	x	-0.00		0	-0.00		14ψ1
	y	**-2.16**	**-1.00**	0	**-1.00**	**-0.99**	14ψ2
	θ	-3.60e-03		0	0.40e-03		15e
10	x	-0.01		0	-0.01		15ψ1
	y	**-3.38**	**-1.00**	0	**-1.00**	**-1.00**	15ψ2
	θ	-4.20e-03		0	-0.90e-03		16e
11	x	-0.01		0	-0.01		16ψ1
	y	**-4.51**	**-1.00**	0	**-1.00**	**-1.07**	16ψ2
	θ	-4.20e-03		0	-0.90e-03		17e
				0			17ψ1
				0			17ψ2
				0			18e
				0			18ψ1
				0			18ψ2
		total actuation (mm)		9.68			

e= bar/beam elongation.   ψ1 & ψ2= beam rotation at ends 1 & 2.

Table 4.3: Displacement control of the structure in Figure 4.1 with four elements of $\mathbf{e_o}$ (MATLAB program is shown in Appendix A.5).

(1)	(2)	(3)	(4)	(5)	(6)	(7)	(8)
		Exp2 (8-Cable model, adjustment in only 4 elements in $\mathbf{e_o}$)					
Joint	Dir	Just $\mathbf{d_P}$, no $\mathbf{e_o}$ (mm)	target disp (mm)	$\mathbf{e_o}$ (mm)	4 elements in $\mathbf{e_o}$ (mm) Theo. results	4 elements in $\mathbf{e_o}$ (mm) Exp. results	Bar actuation
1	x	0.07		**-2.43**	0.07	0.02	1e
	y	0.00		0	0.00		2e
	θ	0.00		**-1.91**	0.00		3e
2	x	0.00		0	0.00		4e
	y	0.00		0	0.00		5e
	θ	0.00		**-1.93**	0.00		6e
3	x	0		0	0	0	7e
(Fixed)	y	0		**-2.47**	0	0	8e
	θ	0		0	0	0	9e
4	x	0.01		0	0.01		9ψ1
	y	**-4.52**	**-1.00**	0	**-0.83**	**-0.84**	9ψ2
	θ	4.10e-03		0	-2.20e-03		10e
5	x	0.01		0	0.01		10ψ1
	y	**-3.52**	**-1.00**	0	**-1.60**	**-1.69**	10ψ2
	θ	4.10e-03		0	1.30e-03		11e
6	x	0.00		0	0.00		11ψ1
	y	**-2.18**	**-1.00**	0	**-0.74**	**-0.75**	11ψ2
	θ	3.60e-03		0	1.60e-03		12e
7	x	0.00		0	0.00		12ψ1
	y	**-0.96**	**-1.00**	0	**-0.60**	**-0.60**	12ψ2
	θ	3.10e-03		0	0.50e-03		13e
8	x	-0.00		0	-0.00		13ψ1
	y	**-1.03**	**-1.00**	0	**-0.67**	**-0.64**	13ψ2
	θ	-3.10e-03		0	-0.50e-03		14e
9	x	-0.00		0	-0.00		14ψ1
	y	**-2.21**	**-1.00**	0	**-0.75**	**-0.67**	14ψ2
	θ	-3.60e-03		0	-1.60e-03		15e
10	x	-0.01		0	-0.01		15ψ1
	y	**-3.49**	**-1.00**	0	**-1.55**	**-1.54**	15ψ2
	θ	-4.10e-03		0	-1.30e-03		16e
11	x	-0.01		0	-0.01		16ψ1
	y	**-4.58**	**-1.00**	0	**-0.84**	**-0.81**	16ψ2
	θ	-4.10e-03		0	2.20e-03		17e
				0			17ψ1
				0			17ψ2
				0			18e
				0			18ψ1
				0			18ψ2
		total actuation (mm)		8.74			

e= bar/beam elongation.   ψ1 & ψ2= beam rotation at ends 1 & 2.
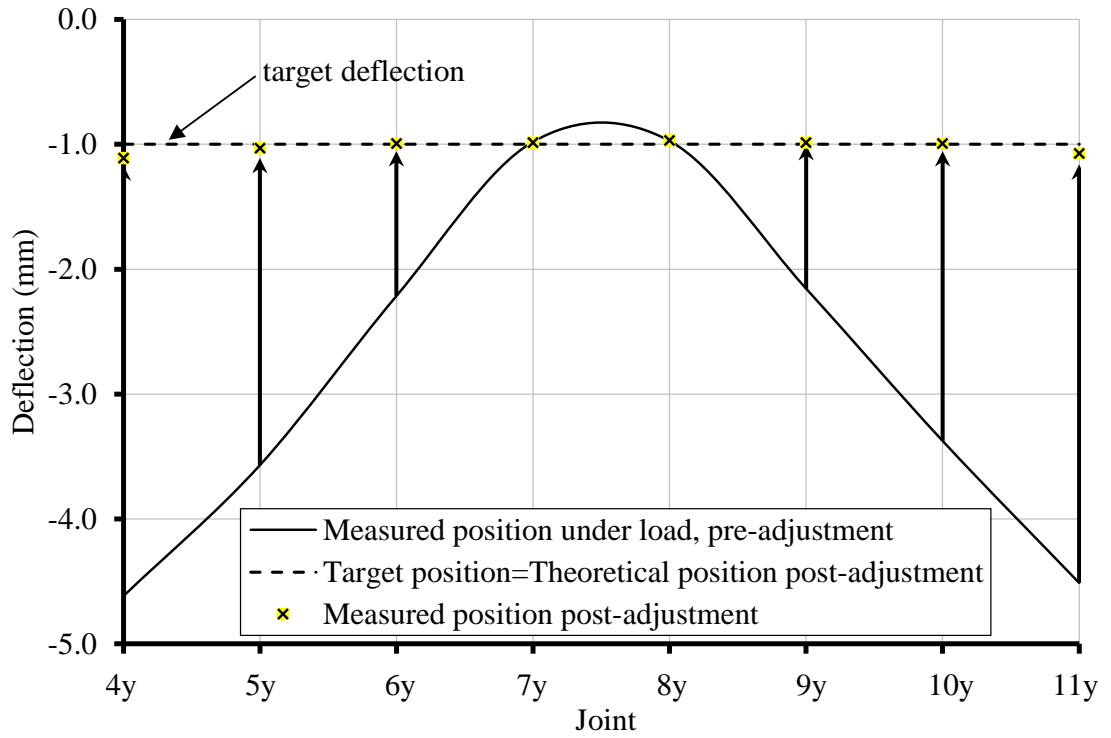
Figure 4.19: Displacement control of the structure in Figure 4.1 with eight elements of $\mathbf{e_o}$.
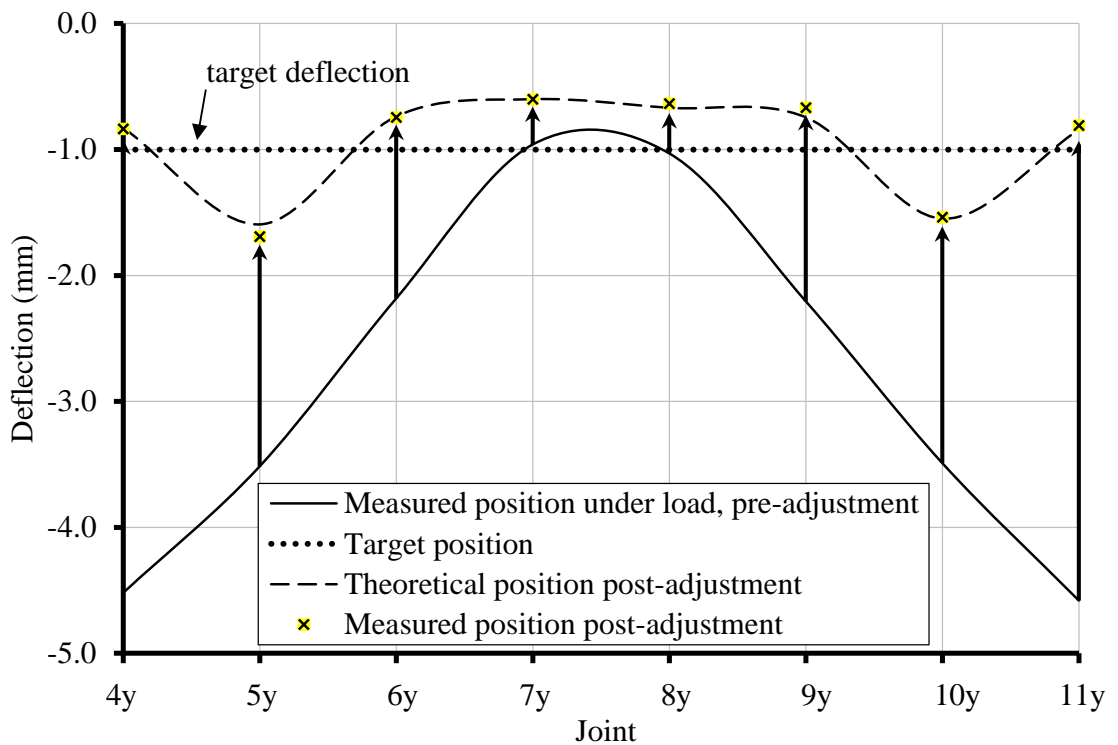
Figure 4.20: Displacement control of the structure in Figure 4.1 with four elements of $\mathbf{e_o}$
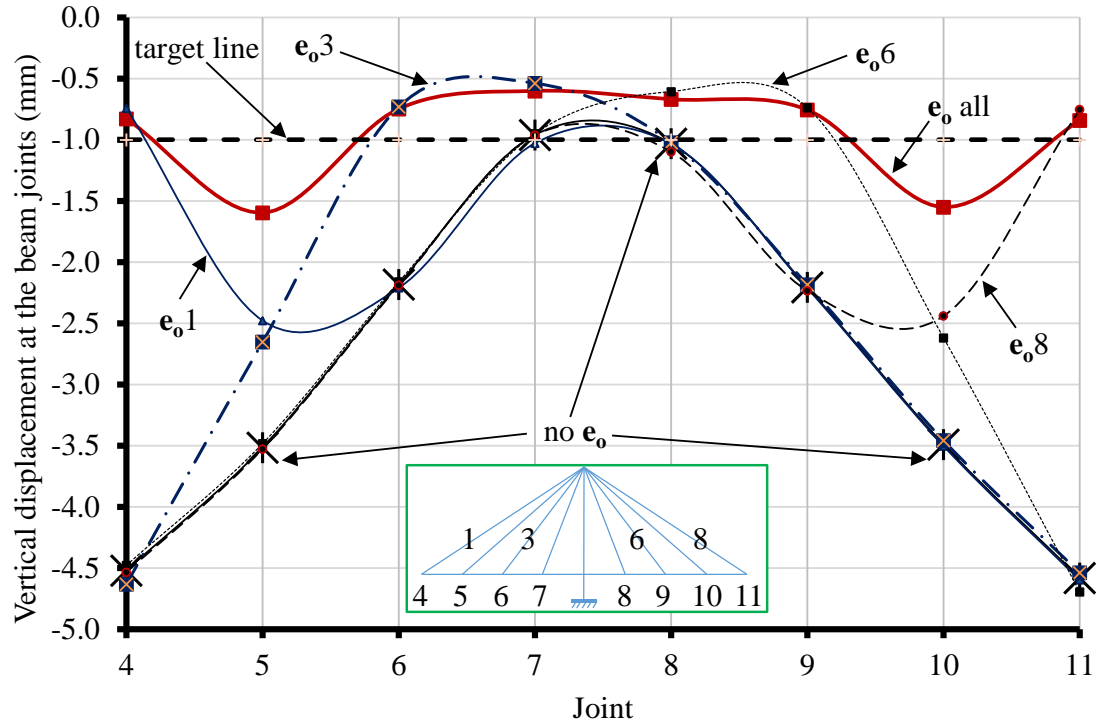
Figure 4.21: Changing vertical displacement of beam joints due to the actuation in individual cable.

4.4.2.1.2 Controlling Bar Forces without Regard to Displacement

Bar force control without regard to displacements as an application of Eqn. 3.16 in Section 3.2.3, is now experimentally explored and shown in Tables 4.4 and 4.5 (Experiments 3 and 4). Similar to controlling the displacements without regard to bar forces, all bar forces can be controlled by having actuators in the cables of the model, see Table 4.4 and the further details in Figure 4.22. Column 4 of Table 4.4 shows the computed e_o which must be applied in order that the cable tension due to load (Column 2) become the target tension value (Column 3) of 34.0N. Column 6 shows the resultant experimentally measured results, which are very close to that theoretically possible (Column 5). This small error is to be expected in practice especially due to imprecise actuation control in the mechanical actuators. However, this type of error can be reduced by extra iteration of adjustment as explained in Section 4.4.2.3.

Table 4.4: Control of bar forces in the structure in Figure 4.1 with eight elements of $\mathbf{e_o}$
(MATLAB program can be found in Appendix A.4).

(1)	(2)	(3)	(4)	(5)	(6)
	Exp3 (8-Cable model, adjustment in only 8 elements in e_o)				
Bar force/ actuation	Just $\mathbf{t_P}$, no $\mathbf{e_o}$ (N)	target tension (N)	$\mathbf{e_{o8}}$ (mm)	8 elements in $\mathbf{e_o}$ (N) Theo. results	8 elements in $\mathbf{e_o}$ (N) Exp. results
1axial	**35.97**	**34.00**	**-0.80**	**34.00**	**34.79**
2axial	**33.77**	**34.00**	**-1.43**	**34.00**	**35.16**
3axial	**34.63**	**34.00**	**-1.73**	**34.00**	**34.16**
4axial	**18.78**	**34.00**	**-1.78**	**34.00**	**34.61**
5axial	**16.84**	**34.00**	**-2.48**	**34.00**	**34.65**
6axial	**33.31**	**34.00**	**-3.27**	**34.00**	**35.85**
7axial	**36.05**	**34.00**	**-3.44**	**34.00**	**34.52**
8axial	**34.20**	**34.00**	**-3.58**	**34.00**	**34.82**
9axial	-30.55		0	-28.83	
9rot.1	0.00		0	0.00	
9rot.2	22.18		0	-315.78	
10axial	-59.80		0	-58.27	
10rot.1	22.18		0	-315.78	
10rot.2	-272.83		0	-900.01	
11axial	-81.66		0	-79.72	
11rot.1	-272.83		0	-900.01	
11rot.2	35.23		0	-1044.59	
12axial	-89.56		0	-93.82	
12rot.1	35.23		0	-1044.59	
12rot.2	-1810.06		0	1635.14	1490.38
13axial	-89.57		0	-95.21	
13rot.1	-1970.78		0	2579.63	2385.31
13rot.2	28.49		0	-753.89	
14axial	-81.68		0	-80.29	
18rot.2	0.00		0	0.00	
	total actuation (mm)		18.51		

axial = bar/beam tension (elongation).

rot.1 & rot.2= beam moment (rotation) at ends 1 & 2.
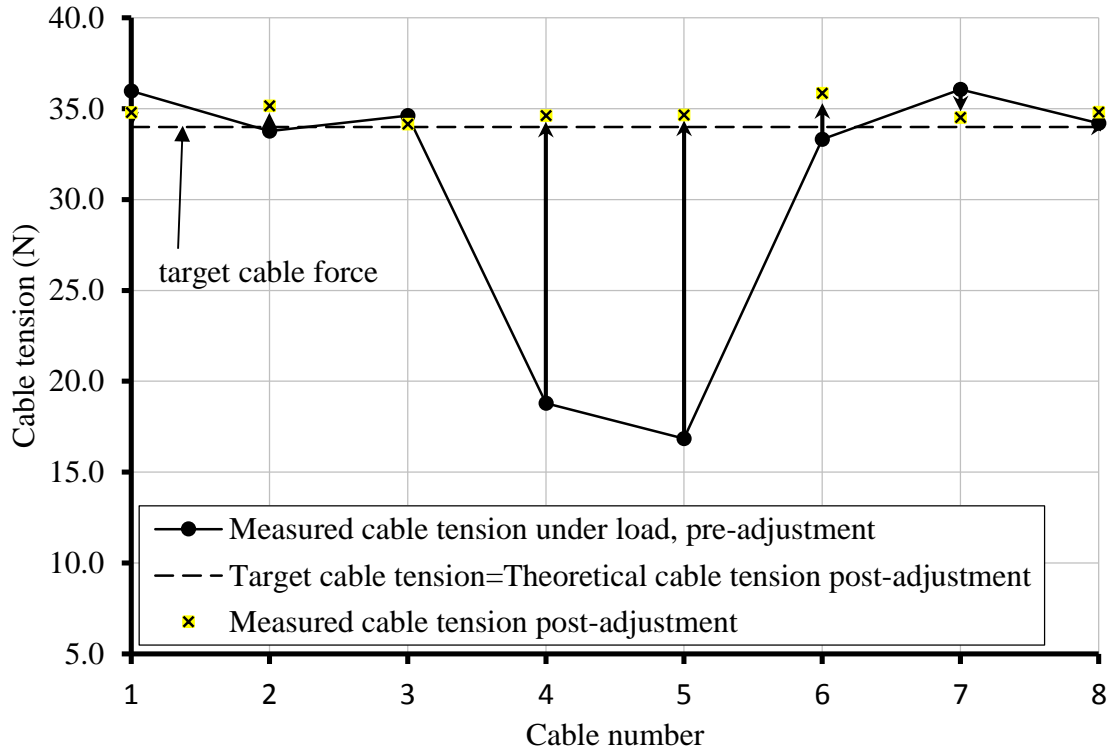
Figure 4.22: Controlling bar forces control of the 8-cable bridge model with eight elements of e_o.

In contrast to controlling in bar force with eight actuators, it is impossible to control the eight cable forces (to change their values to 34.0N) by using just four actuators, as shown in Table 4.5. Just as every single cable of the bridge structure has a direct effect on the one joint to which it is connected, it is also true that the actuator of a cable has high input on the force of that particular cable, but not as much effect on the forces of other cables. In this case, the MATLAB software gives required e_o (Column 4) and resultant set of results as shown in the Column 5 of Table 4.5. The set of e_o values contains both positive and negative amount of actuation, so some tension forces would be reduced while others are increased. Figure 4.23 gives a graphical view of the comparison between theoretical and experimental results, where the experimental results are very close to that theoretically achievable, but neither is all that close to the target state of constant 34.0N for all cables. The extent to which the actuator in one cable can change the tensile force in neighbouring cables is shown in Figure 4.24, where it is clear that each actuator has little effect on cable to other than the cable to which it is connected.

Table 4.5: Control of bar forces in the structure in Figure 4.1 with four elements of e_o (MATLAB program is shown in Appendix A.5).

(1)	(2)	(3)	(4)	(5)	(6)
Bar force/ actuation	**Exp4 (8-Cable model, adjustment in only 4 elements in e_o)**				
	Just t_P, no e_o (N)	target tension (N)	e_{o4} (mm)	4 elements in e_o (N) Theo. results	4 elements in e_o (N) Exp. results
1axial	**35.11**	**34.00**	**-0.62**	**37.20**	**37.58**
2axial	**33.65**	**34.00**	0	**34.31**	**34.65**
3axial	**34.09**	**34.00**	0.67	**27.50**	**27.70**
4axial	**18.47**	**34.00**	0	**22.97**	**23.38**
5axial	**16.52**	**34.00**	0	**21.83**	**22.45**
6axial	**33.80**	**34.00**	0.74	**26.71**	**28.01**
7axial	**35.56**	**34.00**	0	**34.15**	**35.22**
8axial	**33.37**	**34.00**	-1.12	**37.32**	**38.19**
9axial	-30.55		0	-32.37	
9rot.1	0.00		0	0.00	
9rot.2	22.18		0	380.75	
10axial	-59.80		0	-62.14	
10rot.1	22.18		0	380.75	
10rot.2	-272.83		0	582.18	
11axial	-81.66		0	-79.63	
11rot.1	-272.83		0	582.18	
11rot.2	35.23		0	-335.16	
12axial	-89.56		0	-89.36	
12rot.1	27.48		0	-335.16	
12rot.2	-1784.59		0	-1932.09	-1938.28
13axial	-89.57		0	-89.33	
13rot.1	-1957.60		0	-2135.00	-2173.65
13rot.2	28.49		0	-385.12	
14axial	-81.64		0	-79.24	
18rot.2	0.00		0	0.00	
total actuation (mm)			3.15		

axial = bar/beam tension (elongation).

rot.1 & rot.2= beam moment (rotation) at ends 1 & 2.
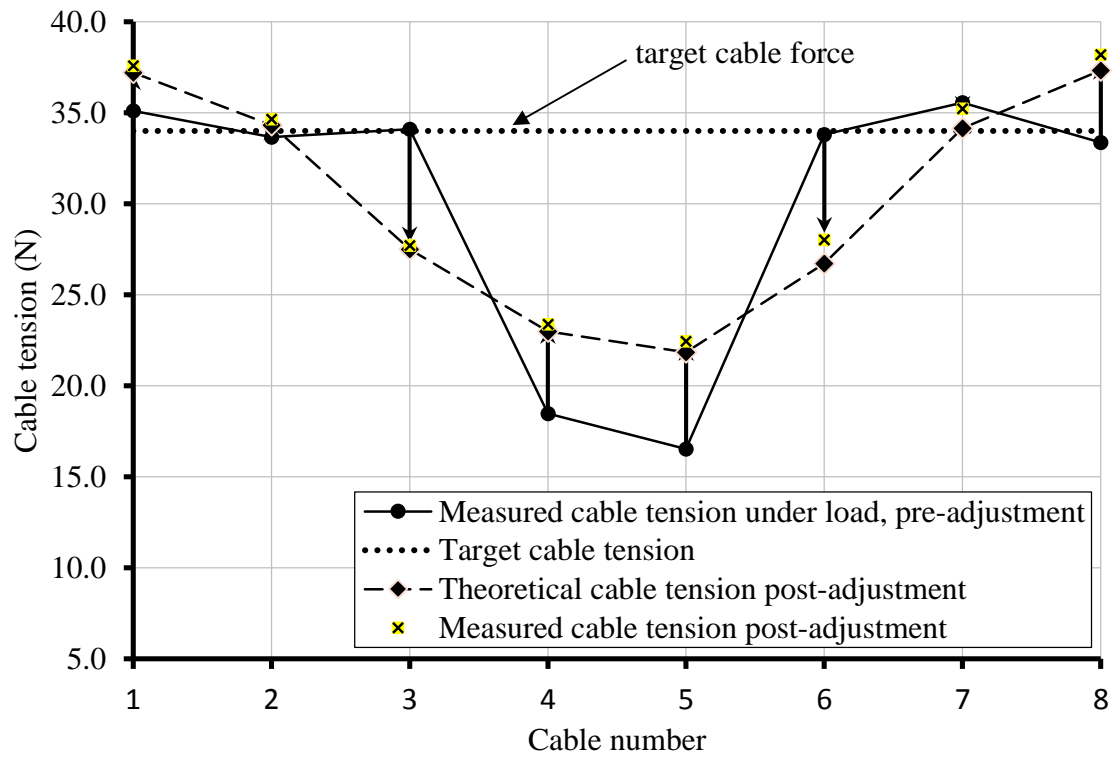
Figure 4.23: Controlling bar forces control of the 8-cable bridge model with four elements of $\mathbf{e_o}$.

Figure 4.24: Changing tension in cables due to the actuation in cables individually

4.4.2.1.3 Simultaneous Control of Displacement and Bar Force

As an application of Eqn. 3.19 in Section 3.2.4 simultaneously controlling both joint displacement and bar force, Experiments 5 and 6 were carried out and the results are shown in Tables 4.6 and 4.7 respectively. In experiment 5, eight joint displacements and eight bar forces were simultaneously controlled by using the eight actuators in the eight cables, while in the experiment 6, the same aim was attempted with only four actuators. Clearly, based on the experience of the last two subsections, it would be difficult to control such large number of displacement and force variables with only a few actuators.

Columns 3 and 4 of Table 4.6 show the measured displacement and cable tension (and two moments) of the loaded bridge model without about control. It is supposed that the desired target is to raise all the joints such that all the beam deflections are 0.0mm (Column 5), while at the same time, the cable forces are all to be a constant 30.0N (Column 8). The calculated set of actuation, with all eight actuators in action, is shown in Column 11. Since there is a certain amount of conflict between the displacement requirements (which would involve shortening of all the turnbuckles) and the cable force requirements (where five of the eight cables need to be lengthened to reduce their tension to 32.0N), the resultant theoretically possible state of displacements and cable tensions was always unlikely to be perfect. Indeed, when the e_0 is applied, Columns 6 and 9 show a good, but not perfect, possible achievement of the desired state of displacements and tension, which is well matched by experimentally measured values in Columns 7 and 10. Figures 4.25 and 4.26 show this comparison.

Although the eventual state was not very close to the originally target state, the experiment merely showed the original target was very exacting, and, with the given actuators, could only be approximated in a least-squares-error sense. Nevertheless, what was achieved was still good, where the root mean square (rms) error for displacement has gone from 3.15mm to 0.53mm, and 7.87N to 2.93N for cable tension.

Table 4.6: Simultaneous displacement and cable forces control of the eight-cable structure with eight actuators in **e₀** (MATLAB program can be found in Appendix A.4).

(1) Joint	(2) Dir	(3)	(4)	(5)	(6)	(7)	(8)	(9)	(10)	(11)	(12)
		Exp5 (8-Cable model, adjustment in only 8 elements in e₀)									Bar force/ actuation
		no **e₀** Theo. & Exp.		target disp	Theo. disp	Exp. measured disp	target tension	Theo. tension	Exp. measured tension	e₀₈	
		d_p	t_p	(mm)	(mm)	(mm)	(N)	(N)	(N)	(mm)	
1	x	0.09	**35.20**		0.18	0.18	**30.00**	**35.05**	**35.38**	**-1.84**	1axial
	y	0.00	**33.24**		0.00		**30.00**	**33.99**	**34.43**	**-1.78**	2axial
	θ	0.00	**36.44**		-0.20e-3		**30.00**	**32.50**	**32.91**	**-1.35**	3axial
2	x	0.00	**17.48**		0.00		**30.00**	**30.86**	**30.56**	**-1.44**	4axial
	y	0.00	**15.27**		0.00		**30.00**	**30.29**	**30.24**	**-2.01**	5axial
	θ	0.00	**28.88**		0.00		**30.00**	**31.04**	**29.36**	**-2.40**	6axial
3	x	0	**36.13**		0.00	0.00	**30.00**	**31.88**	**31.80**	**-1.96**	7axial
(Fixed)	y	0	**32.11**		0.00	0.00	**30.00**	**32.64**	**32.77**	**-2.06**	8axial
	θ	0	-30.55		0.00	0.00		-30.42		0	9axial
4	x	0.01	0.00		0.01			0.00		0	9rot.1
	y	**-4.53**	22.18	**0.00**	**-0.60**	**-0.68**		-2.14		0	9rot.2
	θ	4.10e-3	-59.80		1.50e-3			-60.24		0	10axial
5	x	0.01	22.18		0.01			-2.14		0	10rot.1
	y	**-3.53**	-272.8	**0.00**	**-0.51**	**-0.52**		-164.60		0	10rot.2
	θ	4.10e-3	-81.66		1.50e-3			-79.52		0	11axial
6	x	0.00	-272.83		0.00			-164.60		0	11rot.1
	y	**-2.19**	35.23	**0.00**	**-0.08**	**-0.09**		-752.44		0	11rot.2
	θ	3.60e-3	-89.56		1.10e-3			-92.87		0	12axial
7	x	0.00	35.23		0.00			-752.44		0	12rot.1
	y	**-0.95**	-1773.17	**0.00**	**0.16**	**0.16**		864.03	693.81	0	12rot.2
	θ	3.10e-3	-89.57		-0.80e-3			-94.22		0	13axial
8	x	-0.00	-2015.57		0.00			1671.24	1588.74	0	13rot.1
	y	**-1.08**	28.49	**0.00**	**0.53**	**0.55**		-904.67		0	13rot.2
	θ	-3.10e-3	-81.64		2.80e-3			-80.17		0	14axial
9	x	-0.00	28.49		0.00			-904.67		0	14rot.1
	y	**-2.24**	-270.44	**0.00**	**0.77**	**0.80**		-974.17		0	14rot.2
	θ	-3.60e-3	-59.84		-1.20e-3			-56.93		0	15axial
10	x	-0.01	-270.44		-0.01			-974.17		0	15rot.1
	y	**-3.55**	6.34	**0.00**	**-0.03**	**0.00**		97.30		0	15rot.2
	θ	-4.10e-3	-30.47		-3.00e-3			-30.93		0	16axial
11	x	-0.01	6.34		-0.01			97.30		0	16rot.1
	y	**-4.70**	0.00	**0.00**	**-0.75**	**-0.76**		0.00		0	16rot.2
	θ	-4.10e-3	-162.81		-2.80e-3			-185.53		0	17axial
			0.00					0.00		0	17rot.1
			10.07					1066.69		0	17rot.2
			-171.37					-171.37		0	18axial
			0.00					0.00		0	18rot.1
			0.00					0.00		0	18rot.2
									total actuation (mm)	14.84	

axial = bar/beam tension (elongation).

rot.1 & rot.2 = beam moment (rotation) at ends 1 & 2.

Figure 4.25: Displacement results in the simultaneous control of displacement and cable forces of the eight-cable structure, with eight actuators in $\mathbf{e_0}$.

Figure 4.26: Cable force results in the simultaneous control of displacement and cable forces of the eight-cable structure, with eight actuators in $\mathbf{e_0}$.

As with previous experiments, the same control target was carried out with only four actuators in the eight-cable model, see results for experiment 6 in Table 4.7. The measured displacements (Column 3) and cable tension (Column 4) are to be controlled to achieve the same corresponding targets (Columns 5 and 8), and the 4-element set of calculated actuation is in Column 11. After application of this e_0, the experimentally measured displacements (Column 7) and cable tension (Column 10) show very good correlation with the theoretically possible counterparts (Columns 6 and 9), but the achieved state is expectedly more imperfect than that achieved with eight actuators. For controlling with only four actuators, the rms error for displacement has gone from 3.12mm to 2.64mm, and 7.64N to 6.01N for cable tension. There is only small improvement in the rms error when only four actuators are used for controlling, but the rms error improvement was approximately five and two times better for displacement and cable tension respectively.

The comparative results are also shown in Figures 4.27 and 4.28. While the actuation has been able to considerably "moderate" the cable tension so that the resultant values do fluctuate around 30.0N better than the original values, it is also true that none of the displacements (which are originally all below 0.0mm) has been brought up to 0.0mm. This is probably due to a serious conflict of requirements in the target state: the two outermost beam joints (4 and 11) had the largest deflections and thus required the largest shortening of associated cables (1 and 8) to raise the beam at these points, but yet, the outer cables already had tension values well above 30.0N and thus required the actuations there to lengthen the associated cables. The desired target thus presented an internally conflicting set of requirements, which the algorithm could only partially "solve", giving in the end a compromise where the deflections were raised (though not enough) but the cable tension values were also far more regular with an average value of 31.61 N.

In summary, experiments with the eight-cable model have shown that the shape adjustment algorithms proposed in Chapter 3 have worked very well to even simultaneously control displacements and cable tension. The cable-stayed bridge happened to be a structure where an actuator had a strong direct control on one local area (i.e. its own cable tension and the vertical displacement of the joint to which the cable is connected) but much less control of areas further away; this has resulted in very good control where the target state has been attainable.

Table 4.7: Simultaneous displacement and bar forces control in the eight-cable structure with four actuators in **e$_o$** (MATLAB program is shown in Appendix A.5).

(1)	(2)	(3)	(4)	(5)	(6)	(7)	(8)	(9)	(10)	(11)	(12)
		Exp6 (8-Cable model, adjustment in only 4 elements in e$_o$)									Bar force/ actuation
		no **e$_o$**		target disp	Theo. disp	Exp. measured disp	target tension	Theo. tension	Exp. measured tension	**e$_{o4}$** (mm)	
Joint	Dir	Theo. & Exp.									
		d$_p$	**t$_p$**	(mm)	(mm)	(mm)	(N)	(mm)	(N)		
1	x	0.08	35.97		0.07	0.11	30.00	39.42	39.03	-0.97	1axial
	y	0.00	36.79		0.00		30.00	35.03	34.83	0	2axial
	θ	0.00	34.22		0.00		30.00	29.07	29.55	0.54	3axial
2	x	0.00	19.82		0.00		30.00	23.79	23.89	0	4axial
	y	0.00	17.40		0.00		30.00	22.97	22.98	0	5axial
	θ	0.00	35.76		0.00		30.00	28.52	28.79	0.76	6axial
3	x	0.00	37.03		0.00	0.00	30.00	34.89	34.83	0	7axial
(Fixed)	y	0.00	34.71		0.00	0.00	30.00	39.31	39.01	-1.30	8axial
	θ	5.00e-3	-30.55		0.00	0.00		-33.56		0	9axial
4	x	0.01	0.00		0.01			0.00		0	9rot.1
	y	**-4.52**	22.18	**0.00**	**-3.00**	**-2.86**		615.22		0	9rot.2
	θ	4.10e-3	-59.80		-0.30e-3			-61.40		0	10axial
5	x	0.01	22.18		0.01			615.22		0	10rot.1
	y	**-3.41**	-272.8.	**0.00**	**-3.26**	**-3.23**		544.86		0	10rot.2
	θ	4.10e-3	-81.66		1.00e-3			-79.85		0	11axial
6	x	0.00	-272.83		0.00			544.86		0	11rot.1
	y	**-2.19**	35.2.	**0.00**	**-2.63**	**-2.62**		-267.85		0	11rot.2
	θ	3.60e-3	-89.56		3.50e-3			-89.36		0	12axial
7	x	0.00	35.23		0.00			-267.85		0	12rot.1
	y	**-0.99**	-1826.74	**0.00**	**-1.14**	**-1.14**		-1970.84	-1979.56	0	12rot.2
	θ	3.10e-3	-89.57		4.00e-3			-89.32		0	13axial
8	x	0.00	-2019.08		0.00			-2207.98	-2230.74	0	13rot.1
	y	**-1.05**	28.49	**0.00**	**-1.25**	**-1.28**		-398.74		0	13rot.2
	θ	-3.10e-3	-81.64		-4.40e-3			-79.11		0	14axial
9	x	0.00	28.49		0.00			-398.74		0	14rot.1
	y	**-2.25**	-270.44	**0.00**	**-2.85**	**-2.91**		858.10		0	14rot.2
	θ	-3.60e-3	-59.84		-3.40e-3			-62.14		0	15axial
10	x	-0.01	-270.44		-0.01			858.10		0	15rot.1
	y	**-3.54**	6.34	**0.00**	**-3.34**	**-3.43**		795.41		0	15rot.2
	θ	-4.10e-3	-30.47		0.00e-3			-34.47		0	16axial
11	x	-0.01	6.34		-0.01			795.41		0	16rot.1
	y	**-4.64**	0.00	**0.00**	**-2.60**	**-2.69**		0.00		0	16rot.2
	θ	-4.10e-3	-162.81		1.70e-3			-164.88		0	17axial
			0.00					0.00		0	17rot.1
			10.07					-37.49		0	17rot.2
			-171.37					-171.37		0	18axial
			0.00					0.00		0	18rot.1
			0.00					0.00		0	18rot.2
								total actuation (mm)		3.57	

axial = bar/beam tension (elongation).

rot.1 & rot.2= beam moment (rotation) at ends 1 & 2.
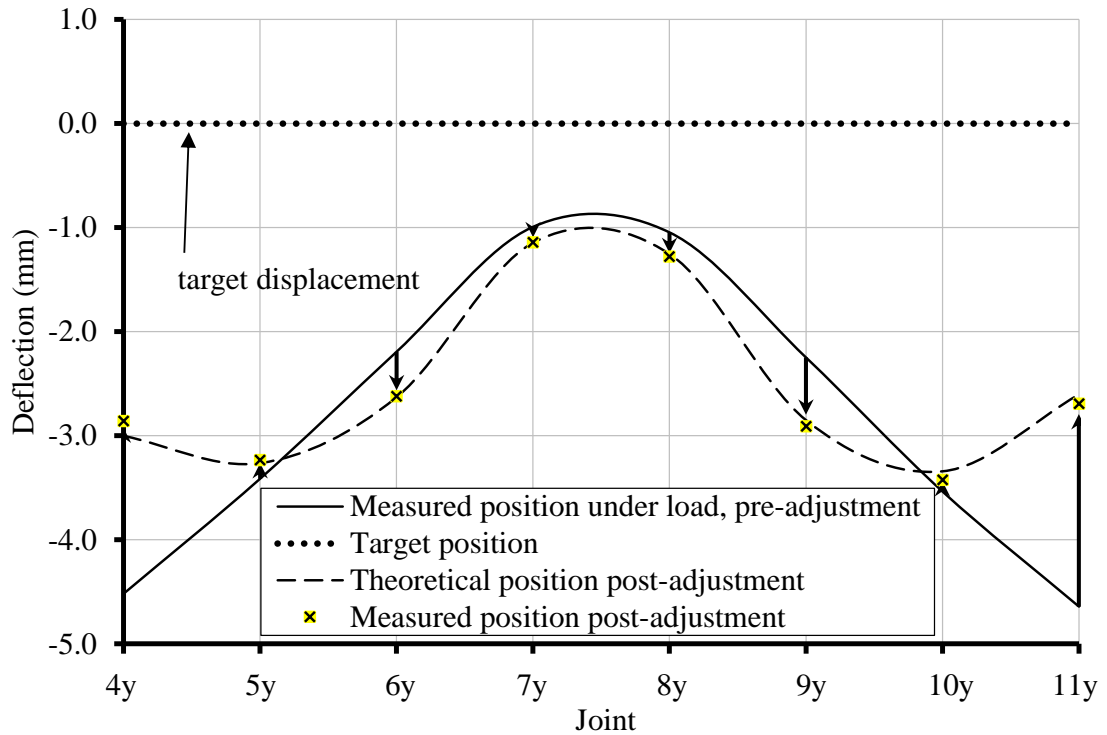
Figure 4.27: Displacement results in the simultaneous control of the structure in Figure 4.1 with four elements of $\mathbf{e_o}$.
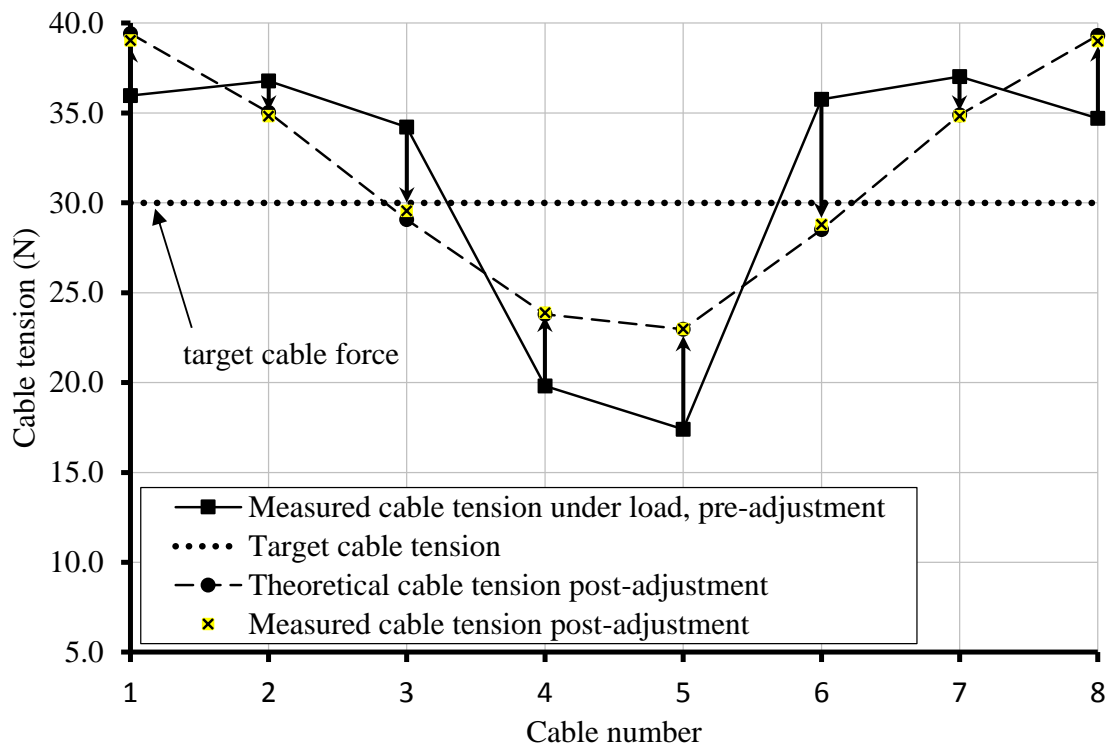
Figure 4.28: Bar force results in the simultaneous control of the structure in Figure 4.1 with four elements of $\mathbf{e_o}$.

4.4.2.2 Four Cables Model of Cable Stayed Bridge

The bridge model in Section 4.4.2.1 contained eight cables, which had the consequence of both the level of prestress being rather low, and there was a significant degree of "interplay" between adjacent cables in that shortening of one to increase its tensile force also simultaneously reduced the tension of its neighbouring cables. Consequently, the bridge model had four cables taken off (two each side, see Figure 4.14), and the shape adjustment exercise were carried out again, and this time, with more than one iteration in attempt to better attain the target geometry. The model was tested under two vertical point loads of 57.12N applied at joints 5 and 9 with another two vertical point loads 28.56N on joints 4 and 11. Displacements were measured for all vertical displacements at beam joints and horizontally at the top joint of the tower. Moreover, cable forces and bending moments at the root both beams were again recorded. Three tests (Experiments 7, 8 and 9) were done for this model to control nodal displacement only, internal bar forces only, and then both nodal displacements and internal bar forces simultaneously. The results are presented in Tables 4.8, 4.9 and 4.10, respectively.

4.4.2.2.1 Control of Joint Displacement without Regard to Bar/Beam Forces

The results of the displacement control without regard to the bar forces for the four cable bridge model by using all four cable actuations is presented in Table 4.8 (Experiment 7). The target displacement of obtaining -2.5mm deflection (Column 5) in four joints connected to the cables was set and Eqn. 3.10 was used. The results comparison between the theoretical (Column 6) and experimental (Column 7) (Figure 4.29), show very good correlation with the target displacements for both, even though there were some large (-7.27 and -7.62) displacements being reduced to -2.50 with only subsequent errors of 3.77% and 2.73%. The results of other joints not connected to the cable were not adjusted to any desired values and were thus free to take any value, but it should be noted that there was also little discrepancy between practical and theoretical values. Furthermore, the theoretical displacement adjustment was also done for joints that were not directly connect to the cables as shown in Columns 8, 9 and 10 in Table 4.8. This test adjustment was done to see how effective could the displacement control of joints could be where those joints could only be indirectly affected by actuators

located in more remote parts of the structure. This results show that the present adjustment technique was capable to control joints that they have not a direct contact with.

Table 4.8: Displacement control of the structure in Figure 4.14 with four elements of $\mathbf{e_o}$ (MATLAB program can be found in Appendix A.6).

(1)	(2)	(3)	(4)	(5)	(6)	(7)	(8)	(9)	(10)	(11)
		Exp7 (4-Cable model, adjustment in only 4 elements in $\mathbf{e_o}$)								
		Joints connected to the cables					Joints did not connect to the cables			Bar actuation
Joint	Dir	Just $\mathbf{d_P}$, no $\mathbf{e_o}$ (mm)	target disp (mm)	$\mathbf{e_o}$ (mm)	4 elements in $\mathbf{e_o}$ (mm) Theo. results	4 elements in $\mathbf{e_o}$ (mm) Exp. results	target disp (mm)	$\mathbf{e_o}$ (mm)	4 elements in $\mathbf{e_o}$ (mm) Theo. results	
1	x	0.07		**-2.38**	0.07	0.02		**-5.40**	0.00	1e
	y	0.00		**-1.12**	0.00			**-0.23**	0.00	2e
	θ	0.00		**-1.34**	0.00			**-0.33**	0.00	3e
2	x	0.00		**-2.57**	0.00			**-5.43**	0.00	4e
	y	0.00		0	0.00			0	0.00	5e
	θ	0.00		0	0.00			0	0.00	5ψ1
3	x	0		0	0	0		0	0	5ψ2
(Fixed)	y	0		0	0	0		0	0	6e
	θ	0		0	0	0		0	0	6ψ1
4	x	0.01		0	0.01			0	0.01	6ψ2
	y	**-7.27**	**-2.50**	0	**-2.50**	**-2.68**		0	2.19	7e
	θ	4.90e-3		0	-0.10e-3			0	-10.00e-3	7ψ1
5	x	0.01		0	0.01			0	0.01	7ψ2
	y	**-5.99**		0	-3.03	2.99	**-1.50**	0	**-1.50**	8e
	θ	5.50e-3		0	0.80e-3			0	-7.30e-3	8ψ1
6	x	0.00		0	0.00			0	0.00	8ψ2
	y	**-4.01**	**-2.50**	0	**-2.50**	**-2.48**		0	-3.00	9e
	θ	7.30e-3		0	3.40e-3			0	0.80e-3	9ψ1
7	x	0.00		0	0.00			0	0.00	9ψ2
	y	**-1.44**		0	-1.02	1.02	**-1.50**	0	**-1.50**	10e
	θ	6.60e-3		0	4.40e-3			0	6.10e-3	10ψ1
8	x	0.00		0	-0.00			0	-0.00	10ψ2
	y	**-1.57**		0	-1.06	1.06	**-1.50**	0	**-1.50**	11e
	θ	-6.60e-3		0	-4.00e-3			0	-5.50e-3	11ψ1
9	x	-0.00		0	-0.00			0	-0.00	11ψ2
	y	**-4.24**	**-2.50**	0	**-2.50**	**-2.53**		0	-2.92	12e
	θ	-7.30e-3		0	-3.10e-3			0	-0.60e-3	12ψ1
10	x	-0.01		0	-0.01			0	-0.01	12ψ2
	y	**-6.30**		0	-2.95	2.99	**-1.50**	0	**-1.50**	13e
	θ	-5.60e-3		0	-0.70e-3			0	7.00e-3	13ψ1
11	x	-0.01		0	-0.01			0	-0.01	13ψ2
	y	**-7.62**	**-2.50**	0	**-2.50**	**-2.64**		0	2.02	14e
	θ	-5.00e-3		0	0.10e-3			0	9.50e-3	14ψ1
				0				0		14ψ2
		total actuation (mm)		7.41				11.16		

e= bar/beam elongation. ψ1 & ψ2= beam rotation at ends 1 & 2.
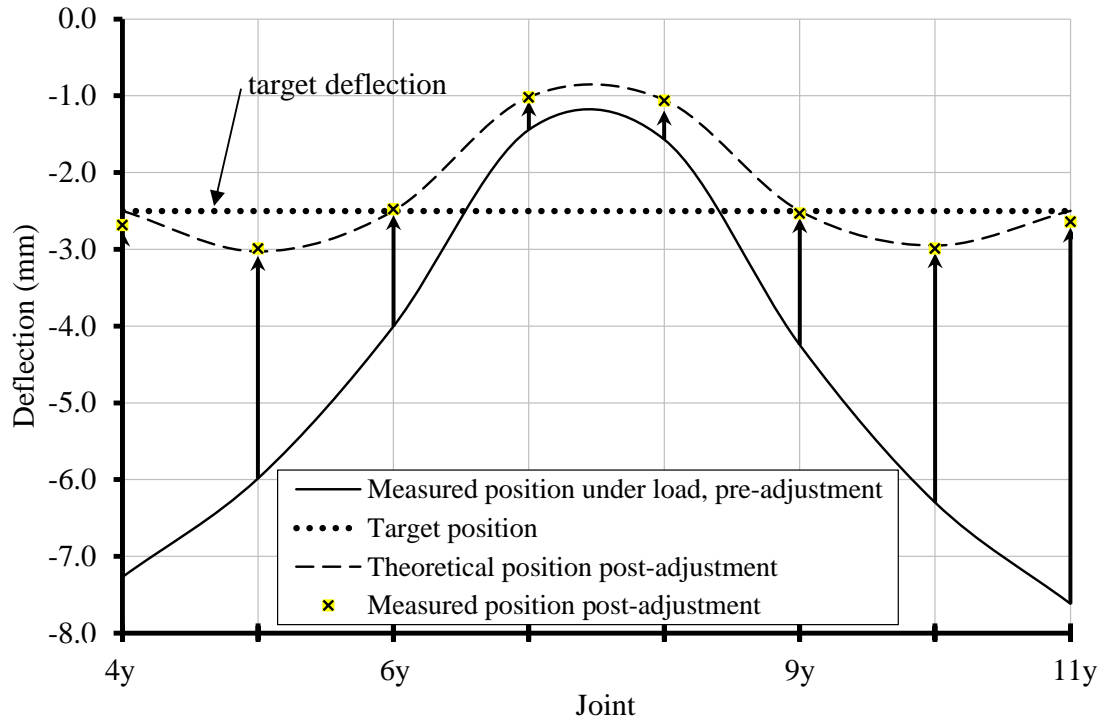
Figure 4.29: Displacement control of the structure in Figure 4.14 with four elements of **e₀**.

4.4.2.2.2 Experimental Bar Forces Control Regardless of Displacement

Table 4.9 and Figure 4.30 (Experiment 8) show the results of controlling four cable cable-stayed bridge model regarding to the bar force only. Theoretical results from the MATLAB program gives a set of **e₀** (Column 4) to control the bar force (Column 2) in all four cables to 61N (Column 3). It is interesting to note that, the magnitude of the components of **e₀** is not near-symmetrical, even though the loaded geometry of the structure is near-symmetrical, and the target geometry is symmetrical. This shows that there are several possible results of **e₀** and MATLAB program has selected one of them. Figure 4.30 shows theoretical results are very close to experimental results, as well as the target cable tension.

Table 4.9: Bar forces control of the structure in Figure 4.14 with four elements of e_o (MATLAB program is shown in Appendix A.6).

(1)	(2)	(3)	(4)	(5)	(6)
Bar force/ actuation	**Exp8 (4-Cable model, adjustment in only 4 elements in e_o)**				
	Just t_P, no e_o (N)	target tension (N)	e_o (mm)	4 elements in e_o (N) Theo. results	4 elements in e_o (N) Exp. results
1axial	**57.92**	**61.00**	**0.38**	**61.00**	**61.14**
2axial	**67.89**	**61.00**	**1.74**	**61.00**	**62.92**
3axial	**68.15**	**61.00**	**0.90**	**61.00**	**62.69**
4axial	**57.13**	**61.00**	**-1.50**	**61.00**	**61.59**
5axial	-52.13		0	-54.82	
5rot.1	0.00		0	0.00	
5rot.2	276.43		0	806.21	
6axial	-52.13		0	-54.82	
6rot.1	274.43		0	806.21	
6rot.2	552.86		0	1612.41	
7axial	-98.68		0	-96.79	
7rot.1	552.86		0	1612.41	
7rot.2	-853.35		0	-1065.53	
8axial	-98.68		0	-96.79	
8rot.1	-853.35		0	-1065.53	
8rot.2	-2278.16		0	-3766.42	-3776.44
9axial	-98.68		0	-97.31	
9rot.1	-2401.99		0	-3557.35	-3629.77
9rot.2	-857.01		0	-730.44	
10axial	-98.68		0	-97.31	
⋮					
14rot.2	0		0	0	
total actuation (mm)			4.52		

axial = bar/beam tension (elongation).

rot.1 & rot.2 = beam moment (rotation) at ends 1 & 2.
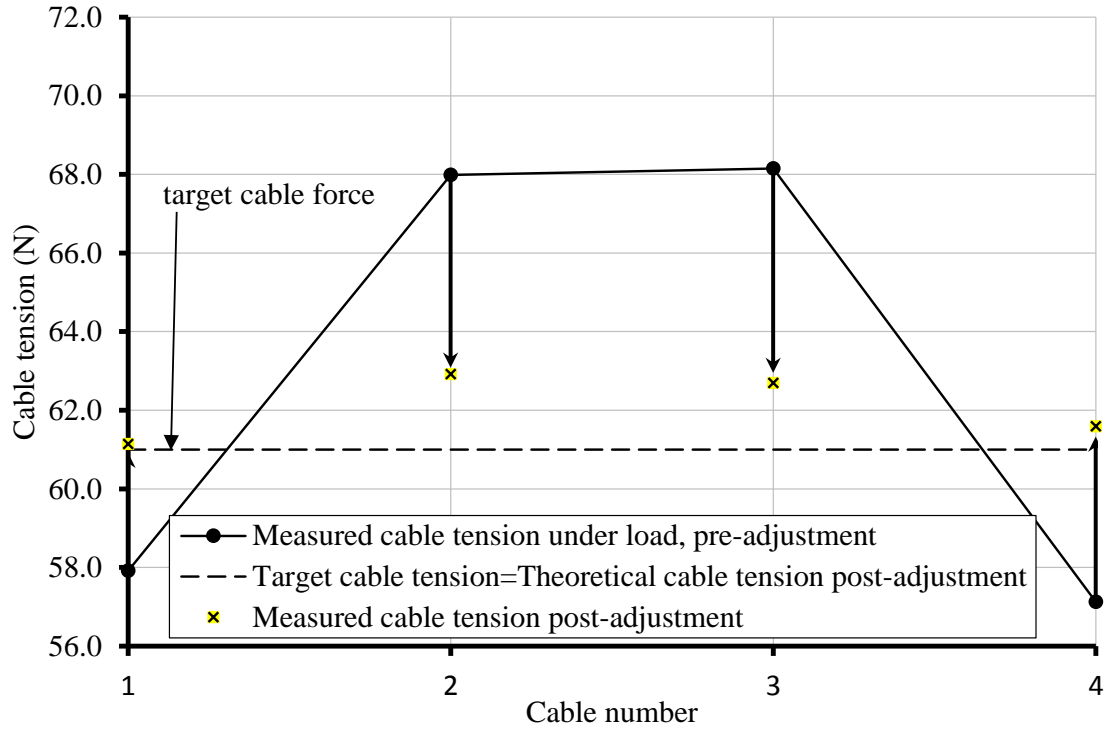
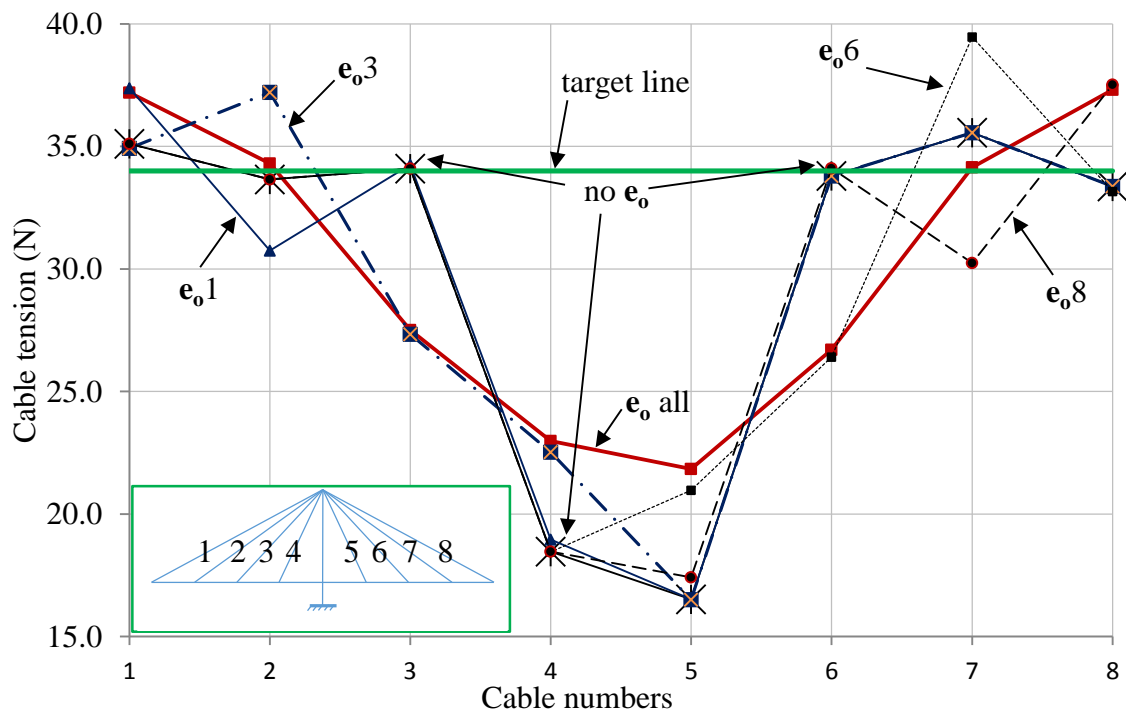Figure 4.30: Controlling bar forces control of the 4-cable bridge model with four elements of $\mathbf{e_o}$.

4.4.2.2.3 Simultaneous Control of Displacement and Bar Force

Experiment 9 was done to simultaneous control four joint displacements and four bar forces in the four cable bridge with actuators in all four cables, as shown in Table 4.10. The initial loaded structure displacements and internal forces as shown in Columns 3 and 4. The target of the experiment is -4.0mm deflection of the four joint selected (Column 5) and equalize all cable forces to 61N (Column 8). Equation 3.19 was used for achieving the set of $\mathbf{e_o}$ in Column11.

The comparisons of the theoretical with experimentally measured results of joint displacements (Column 6 and 7) and bar forces (Column 9 and 10) against joint number are also shown in Figures 4.31 and 4.32 respectively. Again, although the target state of combined displacement and cable force proved to be too demanding, nonetheless, a good approximation to this target state was achieved, and the values obtained experimentally matched again very closely the theoretically best possible results. This shows that had there been more actuators, or a target with less/no internally conflicting demands, then the target would have been achieved.

Table 4.10: Simultaneous displacement and bar forces control of the four-cable structure with four actuators in $\mathbf{e_o}$ (MATLAB program can be found in Appendix A.6).

(1)	(2)	(3)	(4)	(5)	(6)	(7)	(8)	(9)	(10)	(11)	(12)
		\multicolumn{7}{c}{Exp9 (4-Cable model, adjustment in only 4 elements in e_o)}					Bar force/ actuation
Joint	Dir	no $\mathbf{e_o}$		target disp	Theo. disp	Exp. measured disp	target tension	Theo. tension	Exp. measured tension	$\mathbf{e_{o4}}$ (mm)	
		Theo. & Exp.									
		$\mathbf{d_p}$	$\mathbf{t_p}$ (mm)	(mm)	(mm)	(mm)	(N)	(N)	(N)		
1	x	0.08	**58.15**		0.09	0.12	**61.00**	**62.31**	**62.30**	-2.31	1axial
	y	0.00	**68.81**		0.00		**61.00**	**61.71**	**63.31**	0.52	2axial
	θ	0.00	**69.13**		0.00		**61.00**	**61.36**	**62.67**	0.77	3axial
2	x	0.00	**56.95**		0.00		**61.00**	**61.36**	**61.69**	-2.13	4axial
	y	0.00	-52.13		0.00			-55.75		0	5axial
	θ	0.00	0.00		0.00			0.00		0	5rot.1
3	x	0.00	276.43		0.00	0.00		990.38		0	5rot.2
(Fixed)	y	0.00	-52.13		0.00	0.00		-55.75		0	6axial
	θ	0.00	276.43		0.00	0.00		990.38		0	6rot.1
4	x	0.01	552.86		0.01			1980.75		0	6rot.2
	y	**-8.27**	-98.68	**-4.00**	**-4.13**	**-4.21**		-97.58		0	7axial
	θ	4.90e-3	552.86		-3.40e-3			1980.75		0	7rot.1
5	x	0.01	-853.35		0.01			-570.16		0	7rot.2
	y	-6.03	-98.68		-4.64	-4.71		-97.58		0	8axial
	θ	5.50e-3	-853.35		-1.30e-3			-570.16		0	8rot.1
6	x	0.00	-2311.53		0.00			-3142.94	-3183.13	0	8rot.2
	y	**-4.04**	-98.68	**-4.00**	**-4.35**	**-4.43**		-97.36		0	9axial
	θ	7.30e-3	-2444.15		4.90e-3			-3316.83	-3491.50	0	9rot.1
7	x	0.00	-857.01		0.00			-617.55		0	9rot.2
	y	-1.47	-98.68		-1.85	-1.87		-97.36		0	10axial
	θ	6.60e-3	-857.01		7.90e-3			-617.55		0	10rot.1
8	x	0.00	543.63		0.00			2058.78		0	10rot.2
	y	-1.57	-52.10		-2.05	-2.12		-55.95		0	11axial
	θ	-6.60e-3	543.63		-8.30e-3			2058.78		0	11rot.1
9	x	0.00	271.81		0.00			1029.39		0	11rot.2
	y	**-4.25**	-52.10	**-4.00**	**-4.82**	**-5.01**		-55.95		0	12axial
	θ	-7.30e-3	271.81		-5.30e-3			1029.39		0	12rot.1
10	x	-0.01	0.00		-0.01			0.00		0	12rot.2
	y	-6.26	-163.35		-5.22	-5.42		-156.44		0	13axial
	θ	-5.60e-3	0.00		1.20e-3			0.00		0	13rot.1
11	x	-0.01	1.96		-0.01			-173.89		0	13rot.2
	y	**-7.59**	-171.37	**-4.00**	**-3.81**	**-3.96**		-171.37		0	14axial
	θ	-5.00e-3	0.00		3.30e-3			0.00		0	14rot.1
			0.00					0.00		0	14rot.2
							total actuation (mm)			5.73	

axial = bar/beam tension (elongation).
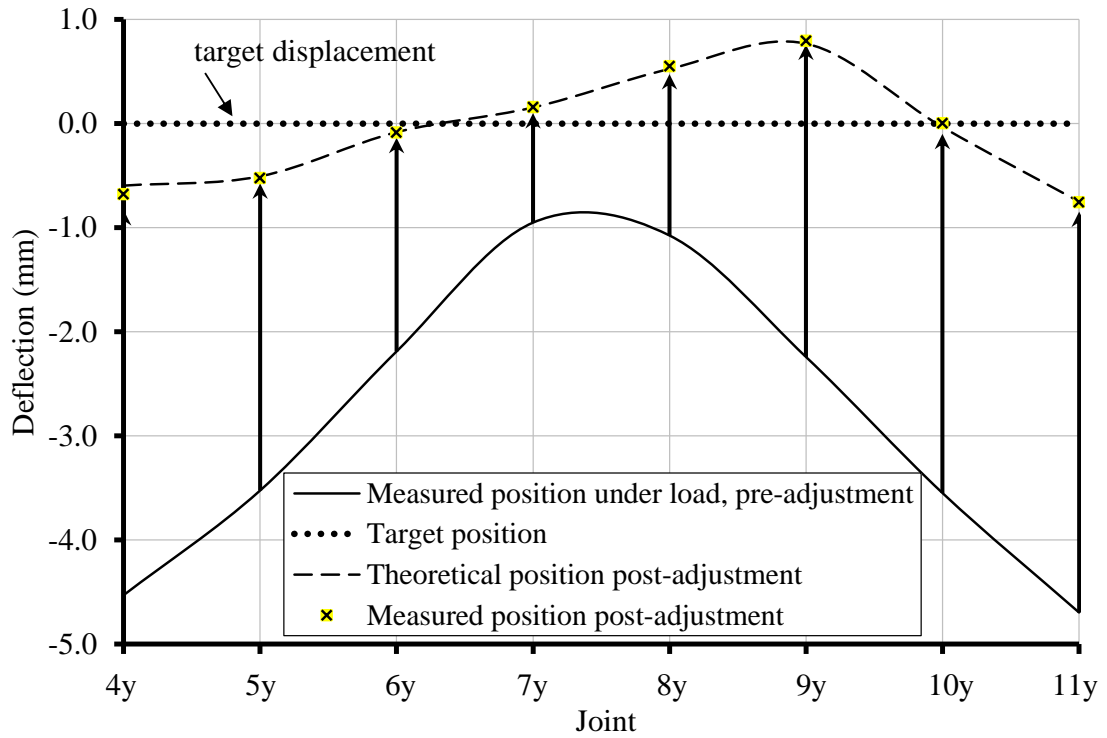
 rot.1 & rot.2= beam moment (rotation) at ends 1 & 2.
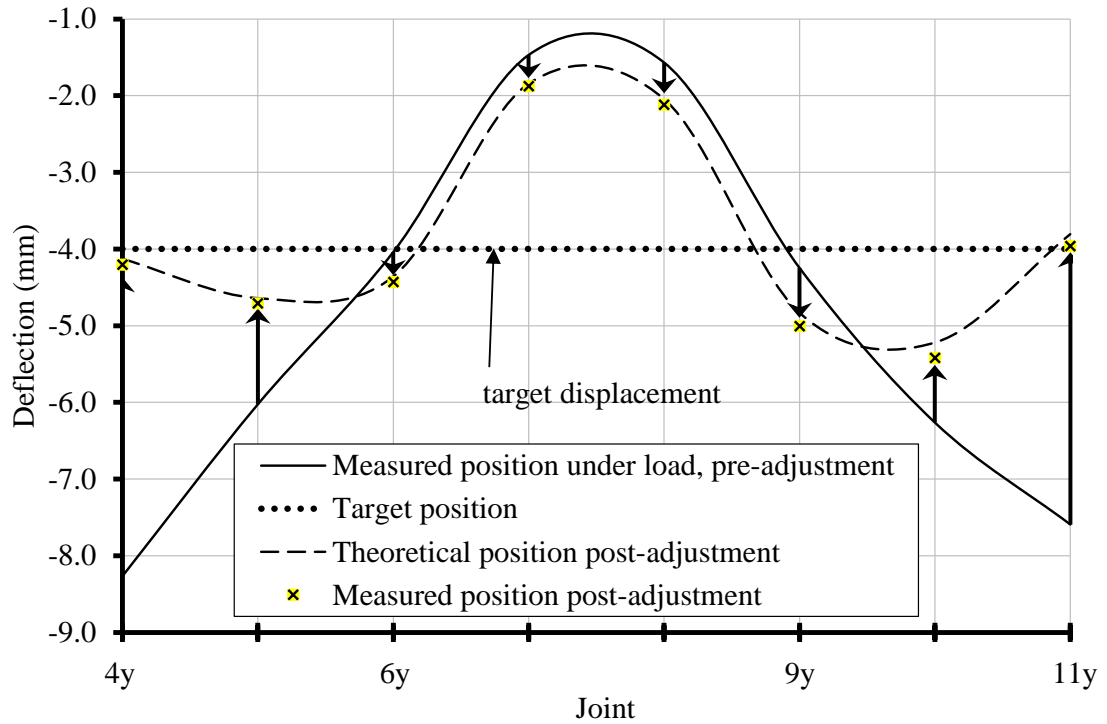
Figure 4.31: Displacement results in the simultaneous control of displacement and cable forces of the four-cable structure, with four actuators in $\mathbf{e_o}$.
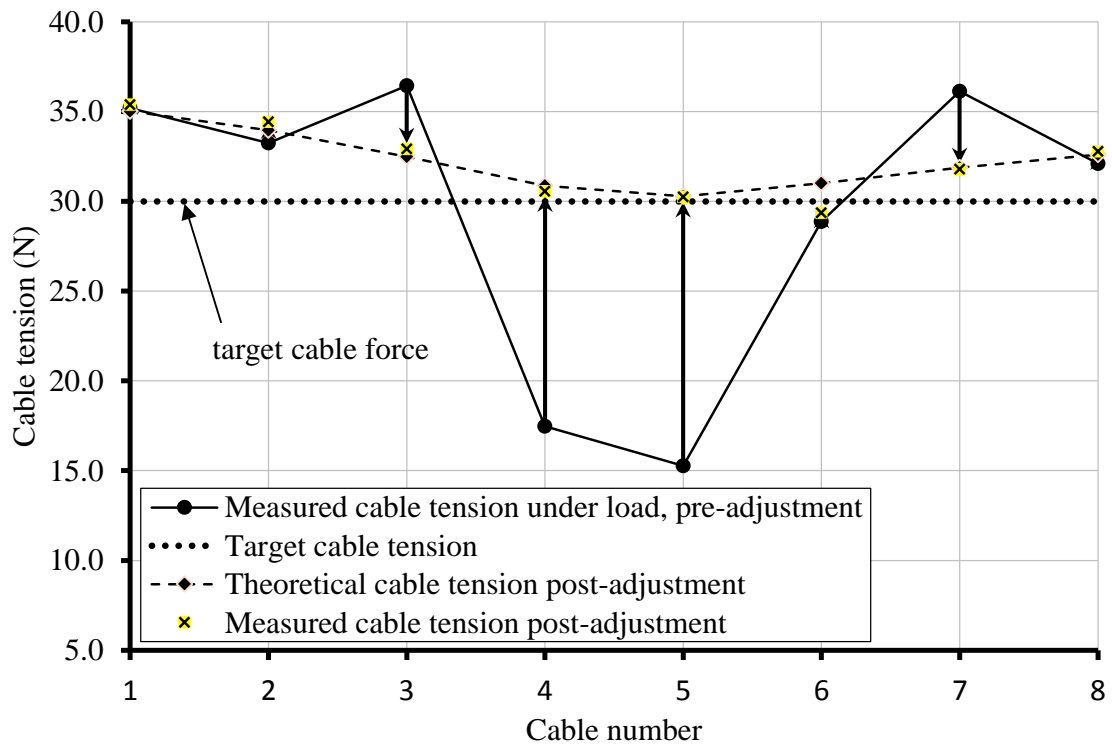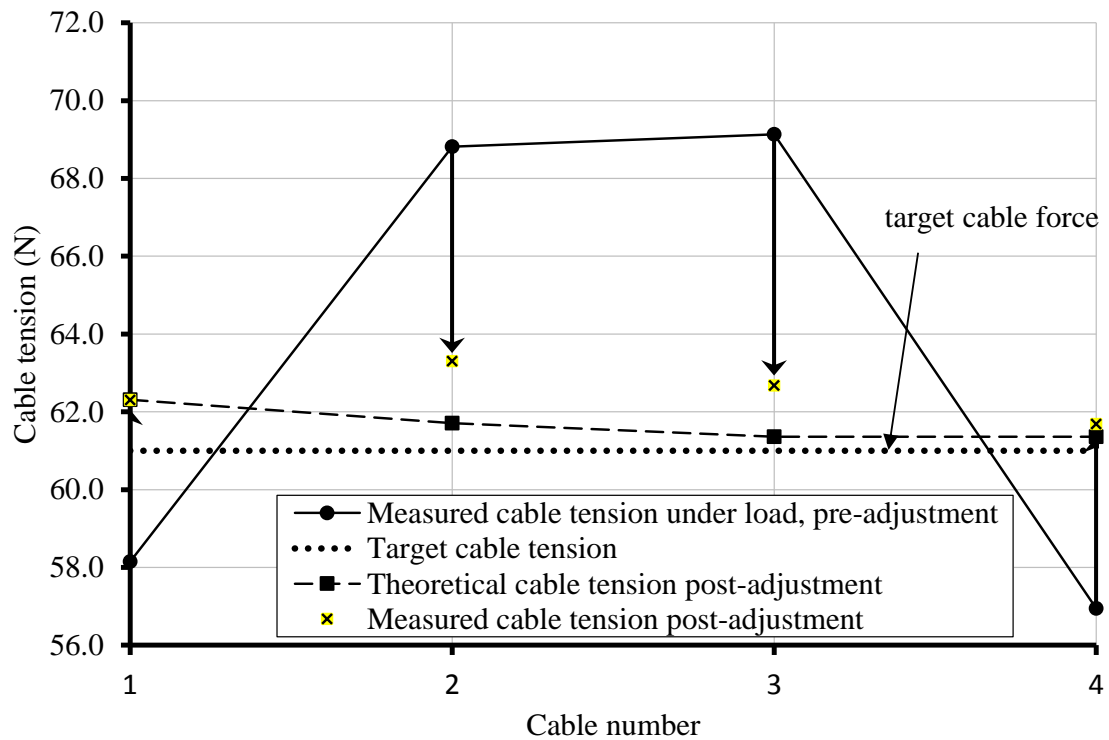

Figure 4.32: Cable forces results in the simultaneous control of displacement and cable forces of the four-cable structure, with four actuators in $\mathbf{e_o}$.

4.4.2.3 Multi-Iteration Adjustment to Remove Experimental Errors

In most cases, the structure adjusted for displacement/force can reach either the target state, or the theoretically possible least-error approximate, well with application of the $\mathbf{e_0}$ actuation calculated with the equations derived in Chapter 3. However, during the adjustment, small errors are possible, and this is principally caused by the difficulty to impose a precise length actuation using the mechanical turnbuckles. Although the turnbuckles have a pitch on their threads such that one revolution equated with a 1mm length change, it was difficult to enforce a rotation with a small hexagonal spanner more accurately than say 25-30°, which in turn is just under 0.1mm. An accuracy of 0.1mm can be significant when the actuations in $\mathbf{e_0}$ were typically only an order of magnitude higher. Furthermore, the steel turnbuckles fitted into the aluminium ends with a small amount of play, which meant that even without rotation of the turnbuckle, there was a free play (of the order of 0.2mm) in the length. Having cables taut generally helped, but it was clear that approaching a prescribed actuation from either tightening or loosening the turnbuckle produced different cable force results. As an additional measure, a micrometer was also used each time to check the amount of actuation. It was also evident that physical disturbance to the rather "fragile" structure also caused some changes to structure, especially bar forces, and hence there were typically still some small inaccuracies in the structure even after adjustment.

One way to minimise error is to have further iterations of adjustment. In this way, the state of the structure after the initial application of $\mathbf{e_0}$ is again measured, and another $\mathbf{e_0}$ is calculated, in attempt to adjust the structure from its current state further towards the target state. Such an experiment was conducted on the four cable model; Table 4.11 shows the results. Some of the nodal displacements after load (Column 3) are required to be controlled to -2.5mm (Column 4) and thus an $\mathbf{e_0}$ (Column 5) has been calculated using Eqn. 3.23. Displacements as a consequence of this adjustment made to the structure are in Column 7 (and also shown in Figure 4.33). Although the improvement is good, the individual displacement errors for joints 4y, 6y, 9y and 11y are 3.77%, 1.32%, 1.72% and 2.73% respectively, and the rms error is still 0.12. The error in the adjusted shape is judged to be too big and a further iteration of adjustment is carried out, using this once-adjusted state as the starting state.

The $\mathbf{e_o}$ for the second iteration (Column 8) is calculated again using Eqn. 3.23, whereby the $\mathbf{d_p}$ is simply the deflection of the post-adjusted structure. The second $\mathbf{e_o}$ is applied to the structure, where the resultant displacements shown in Column 9 are now almost exactly the target values, see also Figure 4.34. The displacement errors in the four joints are now of joint 4y, 6y, 9y and 11y are now 0.84%, 0%, 0% and 0% and the rms error has reduced to 0.02mm, which illustrates the effectiveness of a multi-iterational approach to shape adjustment.

Table 4.11: Double iteraton displacement control of the structure in Figure 4.14 with four elements of $\mathbf{e_o}$ (MATLAB program is shown in Appendix A.6).

(1)	(2)	(3)	(4)	(5)	(6)	(7)	(8)	(9)	(10)
				Iteration (1)			Iteration (2)		Bar actuation
Joints	Dir	Just $\mathbf{d_p}$, no $\mathbf{e_o}$ (mm)	target disp (mm)	$\mathbf{e_o}$ Iter.(1) (mm)	4 elements in $\mathbf{e_o}$ (mm) Theo. results	4 elements in $\mathbf{e_o}$ (mm) Exp. results	$\mathbf{e_o}$ Iter.(2) (mm)	4 elements in $\mathbf{e_o}$ (mm) Exp. results	
1	x	0.10		**-2.38**	0.11	0.09	**-0.10**	0.09	1e
	y			**-1.12**			**0.04**		2e
	θ			**-1.34**			**-0.03**		3e
2	x			**-2.57**			**-0.08**		4e
	y			0			0		5e
	θ			0			0		5ψ1
3	x	0.00		0	0.00	0.00	0	0.00	5ψ2
(Fixed)	y	0.00		0	0.00	0.00	0	0.00	6e
	θ	0.00		0	0.00	0.00	0	0.00	6ψ1
4	x			0			0		6ψ2
	y	**-7.27**	**-2.5**	0	**-2.50**	**-2.68**	0	**-2.54**	7e
	θ			0			0		7ψ1
5	x			0			0		7ψ2
	y	-5.99		0	-3.03	-2.99	0	-2.95	8e
	θ			0			0		8ψ1
6	x			0			0		8ψ2
	y	**-4.01**	**-2.5**	0	**-2.50**	**-2.48**	0	**-2.50**	9e
	θ			0			0		9ψ1
7	x			0			0		9ψ2
	y	-1.44		0	-1.02	-1.02	0	-1.03	10e
	θ			0			0		10ψ1
8	x			0			0		10ψ2
	y	-1.57		0	-1.06	-1.06	0	-1.05	11e
	θ			0			0		11ψ1
9	x			0			0		11ψ2
	y	**-4.24**	**-2.5**	0	**-2.50**	**-2.53**	0	**-2.50**	12e
	θ			0			0		12ψ1
10	x			0			0		12ψ2
	y	-6.30		0	-2.95	-2.99	0	-2.86	13e
	θ			0			0		13ψ1
11	x			0			0		13ψ2
	y	**-7.62**	**-2.5**	0	**-2.50**	**-2.64**	0	**-2.50**	14e
	θ			0			0		14ψ1
				0			0		14ψ2
total actuation (mm)				7.38			0.25		

e= bar/beam elongation.   ψ1 & ψ2= beam rotation at ends 1 & 2.
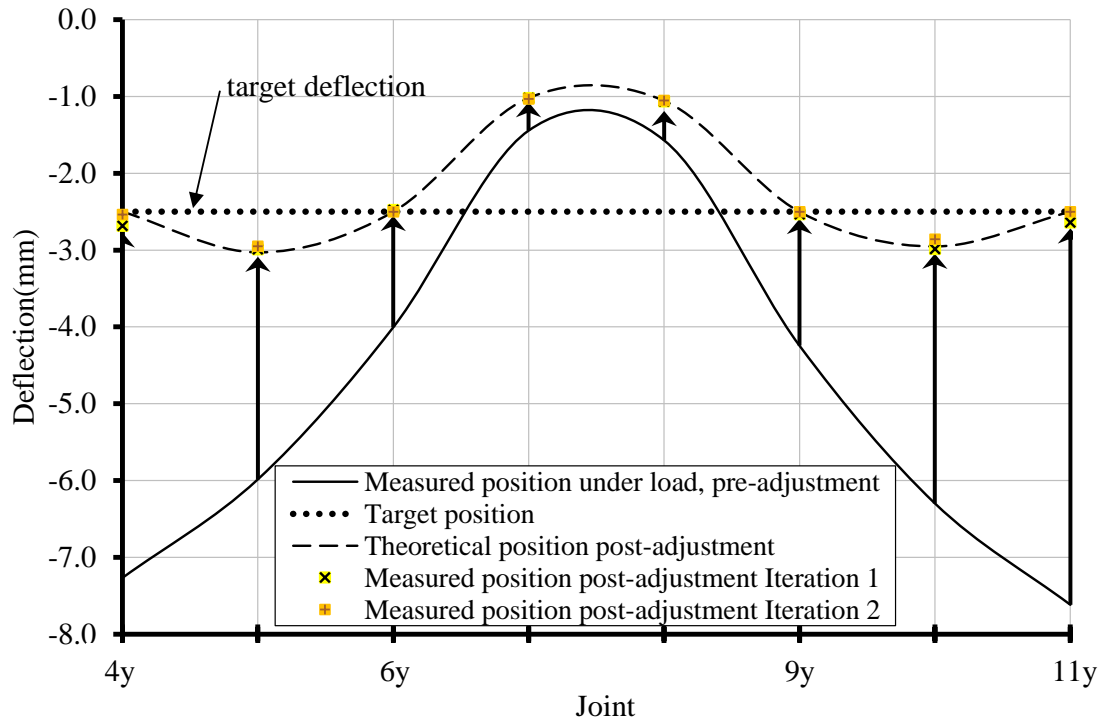
Figure 4.33: First and second iteration displacement control of the structure in Figure 4.14 with four elements of $\mathbf{e_o}$.
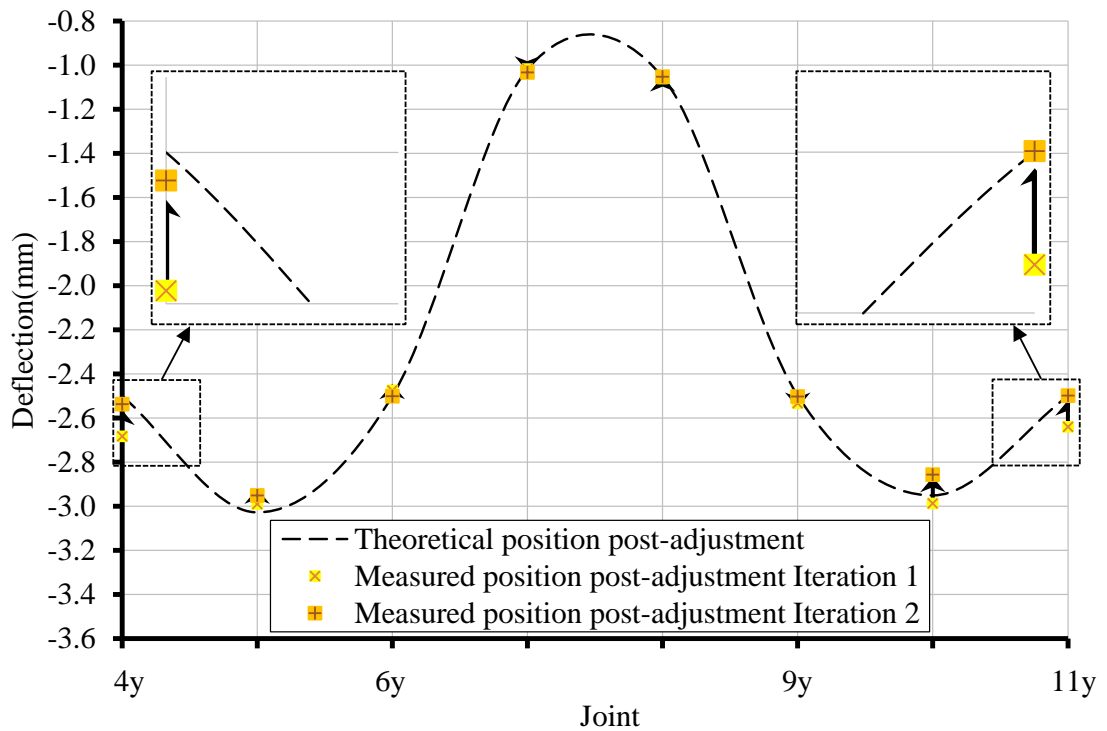
Figure 4.34: Second iteration displacement control of the structure in Figure 4.14 with four elements of $\mathbf{e_o}$.

Chapter 5

Changing Aerodynamic Characteristics of a Morphing Wing Structure

5.1   Introduction and Background

5.1.1   Introduction

A morphing structure is a type of structure which has capability to change its shape according to its application. It has great importance in numerous engineering applications, especially in aerospace, *e.g.* by increasing the ability of engineers to improve designs of a wing. One of the basic inspirations of morphing structures is in the natural world; *e.g.* a bird wing can take several different shapes for different flight requirements.

Initially, from the first successful flight by the Wright brothers, aircraft designers have been trying to progress the aircraft flight efficiency for different flying conditions, such as taking off, landing, as well as for controlling flight attitude, rolling, pitching and yawing performance and for different weather conditions. Since the shape of the aerofoil section is the principal and most responsive parameter for changing the flight characteristics of a wing, researchers working on "smart wings" have focused on finding different ways to control the flight and achieve the different aerodynamic effects under

different flight conditions and environments as currently achieved by a conventional aircraft wing.

The purpose of a morphing wing is to obtain a set of optimal aerofoil shapes to use instead of the traditional hinged control surfaces at different angles separately. Since the shape of the aerofoil's section has the purpose of determining the flight characteristics of a wing, researchers have focused on finding different ways to change the flight efficiency in different flight conditions and environments, *e.g.* by working on smart wings or morphing aircraft. We hereby present a morphing aerofoil concept and we shall use the NACA2415 aerofoil (Jacobs *et al.*, 1933) as the base reference aerofoil.

5.1.1.1 Terminology and Aerodynamic Forces of Aerofoil

An **aerofoil** is the two dimensional cross-sectional shape of a wing, which is used to either generate lift or minimize drag when exposed to a moving fluid (Chandrala *et al.*, 2012). For better understanding, some aerofoil terminologies and their definitions are described in Table 5.1 and illustrated in Figure 5.1:

Table 5.1: Terminology and aerodynamic forces of aerofoil and their definitions.

Term	**Definition** (see also Figures 5.1 and 5.2)
Mean camber line	An imaginary curve on an aerofoil that divides it equally into an upper half and lower half.
Chord line (c)	The straight line connecting the leading edge of an aerofoil with its trailing edge.
Camber	The maximum distance between the mean camber line and the chord line, measured perpendicular to the chord line. In the symmetric aerofoil the camber always equal to zero.
Leading Edge (LE)	The frontal point on the mean camber line.
Trailing Edge (TE)	The most backward point on the mean camber line.
Thickness	Thickness is always given as a percentage of the maximum thickness of the aerofoil to the chord length.

Term	Definition (see also Figures 5.1 and 5.2)
Angle of attack (α)	The angle between the chord line of an aerofoil and the incoming wind.
Flap Angle (FA)	Angle of the flaps, relative to the mean camber line, at the trailing edge of an aerofoil.
Mach number (Mc)	A dimensionless quantity representing object speed relative to speed of sound in air.
Reynolds number (Re)	An important parameter in aerodynamics it is a non-dimensional number that gives the ratio of inertial forces to viscous forces, and consequently quantifies the relative importance of these two types of forces for given flow conditions. Low Reynolds numbers lead to smaller chord lengths or slower flight speeds.
Lift force	Lift is the force on the aerofoil in a direction perpendicular to the flow direction that tends to push the aerofoil upward, see Figure 5.2 (White, 2011).
Lift Coefficient (C_L)	A dimensionless coefficient showing the lift generated by a body. It increases by increasing the camber and the angle of attack until stalling occurs.
Drag force	Drag is the force on the body in the direction of flow. This force increases slowly with increasing angle of attack for producing bigger lift. If the angles of attack increases beyond a certain value, the lift force decreases while the drag forces continues to increase, see Figure 5.2 (White, 2011).
Drag Coefficient (C_D)	A dimensionless coefficient showing the drag force on an object, it presents the amount of air resistance on the object.
Stall	Stalling occurs when there is a sudden loss in the lift due to an increase of angle of attack beyond the critical value which is typically about 15 degrees, see Figure 5.8.
Moment coefficient (Cm)	A non-dimensional number giving a measure of how much nose-over torque the aerofoil is generating. Typically, this coefficient is measured about a location 25% of the distance between the leading edge and trailing edge.

Term	Definition (see also Figures 5.1 and 5.2)
Pressure coefficient (Cp)	A non-dimensional representation of the pressure applied to an aerofoil at one special point. It can be used to generate the lift coefficient by summation of pressure coefficients around an aerofoil.
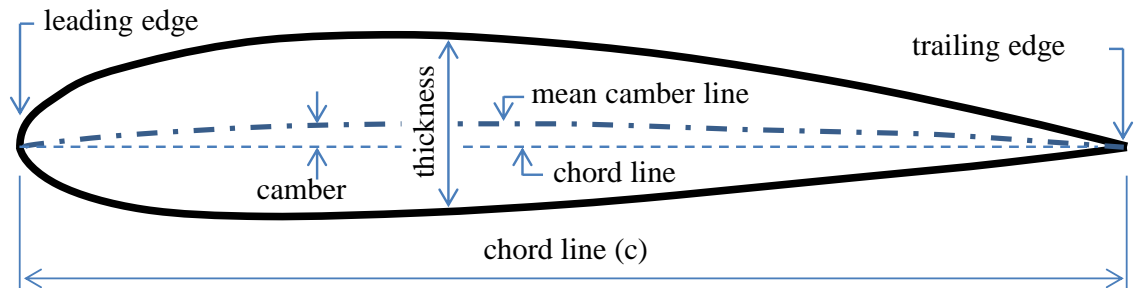
Figure 5.1: Aerofoil terminology.
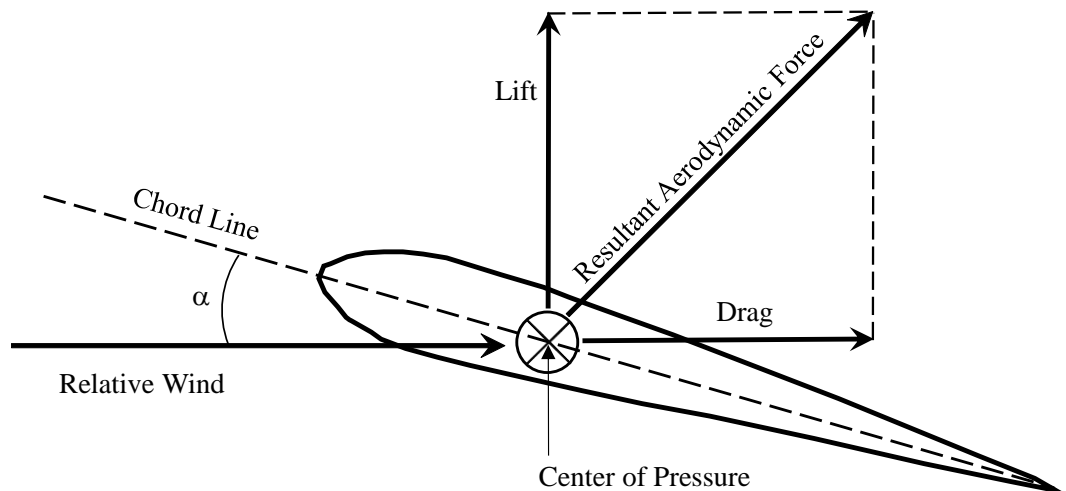
Figure 5.2: Aerodynamic forces of aerofoil.

5.1.2 Background

Du and Ang (2012) proposed a kind of morphing aerofoil (see Figure 5.3) with axial symmetry about the chord, that can deform the configuration into different aerofoil shapes by movement of the leading edge, trailing edge, and the chamber, to fit flight environment and control the attitude. The structure also consists of a stretchable skin material which is

a shape memory polymer. They used a compliant mechanism on the leading and the trailing edge of the morphing aerofoil to control the aerofoil deformation. In addition, two pairs of control points at the leading and trailing edge are used to control the shape of the compliant mechanism with the eight control points in the upper and lower surface. The main core part of the proposed morphing aerofoil is a fixed structure, which is used for attaching all control points and connection of the wing to the fuselage. Du and Ang found that their proposed morphing could replace the traditional hinged control aerofoil to control flight attitude with smaller drag and increased flight efficiency, see Figure 5.4.
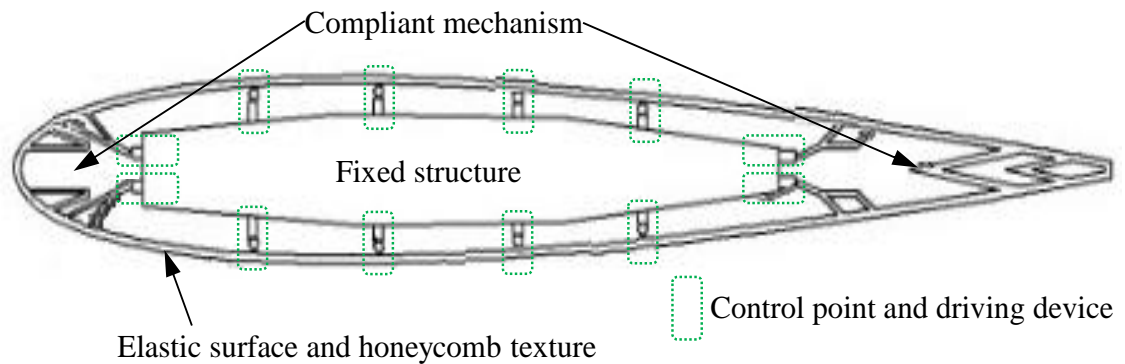
Figure 5.3: Morphing aerofoil structure. Adapted from Du and Ang (2012).
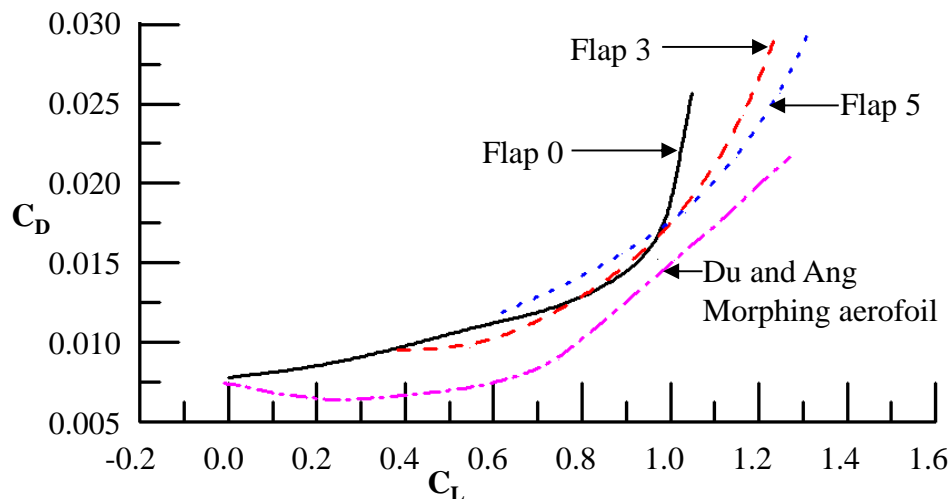
Figure 5.4: The relationship between C_L & C_D of the traditional aerofoil with flaps and the Du and Ang morphing aerofoil. Adapted from Du and Ang (2012).

A morphing aerofoil can be developed and constructed from using different techniques. Bettini *et al.* (2010) investigated a morphing aerofoil technique by using complex composite cellular structures that provides a large shape deformation through deformation of the material of its micro structure, see Figure 5.5. This micro structure appears as a chiral topology that produces macro chiral components to produce their ability to undergo large deformations in the aerofoil, see Figure 5.6. Bettini *et al.* found suitable composite materials for the micro structure, and from analytical and experimental work, they found the chiral composite cores as efficient way to provide morphing capabilities of aircraft structures.
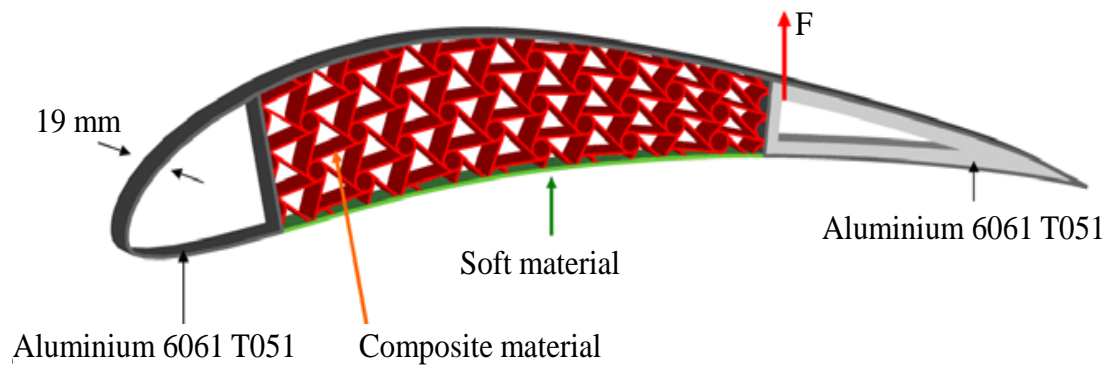
Figure 5.5: Chiral core morphing aerofoil. Source: Bettini *et al.* (2010).

Figure 5.6: Chiral composite element. Source: Bettini *et al.* (2010).

5.2 Numerical Calculation of Lift and Drag Coefficients

Lift and drag calculation comes from understanding the behaviour of solid object in a fluid stream. The total force on the object F_{total} contains of two components: shear stresses (viscous effects) and normal stresses (pressure effects). Figure 5.7 shows distribution pressure and shear stress on a typical aerofoil surface. The total force on the aerofoil is thus (Bar-Meir, 2013):

$$F_{total} = \overbrace{\int_{A_r} p.dA_r}^{\substack{\text{Pressure}\\ \text{effects}}} + \overbrace{\int_{A_r} \tau_w.dA_r}^{\substack{\text{Shear/viscous}\\ \text{effects}}} \qquad (5.1)$$

F_{total} can in turn be divided into two force components: lift and drag forces. By considering a small elemental area on an aerofoil as shown in Figure 5.7, the lift is given by

$$F_L = \int_{Ar} dF_y = -\int_{Ar} (p.dA_r)\sin\varnothing + \int_{Ar} (\tau_w.dA_r)\cos\varnothing . \qquad (5.2)$$

and the drag force is

$$F_D = \int_{Ar} dF_x = \int_{Ar} (p.dA_r)\cos\varnothing + \int_{Ar} (\tau_w.dA_r)\sin\varnothing . \qquad (5.3)$$

The coefficients of lift and drag are obtained by Eqns. 5.2 and 5.3 by *dynamic pressure×Area* :

$$C_L = \frac{lift\ force}{dynamic\ pressure \times Area} = \frac{F_L}{\frac{1}{2}\rho U^2 A_r} \qquad (5.4)$$

$$C_D = \frac{drag\ force}{dynamic\ pressure \times Area} = \frac{F_D}{\frac{1}{2}\rho U^2 A_r} \qquad (5.5)$$

where,

ρ = Air density

A_r= Surface area of wing= chord length x length of blade

U=Wind speed

p= normal stress (air pressure)

τ_w=shear stress (viscosity effects)

It is clear from Eqns. 5.4 and 5.5 that the coefficients C_L and C_D depend on the geometry of the object. For the traditional aerofoil, increasing the angle of attack α makes the aerofoil become more inclined with respect to the relative wind direction. This results in a higher lift coefficient until a certain α when C_L decreases and C_D increases dramatically. Figure 5.8 shows streamlines around a tilted aerofoil in normal (low angle of attack) and stall (higher angle of attack) conditions.
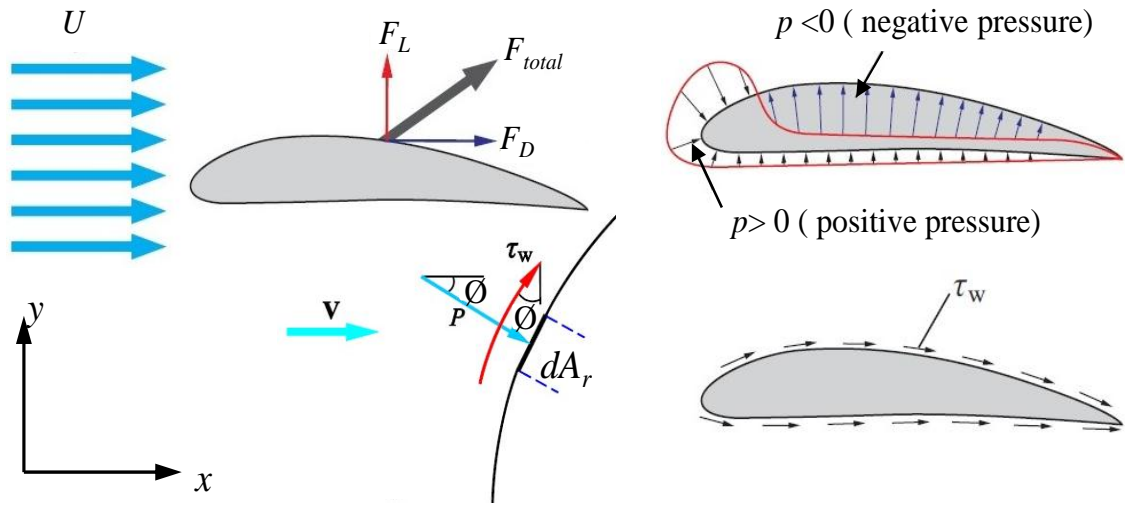
Figure 5.7: Allocation of normal and shear stress for an aerofoil. Adapted from Taheri (2013).

5.3   Standard NACA2415

For this work, the standard NACA2415 aerofoil was chosen as a comparator. This aerofoil is commonly used in light aircraft, and is part of the NACA Four-Digit Series, which is a class of standard NACA (*National Advisory Committee for Aeronautics)* aerofoils. The four digit code provides parameters of the shape (see Figure 5.9) whereby 2 represents the maximum camber in percentage of chord length, and 4 specifies the location of the maximum camber in tenths of chord length measured from leading edge. The last two digits (15) indicate the maximum thickness of the aerofoil in percentage of chord length.
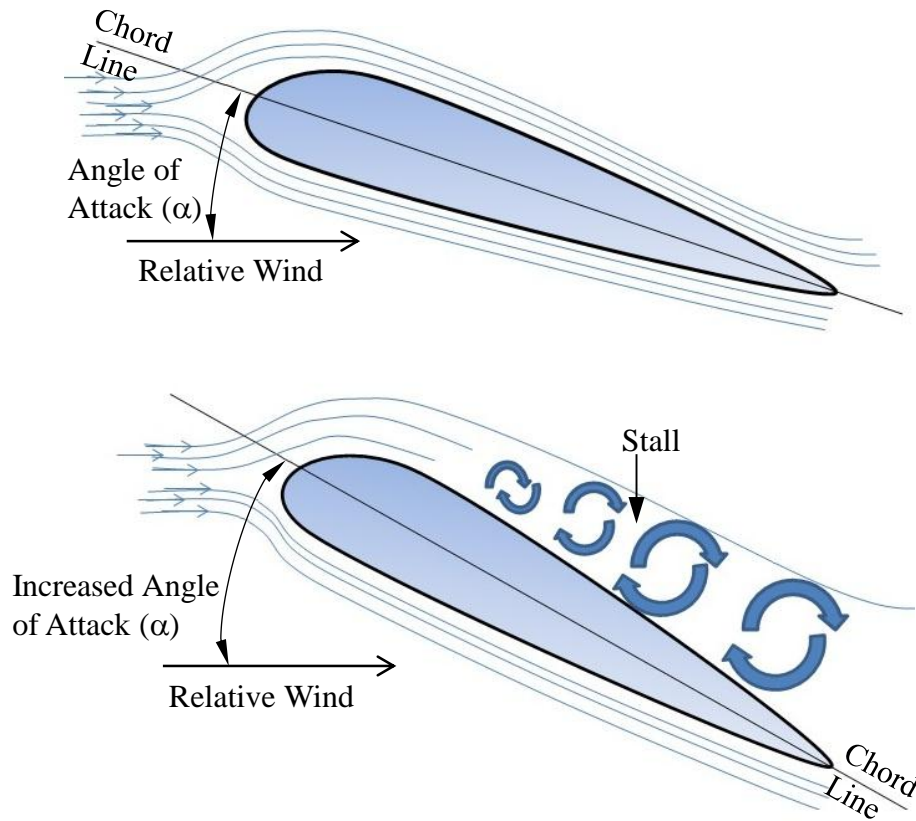
Figure 5.8: Flow streamlines around a tilted aerofoil in normal and stall conditions.
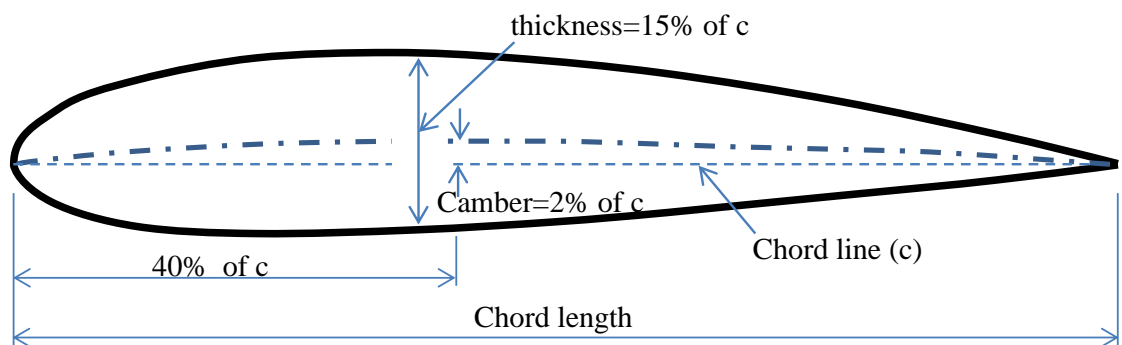
Figure 5.9 : Parameters of the NACA2415 aerofoil.

5.4 Morphing Shape Concept

In the traditional aerofoil, flaps are attached to the trailing edge as a hinged surface, to control the flight by changing the lift force. Morphing aerofoils have been found to be capable of taking the place of traditional aerofoils with flaps, and indeed, to be more

efficient by providing bigger lift coefficient (C_L) and smaller drag coefficient (C_D) (Du and Ang, 2012), as well as Section 5.6 in the present study). This benefit from using a morphing aerofoil can be produced by changing the aerofoil cross sectional configuration. Aerofoil morphing thus changes the key aerofoil parameters, such as chord line length, camber, thickness, leading and trailing edge configuration and position of the mean camber line.

5.5 Structure of Proposed Aerofoils

In this work, two configurations of morphing aerofoil are proposed, both of which are a series of interconnected, curved, single-control pantographs. Aerofoil NACA2415 is chosen as the base-shape for both proposed structures. Configurations of the two morphing structures, MAS1 and MAS2 are shown in Figures 5.10 and 5.11 respectively, with nine morphing stages to highlight the cross-sectional variation achieved through morphing. (Stages 2 and 8 are shown and have been separately re-plotted with greater detail for each structure.) The first structure consists of a small number of big pantographic units while the second consists of a large number of small pantographic units. Both aerofoil structures can provide the different shapes required to give a range of camber, leading and trailing edge *etc* to fit flight environment and control the flight attitude. Both aerofoil structures have the following components.

1-Main structure

The main structure consists of a series of two-dimensional interconnected, curved, single-control pantographs. Each pantographic unit is made from a pair of beams connected by a shear connector (which is central but typically not in the middle of the beam-pairs). The lengths of the beams, as well as the position of the central shear connector, are different from one pantographic unit to the next. All pantographs are connected at their ends by the shear connecters.

2-Morphing control bar

Each morphing structure also has a "control bar" which is a bar of variable length, which is used for controlling the shape configuration of the morphing aerofoil structure. The overall morphing pantograph mechanism has only one degree of freedom, so this control bar can be positioned in many different places, but only one such bar is needed. In the

experimental models in the current work, length actuation has been effected by a turnbuckle built into the control bar.

3-Skin of the aerofoil structure

The morphing aerofoil is really the cross-sectional "backbone" structure of the aerofoil, and hence a "stretchable skin" is also necessary to ensure correct aerodynamic properties (Du and Ang, 2012). The amount of maximum stretching required would be 30.1% and 21.2% for MAS1 and MAS2 respectively. Such a stretchable skin could be made of elastic polymer membrane, or it may even be possible for such a "skin" to mimic the operation of wing feathers of a bird through overlapping plates, or both.
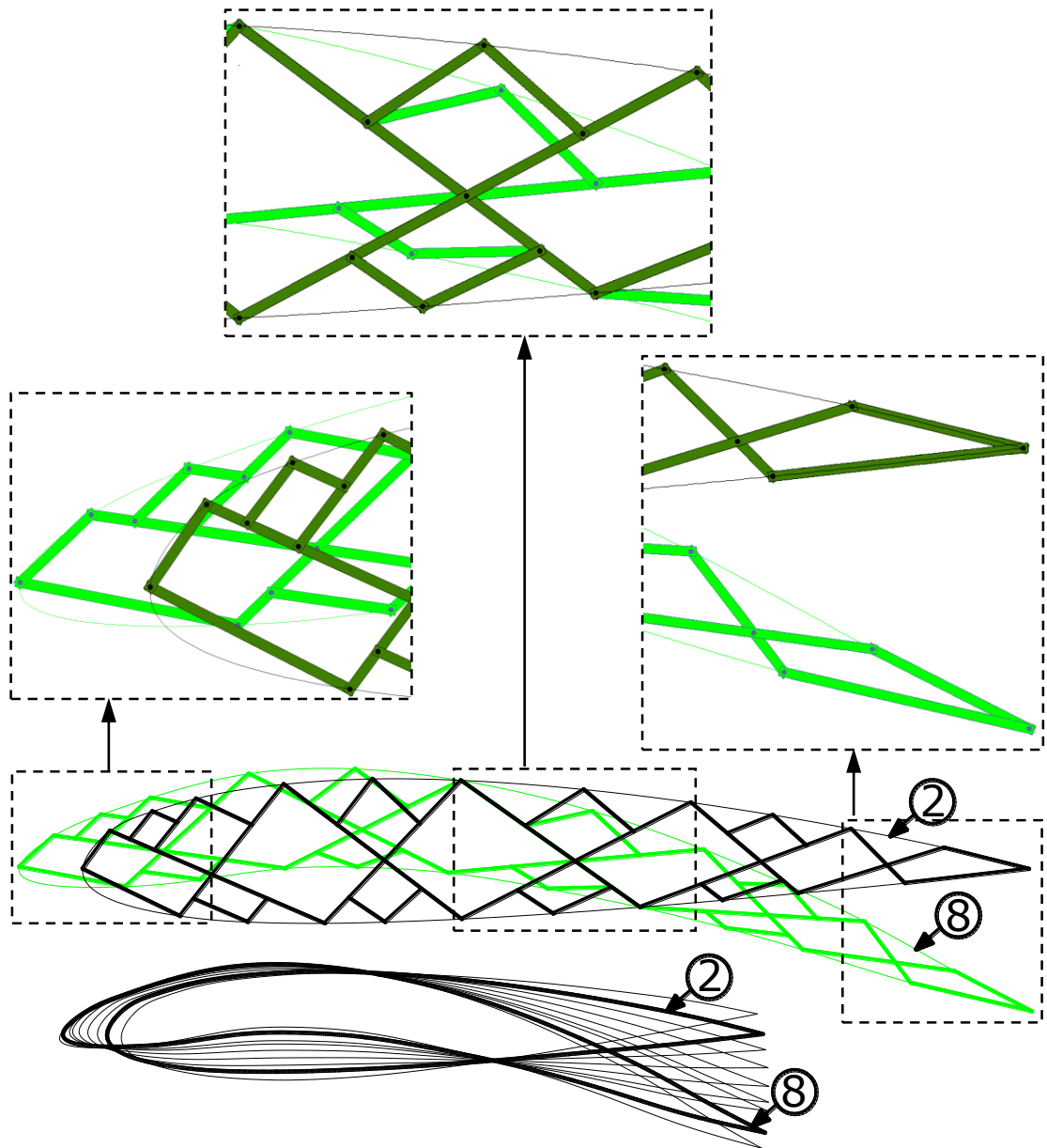
Figure 5.10: Nine morphing stages of MAS1.
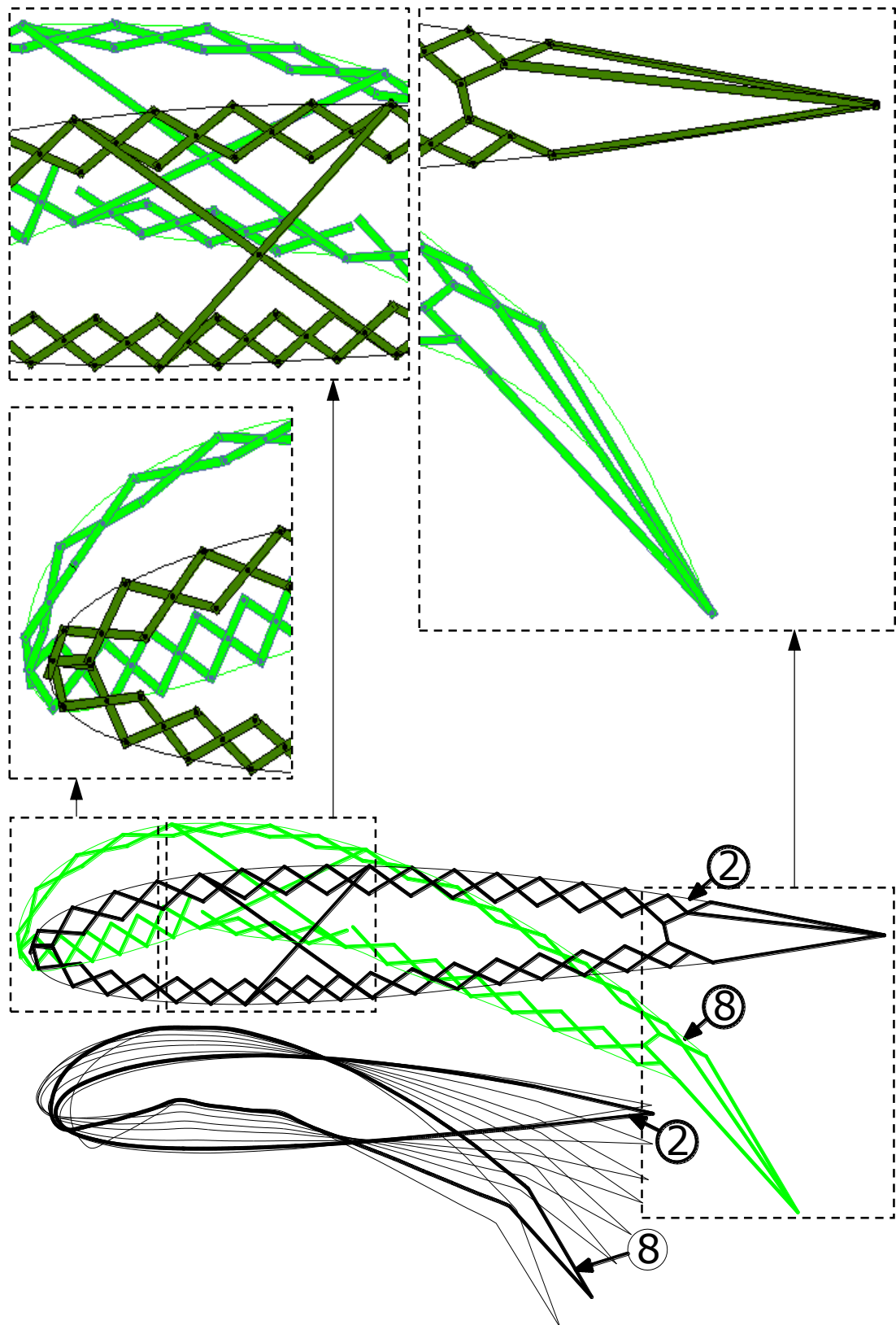
Figure 5.11: Nine morphing stages of MAS2.

5.6   Results and Discussion

For understanding the benefit of the proposed morphing aerofoil structures, their performance should be calculated and compared with that of the standard traditional hinged surface control aerofoil. The JavaFoil (v2.20) software was used for calculating Lift Coefficient (C_L) and Drag Coefficient (C_D) of the proposed and standard NACA aerofoils. Detailed coordinates of the nine morphing stages for each morphing structure was carefully determined, and entered into JavaFoil. A two-dimensional morphing aerofoil structure, which is made from a series of pantograph units, has a single degree of freedom. The overall morphing pantograph mechanism depends on the type of pantograph units used (translational, polar, and angulated) to expand and contract. The different stages in the deployment are shown in Figures 5.10 and 5.11, in which the mechanism deploys gradually in two directions horizontally and vertically. The deployment process was numerically modelled in the Working Model software, which is a dynamic mechanical mechanism modeller. For a given morphing stage, the Working Model model was exported (with fixed geometry) to AutoCAD, and then to DesignFOIL as a .dxf file (since DesignFOIL but not JavaFoil could read AutoCAD files). The outline and profile of the morphing pantograph was then described in DesignFOIL as a series of fixed coordinates for a fixed morphing stage, and then exported into JavaFoil, in which the aerodynamic characteristics were finally calculated. Air speed of Mach 0.045 and Reynolds number 300000 were chosen for the calculations because these values have been used in the literature, and hence a separate verification of the JavaFoil calculations can be obtained.

5.6.1   *Comparing C_L and C_D of the Proposed Aerofoils with NACA2415*

The achieved sets of results of characteristics from the optimal shape of the morphing aerofoil in different stages are shown in Figures 5.12 to 5.15. At each stage, C_L and C_D results are compared with the traditional hinged control standard NACA2415 aerofoil, for a full range of angle of attack and hinged control flaps.

The C_L and C_D relationship for the two morphing aerofoil structures are compared with NACA2415 in Figure 5.12, with changing angle of attacks from -8° to +15°, for

angles of hinged flaps at $+0^{o}$, $+2^{o}$, … $+18^{o}$ separately. These coefficients are calculated from the shape of the nine morphing stages of MAS1 and MAS2.

Figure 5.12 shows that in general both MAS1 and MAS2 provide smaller C_D as compared to NACA2415. In addition, both the maximum C_L of MAS1 and MAS2 are greater than the peak C_L achievable by NACA2415. This C_L versus C_D graph of MAS1 has low C_L and C_D values with stage 1 and C_L rises rapidly until stage 5, before it then rises more gradually thereafter until stage 9, which has maximum C_L and C_D. For MAS2, C_L becomes less and less related to C_D with increasing stages.
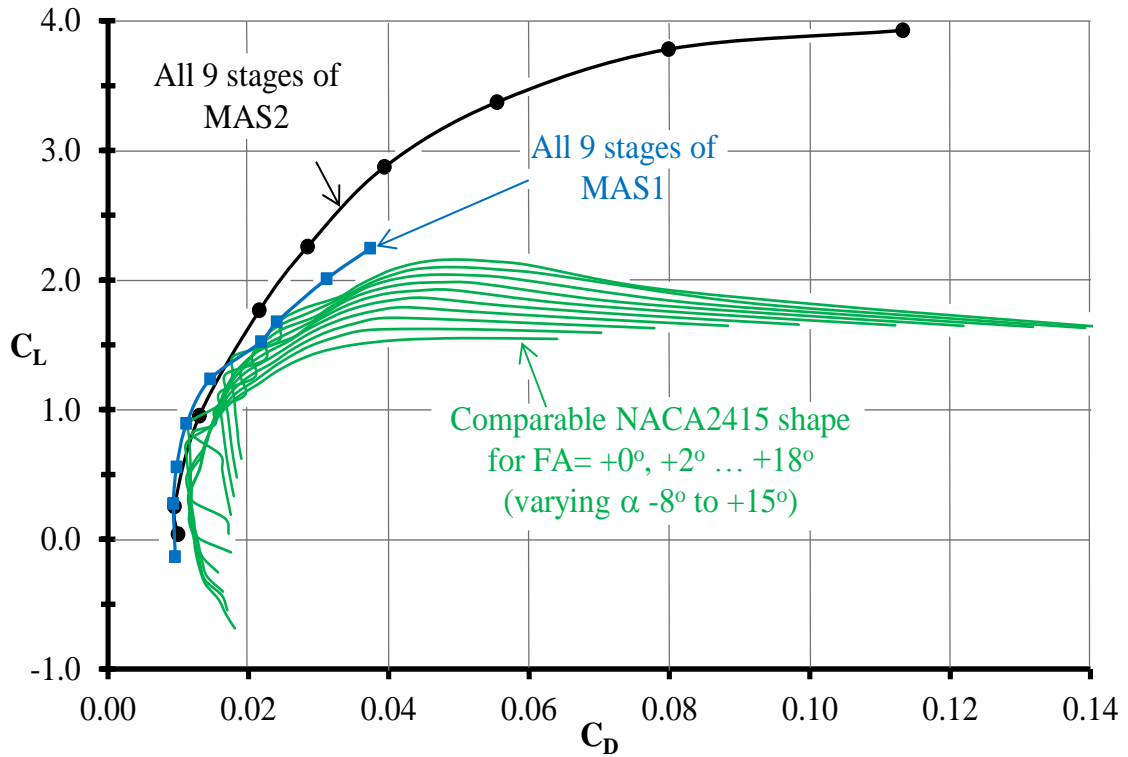
Figure 5.12: Comparing C_L and C_D of NACA2415 (by varying angle of attack for fixed flap angle) with MAS1 and MAS2.

Figure 5.13 presents the comparison of C_L and C_D of MAS1 and MAS2 and standard NACA2415, achieved via increasing flap angles from $+0^{o}$ to 18° (for fixed angles of attack at 0°, 2°, 4°, 6°, 8°, 10° separately). MAS2 and MAS1 exhibit a wider range of C_L and C_D than achievable by standard NACA2415 with flaps. Again, MAS2 shows a smooth relationship throughout, but MAS1 displays a small step change around

C_D =0.02, which is likely to be caused by the aerofoil surface not being smooth enough. A similar step change, but more pronounced, is seen for the NACA aerofoil at around the same C_D =0.02 zone. The reason is that around that angle of attack, the trailing edge of the aerofoil is suddenly no longer "hidden" behind maximum thickness, but protrudes above the wake of the maximum thickness, thus causing additional drag. This thus causes a sudden step change in the C_D.

In summary, it is found that the morphing aerofoil is more effective than NACA2415 by producing bigger C_L for the same amount of C_D. Since the pressure coefficient has a big role in C_L and C_D, the distribution of pressure on the face of the proposed aerofoils MAS1 and MAS2 are shown in Figures 5.14 and 5.15 respectively.
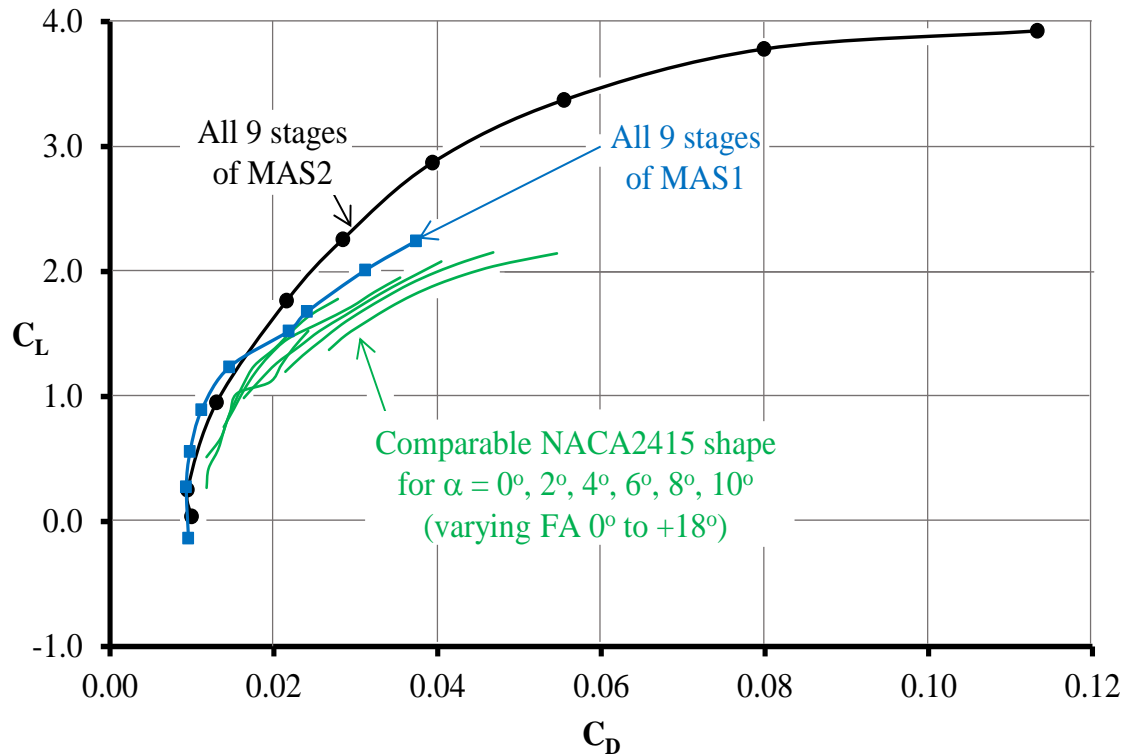
Figure 5.13: Comparing C_L and C_D of NACA2415 (by varying flap angle for fixed angle of attack) with MAS1 and MAS2.
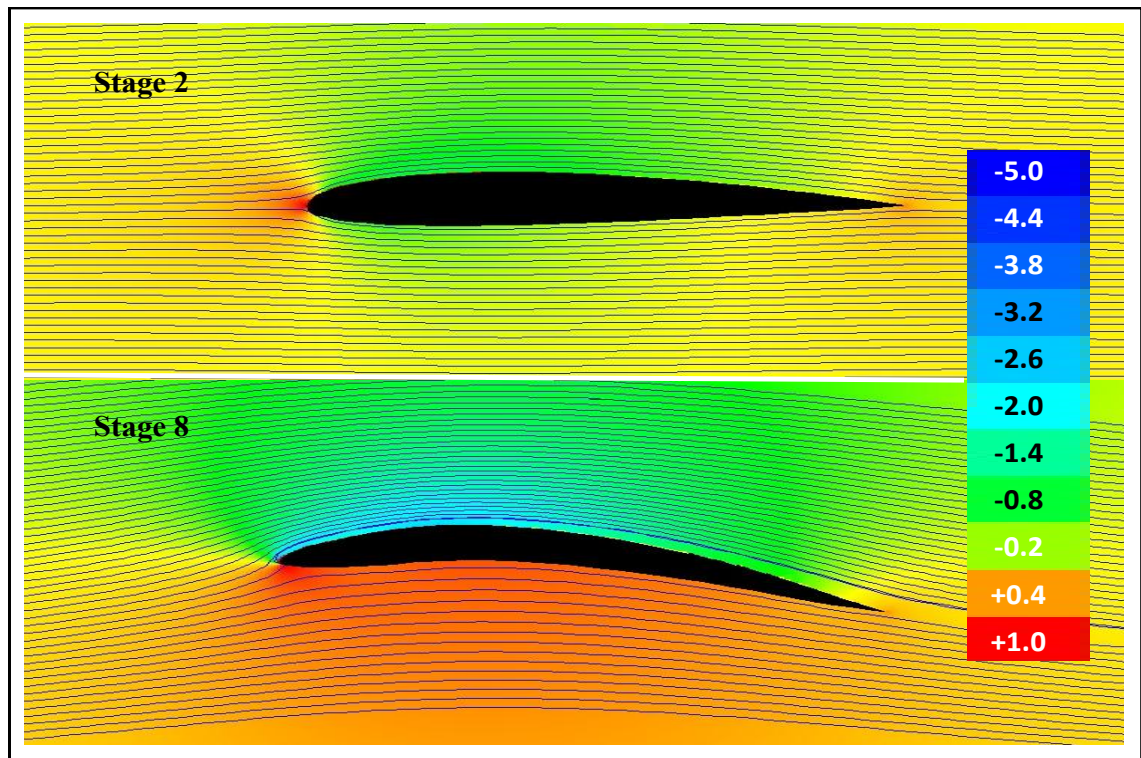
Figure 5.14: Pressure coefficient of MAS1.
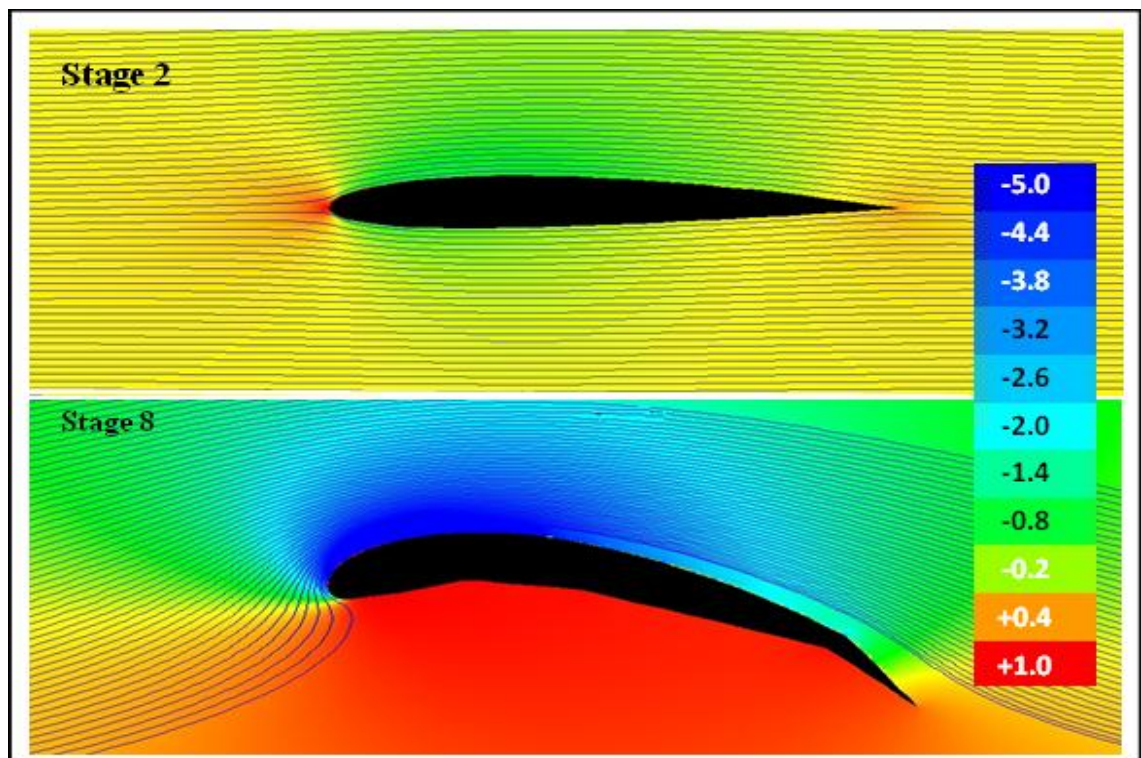
Figure 5.15: Pressure coefficient of the MAS2.

5.6.2   Comparing C_L, C_D of the Proposed Aerofoils with 31 NACA Shapes

Figure 5.16 shows a group of results of aerodynamic characteristics C_L and C_D relationship of MAS1 and MAS2 compared to 31 standard NACA shapes. The C_L and C_D of those 31 standard NACA shapes come via increasing angle of attack from -10° to +25°. MAS2 exhibits a wider range of C_L and C_D than is achievable by the 31 NACA shapes, but results for MAS1 fall within the NACA range. Mostly, for a given C_L, C_D of MAS1 and MAS2 is smaller than the 31 standard NACA shapes. In the zone of $C_L \approx 2.0$, C_D of MAS1 and MAS2 are greater than C_D of shapes NACA6415 to NACA9420. The effect of having a big camber in MAS1/2 over NACA2415 leads to increase in C_L. NACA2415's greater thickness also causes MAS1/2 to have a lower drag pressure due to the decrease of the cross sectional area, and thus a smaller C_D is produced. Therefore, both MAS1 and MAS2 have greater lift (for the same drag) than the whole of the NACA family of aerofoil shapes.

5.6.3   Shape Comparison of Morphing Proposed Aerofoils with NACA2415

The MAS1 shape for various morphing stages is shown superimposed on the corresponding NACA2415 aerofoil (with different angles of attack and hinged flaps) Figures 5.19 to 5.27 with both shapes normalized to their chord length to allow comparison. The same is shown for MAS2 in Figures 5.30 to 5.38. The chosen NACA2415 configuration is the one that provides the same lift coefficient (C_L) in 0° angle of attack.

For MAS1, each figure contains a pair of aerofoils with increasing C_L from low to high (Figures 5.19 to 5.27). Numerical values of C_D and C_m for NACA2415 and MAS1 for a given C_L in different stages are collected in Table 5.2. The data for these figures are also tabulated in Tables 5.2 and 5.3 (for MAS1 and MAS2 respectively), and then plotted in Figures 5.17 and 5.18, and Figures 5.28 and 5.29 (again, for MAS1 and MAS2 respectively) where C_D and C_m are plotted at every point for the same C_L. Not every morphing stage has a corresponding NACA2415 configuration since NACA2415 cannot achieve $C_L=2.213$ and $C_L=3.926$ as produce by MAS1 and MAS2 respectively; $C_L=2.158$ is the maximum producible coefficient of lift by NACA2415. Hence, Figure 5.27 gives

just the configuration of MAS1 and Figures 5.34 to 5.38 give only the configurations for MAS2.

Figures 5.17 and 5.28 show that in general, C_D of MAS1 and MAS2 is much smaller than the drag coefficient produced by NACA2415, see also Tables 5.2 and 5.3. It is also good that the negative moment coefficients are only in the first five stages of MAS1 and the first three stages of MAS2, and they are all less than the moment coefficient achieved by NACA2415. These are very useful results of moment coefficient, which are produced in the early stages of morphing.

Table 5.2: C_D and C_m for the same C_L in different stages of Figures 5.19 to 5.27.

MAS1			C_L	NACA2415				Change (%) from NACA2415 to MAS1	
Stages	C_D	C_m		FA	α	C_D	C_m	C_D	C_m
1	0.00957	-0.016	-0.135	0.00	-3.28	0.01262	-0.045	-24.17	-64.44
2	0.00931	-0.052	0.276	0.09	0.00	0.01182	-0.052	-21.24	0.00
3	0.00977	-0.078	0.559	3.81	0.00	0.01315	-0.094	-25.70	-17.02
4	0.01117	-0.115	0.892	8.30	0.00	0.01479	-0.145	-24.48	-20.69
5	0.01457	-0.160	1.236	12.90	0.00	0.01827	-0.183	-20.25	-12.57
6	0.02182	-0.199	1.524	14.00	2.10	0.02074	-0.195	5.21	2.05
7	0.02406	-0.223	1.678	14.00	3.60	0.02720	-0.197	-11.54	13.20
8	0.03119	-0.282	2.011	14.00	8.50	0.04103	-0.200	-23.98	41.00
9	0.03739	-0.310	2.213						
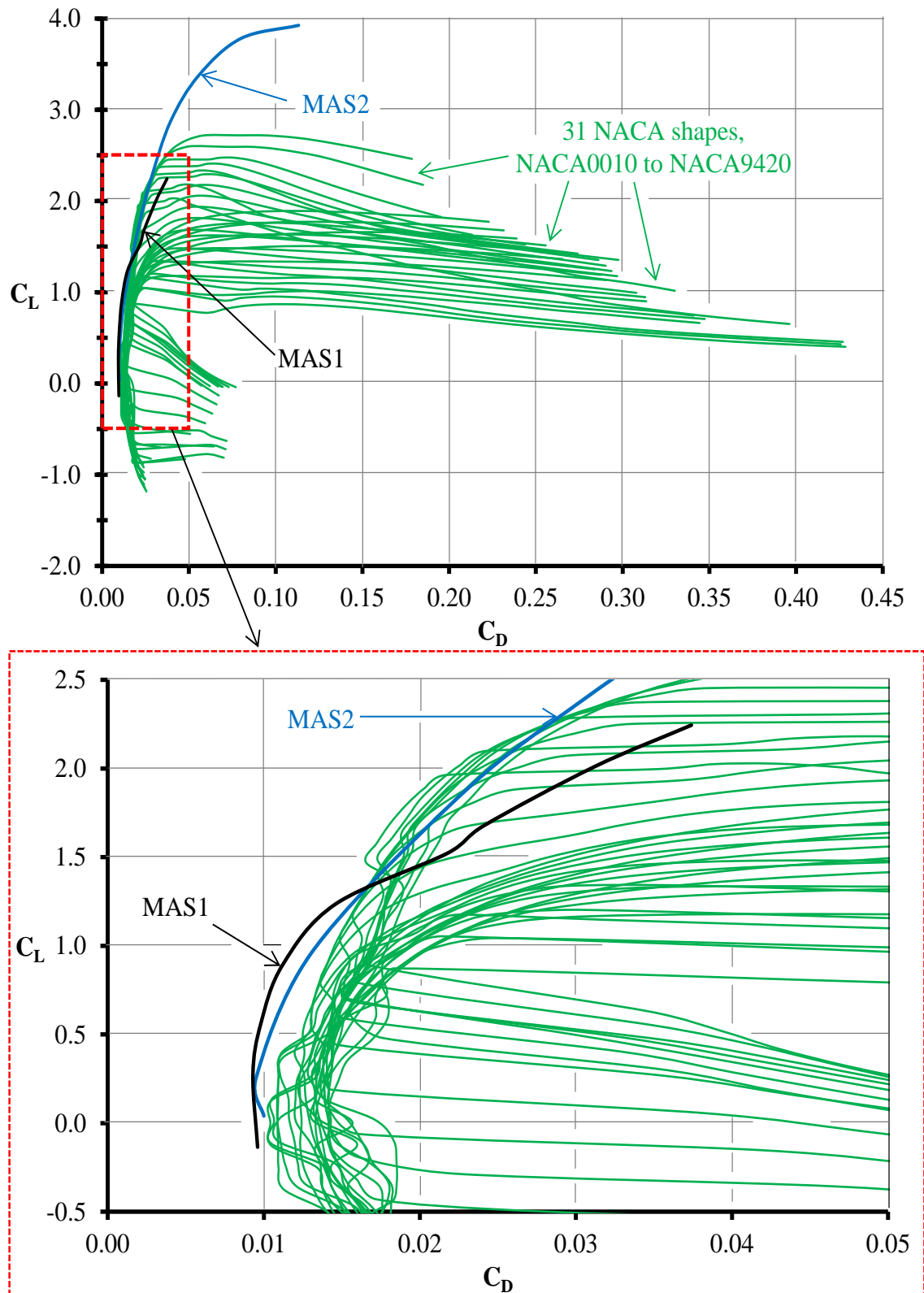
Figure 5.16: Comparing C_L and C_D of 31 NACA shapes with MAS1 & MAS2.
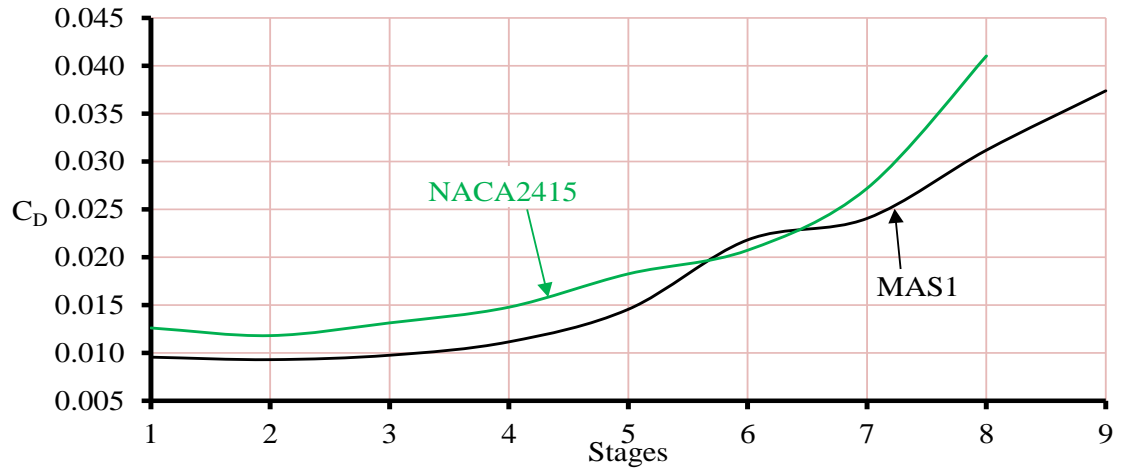
Figure 5.17: C_D for the same C_L in different stages of Figures 5.19 to 5.27.
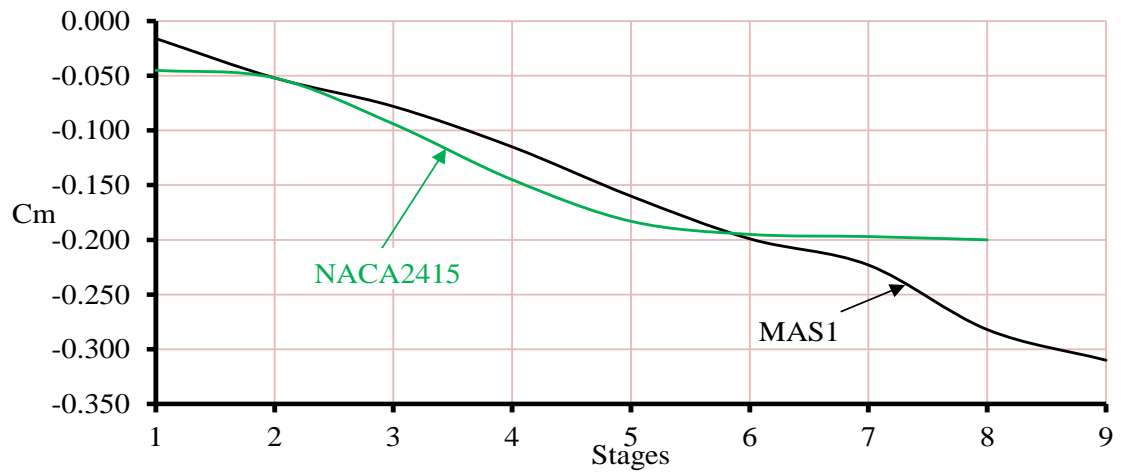
Figure 5.18: C_m for the same C_L in different stages of Figures 5.19 to 5.27.
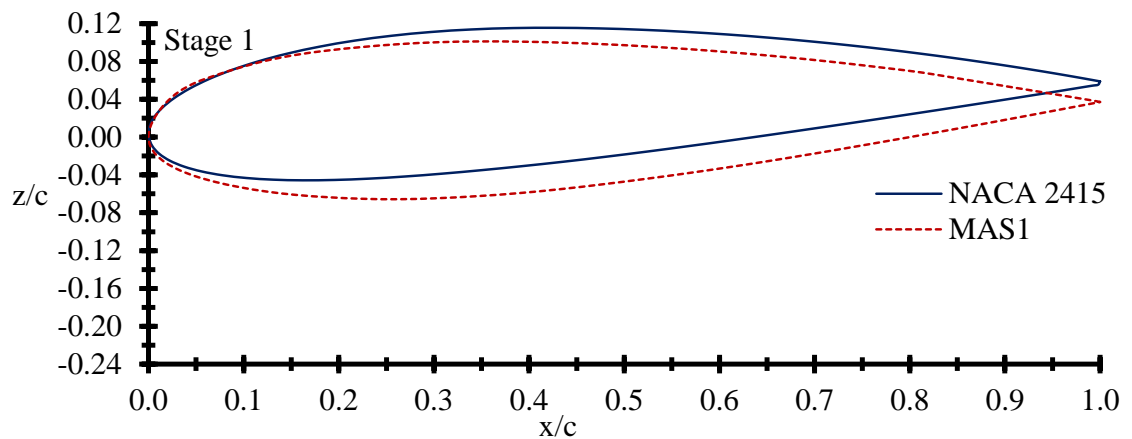
Figure 5.19: Stage 1 of normalised MAS1 and same C_L of NACA2415 aerofoil shape.
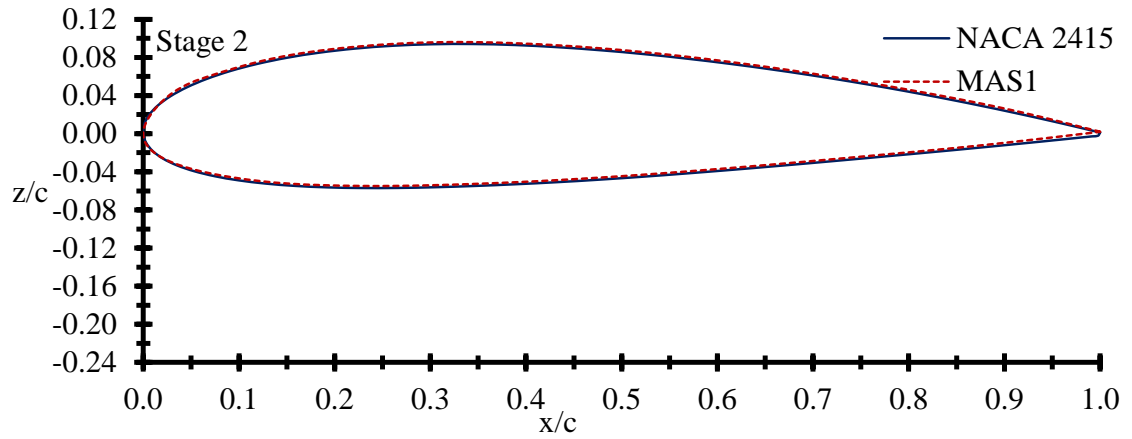
Figure 5.20: Stage 2 of normalised MAS1 and same C_L of NACA2415 aerofoil shape.
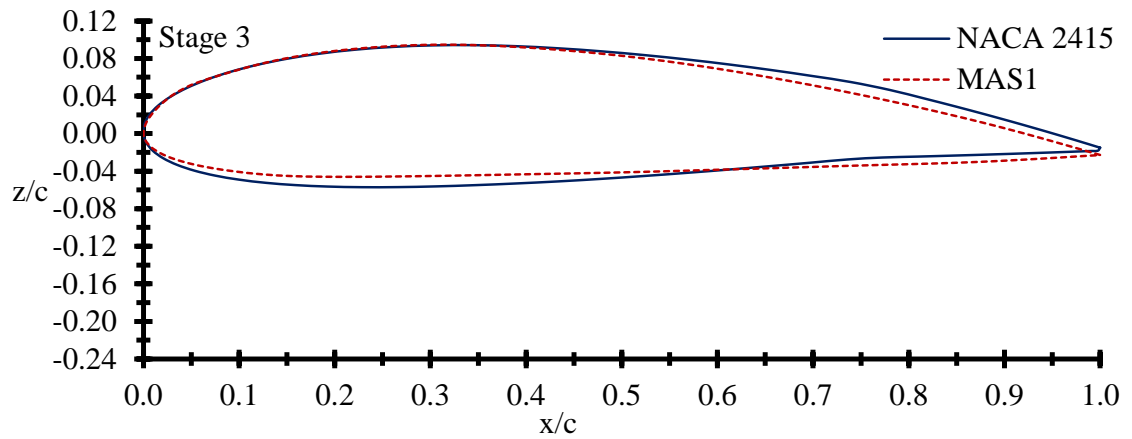
Figure 5.21: Stage 3 of normalised MAS1 and same C_L of NACA2415 aerofoil shape.
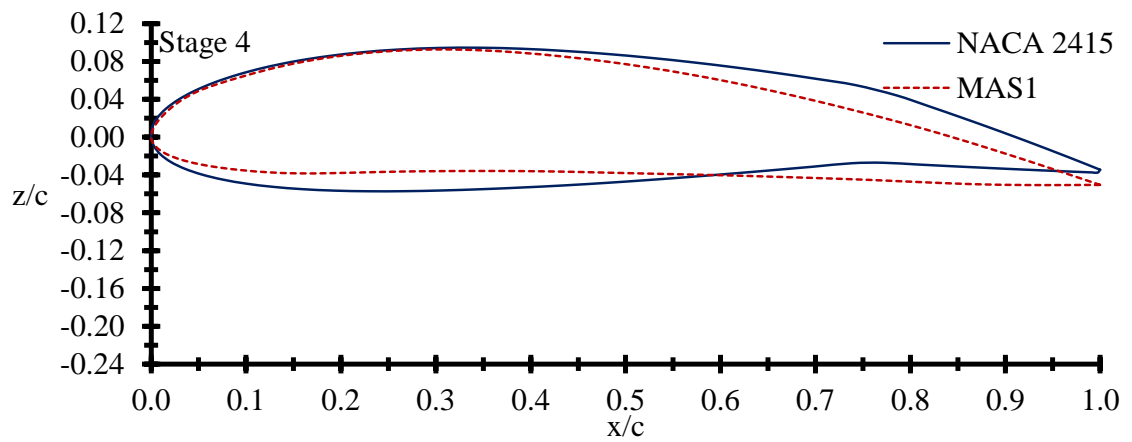
Figure 5.22: Stage 4 of normalised MAS1 and same C_L of NACA2415 aerofoil shape.
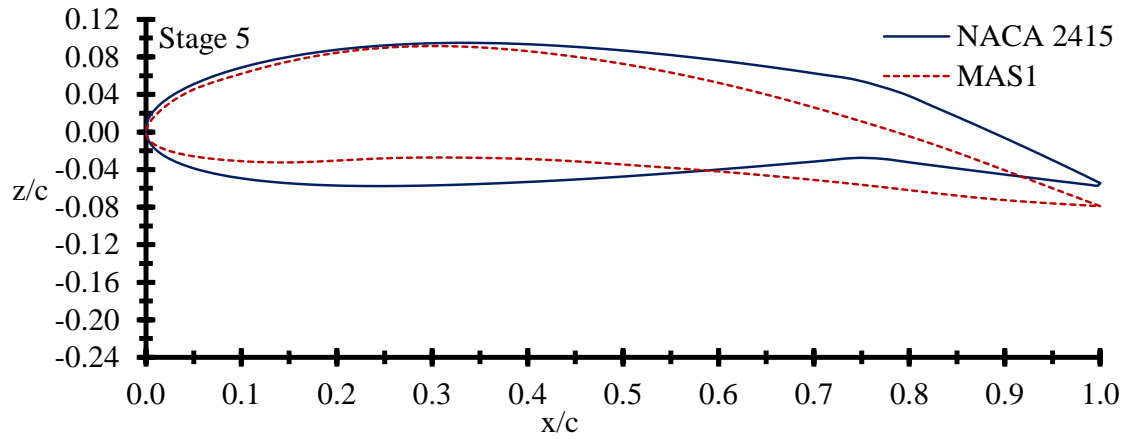
Figure 5.23: Stage 5 of normalised MAS1 and same C_L of NACA2415 aerofoil shape.
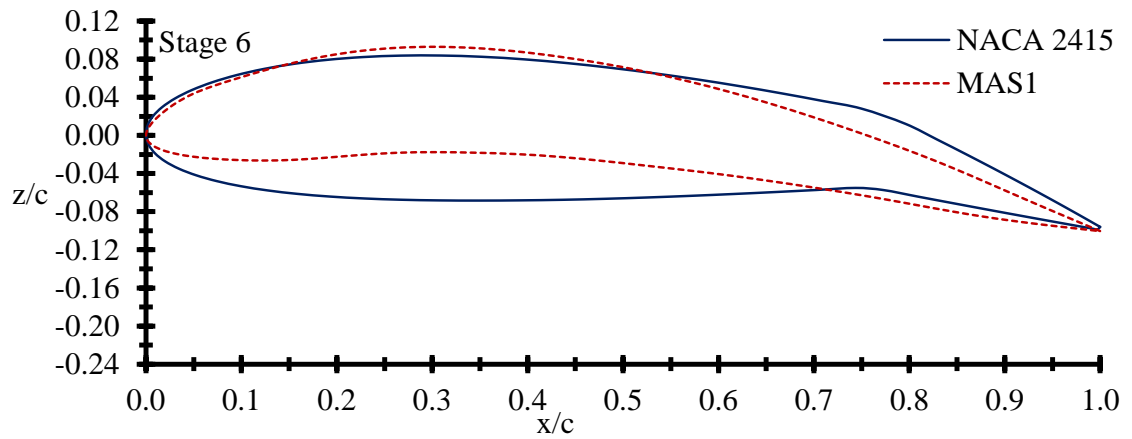
Figure 5.24: Stage 6 of normalised MAS1 and same C_L of NACA2415 aerofoil shape.
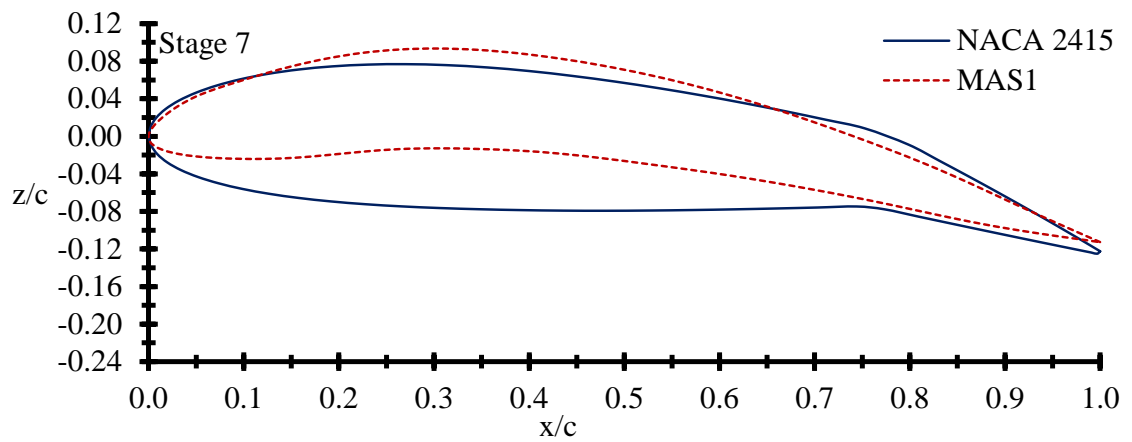
Figure 5.25: Stage 7 of normalised MAS1 and same C_L of NACA2415 aerofoil shape.
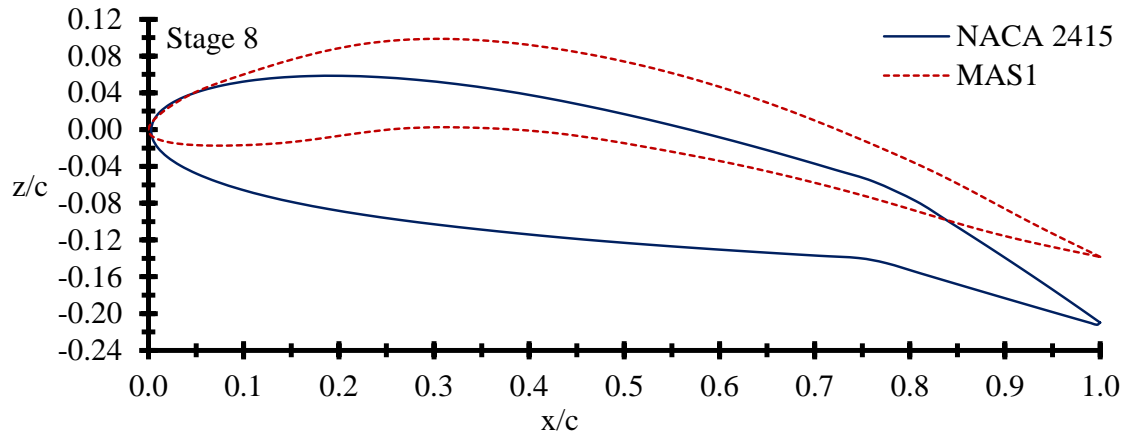
Figure 5.26: Stage 8 of normalised MAS1 and same C_L of NACA2415 aerofoil shape.
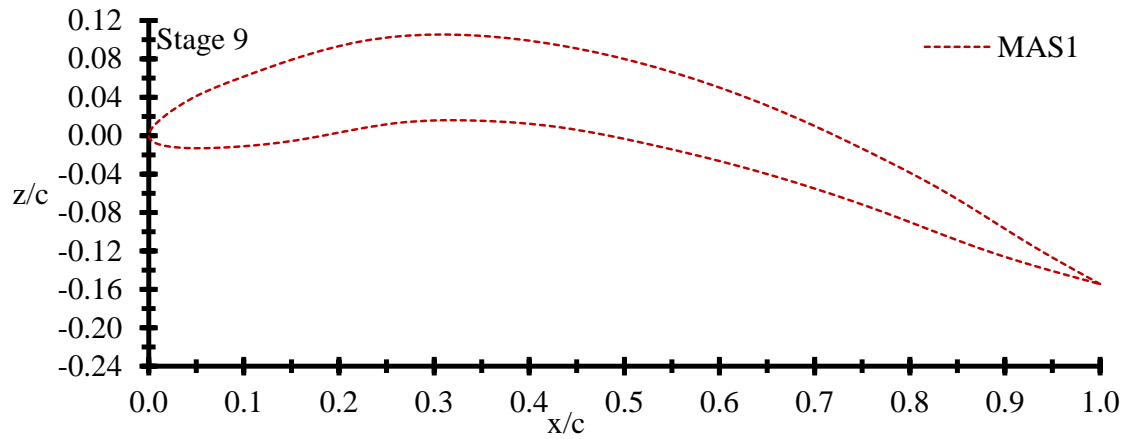
Figure 5.27: Stage 9 of normalised MAS1.

Table 5.3: C_D and C_m for the same C_L in different stages of Figures 5.30 to 5.38.

MAS2			C_L	NACA2415				Change (%) from NACA2415 to MAS2	
Stages	C_D	C_m		FA	α	C_D	C_m	C_D	C_m
1	0.00996	-0.029	0.041	0.00	-1.85	0.01210	-0.047	-17.69	-38.30
2	0.00946	-0.047	0.254	-0.19	0.00	0.01158	-0.049	-18.31	-4.08
3	0.01302	-0.130	0.954	9.01	0.00	0.01508	-0.152	-13.66	-14.34
4	0.02157	-0.211	1.766	14.00	4.60	0.03058	-0.198	-29.46	6.57
5	0.02843	-0.269	2.258						
6	0.03939	-0.252	2.872						
7	0.05545	-0.289	3.373						
8	0.07989	-0.277	3.781						
9	0.11328	-0.260	3.926						
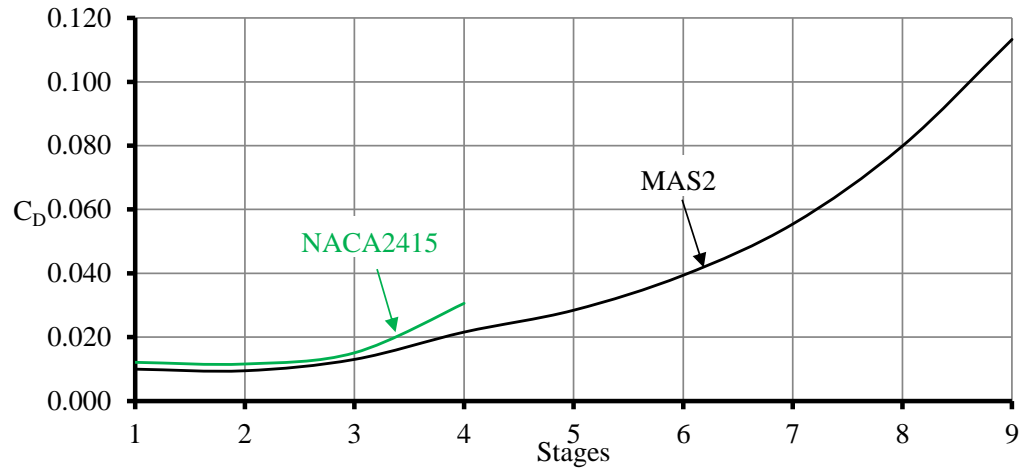
Figure 5.28: C_D for the same C_L in different stages of Figures 5.30 to 5.38.
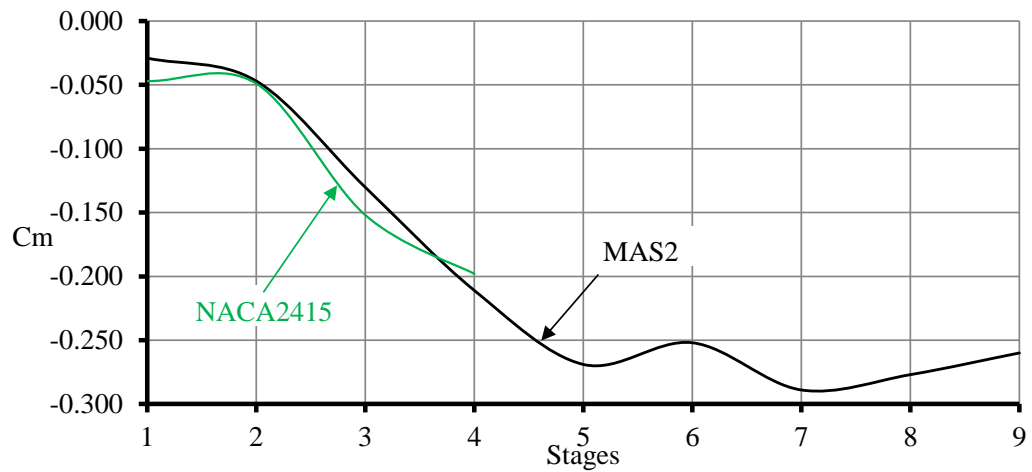
Figure 5.29: C_m for the same C_L in different stages of Figures 5.30 to 5.38.
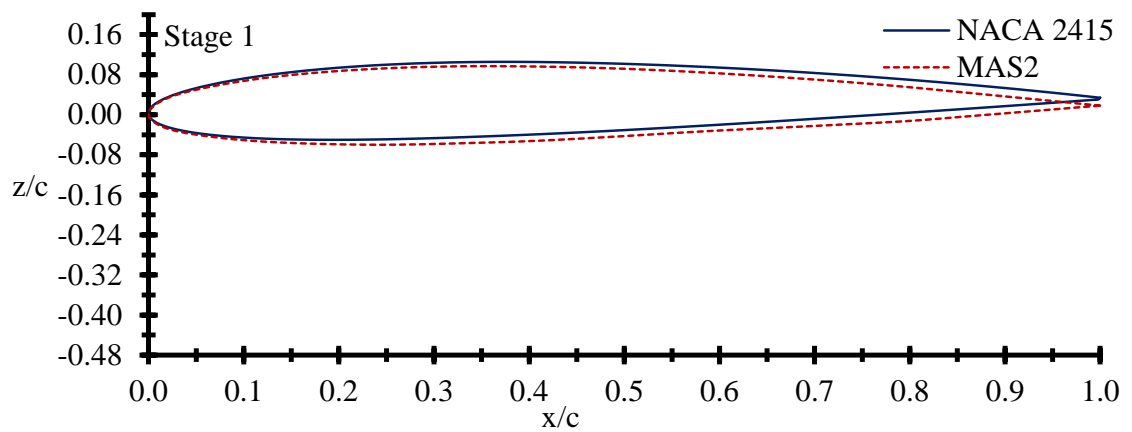
Figure 5.30: Stage 1 of normalised MAS2 and same C_L of NACA2415 aerofoil shape.
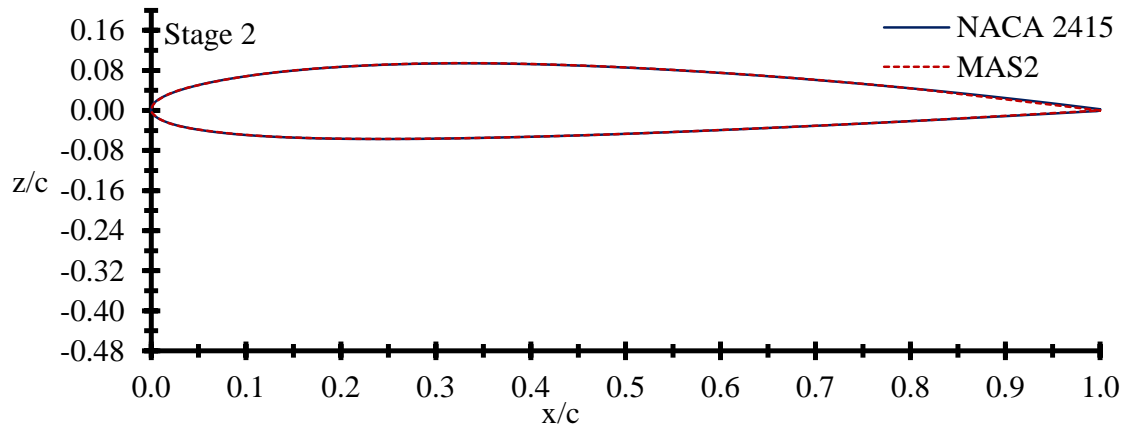
Figure 5.31: Stage 2 of normalised MAS2 and same C_L of NACA2415 aerofoil shape.
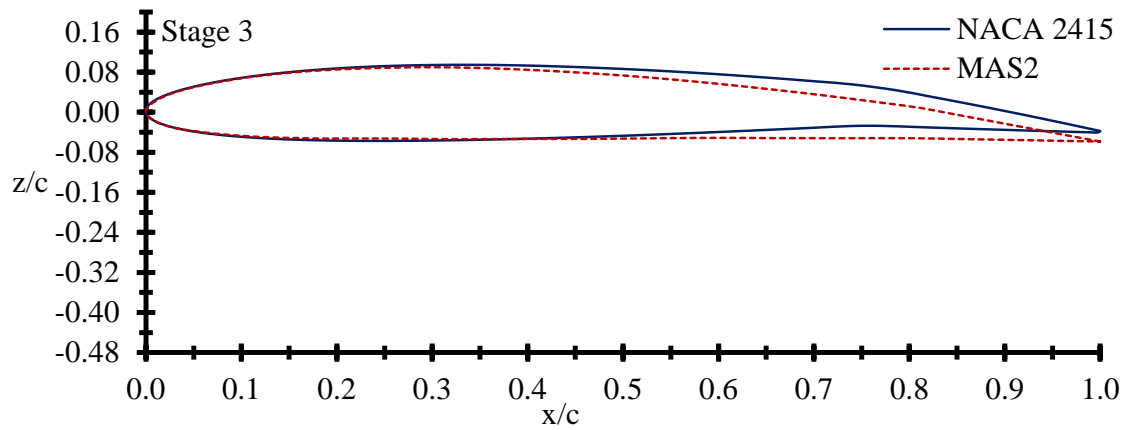
Figure 5.32: Stage 3 of normalised MAS2 and same C_L of NACA2415 aerofoil shape.
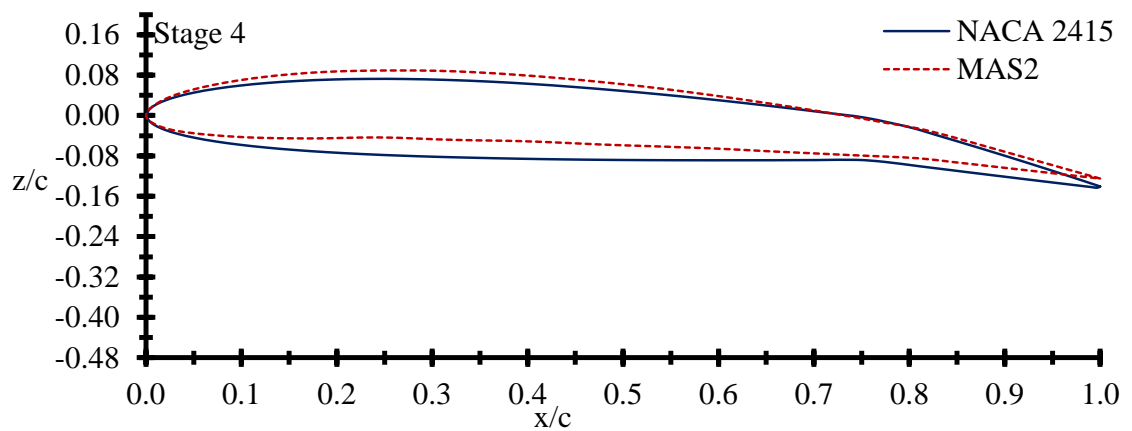
Figure 5.33: Stage 4 of normalised MAS2 and same C_L of NACA2415 aerofoil shape.
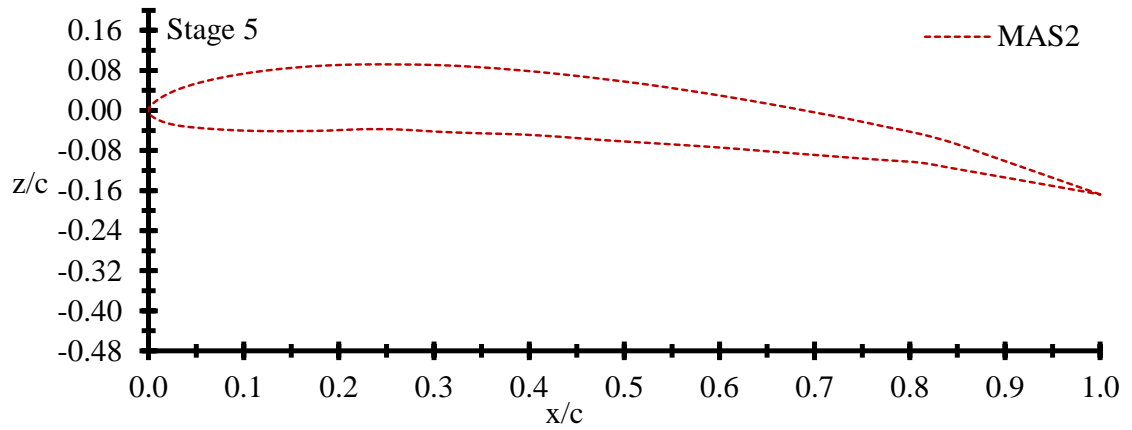
Figure 5.34: Stage 5 of normalised MAS2.
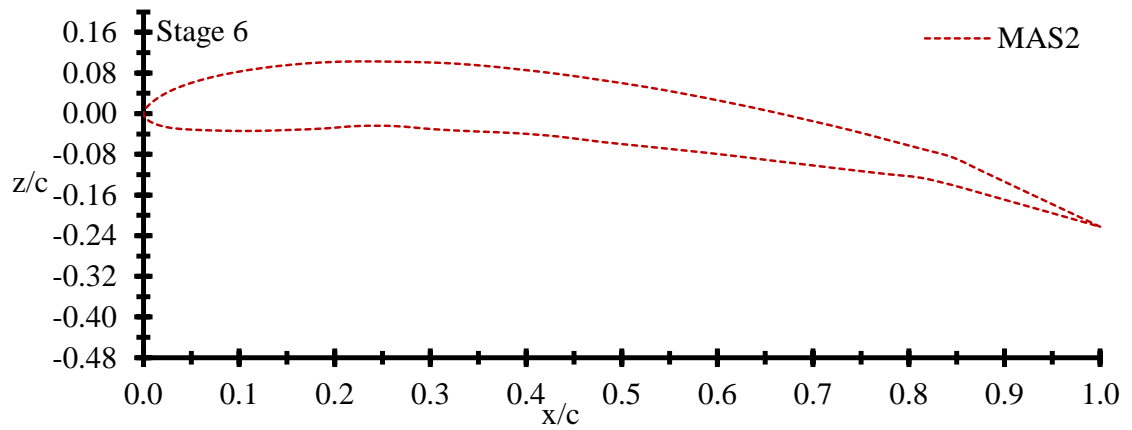
Figure 5.35: Stage 6 of normalised MAS2.
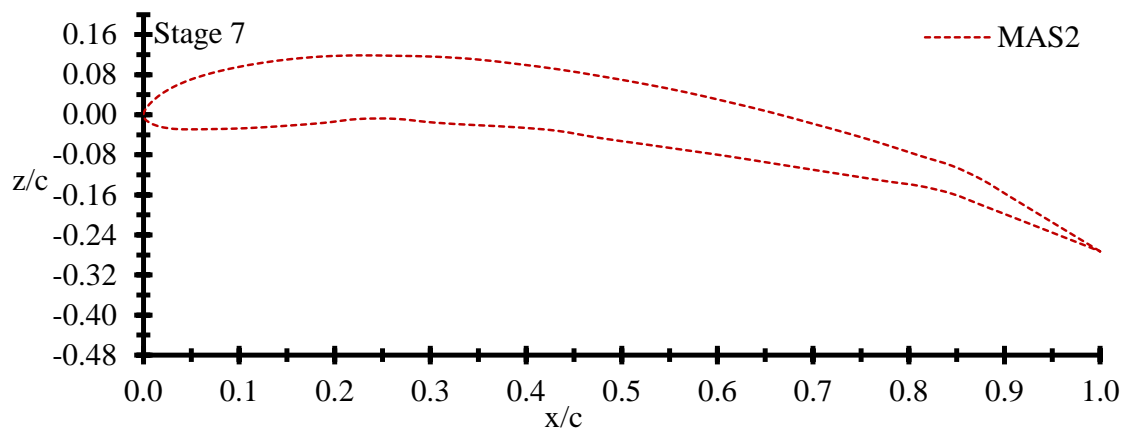
Figure 5.36: Stage 7 of normalised MAS2.
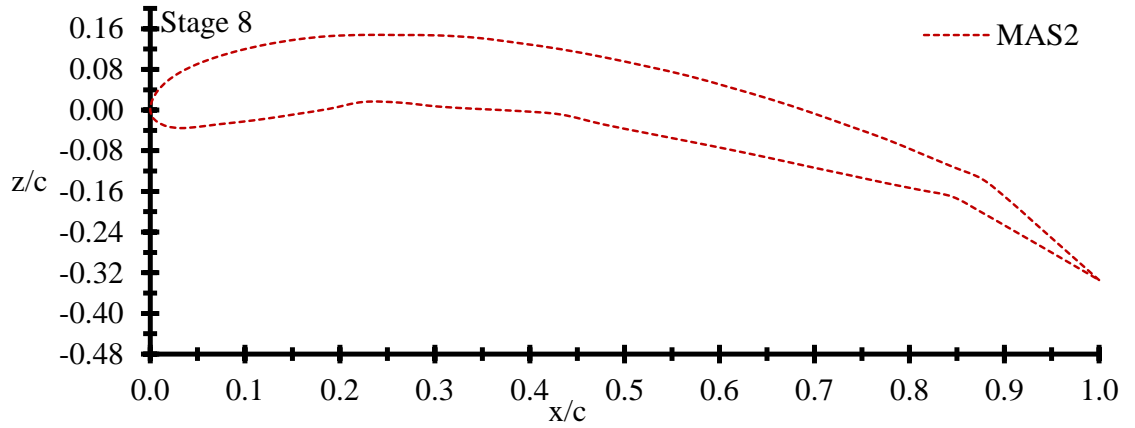
Figure 5.37: Stage 8 of normalised MAS2.
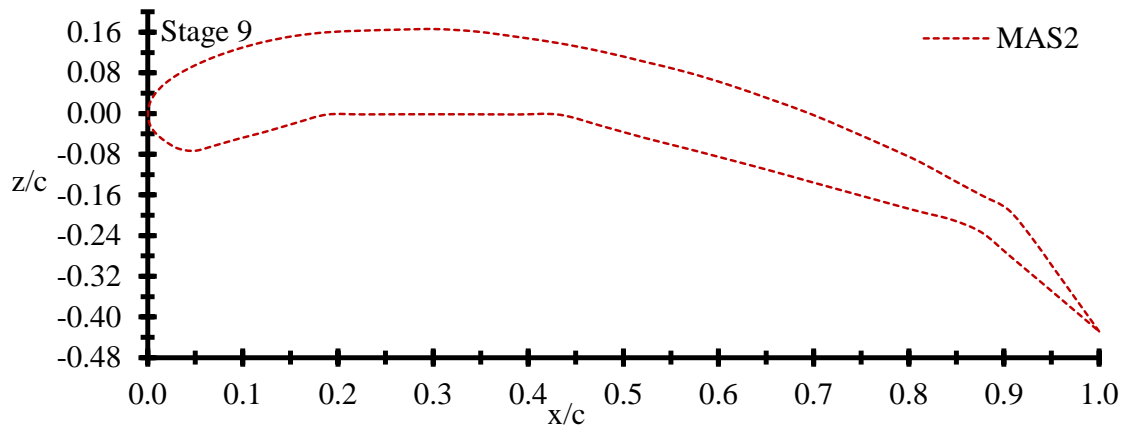
Figure 5.38: Stage 9 of normalised MAS2.

5.6.4 Cross-Sectional Area Comparison of Proposed Morphing Aerofoils with NACA2415

While changes are made to C_L and C_D in NACA2415 arising from increasing angle of attack and hinged flaps, there is little corresponding change of cross-sectional area. On the other hand, changes to C_L and C_D of MAS1 and MAS2, are achieved by deforming the configuration of the morphing aerofoil, so this leads to some change of cross-section of the aerofoil. Essentially, increasing stages also lead to reducing thickness, increasing chord length and changing camber. Figure 5.39 shows the cross-sectional area comparison, normalised to NACA2415 as 100%. There is a significant area decrease in

MAS1 and MAS2 with stages, while the changing of flap angles has resulted in negligible cross-sectional area change for the NACA2415.

Since the cross-section of aircraft wings is often used for fuel storage, it could be argued that the present concepts for morphing aerofoils are unacceptable, due to the cross-sectional area being smaller than that of for NACA2415, to which they are being compared. For this reason, a further morphing aerofoil (MAS3, which is similar to MAS2, see Figure 5.40) is proposed, with the deliberate property such that at its minimum cross-sectional area (*i.e.* morphing stage 9), it still has a cross-sectional area greater than that of NACA2415. At the same time, since MAS3 is designed to have at all times a cross-sectional area greater than that of NACA2415, then at its largest cross-sectional area (stage 1), MAS3 does have an area significantly larger (114%) than is required.

C_L and C_D relationship of MAS3 is compared with MAS1 and MAS2 in Figure 5.41, where the behaviour of MAS3 is very close to that of MAS2 with just a slightly smaller C_L for the same C_D.
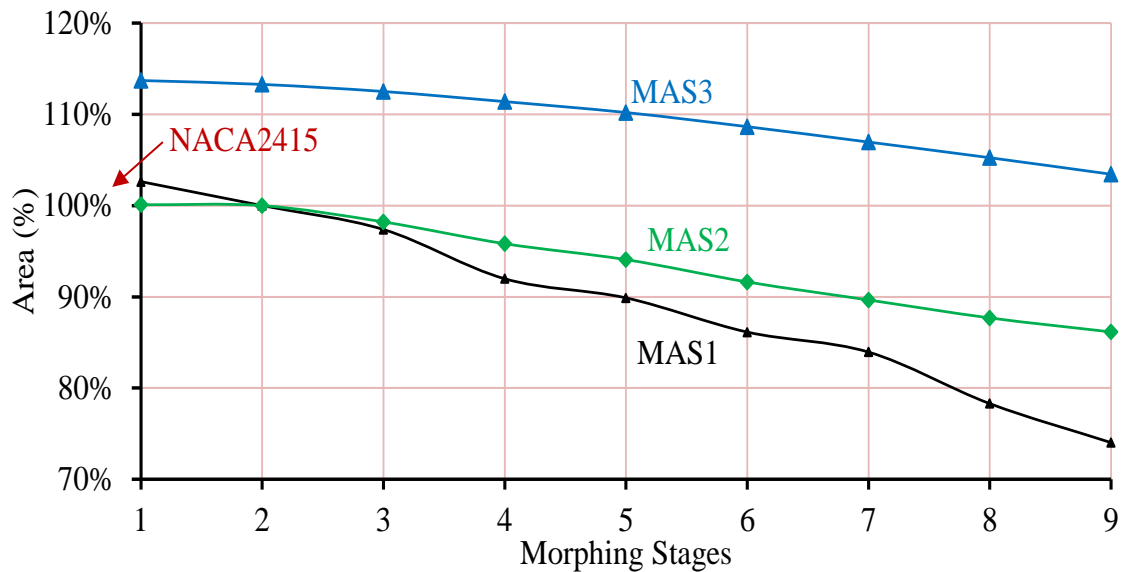
Figure 5.39: Cross-sectional area comparison of MAS1, MAS2 and MAS3
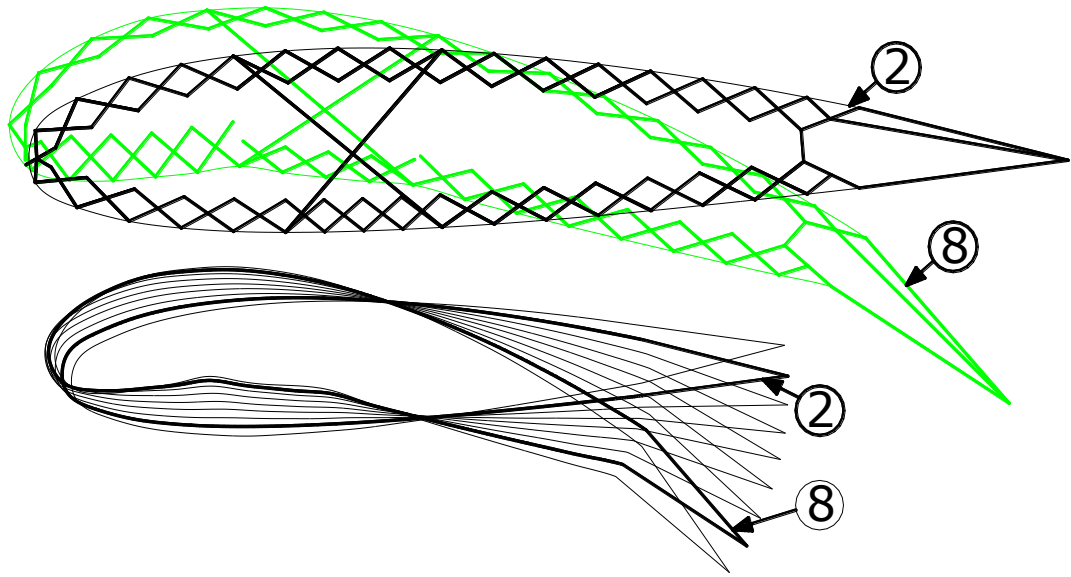
Figure 5.40: Nine morphing stages of MAS3.
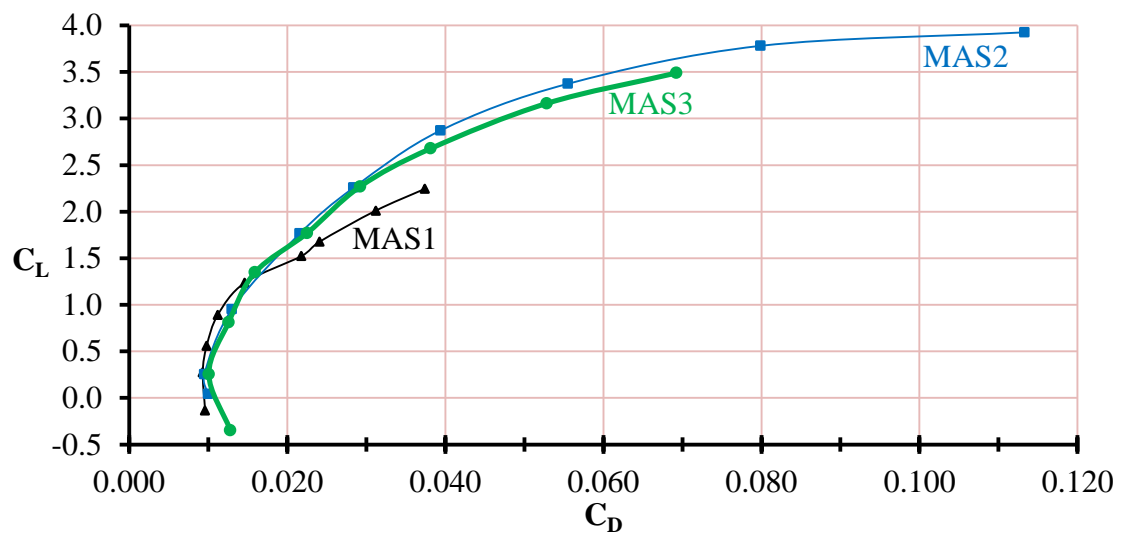
Figure 5.41: Lift versus drag comparison of MAS1, MAS2 and MAS3.

Since it is possible to control the C_L and C_D via a morphing aerofoil, the work in this Chapter has shown the advantages of such an approach over the traditional fixed aerofoil with hinged flaps. The morphing aerofoils can provide different shape configurations for changing camber, leading and trailing edge to fit varying flight environments and control the attitude. In partial as the morphing wing is more effectiveness for having less drag for a given lift.

Chapter 6

Experiment, Results and Discussion of Morphing Pantographic Structure

6.1 Introduction

This chapter discuses constructing and testing a morphing pantographic structure and compares experimental results with the theoretical results coming from displacement control without regard to bar force through using the condensed matrix technique (because of pantograph elements) as presented in Section 3.2.2. This chapter gives details of the designing and modelling of the structure, measurement system with instruments, data collecting and then comparing experimental results obtained with theoretical results.

6.2 Pantographic Morphing Structure

A model of the morphing aerofoil structure was constructed for experimental purposes. This model follows the geometry and configuration of the morphing aerofoil cross-section presented in Chapter 5, as an application of the pantographic morphing structure. The model is built via series of interconnected, irregular, single-control pantographs as shown in Figure 6.1. Each pantograph unit consists of two coplanar beam elements of

different lengths connected together by a shear connector (scissor-like hinge) with axis perpendicular to the plane of the beams. Two adjacent pantograph-units are connected by a further shear connector at the ends of the coplanar beams. A model was constructed for the purpose of adjustment experiment of the external joint displacement. There was no adjustment of internal bar forces in any of experiments done in this chapter mainly because the beams of the model are comparatively thick and thus able to sustain big axial forces, but also because the principal control of interest in the aerofoil is getting the right shape accurately, in order to obtain the desired aerodynamic characteristics. The morphing in the structure is activated through length change in the bar designated "bar 36" in Figure 6.1, and the description and explanation of pantographic morphing structure components are detailed in the next sections.

6.2.1 Beams

Rectangular ($6.0\text{mm} \times 9.0\text{mm}$) aluminium bars with different lengths have been chosen for all members of the model. The reason behind choosing the aluminium material is its light weight, since the aerofoil structure without any edge members is very flexible and very sensitive to vertical loading. Although all the structural members are made of the same aluminium bar, there are in fact two types of members based on the internal forces carried by the bars. The first group carry just axial force since both ends of the bar are hinged (*e.g.* bar 1). On the other hand, the second group (which covers the majority of members, forming the pantographs) are beams with both axial force and bending moment. The pantograph beams carry a maximum bending at the central shear-connector joint in each of its beams, which diminishes to zero at each of the remote ends.

Morphing Control Bar

Members	Length (mm)	Members	Length (mm)	Members	Length (mm)	Members	Length (mm)	All Members		
1	58.4	11	113.1	21	116.1	31	118.3	Height	9.0	mm
2	70.1	12	116.7	22	117.5	32	118.9	Width	6.0	mm
3	52.6	13	118.8	23	117.6	33	119.4	EA	3,780	kN
4	113.7	14	111.8	24	117	34	310.4	EI	25,515	kN.mm^2
5	76	15	110.7	25	119.3	35	208.1			
6	111.7	16	117.1	26	114.2	36	200.5			
7	107.1	17	117.8	27	113.9					
8	120.6	18	111.5	28	119.8					
9	118.3	19	112.5	29	117.3					
10	111.3	20	119.3	30	117.8					

Figure 6.1: Pantographic morphing structure model (Demonstration morphing of Aerofoil)

The "control" for length change is the turnbuckles, which was introduced in Section 5.2.5 for cables. Similarly, turnbuckles were introduced into some of the beams/bars for length change actuation. In the case of bars (which carry only axial force), the position of the turnbuckle along the length of the bar was not too critical. However, the positioning of the turnbuckle for a beam was more important, since the turnbuckle (with little cross-section depth) is not a good device for transmission of bending moment. Indeed, the (necessary) slight play in the thread of the turnbuckle also makes it difficult to determine the actual bending moment there. Therefore, turnbuckles for beams were placed near the remote ends of the pantographs, where the bending moment is at its lowest, as shown in Figure 6.2.

Initially, the intention was to include a turnbuckle in every beam/bar (even though some of these might not be used). However, it was noticed that such a structure had too much flexibility, because, however well constructed was each turnbuckle, the slight play in the threaded joint meant it behaved to a certain extent as a pin joint with limited rotation. With multiple turnbuckles, and therefore a compounding of the rotations from multiple turnbuckles even though each has only limited rotation, the other ends of the overall structure were rather (uncontrollably) flexible. This could be countered if the morphing aerofoil structure had edge cables which could then induce a state of prestress, but this model consisted only of the deployable backbone. Instead, a second model was made where the members had accurately "perfect" lengths and no turnbuckles, and invidual beams/bars were exchanged between the two models only when a turnbuckle in a particular member was actually needed in a particular test.

Bar 36 is known as the "morphing control" bar since this is the bar responsible for controlling the shape configuration of the morphing aerofoil structure model. This bar can be attached to any of the single pantograph units. The capability of this bar to shorten and lengthen gives different shape configurations to the structure. A slightly longer turnbuckle (with 75mm of actuation) was used for this bar. Figure 6.2 also shows loading hooks attached to the top and end joints of the structure, and loads were applied in the form of fixed weights (and calibrated steel bolts proved to be useful for this purpose).

6.2.2   Joints

Although there are two types of joints in the morphing structure, practically, the two types are both the same and involve a 3mm diameter frictionless pin inserted through two beams/bars perpendicularly to the plane containing those two members, to form a revolute joint (also known as a "scissor-hinge"), see Figure 6.3. Such a joint always allows free rotation of the two beams/bars in their common plane, but is capable of transmitting all other forces through the joint. The difference between the two joints is only in whether an inplane bending moment is transmitted across the joint, and this is determined by the location of the joint (i.e. somewhere along the length of a beam-pair, rather than at the ends), rather than the physical nature of the connection.
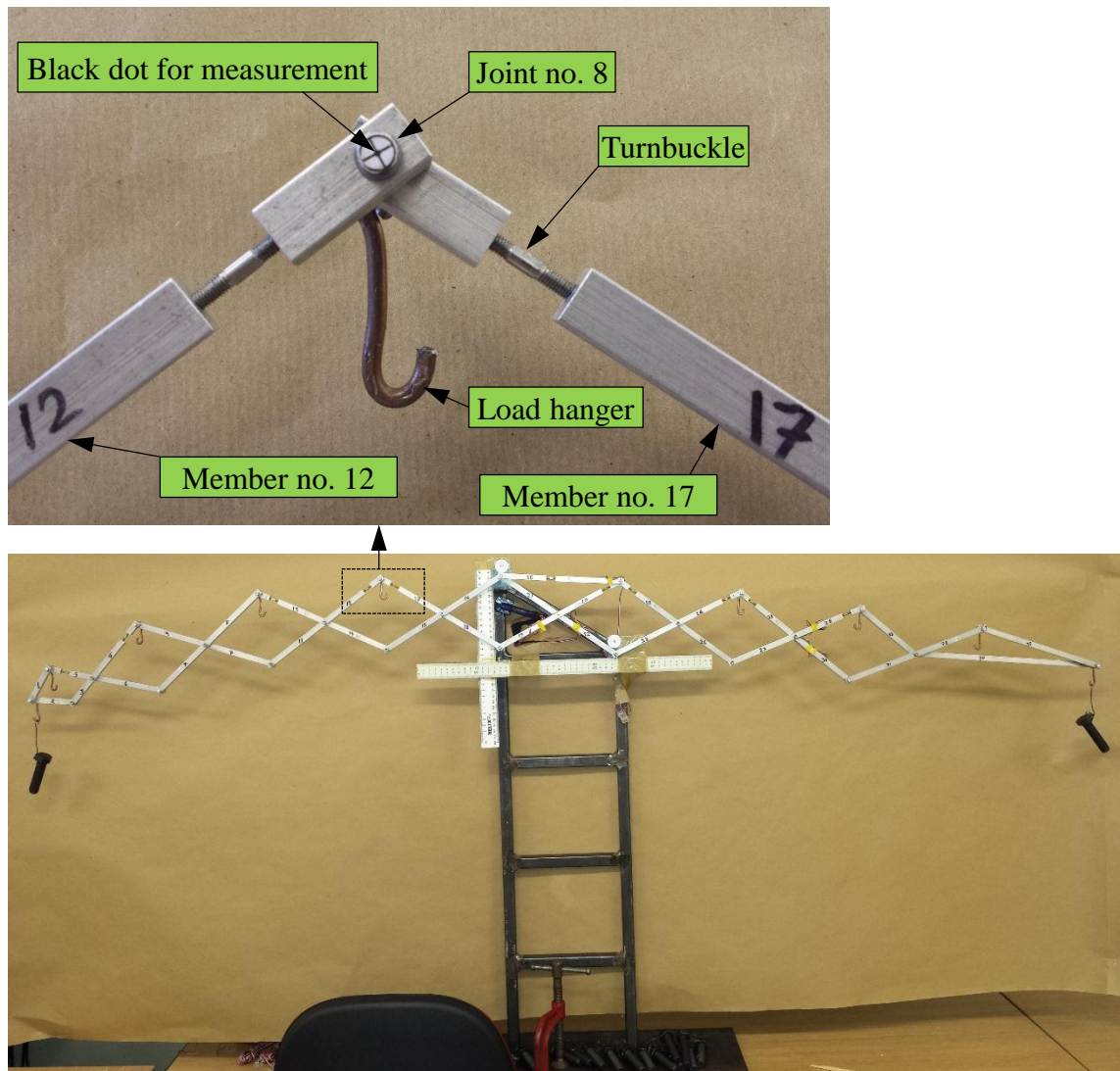
Figure 6.2: The photograph of the pantographic morphing structure
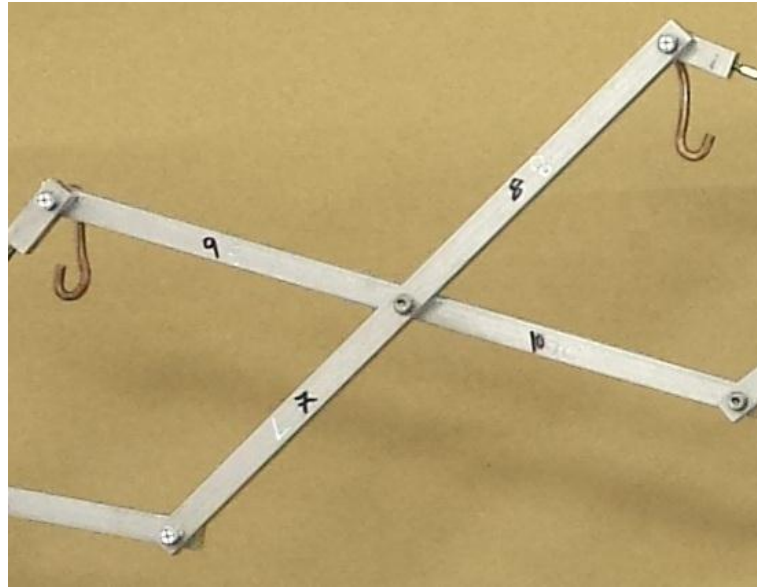
Figure 6.3: A two-dimensional Pantograph unit

6.2.3   Supporting System

In Figure 6.2 shows the support system built for the morphing structure, which is a simple and stiff frame to provide pin-support at two locations, i.e. joints 10 and 13. The detailed shape and dimensions are shown in Figure 6.4 , and the frame contains of two columns with five welded beam between them stiffness minimising any movement of the model due to unsymmetrical loading during the tests. The frame of the support was welded to an 8mm thick steel base plate at the bottom which was in turn fixed to the test bench via G-clamps. All support frame connections were full welds

6.2.4   Measurement of Joints Displacement

For measuring joint horizontal and vertical displacements of the pantographic morphing structure model, an attempt was made through using low resistance dial gauges, which was not successful for the reason of high flexibility of the model the measurements were distorted under plunger force of the dial gauges themselves. A non-contact measuring technique was needed. Endeavour was made to use the Qualisys Track Manager (QTM) system for measurement which is a system involving a set of cameras taking pictures of reflective targets, from which the coordinates of the targets could be found from a

computer system linked to the cameras. However, there was limited availability of this system, which is largely designed for dynamic monitoring (*e.g.* in gait studies). It is also to be noted that the QTM system is principally a 3D system, which would work for the principally 2D model, but was overly complicated for it. The potential extra level of accuracy of the QTM system over a simple 2D digital photography was also not necessary due to the relatively large displacements exhibited by the flexible model.
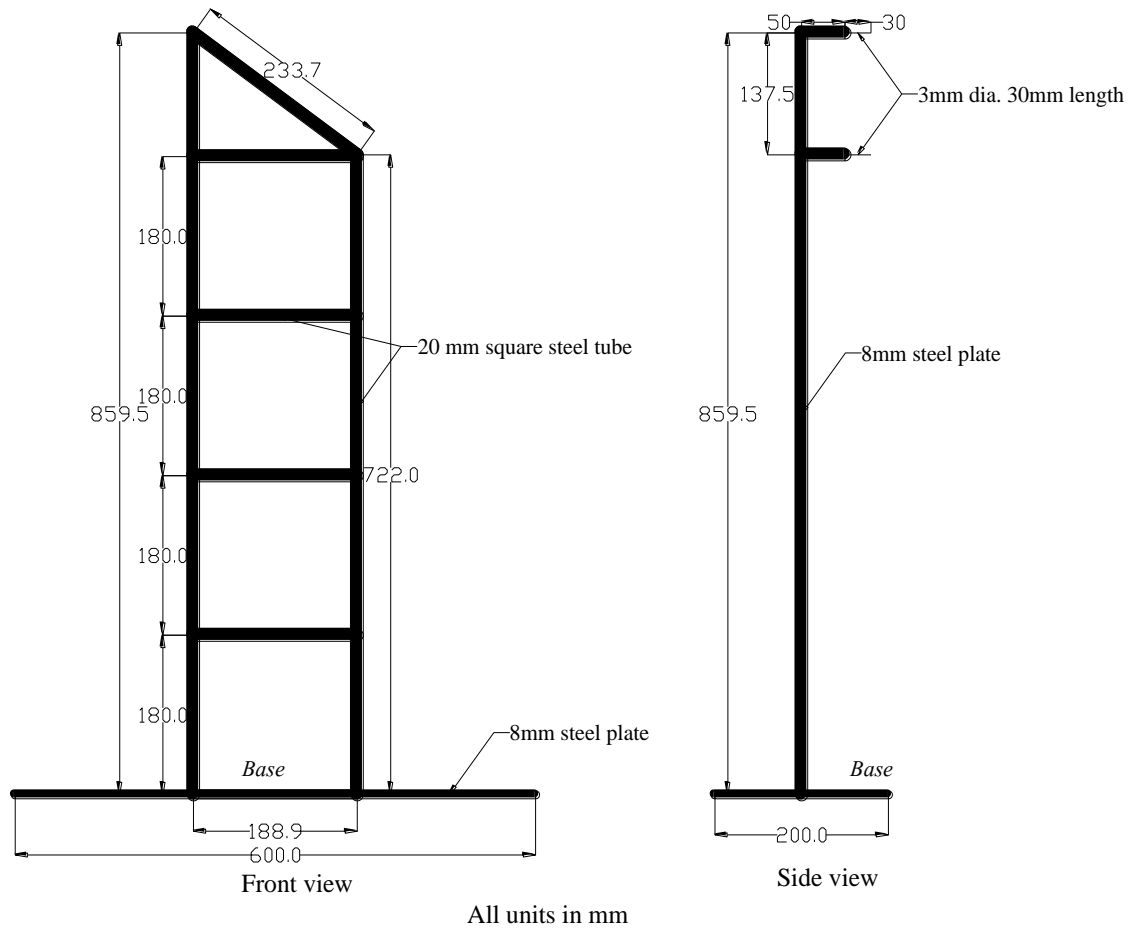
Figure 6.4: Details of the support structure for the pantographic morphing model.

The procedure of measurements starts by placing small black dots (diameter $\approx$ 1mm) in the black circle of 5mm diameter as visual targets on white paper glued to the joints of the model. A 13MP digital camera mounted on a tripod was used for taking photographs of the structure model with using "Pattern monitoring mode" which is also called by other names according to different manufactures, *e.g.* Evaluative (for Canon

Cameras), or Matrix (for Nikon Cameras) (Arbabi, 2012). This technique of metering is the most accurate and applies the correct exposure of all metering modes for our purpose Figure 6.5 shows the different metering modes of the camera. The chosen technique reads the light intensity at several points around the frame and the final exposure is the average of all points. In contrast, the Spot or Partial metering reads the light from a small section in the centre of the frame usually (1%-5%) and (5%-9%) respectively without the influence of any other area. This mode type gives more control to small areas of the overall photograph.

The camera was fixed on a firm tripod stand opposite the centre of the structure model in an appropriate distance in such a way as far enough to get minimal edge distortion of the picture, while near enough to simultaneously have all the target black dots on all joints seen clearly on the photograph. During the experiment, a picture of the structure model was taken before and after any change of external loading and bar actuation, together with scaled rulers for calibration. Displacements were calculated by measuring the distance moved by the black dots in each joints. The process of calculation was done in both AutoCAD software and by pixel count, with both software giving an accuracy of ±0.4mm on average.
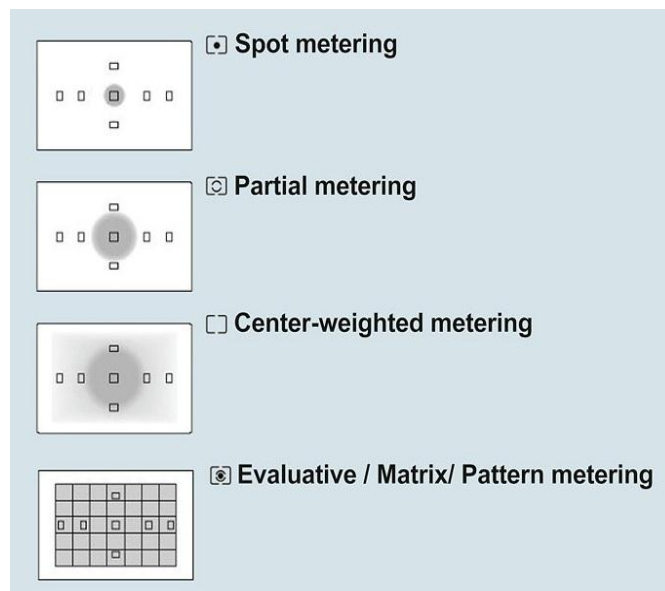
Figure 6.5: Metering modes of the camera: Source: Arbabi (2012).

The procedure of calculation in AutoCAD was done by superimposing two photos to find their displacements change. The combined photos had common points on the base and background selected as origin points to eliminate any errors, and to make sure the superimposing fit together properly. Then by using the vertical and horizontal dimension command of AutoCAD, the distance of the middle pixel of a given joint in both photos was measured, as shown in Figure 6.6. Calculating the displacement of the joint by pixel count involved using Microsoft Excel. The procedure involved dividing the total length and width in the photo by the number of pixels horizontally and vertically, to give the actual distance represented by a pixel for a given picture. The distance moved by the joint can be counted in terms of pixel, and the associated distance then calculated. The accuracy of calculation in both methods is approximate ±0.4mm, which is equal to the size of one pixel.

6.2.5 *Properties of Materials*

All bars/beams used in constructing of the model of the pantographic morphing structure were of the same material and size, which is all aluminium alloy, rectangular cross-section solid bar, with 9mm height and 6mm width. The stiffness of the beam/bar used was based on Young's Modulus E=70kN/mm^2, thus EA=3.78MN and EI=25.515MN.mm^2.

6.3 **Testing Procedure**

Various preparations were carried out before the model of the pantographic morphing structure was tested. These were performed for all tests: adjustment of displacements, morphing and adjustments after morphing. After fixing the model support to the test bench via several G-clamps all the black dot target was were glued to the target joints, and two scale rules (horizontally and vertically) were fixed to the support of the model to provide calibration scale and check against distortion in the photographing process. In addition, the camera was fixed and aligned properly along the centreline perpendicular to the model. Next, the weights were hung to the structure according to the tests through the loading hooks, after checking the weights on a sensitive electronic balance.
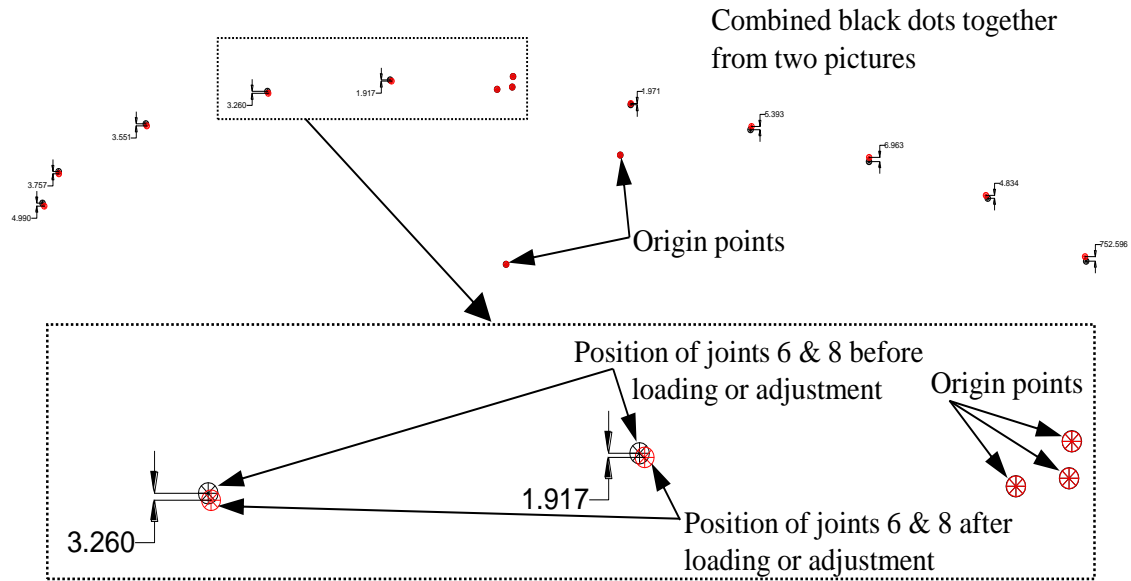
Figure 6.6: Calculating joint displacements by AutoCAD software

The "pre-adjustments" due to the loads applied to the structure are calculated from the two pictures taken before and after the application of the weights. A certain desired shape for the loaded structure is then prescribed, and hence a set of desired displacements for each joint to be controlled was obtained for the adjustment technique. Following calculation in the MATLAB program, the theoretical amount of actuation can be calculated for each active member necessary to move joints to the required position. This adjustment had to be applied with care so as to not accidently disturb the structure, or knock some parts of it or the support structure. It should be noted that this is a slow process, since the joint displacement measurement requires careful visual analysis of photographs, and applying the actuation is a delicate process. There is thus possibility of accidental disturbance, and also systematic error in the gradual "relaxation" in the joints/turnbuckles. Once all actuations have been applied, the joint movements are again measured via taking photographs. For validation of the results, both experimental results are compared to the theoretical results from the MATLAB program. In this chapter different experiments were done for adjustment and morphing as discussed in Sections 6.4 and 6.5.

6.4 Experimental and Theoretical Adjustment Comparison and Discussion

There is a linear method used for the nodal displacement control of the pantographic morphing structure. The technique of condensation matrix is applied to control this model, using reduced matrices of equilibrium, compatibility and flexibility since this model is constructed from interconnecting a series of pantographic units as detailed in Section 3.3. This technique can be applied to the pantographic morphing structure model in Figure 6.1 with few points and observation.

The complete global equilibrium matrix ($\mathbf{A}$) of the given example is of size 105×108, since this model consists of 36 beams and 35 joints. In order to condense the equilibrium matrix some steps must be done. Firstly, removing four rows relating to four constraints of the two supports (*i.e.* dx_{10}, dy_{10}, dx_{13} and dy_{13}) therefore the size of the $\mathbf{A}$ matrix becomes 101×108. Secondly, since there is no external couple applied to the internal joints, the bending moment there will be continuous in each beam-pair of the pantograph unit, therefore the moment of both beams of a beam-pair can be replaced by a single variable. In the given example there were seven pantograph units with two half pantograph beams 31 and 32, see Figure 6.1, thus 30 mid-joint moments of all beams of pantographs can be replaced by 15 new variables, hence the size of $\mathbf{A}$ becomes 101×93. Thirdly, since the pantograph units are connected to each other at their remote ends by pin-joints, then the internal bending moment of each beam-pair at these ends are always equal to zero, and consequently all the 42 columns corresponding to these moments can be removed and the size of the $\mathbf{A}$ matrix is reduced to 101×51. Fourthly, since no external couples are applied to the mid- and end-joints of the pantograph units of the given example, the corresponding 35 rows are removed so the size of the $\mathbf{A}$ matrix reduced to 66×51. Fifthly, as there is no external load applied to the internal joints of the pantograph unit, which is just a shear-connector between two beam-pairs, the two horizontal component of load at both mid joints can be replaced by one new horizontal component, which is equal to the sum of both horizontal components. Similarly, the same can also be done for the vertical components. The given example has sixteen mid joints as shown in Figure 6.1, thus all 32 components of the mid-joints of the model can be replaced by 16 new components, hence the size of $\mathbf{A}$ becomes 50×51. Now the equilibrium matrix can be condensed to $\mathbf{A}^*$ by using Eqn. 3.25 to a size of 35×36.

Similarly, the condensed compatibility and flexibility matrix must be calculated using the same process. Briefly, since compatibility matrix is the transpose of equilibrium matrix, the global size of $\mathbf{B}$ is 108×105, and after condensation the size $\mathbf{B}^*$ reduces to 36×35. While the global flexibility matrix starts with size 108×108, is reduced to 51×51, and after completion of condensation process, $\mathbf{F}^*$ has size 36×36.

6.4.1   Linear Adjustment

An attempt was made to control displacements of joint by using the reduced matrices for equilibrium, compatibility and flexibility matrix of the pantographic morphing structure linearly through finding a required set of actuations $\mathbf{e_0}$ directly in one cycle of actuation. Then the adjustment was done theoretically in MATLAB program and experimentally on the model, applying the calculated set of $\mathbf{e_0}$ actuations to all selected bars to reach the target shape.

Some experiments were done as shape adjustment on the model, after morphing other experiments were done for adjustment of the model with attached elastic bands between two adjacent external joints of the model, to simulate the effect of high strain stretchable skin on the surface of the aerofoil. Furthermore, experiments of multi-iteration adjustment were also done to reduce and remove errors arising from experimental work. Since this work is on the demonstration of the morphing aerofoil structure as an application of a morphing pantographic structure, the emphasis will be to control the shape of the structure, especially the upper surface, lower surface and the leading edge of the aerofoil, due to their role on the coefficients of lift and drag.

6.4.1.1 Adjustments for Distributed Vertical Load

An aerofoil structure must be designed to withstand a large number of different types of loads and one of them is the aerodynamic load which is a distributed load as the result of pressures and shear stresses distributed over the aerofoil surface (Brandt *et al.*, 2004). Therefore, the adjustment in this experiment was done under "distributed" vertical load at the joints. Vertical displacement control of the top surface of the structure in Figure 6.1 is illustrated in Table 6.1 (Experiment 1) which is carried out without regard to the bar

forces. Actuation is applied in ten beams of the structure. After entering the target shape for the pre-adjustment displacement of the desired joints into the MATLAB program, the amount of actuation of each member with an actuator already embedded was calculated using Eqn. 3.54.

Generally, the number of bars selected for actuation was sufficient, *i.e.* the possibility of achieving desired displacement target could be guaranteed in this structure. All the selected bar elongations were among non-vanishing components in the condensation process. The structure was thus adjusted practically in the laboratory according to the set of actuations from the program.

Values of various parameters for the measured structure are shown in Columns 1 to 5 of Table 6.1. For the purpose of examining the efficiency of adjustment, it is presumed that the desired displacements are those shown in Column 7 of Table 6.1, which represent a more smooth top surface shape. This set of desired displacements represents significant deviation from the existing measured displacements in Column 5 and hence it is a reasonably good test of adjustment of a distorted model. The computed set of e_0 is shown in Column 6 of Table 6.1. Post-adjustment vertical displacement results (Column 8) are in good agreement with the target position (Column 7) as also shown in Figure 6.7, with only small deviations. The source of this deviation is the combination of errors from imperfection in the geometrical construction of the structure and measurement of its coordinates, and additional flexibility in the structure due to turnbuckles with some slack in the bars. It is clear that the joints furthest from the support have more deviation than those closer. The total actuation in this experiment was 10.05mm, through the same results could have been achieved with less actuation by selecting the most effective bars for these displacements, see Section 6.4.1.7 later on, which gives minimum actuation for controlling vertical displacement of the upper surface for any loading and any target position. For this set of actuators which have not been optimally chosen according to any objective, some of the selected bars would likely be working to some extent against each other.

Table 6.1: Vertical displacement control of the upper surface joints of the structure in Figure 6.1 under distributed vertical load (MATLAB program is shown in Appendix A.7).

(1)	(2)	(3)	(4)	(5)	(6)	(7)	(8)	(9)	(10)
Joints	Cond. Disp.	Dir	Loads (P) N	Just d_p, no e_o Theo. & Prac. (mm)	(e_o) (mm)	displacement after applying e_o with 10 components (mm)		Cond. Bars	Bar
						Theo.	Prac.		
1		x	0		0				1
		y	-2.286	**-13.44**	0	**-9**	**-9.45**		2
2		x	0		0				3
		y	-2.286	**-12.85**	0.89	**-8**	**-8.58**		4
3		x	0		0.84				5
		y	0		0				6
4		x	0		0				7
		y	-2.286	**-9.56**	0	**-5**	**-5.11**		8
5		x	0		0				9
		y	0		0				10
6		x	0		0				11
		y	-2.286	**-5.44**	-1.72	**-3**	**-2.99**		12
7		x	0		-0.82				13
		y	0		0				14
8		x	0		0				15
		y	-2.286	**-2.13**	0	**-1**	**-1.13**		16
9		x	0		1.58				17
		y	0		0				18
10		x	0	0	0			t_n	19
	d_m	y	0	0	-0.24				20
11		x	0		0				21
		y	0		0				22
12		x	0		0				23
		y	0	**0.47**	1.60	**0**	**0.13***		24
13		x	0	0	-0.11				25
		y	0	0	0				26
14		x	0		0				27
		y	-2.286	**-0.41**	-0.79	**0**	**0.23***		28
15		x	0		-1.46				29
		y	0		0				30
16		x	0		0				31
		y	-2.286	**-2.14**	0	**-1**	**-0.96**		32
17		x	0		0				33
		y	0		0				34
18		x	0		0				35
		y	-2.286	**-4.33**	0	**-2**	**-2.13**		36
19		x	0		0				m(3,4)
		y	-2.286	**-7.31**	0	**-3**	**-3.07**		m(4,6)
34,35		x	0		0				m(7,8)
		y	0		0				m(9,10)
20,21		x	0		0				m(11,12)
		y	0		0				m(13,14)
22,23		x	0		0				m(15,16)
		y	0		0			t_p	m(17,18)
24,25		x	0		0				m(19,20)
		y	0		0				m(21,22)
26,27	d_p	x	0		0				m(23,24)
		y	0		0				m(25,26)
28,29		x	0		0				m(27,28)
		y	0		0				m(29,30)
30,31		x	0		0				m(31,32)
		y	0		0				
32,33		x	0		0				
		y	0		0				
				total (mm) 10.05					

*Within the range of the precision of 0.4mm

Figure 6.7: Vertical displacement control of the upper surface joints of the structure in Figure 6.1 under distributed vertical load

6.4.1.2 Adjustments for Distributed Vertical Load after Morphing

In this experiment (Experiment 2), the structure is tested under the same loading case as in Experiment 1 and also the same joint displacements are desired to be controlled, but Experiment 2 differs in that the starting shape of the structure is different since the structure is tested after shape morphing. The morphing is the result of lengthening the control bar by +10mm and the structure increases in both overall length and curvature. The new shape (in nodal coordinates) and different nodal displacements under load (Column 5) in Table 6.2, the target position of the of those joints required to be control are also consequently different as shown in Column 7 of Table 6.2.

The actuation $\mathbf{e_o}$ for this experiment is calculated in the MATLAB program with equation for displacement control (without regard to the bar force), Eqn. 3.54, together with including the +10mm initial elongation to the morphing control bar (bar-36). The set of $\mathbf{e_o}$ for this experiment is shown in Column 6 of Table 6.2, with the total actuation of 14.22mm.

Consequent to the adjustment, the measured displacements are as shown Column 8 of Table 6.2 and graphically compared with the target position in Figure 6.8. Again, the difference between post-adjustment measurement and target position is small.

From this, it can be concluded that shape adjustment or refinement is likely to be possible for similar morphing structures for some specified joint displacements, with a fixed set of actuation members, in any stage of morphing. This is a good result for the technology of designing morphing aerofoils, since not only have the static stages morphing aerofoil itself shown to have better aerodynamic characteristics than the equivalent fixed shape NACA aerofoil with flaps, but here, we see that a morphing aerofoil which has gone "out of shape" due to changes in load or weight (*e.g.* through the burning of fuel normally stored within the voids of the aerofoil) can be corrected via shape adjustment. Furthermore, this leads to the possibility that a desired change in lift/drag characteristics could be obtained from either a morphing change or a smaller refining shape change, and thus the choice could be made dynamically during flight, and be optimised for best economy of flight operational parameters.

Figure 6.8: Vertical displacement control of the upper surface joints of the morphed shape of the structure in Figure 6.1 with (+10mm) e_0 of bar-36, under distributed vertical load.

Table 6.2: Vertical displacement control of the upper surface joints of the morphed shape of the structure in Figure 6.1 with (+10mm) e_o of bar-36, under distributed vertical load (MATLAB program can be found in Appendix A.8).

(1)	(2)	(3)	(4)	(5)	(6)	(7)	(8)	(9)	(10)
Joints	Cond. Disp.	Dir	Loads (P) N	Just d_p, no e_o Theo. & Prac. (mm)	(e_o) (mm)	displacement after applying e_o with 10 components (mm) Theo.	Prac.	Cond. Bars	Bar
1		x	0		0				1
		y	-2.286	20.73	0	15	15.74		2
2		x	0		0				3
		y	-2.286	19.12	-0.29	15	15.36		4
3		x	0		2.51				5
		y	0		0				6
4		x	0		0				7
		y	-2.286	19.45	0	15	15.90		8
5		x	0		0				9
		y	0		0				10
6		x	0		0				11
		y	-2.286	18.30	1.26	15	15.04		12
7		x	0		0.17				13
		y	0		0				14
8		x	0		0				15
		y	-2.286	11.76	0	10	9.84		16
9		x	0		-1.32				17
		y	0		0				18
10		x	0	0	0			t_n	19
	d_m	y	0	0	0.89				20
11		x	0		0				21
		y	0		0				22
12		x	0		0				23
		y	0	-16.71	3.29	-15	-14.74		24
13		x	0	0	-1.07				25
		y	0	0	0				26
14		x	0		0				27
		y	-2.286	-35.50	1.72	-30	-30.11		28
15		x	0		-1.70				29
		y	0		0				30
16		x	0		0				31
		y	-2.286	-57.51	0	-50	-50.55		32
17		x	0		0				33
		y	0		0				34
18		x	0		0				35
		y	-2.286	-80.76	0	-75	-75.93		36
19		x	0		0				m(3,4)
		y	-2.286	-119.36	0	-110	-111.83		m(4,6)
34,35		x	0		0				m(7,8)
		y	0		0				m(9,10)
20,21		x	0		0				m(11,12)
		y	0		0				m(13,14)
22,23		x	0		0				m(15,16)
		y	0		0			t_p	m(17,18)
24,25		x	0		0				m(19,20)
		y	0		0				m(21,22)
26,27	d_p	x	0		0				m(23,24)
		y	0		0				m(25,26)
28,29		x	0		0				m(27,28)
		y	0		0				m(29,30)
30,31		x	0		0				m(31,32)
		y	0		0				
32,33		x	0		0				
		y	0		0				
				total (mm) 14.22					

6.4.1.3 Adjustments for Large Vertical Point Load

In this section two experiments (Experiments 3 and 4) are done for two purposes, first to show that shape adjustment for a morphing structure is achievable for a concentrated load, and second to show that the choice of target position can have a large impact on the amount of total actuation in the adjustment process, through comparison results of these two experiments.

For the first purpose, the important point for designing an aerofoil is the very effectiveness in response and safety when unexpected forces act on the aerofoil, *e.g.* in storm conditions, as well as in more routine changes due to changing flight attitude, landing and take-off of an aircraft. While the aerofoil is expected to be subjected to distributed (and thus to a certain extent, even) loading when it is in service, sudden changes can cause a significant uneven loading that additionally twists the aerofoil. Therefore, a concentrated load was applied at the leading edge (frontal point) of the aerofoil to see how the adjustment techniques developed herein would help the distorted aerofoil to recover its shape and still meet design requirements of aerodynamic characteristics.

In the given model as a demonstration of the aerofoil morphing structure, a single 10.287N load was vertically applied to joint 1 for both experiments. The pre-adjusted displacements are shown in Column 5 of Table 6.3. The same bars were chosen for actuation in both experiments with the different targets.

The new objective in these experiments is to control ten displacements through using only six bars for actuation. This case should thus be over-determinate and insoluble, and only a least-squares "approximate" is possible for $\mathbf{e_0}$. However in this particular structure, all five displacements chosen on the right hand side of the model (12y, 14y, 16y, 18y and 19y) (see Figure 6.1) are affected by beam-pairs 19 and 20 and hence all these displacements can be controlled through actuation in bar 20 in this experiment. The other five displacements on the left hand side of the supports can be controlled by the other five actuators. Therefore, although the number of actuator is only six, there is still good control for the 10 joint displacements, as shown in Column 8 of Table 6.3. The measured results show good correlation with the desired displacements, which is restoring all displacement to the original pre-loading position with relatively only small deviations from the desired position is found in the plot in Figure 6.9.

Table 6.3: Vertical displacement control of the upper surface joints of the structure in Figure 6.1 under big vertical point load (MATLAB program is shown in Appendix A.9).

(1)	(2)	(3)	(4)	(5)	First target position			Second target position			(12)	(13)
					(6)	(7)	(8)	(9)	(10)	(11)		
Joints	Cond. Disp.	Dir	Loads (P) N	Just d_p, no e_o Theo. & Prac. (mm)	(e_o) (mm)	displacement after applying e_o with 6 components (mm)		(e_o) (mm)	displacement after applying e_o with 6 components (mm)		Cond. Bars	Bar
						Theo.	Prac.		Theo.	Prac.		
1		x	0		0			0				1
		y	-10.287	-21.54	0	0	1.36	0	0	2.75		2
2		x	0		0			0				3
		y	0	-20.55	-0.153	0	1.39	-0.197	0	2.76		4
3		x	0		-0.442			0.089				5
		v	0		0			0				6
4		x	0		0			0				7
		y	0	-15.19	0	0	1.23	0	0	2.03		8
5		x	0		0			0				9
		v	0		0			0				10
6		x	0		0			0				11
		y	0	-8.59	-5.820	0	0.97	-3.314	0	1.17		12
7		x	0		-1.975			-0.109				13
		v	0		0			0				14
8		x	0		0			0				15
		y	0	-3.40	0	0	0.24*	0	-3	-2.45		16
9		x	0		4.917			-0.699				17
		v	0		0			0			t_n	18
10	d_m	x	0	0	0			0				19
		y	0	0	-0.650			-0.650				20
11		x	0		0			0				21
		y	0		0			0				22
12		x	0		0			0				23
		y	0	1.25	0	0.00	0.13*	0	0.00	-0.11*		24
13		x	0	0	0			0				25
		v	0	0	0			0				26
14		x	0		0			0				27
		y	0	1.39	0	0.00	0.05*	0	0.00	0.06*		28
15		x	0		0			0				29
		v	0		0			0				30
16		x	0		0			0				31
		y	0	1.71	0	0.00	-0.05*	0	0.00	-0.06*		32
17		x	0		0			0				33
		v	0		0			0				34
18		x	0		0			0				35
		y	0	2.10	0	0.00	0.36*	0	0.00	-0.11*		36
19		x	0		0			0				m(3,4)
		y	0	3.60	0	0.00	0.11*	0	0.00	0.07*		m(4,6)
34,35		x	0		0			0				m(7,8)
		y	0		0			0				m(9,10)
20,21		x	0		0			0				m(11,12)
		y	0		0			0				m(13,14)
22,23		x	0		0			0				m(15,16)
		y	0		0			0			t_p	m(17,18)
24,25		x	0		0			0				m(19,20)
		y	0		0			0				m(21,22)
26,27	d_p	x	0		0			0				m(23,24)
		y	0		0			0				m(25,26)
28,29		x	0		0			0				m(27,28)
		y	0		0			0				m(29,30)
30,31		x	0		0			0				m(31,32)
		y	0		0			0				
32,33		x	0		0			0				
		y	0		0			0				
			total (mm)		13.96			5.06				

* Within the range of the precision of 0.4mm

The second purpose in this section is comparing the total required actuation for adjustment of the same structure (same loading, actuator position and number of actuators) with slightly different target positions for the selected joints. The only difference between Experiment 4 and Experiment 3 is that the target 8y displacement is -3mm, *i.e.* very close to the pre-adjustment displacement of -3.40mm instead of zero, while the amount of total actuation decreases from 13.96mm to 5.06mm, which is a significant amount.

The comparison of the post-adjustment displacements of Experiment 4 with pre-adjustment is shown in Figure 6.10, which again shows good attainment. Actually, the post-adjustment displacement results of Experiment 3 (Column 8 of Table 6.3 and Figure 6.9) are much better than the post-adjustment displacement results of Experiment 4 (Column 7 of Table 6.3 and Figure 6.10). This difference is not related to the theoretically achievable required actuation for controlling, since it was possible to control the required displacements in both experiments as shown in Columns 7 and 10 of Table 6.3. Experiment 4 shows that sometimes selecting targets for the experiment is challenging and needs high effort to control.
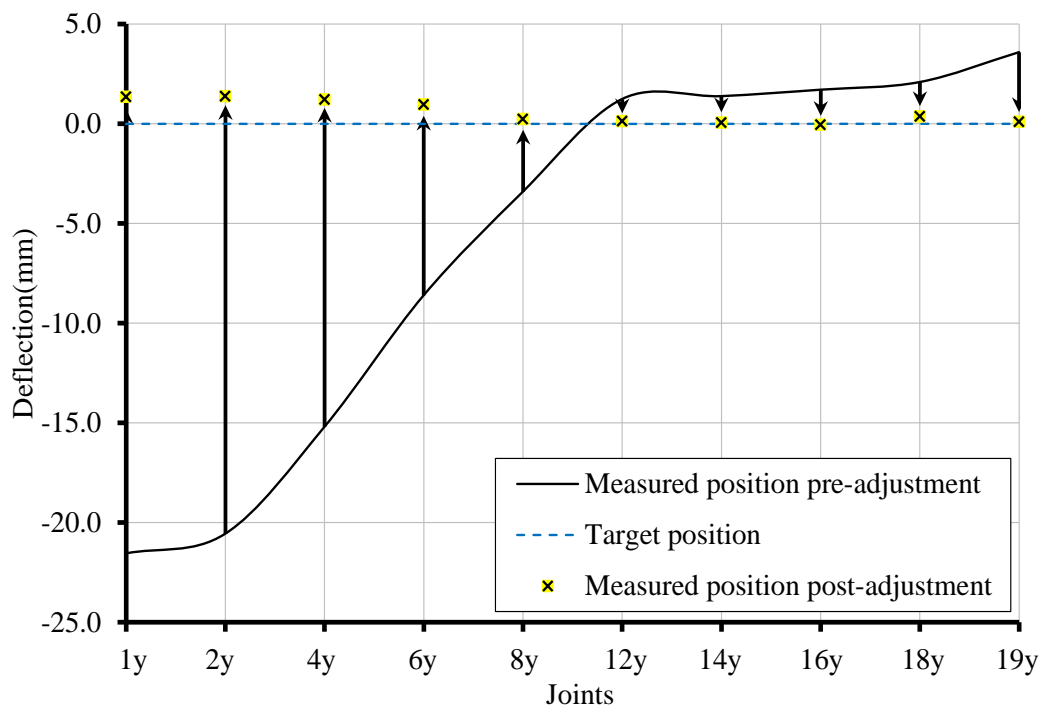
Figure 6.9: Vertical displacement control of the upper surface joints of the structure in Figure 6.1 under a single vertical point load for the first target position.
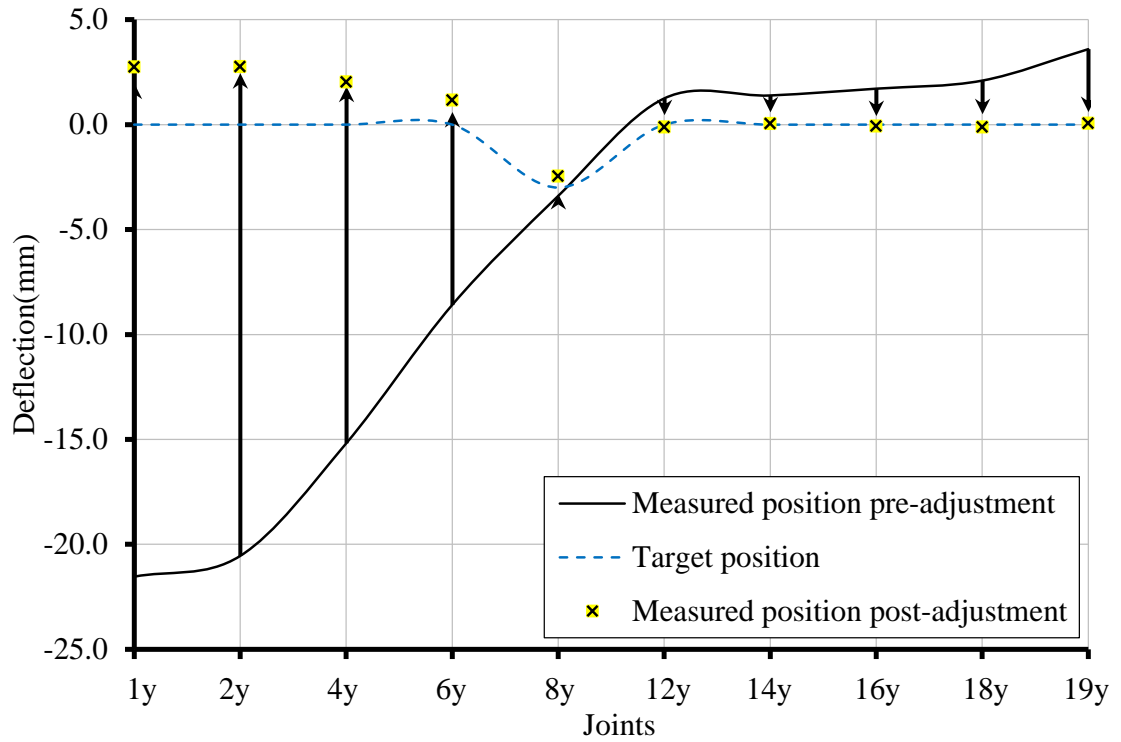
Figure 6.10: Vertical displacement control of the upper surface joints of the structure in Figure 6.1 under a single vertical point load for the second target position.

6.4.1.4 Adjustments for Distributed Horizontal Load

In this section (Experiment 5), an attempt was made to control horizontal displacements of the frontal joints of the structure of Figure 6.1 against distributed horizontal loading which comes from the drag force of the wind during flying. The horizontal pre-adjustment displacements of the joints for control are shown in Column 5 of Table 6.1 due to the horizontal loading in Column 4. Through using only five actuators embedded to five beams, the aim of controlling those displacements was achieved. The amount of required actuation was calculated in the MATLAB program and shown in Column 6 with a total actuation of 7.04mm. Figure 6.1 shows the post-adjustment displacements of the chosen joints relative e_0 the target position since the number of actuators is adequate for achieving the goal to secure this structure against horizontal loading.

Table 6.4: Horizontal displacement control of the front joints of the structure in Figure 6.1 against distributed horizontal load (MATLAB program can be found in Appendix A.10).

(1) Joints	(2) Cond. Disp.	(3) Dir	(4) Loads (P) N	(5) Just d_p, no e_o Theo. & Prac. (mm)	(6) (e_o)	(7)(8) displacement after applying e_o with 6 components (mm) Theo.	Prac.	(9) Cond. Bars	(10) Bar
1		x	2.286	**4.24**	0	**1**	**1.98**		1
		y	0		0				2
2		x	2.286	**4.00**	0	**0**	**0.78**		3
		y	0		-1.27				4
3		x	0		1.06				5
		y	0		0				6
4		x	2.286	**2.99**	0	**0**	**0.41**		7
		y	0		0				8
5		x	0		0				9
		y	0		0				10
6		x	2.286	**1.72**	0	**0**	**0.22***		11
		y	0		2.25				12
7		x	0		-1.68				13
		y	0		0				14
8		x	2.286	**0.65**	0	**0**	**0.13***		15
		y	0		0				16
9		x	0		0.39				17
		y	0		0				18
10		x	0	0	0			t_n	19
	d_m	y	0	0	-0.38				20
11		x	0		0				21
		y	0		0				22
12		x	0		0				23
		y	0		0				24
13		x	0	0	0				25
		y	0	0	0				26
14		x	0		0				27
		y	0		0				28
15		x	0		0				29
		y	0		0				30
16		x	0		0				31
		y	0		0				32
17		x	0		0				33
		y	0		0				34
18		x	0		0				35
		y	0		0				36
19		x	0		0				m(3,4)
		y	0		0				m(4,6)
34,35		x	0		0				m(7,8)
		y	0		0				m(9,10)
20,21		x	0		0				m(11,12)
		y	0		0				m(13,14)
22,23		x	0		0				m(15,16)
		y	0		0			t_p	m(17,18)
24,25		x	0		0				m(19,20)
		y	0		0				m(21,22)
26,27	d_p	x	0		0				m(23,24)
		y	0		0				m(25,26)
28,29		x	0		0				m(27,28)
		y	0		0				m(29,30)
30,31		x	0		0				m(31,32)
		y	0		0				
32,33		x	0		0				
		y	0		0				
				total (mm)	7.04				

* Within the range of the precision of 0.4mm
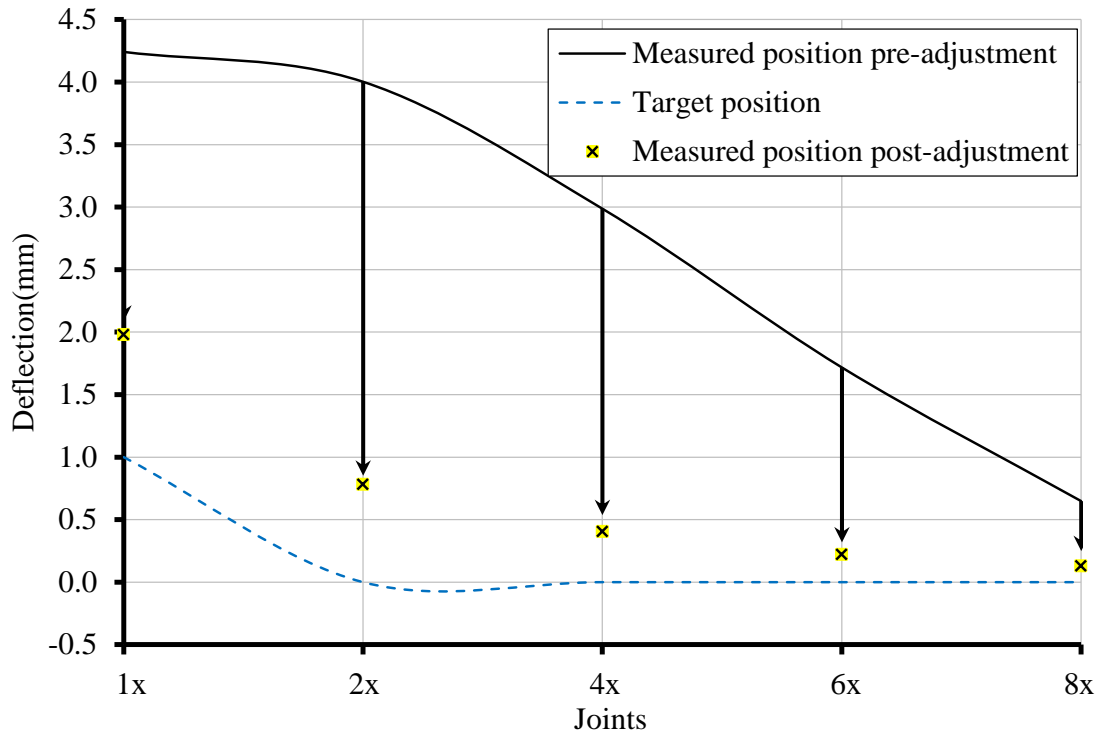
Figure 6.11: Horizontal displacement control of the front surface joints of the structure in Figure 6.1 against distributed horizontal load.

6.4.1.5 Adjustments for Vertical Distribute Loading with Elastic Band

The pantographic morphing structure model is of a demonstration morphing of aerofoil, hence a "stretchable skin" is also necessary to provide an external surface that can ensure correct aerodynamic properties (Du and Ang, 2012). In Experiment 6, 15 elastic bands were stretched between each two adjacent external top and bottom joints of structure, as shown in Figure 6.12. Again, joint displacement is controlled without regard to the bar forces, and the vertical displacement of the upper external joint joints after prestressing with the elastic bands are to be controlled. The axial stiffness of the elastic bands (EA) is 10N. Approximately, an even prestress level of 2N is achieved in all elastic bands by using the algorithm suggested by Kwan and Pellegrino (1993) via shortening the length of each elastic rubber band by 20.5%. The prestressing of the structure removed any joint slack and also reduced geometric flexibility of the structure.
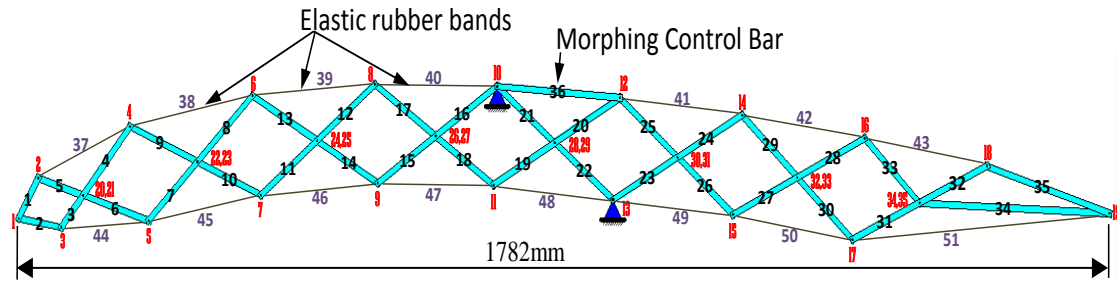
Figure 6.12: Structure in Figure 6.1 after increasing elastic rubber bands.

The structure was tested for adjustment of vertical displacement of the upper joints under vertical distributed load as shown in Column 4 in Table 6.5. The measured positions of the joints and the target position were introduced to the MATLAB program from which a set of actuations (Column 6) was obtained to adjust the pre-adjustment displacement in Column 4. All the chosen bars for actuation are the most effective bars (see Section 6.4.1.7) for this adjustment, except for bars 5 and 34 which were "second best" options but nonetheless chosen instead of the best bars 1 and 35 because these two bars did not actually have an actuator. Consequently, the total actuation was 4.34mm which was relatively very small. The numerical results are shown in Column 8, and graphically in Figure 6.13, which shows the adjustment process is capable of countering the displacement due to the prestress and loading.

This experiment shows that using an elastic stretchable material is a suitable technique for the pantographic morphing structure skin to ensure correct aerodynamic properties of the aerofoil. In addition, it was also shown that the direct method of controlling displacement is valid and practical, and good for adjusting static shape induced by both loads (routine and unpredicted) and other factors such as from prestressing in the pantographic structures via using elastic bands. The prestress level of the elastic bands was not much affected by the adjustment process since the prestress was produced by shortening of the order of 20% strain, which is many times greater than the strain change due to the adjustment process.

Table 6.5: Vertical displacement control of the upper surface joints of the structure in Figure 6.12 with elastic rubber bands under distributed vertical load (MATLAB program is shown in Appendix A.11).

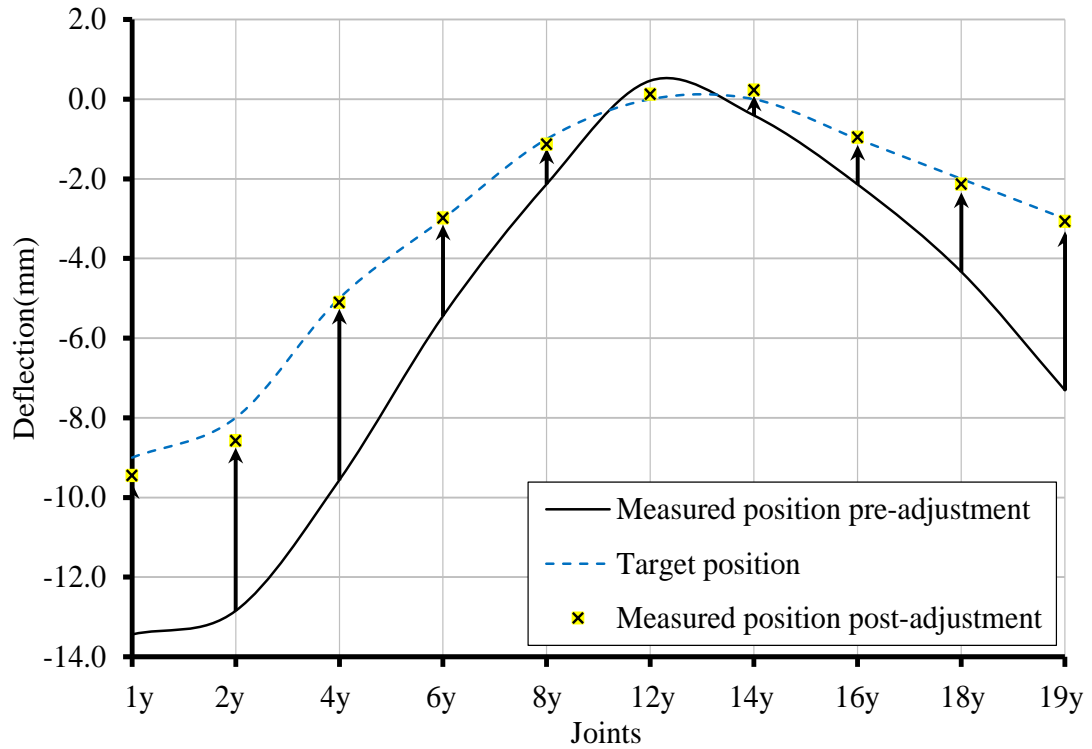| (1)	(2)	(3)	(4)	(5)	(6)	(1)	(7)	(8)	(9)	(10)
Joints	Cond. Disp.	Dir	Loads (P) N	Just d_p, no e_o Theo. & Prac. (mm)	(e_o) (mm)		displacement after applying e_o with 10 components (mm) Theo.	Prac.	Cond. Bars	Bar
1		x	0		0					1
		y	-2.286	-13.672	0		-1	-2.439		2
2		x	0		0					3
		y	-2.286	-12.976	-0.237		-1	-1.823		4
3		x	0		-0.226					5
		y	0		0					6
4		x	0		-1					7
		y	-2.286	-9.829	-0.513		-1	-1.058		8
5		x	0		0					9
		y	0		0					10
6		x	0		0					11
		y	-2.286	-5.838	-1.152		-1	-1.227		12
7		x	0		0					13
		y	0		0					14
8		x	0		0					15
		y	-2.286	-2.395	-0.495		-1	-1.001		16
9		x	0		0					17
		y	0		0					18
10		x	0	0	0					19
	d_m	y	0	0	-0.364					20
11		x	0		0					21
		y	0		0					22
12		x	0		0					23
		y	0	0.700	0		0	0.285*		24
13		x	0	0	-0.378					25
		y	0	0	0				t_n	26
14		x	0		0					27
		y	-2.286	0.020*	0		0	0.762		28
15		x	0		-0.068					29
		y	0		0					30
16		x	0		0					31
		y	-2.286	-1.501	0		-1	-0.489		32
17		x	0		-0.743					33
		y	0		0.171					34
18		x	0		0					35
		y	-2.286	-3.501	0		-1	-0.169*		36
19		x	0		0					37
		y	-2.286	-5.640	0		-1	0.508		38
34,35		x	0		0					39
		y	0		0					40
20,21		x	0		0					41
		y	0		0					42
22,23		x	0		0					43
		y	0		0					44
24,25		x	0		0					45
		y	0		0					46
26,27	d_p	x	0		0					47
		y	0		0					48
28,29		x	0		0					49
		y	0		0					50
30,31		x	0		0					51
		y	0		0					m(3,4)
32,33		x	0		0					m(4,6)
		y	0		0					m(7,8)
					0					m(9,10)
					0					m(11,12)
					0					m(13,14)
					0					m(15,16)
					0				t_p	m(17,18)
					0					m(19,20)
					0					m(21,22)
					0					m(23,24)
					0					m(25,26)
					0					m(27,28)
					0					m(29,30)
					0					m(31,32)
			total (mm)	4.34						

* Within the range of the precision of 0.4mm
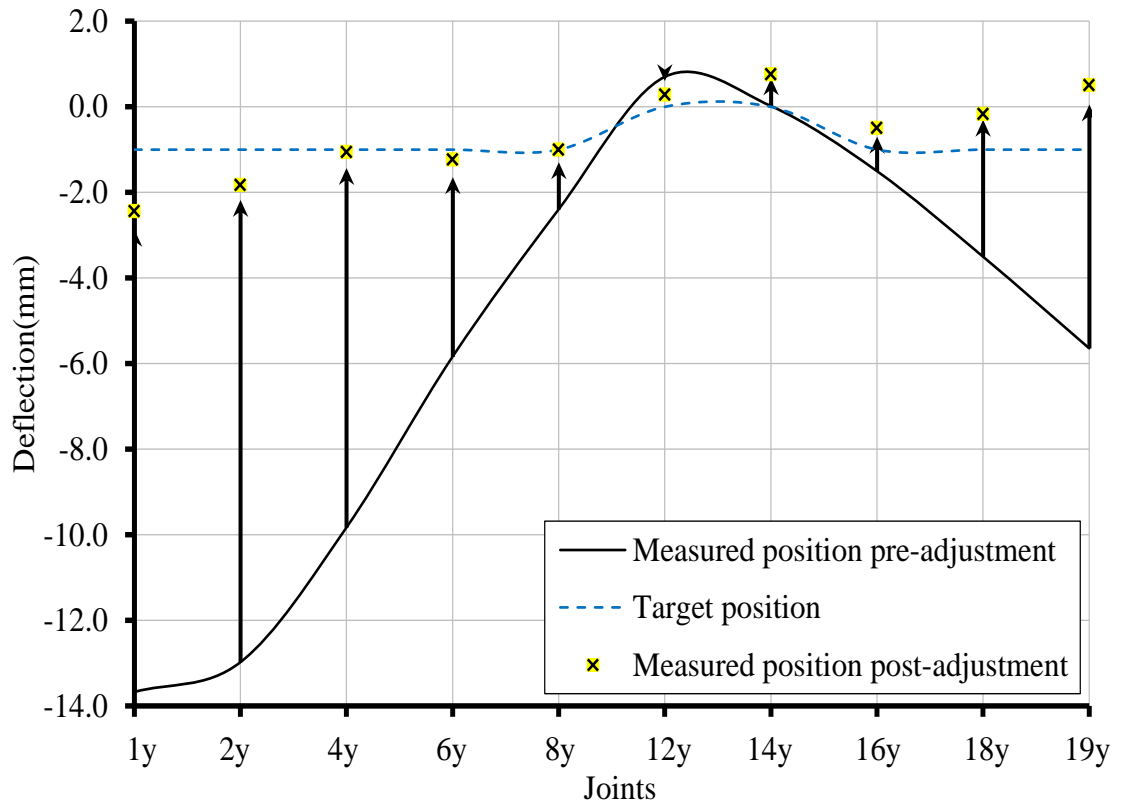
Figure 6.13: Vertical displacement control of the upper surface joints of the structure in Figure 6.12 with elastic band under distributed vertical load.

6.4.1.6 Multi-Iteration Adjustment to Remove Practical Errors

The nodal position defines the shape of the structure, and in this chapter so far the control of the nodal displacements to restore structural shape has been carried out by a single application of the length actuation. Sometimes a very high geometric accuracy is necessary in some structures. One of these is the proposed pantographic morphing structure as an aerospace structure, where its functions, and the efficiency with which it carries out those functions, are very sensitive to structural shape. At other times, the target shape may be quite different from the starting shape.

It may be too difficult to achieve the required high geometric accuracy through only one iteration of the adjustment process, and a second or more iteration is necessary to deal with residual errors remaining after the first round. For solving this issue, the process of multi-iteration adjustment was applied through using Eqn. 3.54 in two or more iterations in Experiment 6. In this technique, simply the post-adjustment displacement

from the first iteration is re-introduced as a pre-adjustment displacement in the next iteration, and so on, until the best possible adjustment is achieved. Again, in this test, the external joint of the morphing aerofoil was been controlled.

Table 6.6 Column 8 illustrates the results of adjustment, which comes from modifying the measured position of joints through applying the set of $\mathbf{e_0}$ obtained from Eqn. 3.54 to the structural model in the first iteration as shown in Figure 6.14. The rms of the error after the first adjustments in Table 6.6 is still 0.49mm. This result is good but it was supposed that extra accuracy was necessary in the chosen nodes. To reduce the errors even further, a second iteration was done using the post–adjustments displacements of the first iteration, as shown in Column 8, as the starting values for the second iteration, and the results of the second iteration are shown in Column 10, where the rms error is now reduced to 0.12mm. For extra clarity, the results of the second iteration, illustrated in Figure 6.15, are found to be very close to the theoretical results.

On the basis of this Experiment 6, it could be concluded that the technique of multi-iteration adjustment was effective in eliminating errors that occur in the practical adjustment process itself. The only problem in this experiment is the degree of measurement precision possible was of the order of the error in the second adjustment and hence it was difficult to particularly quantify the degree of improvement possible in a second iteration. It can be recommended that a very accurate non-contact measurement system should be used for the displacement measurement involving multi-iteration adjustment.

Table 6.6: Double iteration displacement control of the structure in Figure 6.12 (MATLAB program can be found in Appendix A.12).

(1)	(2)	(3)	(4)	(5)	(6)	(7)	(8)	(9)	(10)	(11)	(12)
						Iteration (1)			Iteration (2)		
Joints	Cond. Disp.	Dir	Loads (P) N	Just d_p, no e_o Theo. & Pra. (mm)	(e_{o1}) (mm)	displacement after applying e_o with 10 components (mm)		(e_{o2}) (mm)	displacement after applying e_o with 10 components (mm), Prac.	Cond. Bars	Bar
						Theo.	Prac.				
1		x	0		0			0			1
		y	-2.286	**-13.672**	0	**0**	**-0.293***	0	**0.035***		2
2		x	0		0			0			3
		y	-2.286	**-12.976**	-0.203	**0**	**0.208***	-0.327	**0.111***		4
3		x	0		-0.215			-0.771			5
		v	0		0			0			6
4		x	0		-1			-1			7
		y	-2.286	**-9.829**	-0.396	**0**	**0.379***	0.003	**-0.123***		8
5		x	0		0			0			9
		v	0		0			0			10
6		x	0		0			0			11
		y	-2.286	**-5.838**	-0.757	**0**	**0.127***	0.160	**0.107***		12
7		x	0		0			0			13
		y	0		0			0			14
8		x	0		0			0			15
		y	-2.286	**-2.395**	-1.009	**0**	**-0.121***	0.029	**-0.111***		16
9		x	0		0			0			17
		v	0		0			0			18
10	d_m	x	0	0	0			0			19
		y	0	0	-0.363			-0.151			20
11		x	0		0			0			21
		v	0		0			0			22
12		x	0		0			0			23
		v	0	**0.700**	0	**0**	**0.290***	0	**-0.103***		24
13		x	0	0	-0.378			0.126		t_n	25
		y	0	0	0			0			26
14		x	0		0			0			27
		v	-2.286	**0.020**	0	**0**	**0.574**	0	**0.098***		28
15		x	0		-0.542			0.055			29
		y	0		0			0			30
16		x	0		0			0			31
		v	-2.286	**-1.501**	0	**0**	**0.948**	0	**-0.012***		32
17		x	0		-0.402			0.425			33
		v	0		0.097			-0.108			34
18		x	0		0			0			35
		v	-2.286	**-3.501**	0	**0**	**0.424**	0	**-0.131***		36
19		x	0		0			0			37
		v	-2.286	**-5.640**	0	**0**	**0.760**	0	**-0.216***		38
34,35		x	0		0			0			39
		v	0		0			0			40
20,21		x	0		0			0			41
		v	0		0			0			42
22,23		x	0		0			0			43
		v	0		0			0			44
24,25		x	0		0			0			45
		v	0		0			0			46
26,27	d_p	x	0		0			0			47
		y	0		0			0			48
28,29		x	0		0			0			49
		v	0		0			0			50
30,31		x	0		0			0			51
		v	0		0			0			m(3,4)
32,33		x	0		0			0			m(4,6)
		y	0		0			0			m(7,8)
					0			0			m(9,10)
					0			0			m(11,12)
					0			0			m(13,14)
					0			0			m(15,16)
					0			0		t_p	m(17,18)
					0			0			m(19,20)
					0			0			m(21,22)
					0			0			m(23,24)
					0			0			m(25,26)
					0			0			m(27,28)
					0			0			m(29,30)
					0			0			m(31,32)
total (mm)					4.36			2.15			

* Within the range of the precision of 0.4mm
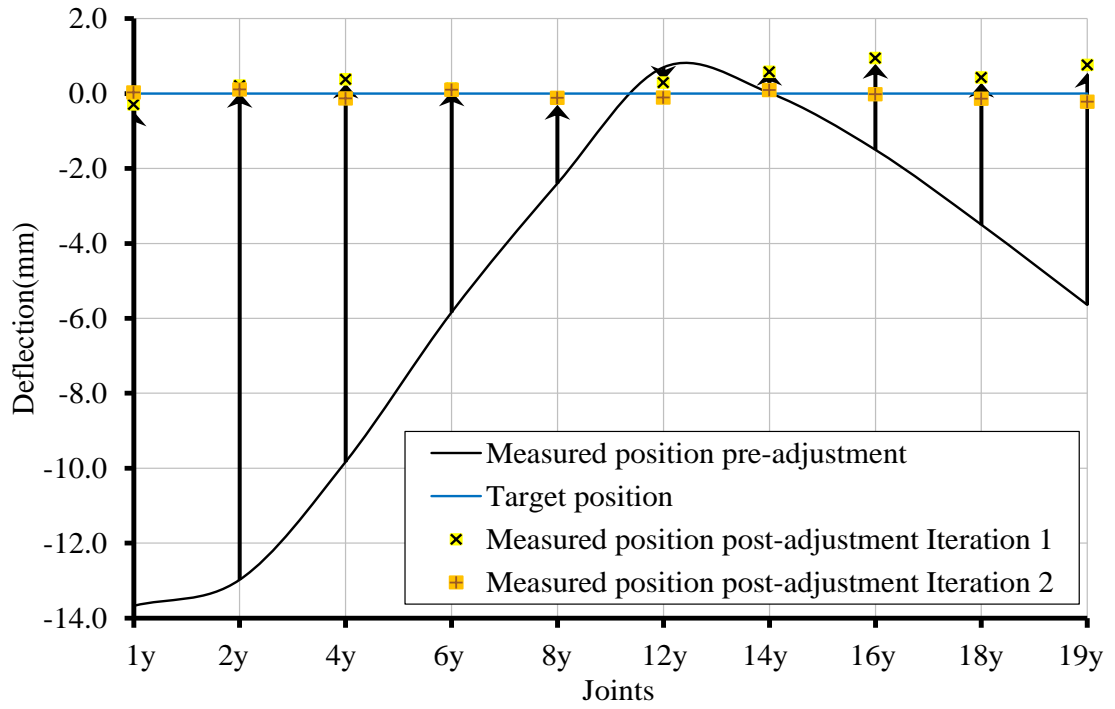
Figure 6.14: First and second iteration displacement control of the structure in Figure 6.12
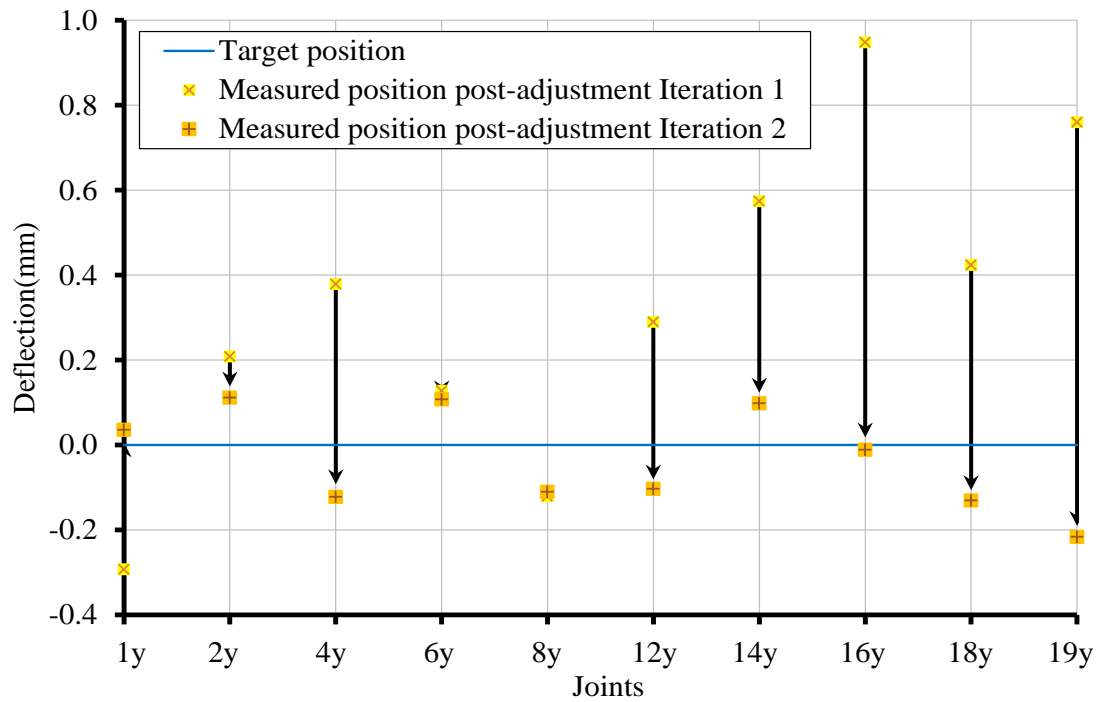
Figure 6.15: Second iteration displacement control of the structure in Figure 6.12

6.4.1.7 Finding Most Effective Bars through Calculating Bar Sensitivity to Displacement

All prior adjustment experiments in this chapter were carried out on actuators which were already in place, and consequently the question of which bars could be actuated did not arise; only the amount of actuation for the actuators available had to be calculated. Alternatively, at the early design stage where the location of actuators is still undecided, it is very important to locate the actuators in the components of the structure so that they could be of most effective in controlling future displacements. Section 3.2.2.2 detailed the case where effectiveness of actuation in any bar in controlling a particular displacement is indicated by the associate coefficient in the **Y** matrix for that bar, thus the most effective bars are those with the largest coefficients in **Y**.

In this section, another technique was used to highlight the most effective bars to carry the actuators, which we call the "bar sensitivity" technique. Table 6.7 shows the vertical displacement of the upper surface pins due to successive unit actuation of each of the bars of Figure 6.1. The table is compiled by assigning a unit elongation to each bar in turn, and the consequent values of these displacements are recorded. For example, when a unit elongation is applied to bar 1, a -1.08mm displacement in d_{1y} results, but no other monitored displacement changes. On the other hand, when a unit elongation is applied to bar 20, all the monitored displacements are changed. Therefore, the non-zero values in this table show which bars are capable of controlling a certain displacement, and the largest coefficient for a particular displacement shows which bar has the most effective control for that displacement, while a "zero" shows a given bar has no control over these displacements. The computation of this technique was done through a specially used MATLAB program in such a way the adjustment process follows the prepared data of Table 6.7.

To illustrate the process, Experiment 1 in Section 6.4.1.1 was chosen as an example to apply this technique. In the original Experiment 1, the set of the vertical displacements $\{-13.44\ -12.85\ -9.56\ -5.44\ -2.13\ 0.47\ -0.41\ -2.14\ -4.33\ -7.31\}$ for the upper surface joints $\{d_{1y}\ d_{2y}\ d_{4y}\ d_{6y}\ d_{8y}\ d_{12y}\ d_{14y}\ d_{16y}\ d_{18y}\ d_{19y}\}$ was adjusted through actuation in a set of pre-selected actuators in bars {4 5 12 13 17 20 24 25 28 29}. The attempt to control all selected displacements was successful through the set of

actuations $\{0.89\ 0.84\ -1.72\ -0.82\ 1.58\ -0.24\ 1.60\ -0.11\ -0.79\ -1.46\}$. However, the total actuation was 10.05mm, which was relatively big, which we will reduce using the bar sensitivity technique.

Table 6.7: Bar sensitivity to the vertical displacement of the upper surface joints of the structure in Figure 6.1.

bar	e_o	d_{1y}	d_{2y}	d_{4y}	d_{6y}	d_{8y}	d_{12y}	d_{14y}	d_{16y}	d_{18y}	d_{19y}
1	1.0	-1.08	0	0	0	0	0	0	0	0	0
2	1.0	0.60	0	0	0	0	0	0	0	0	0
3	1.0	0.33	0	0	0	0	0	0	0	0	0
4	1.0	-1.98	-1.81	0	0	0	0	0	0	0	0
5	1.0	-0.32	0.28	0	0	0	0	0	0	0	0
6	1.0	1.37	1.08	0	0	0	0	0	0	0	0
7	1.0	1.32	1.13	0	0	0	0	0	0	0	0
8	1.0	-3.49	-3.30	-2.15	0	0	0	0	0	0	0
9	1.0	-0.93	-0.65	0.36	0	0	0	0	0	0	0
10	1.0	2.56	2.31	1.33	0	0	0	0	0	0	0
11	1.0	2.96	2.75	1.55	0	0	0	0	0	0	0
12	1.0	-5.14	-4.93	-3.67	-2.05	0	0	0	0	0	0
13	1.0	-1.89	-1.64	-0.76	0.46	0	0	0	0	0	0
14	1.0	3.75	3.51	2.62	1.38	0	0	0	0	0	0
15	1.0	4.70	4.48	3.19	1.53	0	0	0	0	0	0
16	1.0	-6.83	-6.60	-5.26	-3.52	-1.95	0	0	0	0	0
17	1.0	-2.93	-2.70	-1.89	-0.76	0.53	0	0	0	0	0
18	1.0	4.89	4.66	3.84	2.69	1.41	0	0	0	0	0
19	1.0	6.45	6.21	4.86	3.10	1.48	0	0	0	0	0
20	1.0	-2.92	-2.74	-2.48	-2.03	-1.19	1.93	2.14	2.64	3.22	5.54
21	1.0	-3.76	-3.55	-3.05	-2.30	-1.27	0.44	0.48	0.60	0.73	1.25
22	1.0	3.71	3.51	3.01	2.27	1.25	-0.43	-0.48	-0.59	-0.72	-1.24
23	1.0	0	0	0	0	0	0	1.34	2.60	3.84	4.63
24	1.0	0	0	0	0	0	0	0.44	-0.86	-2.14	-2.92
25	1.0	0	0	0	0	0	0	-2.01	-3.49	-4.99	-6.98
26	1.0	0	0	0	0	0	0	0	1.50	3.03	5.01
27	1.0	0	0	0	0	0	0	0	1.34	2.66	3.52
28	1.0	0	0	0	0	0	0	0	0.40	-0.89	-1.71
29	1.0	0	0	0	0	0	0	0	-2.11	-3.60	-5.60
30	1.0	0	0	0	0	0	0	0	0	1.44	3.33
31	1.0	0	0	0	0	0	0	0	0	1.31	2.16
32	1.0	0	0	0	0	0	0	0	0	0.38	-3.32
33	1.0	0	0	0	0	0	0	0	0	-2.08	-3.97
34	1.0	0	0	0	0	0	0	0	0	0	4.06
35	1.0	0	0	0	0	0	0	0	0	0	-4.22
36	1.0	3.42	3.20	2.90	2.37	1.39	-1.72	-3.51	-5.54	-7.64	-11.21

The program starts with the control of d_{12y}, because it is affected by the least number of actuators, which are bars 20, 21 and 22. Then from these three bars, the most effective for an actuator is bar 20 with a 1.93 "bar sensitivity" so in the first cycle d_{12y} is directly controlled via actuation in bar 20 with the actuation of -0.24mm. The calculated set of displacements for the second cycle after applying the actuation of bar 20 is {-12.73 -12.19 -8.96 -4.95 -1.84 d_{12y}=0 -0.93 -2.78 -5.11 -8.65} . The actuation of bar 20 has effect on all displacements as shown in Table 6.7, and the displacement of joints on the left hand-side of supports are relatively reduced while the displacements of these right had-side are increased.

In the second cycle, d_{14y} is chosen for controlling since, with only six bars (20, 21, 22, 23, 24, and 25) able to affect it, it is the displacement with the next least number of possible actuators. Bar 25 is highlighted as the most effective bar, since even though bar 20 has a larger "bar sensitivity", bar 20 has already been highlighted for controlling d_{12y}. Furthermore, bars 21 and 22 cannot be used for controlling d_{14y} either, because they are grouped with bar 20 for d_{12y} and any actuation now in bars 21 and 22 would affect d_{12y} . Consequently, for d_{14y}, out of the six possible bars, only the bottom three can be used, and bar 25 (second biggest bar sensitivity at -2.01) is the most effective of these three, and is thus selected. Together with the actuation in bar 20 for d_{12y}, the calculations show d_{14y} is directly controlled via actuation in bar 25 of -0.46mm. The set of displacements after the second cycle becomes {-12.73 -12.19 -8.96 -4.96 -1.84 d_{12y}=0 d_{14y}=0 -1.17 -2.82 -5.44}.

In the same way, d_{8y} is controlled in cycle three via -0.43mm actuation in bar 16 and the displacements then become {-9.78 -9.33 -6.69 -3.43 d_{8y}=-1 d_{12y}=0 d_{14y}=0 -1.17 -2.82 -5.44}. In the fourth cycle d_{6y} is controlled with its most effective bar, bar 12, with a -2.05 bar sensitivity coefficient, and an actuation of 0.21mm the results of displacements are {-8.71 -8.30 -5.90 d_{6y}=-3 d_{8y}=-1 d_{12y}=0 d_{14y}=0 -1.17 -2.82 -5.44}. The technique as described so far thus will continue until all displacements have achieved their targets. In this example, the MATLAB program needed ten cycles to choose ten actuators for the 10 displacements to control. The of whole set actuation is {0.53 0.62 -0.43 -0.21 -0.43 -0.24 -0.46 -0.08 -0.25 -0.23} with total actuation of 3.48mm, while the total actuation in Experiment 1 (with the same target displacements, but non-optimised actuator location) was of 10.05mm. The difference is significantly big, the use of the "bar sensitivity" technique has reduced the amount of actuation to around a third.

For highlighting the most effective bars for controlling horizontal displacements of joints in this structure, Table 6.8 was prepared which illustrates coefficients of bar sensitivity to the horizontal displacements of the upper surface joints of the model. In a process similar to that for vertical displacements, it was shown that the most effective for effective bars for controlling $\{d_{1x}\ d_{2x}\ d_{4x}\ d_{6x}\ d_{8x}\ d_{12x}\ d_{14x}\ d_{16x}\ d_{18x}\ d_{19x}\}$ are bars {2 5 9 12 16 20 25 28 32 35}. The attempt was made to re-analyse the case of Experiment 5 in Section 6.4.1.4. The new results show that the displacement can be controlled with using only five actuating bars {2 5 9 12 16} with a set of actuations of $\{2.67\ 2.41\ 1.28\ 0.88\ 0.53\}$ respectively, and with the total actuation of 7.77mm. This amount of total actuation is slightly greater than that found in Experiment 5 which is (which is 7.03mm), but only five actuators were used here while in Experiment 5, it was six. Using the technique of bar sensitivity if a further bar was adopted, then it would be bar 20, and then the same adjustment effect can be achieved with 2.53mm total actuation, and a set of actuation as $\{-0.25\ 0.63\ 0.41\ 0.24\ -0.09\ -0.91\}$.

In this example, bar 36 does have the ability to affect all displacements of all joints, but bar 36 was not used in the process of controlling, since the actuator in bar 36 was used for controlling morphing of the structure, *i.e.* the morphing control bar in Figure 6.1.

In conclusion, through using this bar sensitivity technique the decision of where the actuator should be place can be taken before the designing of the structures. The effectiveness of actuation in a particular bar in controlling a particular displacement is indicated by the associated coefficient in the bar sensitivity to displacement table. The first advantage of this technique is minimizing the total actuation necessary for controlling a particular set of displacements. Secondly, it is possible to choose a just sufficient number of actuators. In other words, both the minimum number of actuators as well as minimum actuation can be obtained, resulting in less expense and probably easier provision for control of structures.

Table 6.8: Bar sensitivity to the horizontal displacement of the upper surface joints of the structure in Figure 6.1.

bar	e_o	d_{1x}	d_{2x}	d_{4x}	d_{6x}	d_{8x}	d_{12x}	d_{14x}	d_{16x}	d_{18x}	d_{19x}
1	1.0	-0.17	0	0	0	0	0	0	0	0	0
2	1.0	-0.92	0	0	0	0	0	0	0	0	0
3	1.0	-0.51	0	0	0	0	0	0	0	0	0
4	1.0	-0.25	-0.52	0	0	0	0	0	0	0	0
5	1.0	-0.05	-0.96	0	0	0	0	0	0	0	0
6	1.0	-1.16	-0.73	0	0	0	0	0	0	0	0
7	1.0	-0.53	-0.23	0	0	0	0	0	0	0	0
8	1.0	-0.37	-0.66	-0.84	0	0	0	0	0	0	0
9	1.0	0.24	-0.19	-0.93	0	0	0	0	0	0	0
10	1.0	-1.59	-1.20	-0.55	0	0	0	0	0	0	0
11	1.0	-0.53	-0.22	0.03	0	0	0	0	0	0	0
12	1.0	-0.57	-0.89	-1.12	-1.06	0	0	0	0	0	0
13	1.0	0.73	0.36	-0.30	-0.89	0	0	0	0	0	0
14	1.0	-1.97	-1.60	-0.97	-0.41	0	0	0	0	0	0
15	1.0	-0.42	-0.08	0.21	0.20	0	0	0	0	0	0
16	1.0	-0.90	-1.25	-1.52	-1.48	-1.23	0	0	0	0	0
17	1.0	1.18	0.83	0.19	-0.39	-0.85	0	0	0	0	0
18	1.0	-2.18	-1.83	-1.23	-0.69	-0.29	0	0	0	0	0
19	1.0	-0.12	0.25	0.55	0.55	0.34	0	0	0	0	0
20	1.0	3.83	3.54	2.72	1.75	0.84	0.13	-1.04	-2.17	-3.29	-2.62
21	1.0	3.04	2.73	2.02	1.26	0.58	0.03	-0.23	-0.49	-0.74	-0.59
22	1.0	-3.00	-2.69	-1.99	-1.24	-0.58	-0.03	0.23	0.49	0.73	0.59
23	1.0	0	0	0	0	0	0	0.46	0.96	1.49	1.72
24	1.0	0	0	0	0	0	0	0.90	0.37	-0.19	-0.42
25	1.0	0	0	0	0	0	0	0.97	1.10	1.18	0.61
26	1.0	0	0	0	0	0	0	0	-0.12	-0.18	0.39
27	1.0	0	0	0	0	0	0	0	0.51	1.06	1.30
28	1.0	0	0	0	0	0	0	0	0.92	0.36	0.13
29	1.0	0	0	0	0	0	0	0	0.91	1.01	0.44
30	1.0	0	0	0	0	0	0	0	0	-0.08	0.47
31	1.0	0	0	0	0	0	0	0	0	0.55	0.79
32	1.0	0	0	0	0	0	0	0	0	0.93	-0.14
33	1.0	0	0	0	0	0	0	0	0	0.85	0.30
34	1.0	0	0	0	0	0	0	0	0	0	1.17
35	1.0	0	0	0	0	0	0	0	0	0	-0.17
36	1.0	-4.48	-4.14	-3.18	-2.05	-0.98	0.88	1.70	2.44	3.11	2.08

6.5 Experimental and Theoretical Morphing Comparison and Discussion

6.5.1 Introduction to Morphing Structures

Structural morphing is the ability of the structure to change shape configuration according to its application, to adapt to environmental conditions to optimise certain performance design requirements. It has great importance in multiple engineering applications, especially in aerospace. Morphing has increased the ability of engineers to progress wing technology in order to increase the efficiency or safety of the structure.

Morphing requires structure to possess some form of mechanisms for mobility, for instance convenient arrangement of hinges and bars to allow shape re-configuration. In any structure the process of morphing will not work without an external source of energy or actuation of members, which is done via actuators embedded to the members of the structure.

6.5.2 Experimental Structure Morphing

A pantographic morphing structure in Figure 6.1 was prepared for the purpose of morphing as well as for adjustment/controlling. In the morphing mechanism the structure changes significantly from one shape configuration to another, with the same number of hinges and bars, that is a large geometric change in the structure through actuation in one or more morphing control bars. In the present experimental model, just one bar was selected for achieving the morphing process. Morphing is distinct to shape adjustment/controlling, since the adjustment process moves only small refinements in displacement and/or force changing, within essentially the same geometry, for the removing or reduction of any undesirable displacement and/or force, which can be carried out on either an unmorphable structure, or after morphing. The number of actuators for adjustment depends on the number of displacement or force variables, as shown in Section 6.4.

As mentioned in the previous sections in this chapter the structure of Figure 6.1 is the demonstration of the morphing aerofoil structure. No doubt, many different shape configurations are necessary in any aircraft wing in order to achieve different lift and drag

coefficients in the different stages of flight. In the experimental model, bar-36 was the morphing control bar, and the change in geometry achievable through actuation in bar 36 is shown in Figure 6.16.
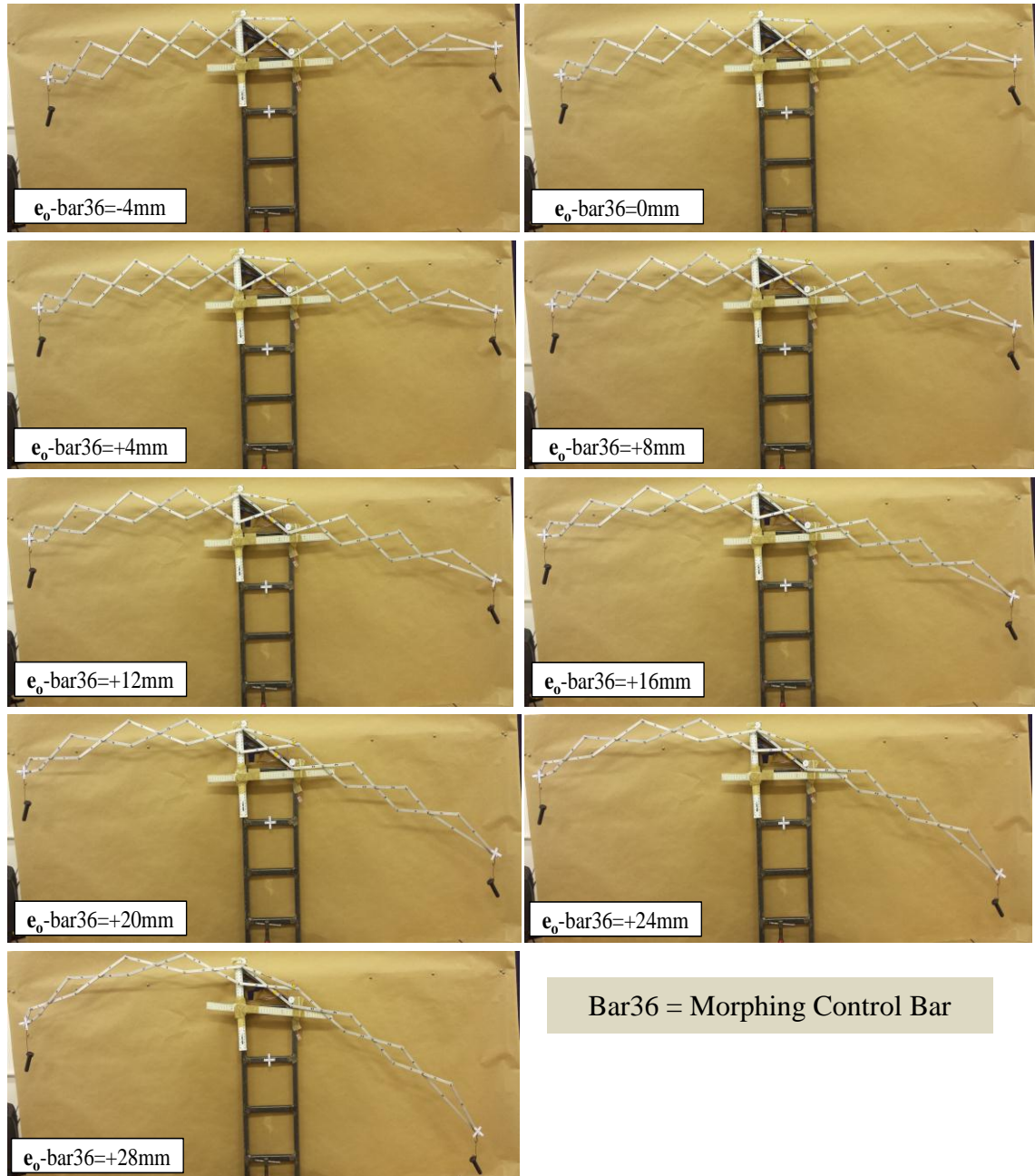
Figure 6.16: Nine morphing stages of morphing structure in Figure 6.1

The comparison of experimental and analytical models is very important as a proof of concept for a morphing aerofoil as an effective way to enhance/replace the traditional aerofoil. The deflection analysis due to the loading and actuation of morphing control bar was calculated via Eqn. 3.54 and furthermore, condensation in the force method was used for calculation where some of the displacements were "hidden" since they relate to unloaded joint components which were then condensed out from the primary equations. This is a novel approach and application. Two methods for calculating theoretical nodal displacement of the pantographic morphing structure were introduced: linear and non-linear methods.

6.5.3   Linear Calculation Method

In the linear method nodal displacements of the structures were calculated through a single use of Eqn. 3.54 in Chapter 3 in one iteration, with the same joint coordinates from the original shape of the model. Morphing inaccuracies and any displacements due to external loading on the structure were thus adjusted for. Theoretical results of this method were compared with the experimental results as illustrated in Figures 6.17 to 6.26, where the theoretically computed results were labelled as "Theoretical Linear" with solid lines. The results have a good correlation with the experimental results in the early stages of the structural shape morphing, typically until around $\mathbf{e_o}$=+10. Beyond that point, all the linear results begin to separate from the experimental trend line, except for *dx4* in Figure 6.19, *dx6* and *dy6* in Figure 6.20, and *dx8* in Figure 6.21 which continued in a straight line until approximately the end stages of the morphing. This separation is the result of non-linear behaviour of the structure for the morphing. Thus, the linear method is not valid for the full range of morphing and non-linear modification was proposed.

6.5.4   Non-Linear Calculation Method (Coordinate Update Method)

Since the nonlinearity in the morphing structure was geometric, due to its flexibility and thus relatively large movements and displacements, the non-linear method for calculating the nodal displacements of the given model was based on updating the coordinate of the structure. In this method, Eqn. 3.54 in Chapter 3 was used in the linear calculation

method, within a number of cycles during which coordinates of the structure were updated with the displacements in each iteration. The matrices of Equilibrium, Compatibility and Flexibility of the assembly are recalculated in each cycle although **F** changes only by a small amount due to very slight change in bar length from the changing coordinates. In other words, the calculation in each cycle is done for a "new" structure: the MATLAB program for this is shown in Appendix A.13. The accuracy of the calculation increases with increasing the number of the iterations beyond the linear limit of displacement. Theoretical displacement results of this method have shown a very good correspondence with the experimental measured displacement values (horizontal and vertical) of all joints as shown in Figures 6.17 to 6.26.
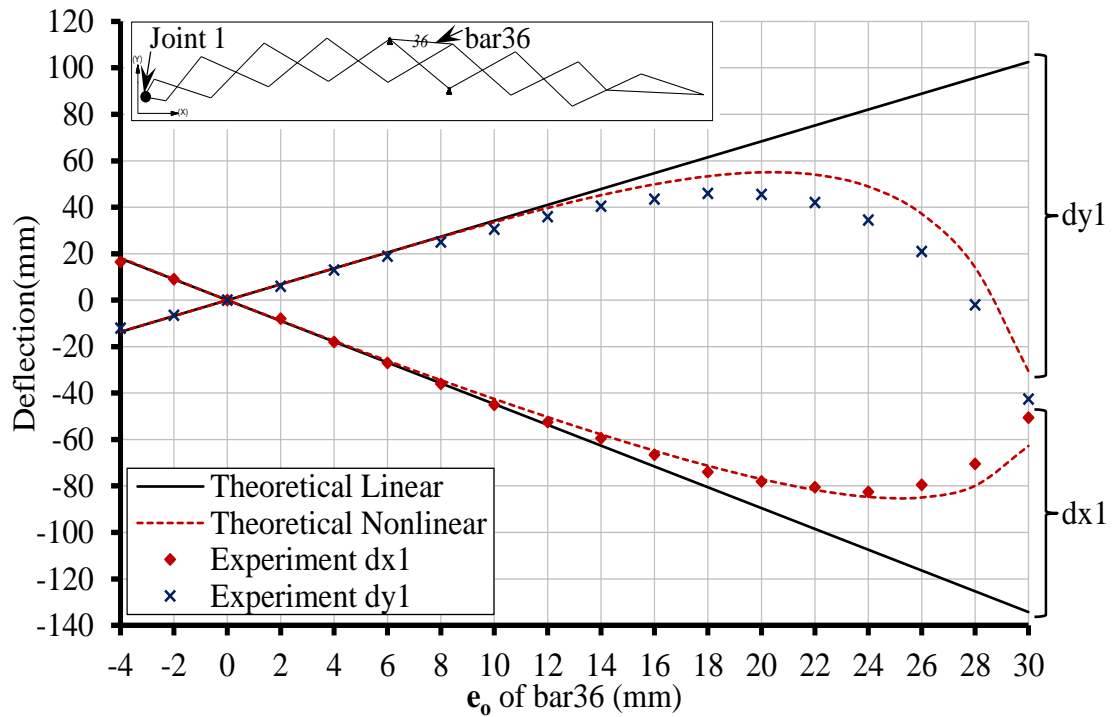
Figure 6.17: Theoretical and experimental deflection of joint 1 in x and y direction versus morphing control bar actuation.
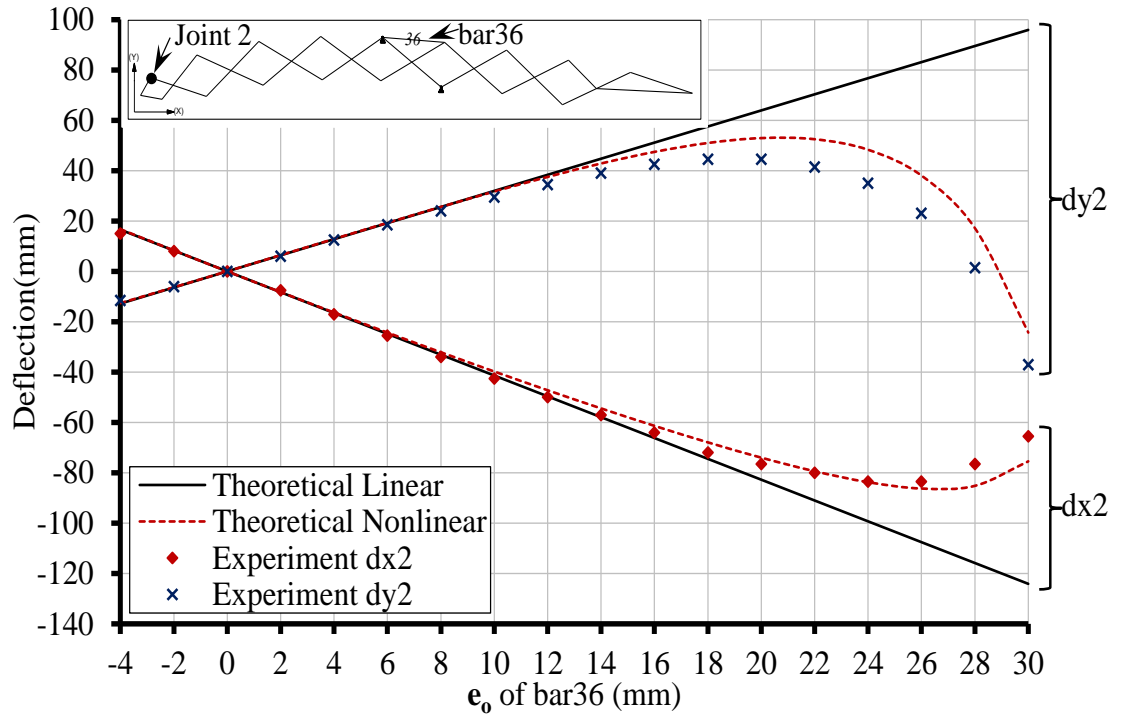
Figure 6.18: Theoretical and experimental deflection of joint 2 in x and y direction versus morphing control bar actuation.
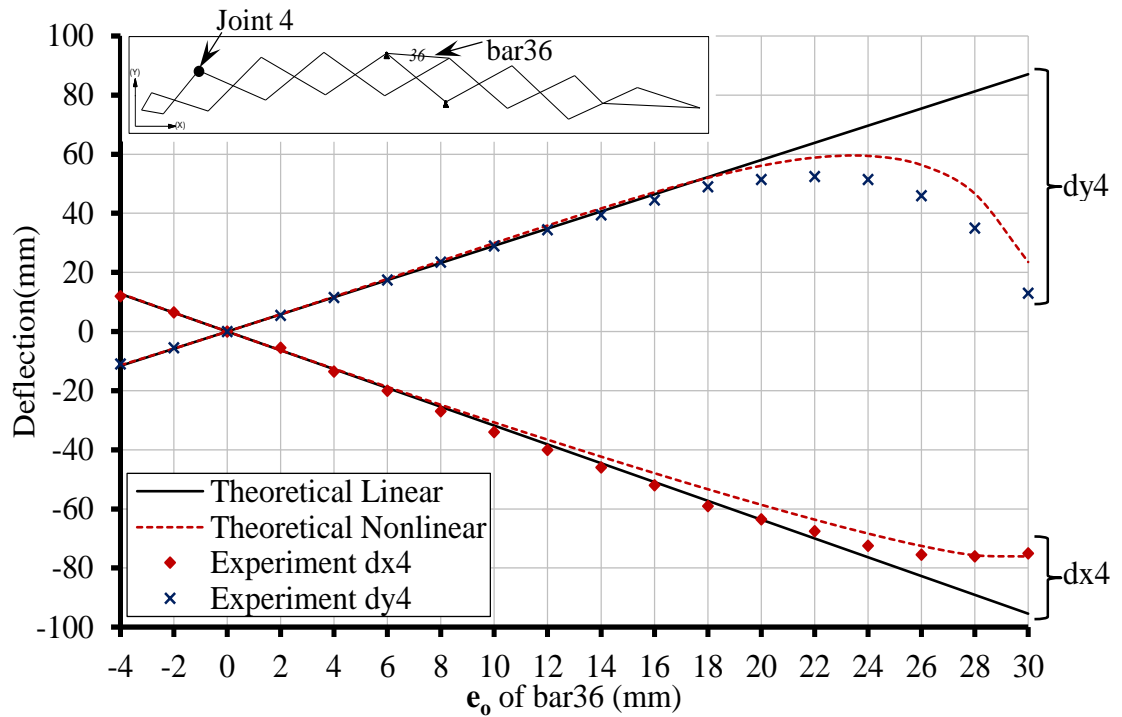
Figure 6.19: Theoretical and experimental deflection of joint 4 in x and y direction versus morphing control bar actuation.
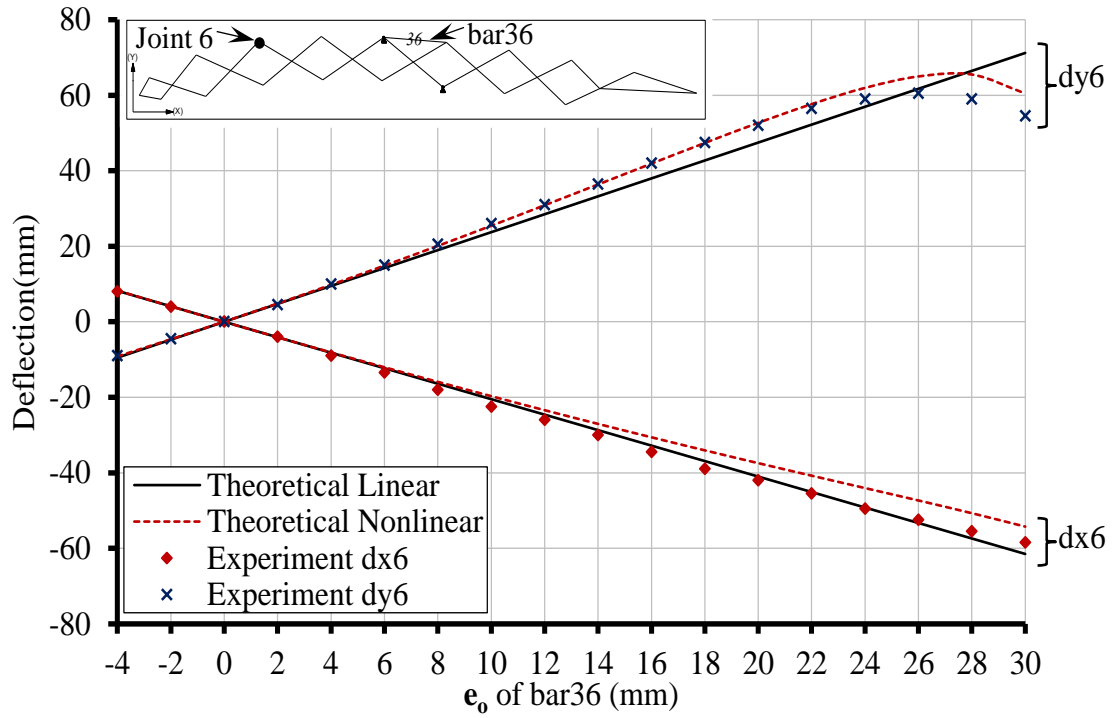
Figure 6.20: Theoretical and experimental deflection of joint 6 in x and y direction versus morphing control bar actuation.
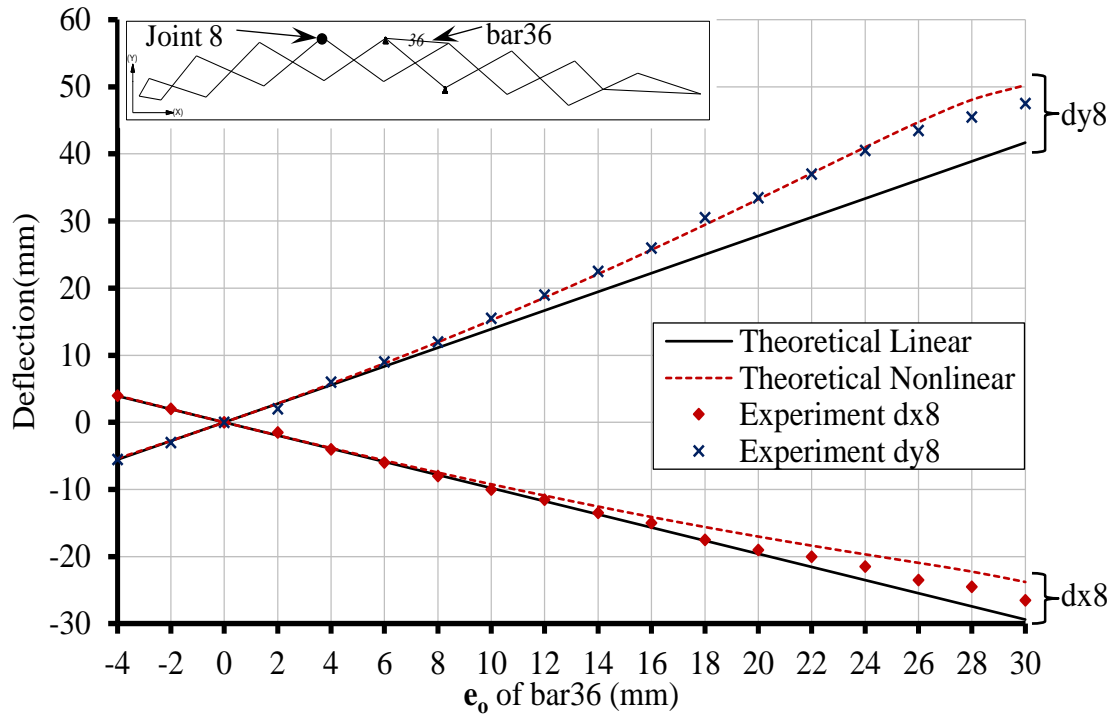
Figure 6.21: Theoretical and experimental deflection of joint 8 in x and y direction versus morphing control bar actuation.
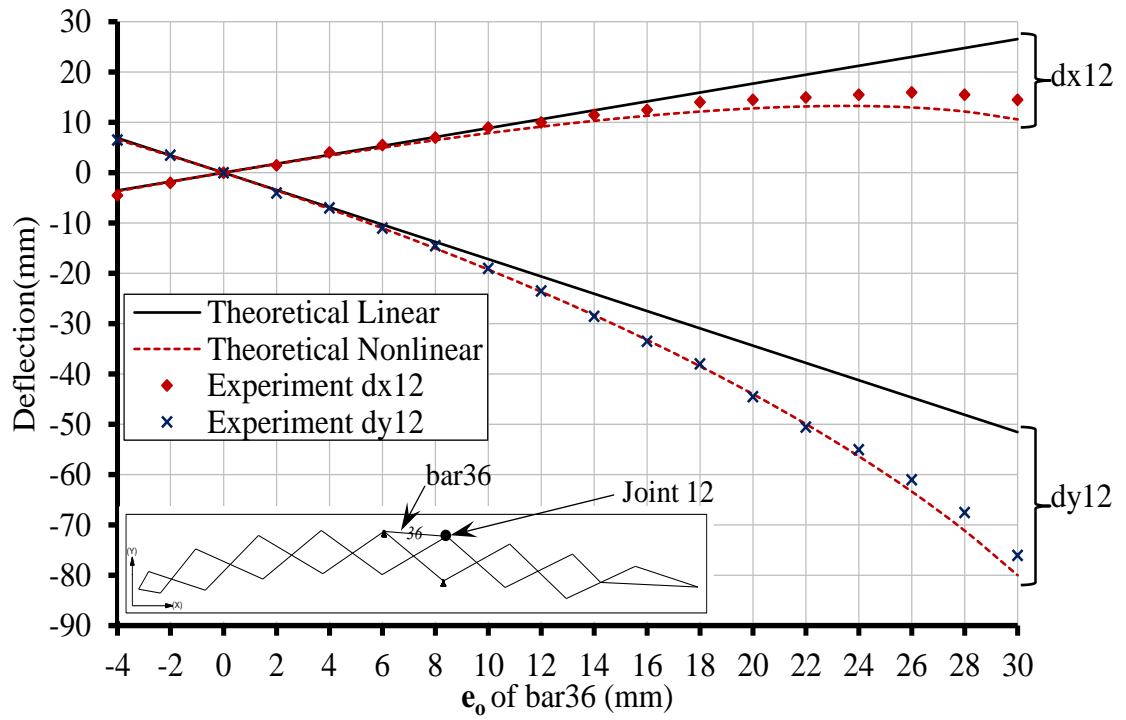
Figure 6.22: Theoretical and experimental deflection of joint 12 in x and y direction versus morphing control bar actuation.
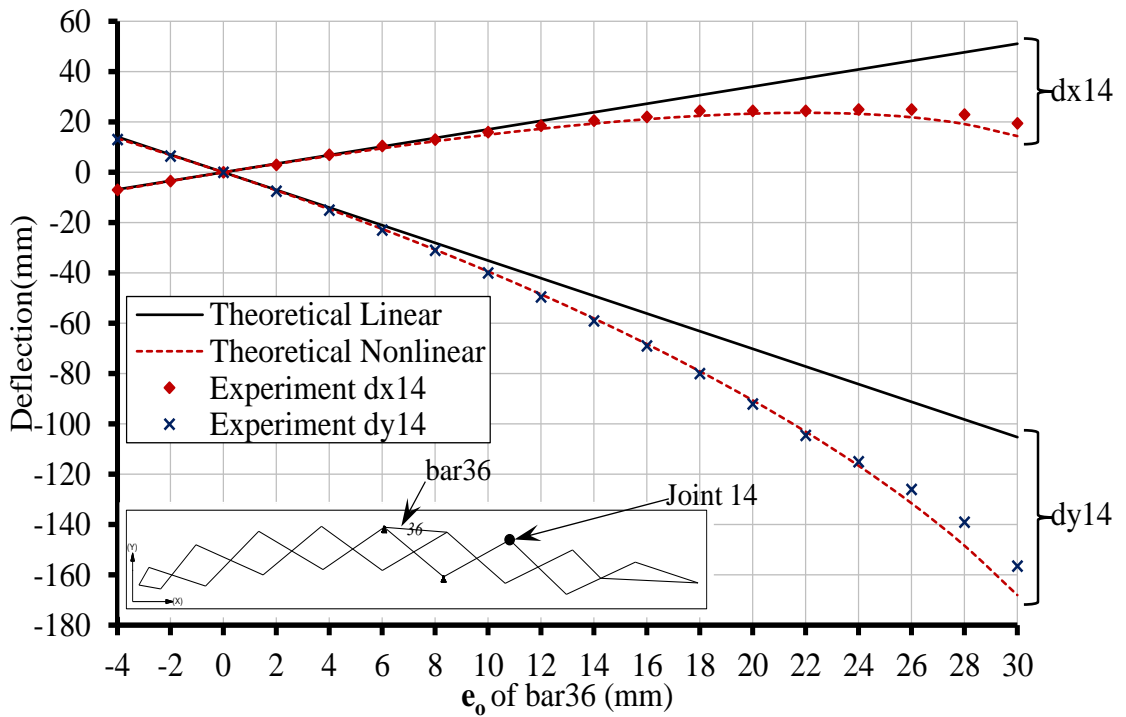
Figure 6.23: Theoretical and experimental deflection of joint 14 in x and y direction versus morphing control bar actuation.
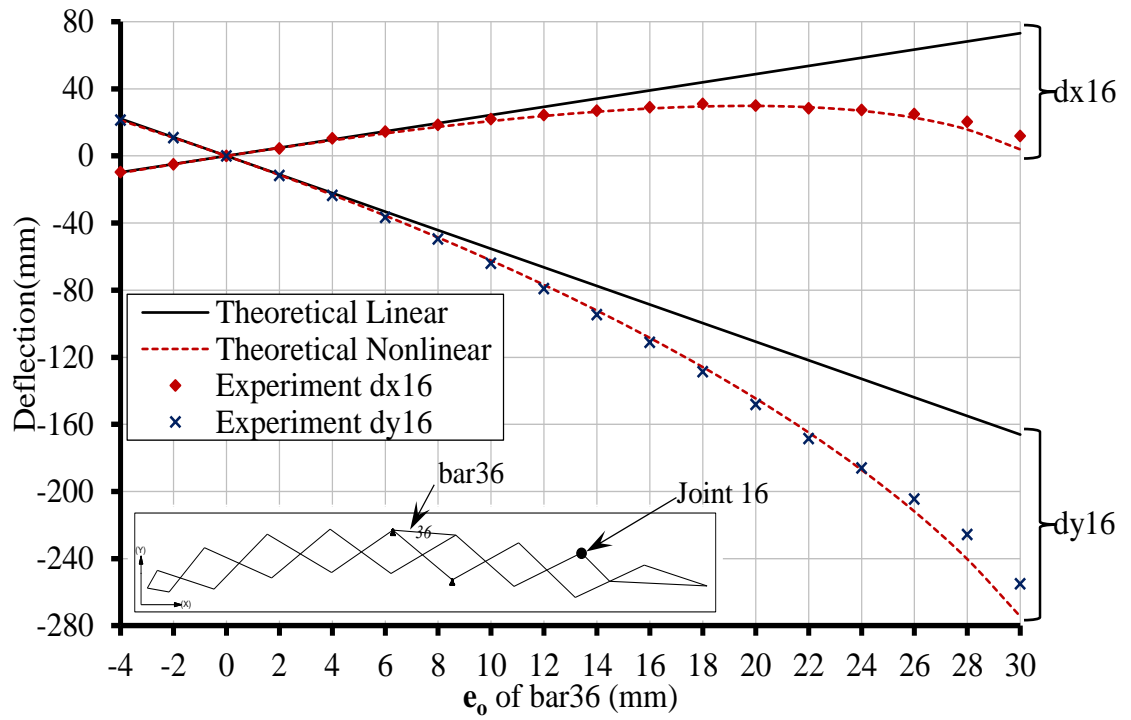
Figure 6.24: Theoretical and experimental deflection of joint 16 in x and y direction versus morphing control bar actuation.
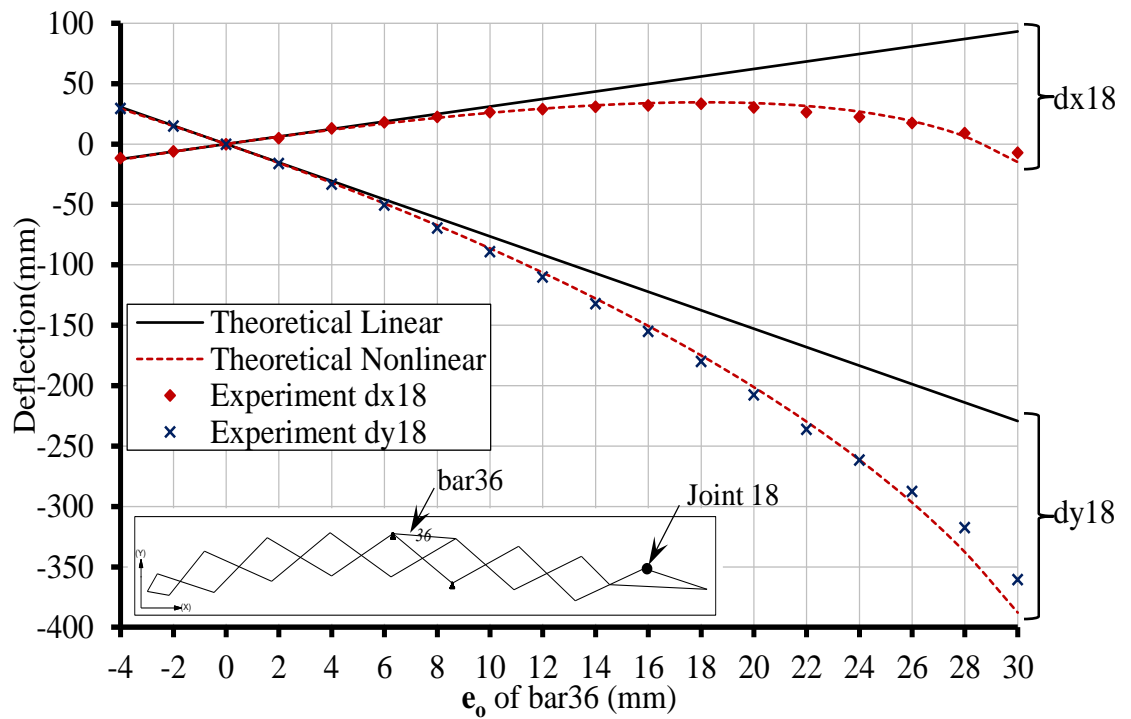
Figure 6.25: Theoretical and experimental deflection of joint 18 in x and y direction versus morphing control bar actuation.
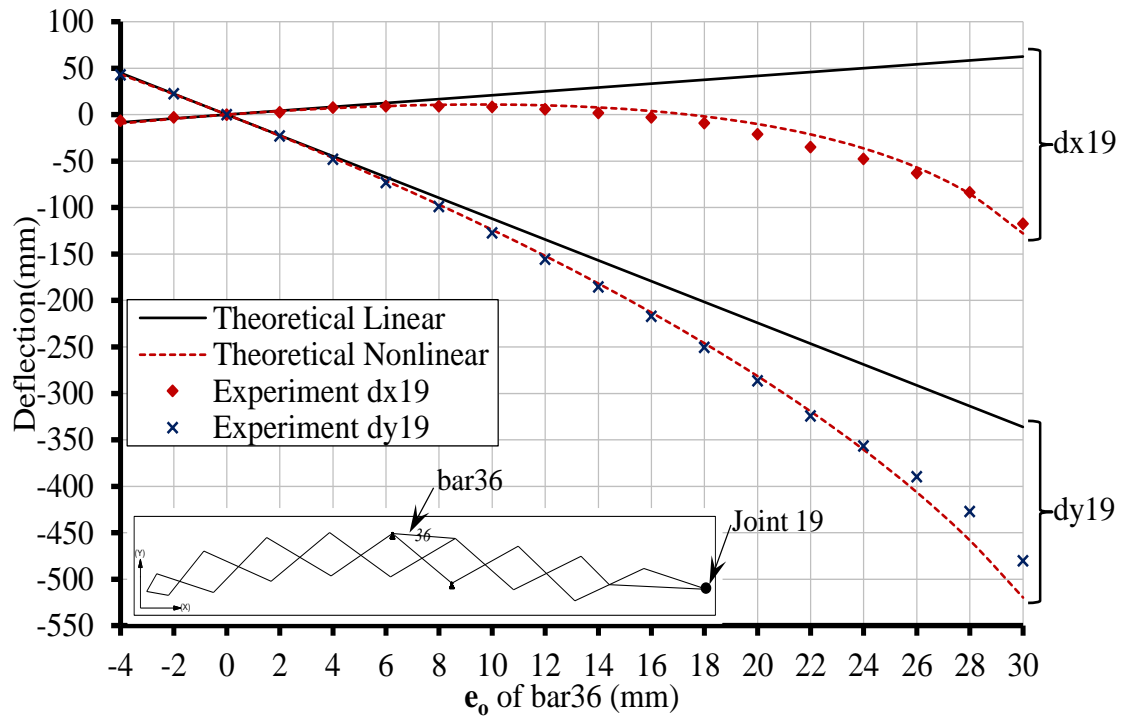
Figure 6.26: Theoretical and experimental deflection of joint 19 in x and y direction versus morphing control bar actuation.

In summary, as shown in Figures 6.17 to 6.26, all the three curves (linear, non-linear and experiment) correlate closely to each other at the early stages of morphing. Horizontal displacement results agree better with theoretical predictions than the vertical displacements in general. Some of the difference between non-linear and theoretical results could result from the shape of the physical model being imperfect from construction, and the imperfections exacerbate the distortion from theoretical shape at the later stages of morphing. However, as shown by the close correlation between the theoretical non-linear computation results and the experimental values, the main source of nonlinearity is geometric, and is due to the displacement prediction from a given structural geometry being no longer accurate or valid because that geometry had undergone significant change due to the morphing process.

Chapter 7

Conclusions and Future Work

7.1 Introduction

The main conclusions of the present work are summarised in this chapter, under two headings according to the aim and objectives in Chapter 1. Furthermore, this chapter contains also the recommendations for future work concerning issues of this research that can be more developed, arising from the findings of the present study.

7.2 Conclusion of the Research Work

Nine objectives were identified for the two stated aims in Section 1.2. The conclusions made during the course of the current work relating to these objectives are now re-presented in this section.

7.2.1 Objective 1 concerned reviewing the available literature on analytical and numerical techniques on shape control, with view to find an efficient and comprehensive technique on shape control. This objective was explored in Section 2.2. The conclusion from this section relating to this objective is:

7.2.1.1 Conclusion 1. Although many different techniques have been proposed by different researchers in the last three decades, there has not been one method which is direct, effective, and can comprehensively deal with the problem of displacement and force constraints simultaneously. This conclusion from chapter 2 led to the theoretical work developed in Chapter 3 [Section 2.2].

7.2.2 Objective 2 concerned the derivation of a direct method for nodal displacement, bar force and simultaneously nodal displacement and bar force control for pin-jointed bar assembly. This objective was explored in Sections 3.2.2, 3.2.3 and 3.2.4. The conclusions from those sections relating to this objective are:

7.2.2.1 Conclusion 2. A useful and relatively simple method (Eqn. 3.10) has been presented, which provides a direct method for calculating required length actuations for a pin-jointed bar assembly requiring shape control within a single formulation. It can be said that this method is complementary to, and an extension of, the work presented by You (1997), since his interest was in shape control of *unloaded* prestressed structures [Section 3.2.2].

7.2.2.2 Conclusion 3. In this dissertation also a useful and relatively simple method has been presented (Eqn. 3.16) for providing a direct calculation for required length actuations for a structural assembly requiring force control within a single formulation. This method is very important to control force of structures under some loading conditions, a cable member could approach slack and thus needs to be re-tightened to remain structurally existent, or a slender strut could be approaching instability and thus needs its compressive force reduced [Section 3.2.3].

7.2.2.3 Conclusion 4. A useful and relatively simple method has been presented (Eqn. 3.19) for providing a direct calculation for required length actuations for a structural assembly requiring simultaneous nodal displacement and bar force control. The changes for both force and displacement regimes are within a single formulation. Ability for simultaneous control has vital role, since in practice, it is highly likely that situations requiring control of one will also have some requirements on the other [Section 3.2.4].

7.2.2.4 Conclusion 5. Equations 3.19 and 3.59 which are used for controlling nodal displacement and bar force simultaneously, were found to be over-determinate and thus

insoluble, (because of typically high number of equations ($ij - c$ in **Y** and b in **Z**) while there are only b unknowns in $\mathbf{e_o}$) and hence only a least-squares "approximate" was used for $\mathbf{e_o}$ which was found to work well. [Section 3.2.4].

7.2.3 Objective 3 concerned the extension of the direct method for adjusting nodal displacement, bar force and simultaneous nodal displacement and bar force control for structures made up of more complex structural components (*i.e.* those with "macro-elements"), *e.g.* the pantographic element. This objective was explored in Sections 3.3.2, 3.3.3 and 3.3.4. The conclusions from those sections relating to this objective are:

7.2.3.1 Conclusion 6. Equation 3.54 was developed which offers a direct method for calculating required length actuations for structures made up of more complex structural components (*i.e.* those with "macro-elements"), *e.g.* the pantographic element requiring shape control. This technique involved structural matrices being built up from matrices of elementary elements, and then processed with "matrix condensation" [Section 3.3.2].

7.2.3.2 Conclusion 7. Two equations (Eqns. 3.48 and 3.53) provided the non-vanishing and vanishing displacements of the structure respectively, without regard of each other for structures made up of more complicated structural components requiring shape through using the condensed matrix method. Both equations were found to work in calculating displacements of morphing structure after adjusting bar length actuation. Equation 3.48 was important to provide non-vanishing displacements of the pantographic morphing aerofoil structure, since in this structure, only displacements of the outer surface of the aerofoil were primary non-vanishing displacements [Section 3.3.2].

7.2.3.3 Conclusion 8. For structures made up of complex structural components, a direct and relatively simple method has also been presented (Eqn. 3.58), for providing a direct calculation for required length actuations required for internal force control within a single formulation [Section 3.3.3]. In the same section, also Equations 3.56 and 3.57 provided for controlling bar force without regarding to joint displacement for the non-vanishing and vanishing member force respectively.

7.2.3.4 Conclusion 9. Similarly, a direct simple technique (Eqn. 3.59) has also been developed for structures with complex structural components for calculating required

length actuations where nodal displacement and bar force control are simultaneously controlled [Section 3.3.4].

7.2.4 Objective 4 concerned identifying the best location of actuators and determine the minimum amount of actuation and minimum number of actuators required. This objective was explored in Sections 3.2.2.2 and 6.4.1.7. The conclusions from those sections relating to this objective are:

7.2.4.1 Conclusion 10. It was shown that the effectiveness of a particular actuation in controlling a particular displacement is indicated by the size associated coefficient in the **Y** matrix [Section 3.2.2.2] which was found to work well.

7.2.4.2 Conclusion 11. It was concluded through using the (bar sensitivity technique) that the decision of where the actuator should be placed indicated by the associated coefficient in the bar sensitivity to displacement table which was shown to lead to minimal amount of actuation and that it is possible to choose a just sufficient number of actuators. In other words, it was shown that both the minimum number of actuators as well as minimum actuation can be obtained via this simple technique [Section 6.4.1.7].

7.2.5 Objective 5 concerned correcting manufacture or assembly imperfection, or restoring of the structural shape or internal force due to environmental effects. This objective was explored in Section 3.2.5. The conclusion from this section relating to this objective is:

7.2.5.1 Conclusion 12. Equation 3.23 was developed which corrected manufacture or assembly imperfection. This equation could restore structural shape or internal force due to environmental effects (*e.g.* thermal distortion) or structural movements (*e.g.* foundation settlement, or the structure moving, as in a mobile support structure) [Section 3.2.5].

7.2.6 Objective 6 concerned the development of a morphing aerofoil structure as an effective way to enhance/replace the tradition aerofoil. This objective was explored in Sections 5.6, 5.7 and 5.7.4. The conclusions from those sections relating to this objective are:

7.2.6.1 Conclusion 13. Two morphing aerofoils (Figures 4.10 and 4.11) have been formed via a series of interconnected curved controlled pantograph units. It was concluded that Morphing Aerofoil Structure 2 exhibited a wider range of Coefficients of Lift (C_L) and Drag (C_D) than achievable by Morphing Aerofoil Structure 1, and the standard NACA2415 with flaps. It was shown Morphing Aerofoil Structure 2 could take the place of the traditional fixed shape aerofoil with flaps, with its smaller drag and associated bigger lift [Section 5.6]. It was shown that Morphing Aerofoil Structure 1 and 2 can have 18% and 19.5% respectively lower drag on average than the standard NACA2415 especially in the starting stages of morphing. The maximum C_L value of Morphing Aerofoil Structure 2 was 1.82 times higher than the C_L of the NACA2415. In addition, the two morphing aerofoils produced a good coefficient of moment (C_m) in the early stages of morphing [Sections 5.6 and 5.7].

7.2.6.2 Conclusion 14. Morphing Aerofoil Structure 3 was developed (Figure 5.40) as an alternative to Morphing Aerofoil Structures 1 and 2, because they had significant cross-sectional area decrease during morphing, which might be deemed unacceptable. It was concluded that it was indeed possible to have a morphing shape that had a cross-sectional area exceeding that of NACA2415 in all morphing stages, which still had the advantageous aerodynamic characteristics of Morphing Aerofoil Structure 2 (*i.e.* only a slightly smaller C_L for the same C_D) [Section 5.7.4].

7.2.7 Objective 7 concerned calculating theoretical nodal displacements of the pantographic morphing structure. This objective was explored in Section 6.5. The conclusion from this section relating to this objective is:

7.2.7.1 Conclusion 15. The concept for a novel morphing aerofoil as an effective way to enhance/replace the tradition aerofoil was proved in Section 6.5 through the comparison of experimental and analytical model. While two methods for calculating theoretical nodal displacement of the pantographic morphing structure were introduced (linear and non-linear methods), it was found correlation between the theoretical computational results and the experimental values was good only for early stages of morphing and geometric nonlinearity due to large and significant geometry change, mean only a non-linear coordinate update method could sufficiently track the geometry of the morphing aerofoil accurately through all stages of morphing [Section 6.5].

7.2.8 Objective 8 concerned examining shape adjustment of a morphing structure. This objective was explored in Section 6.4.1.2. The conclusion from this section relating to this objective is:

7.2.8.1 Conclusion 16. It was concluded that shape adjustment or refinement can be done for any morphing structure for some specified joint displacements, with a fixed set of actuation members, in any stage of morphing. This is a good result for the technology of designing morphing aerofoils, since not only have the static stages morphing aerofoil itself shown to have better aerodynamic characteristics than the equivalent fixed shape NACA aerofoil with flaps, but here, we see that a morphing aerofoil which has gone "out of shape" due to changes in load or weight (*e.g.* through the burning of fuel normally stored within the voids of the aerofoil) can be corrected via shape adjustment. Furthermore, this leads to the possibility that a desired change in lift/drag characteristics could be obtained from either a morphing change or a smaller refining shape change, and thus the choice could be made dynamically during flight, and be optimised for best economy of flight operational parameters [Section 6.4.1.2].

7.2.9 Objective 9 concerned examining objectives 2 to 8 experimentally. This objective was explored in Sections 4.4.2, 4.4.2.1.1, 4.4.2.2.1, 4.4.2.3, 6.4.1.6, 6.4.1, 6.4.1.3 and 6.4.1.5. The conclusions from those sections relating to this objective are:

7.2.9.1 Conclusion 17. It was established that all experimental results of the physical model of the cable stayed bridge and pantographic morphing structure agreed well with theoretically computed predictions from Eqns. 3.10, 3.16, 3.19 and 3.54, hence the validation of those equations were conclusive for linear shape and internal force adjustment of different structural assembly [Sections 4.4.2 and 6.4.1].

7.2.9.2 Conclusion 18. It was proven experimentally and practically that the desired targets could be achieved for nodal displacement and bar forces, depending on the number of actuators. It was shown that if the number of actuators not sufficient it is impossible to obtain (even theoretically) the target results [Section 4.4.2.1.1].

7.2.9.3 Conclusion 19. For the physical model of the cable-stayed bridge eight cables in Chapter 4, a theoretical calculation was done for each actuator individually. It was shown

in Figure 4.21 with "$\mathbf{e_o}$" that each cable actuation has a direct effect on its joint with the beam of the structure [Section 4.4.2.1.1].

7.2.9.4 Conclusion 20. It was also concluded that if the number of actuators are sufficient the nodal displacement controlling could be done in all joints of the cable stayed bridge model, even if the controlled joints did not directly contact with members that had the actuators for the purpose of adjustment [Section 4.4.2.2.1].

7.2.9.5 Conclusion 21. It could be concluded that the technique of multi-iteration adjustment was effective in eliminating errors that occur in the practical adjustment process itself, as demonstrated by the experiments on the cable stayed bridge and pantographic morphing models [Sections 4.4.2.3 and 6.4.1.6].

7.2.9.6 Conclusion 22. It was proven in Experiments 3 and 4 that choosing a wrong target has a very big effect on the amount of total actuation, where a slightly different target positions for the one selected joint led to significant difference in the amount of total actuation of 8.9mm [Section 6.4.1.3].

7.2.9.7 Conclusion 23. Using an elastic stretchable material was found to be a suitable technique for the pantographic morphing structure skin to ensure correct aerodynamic properties of the aerofoil. In addition, it was also shown that the direct method of controlling displacement is valid and practical, and good for adjusting static shape induced by both loads (routine and unpredicted) and other factors such as from prestressing in the pantographic structures via using elastic bands [Section 6.4.1.5].

An analysis of the conclusions 1 to 23 above shows that Objectives 1 to 5, and 7 to 9 were fully met. However, Objective 6 was only partially met because the proposed morphing aerofoils must still be checked experimentally for validation of the calculated aerodynamic properties such as coefficients of Lift (C_L) and Drag (C_D). With the near fulfilment of all the objectives, it can be concluded that the original two aims of the thesis as stated in Section 1.2 have been achieved.

7.3   Recommendations for Future Work

Objective 6 was only partially met in the present study, since C_L and C_D were not experimentally verified, and hence:

- It is proposed that further experimental work be carried out on the proposed morphing aerofoil shapes in this dissertation to experimentally verify C_L and C_D values.
- It is also proposed to construct a larger scaled three-dimensional morphing wing structure with a proper stretchable surface material and better joints, to further verify the morphing concept.

Apart from meeting all the original objectives in this work:

- In the course of the work, it was clear that only a two-dimensional morphing structure was proposed and examined (Section 5.6), i.e. the morphing occurred only in one vertical plane. Accordingly, it is proposed that three-dimensional morphing aerofoils be examined, such that the morphing allows a changing geometry both in the cross-section as well as in the long-section. This could perhaps combine the current two-dimensional cross-sectional morphing aerofoil with a swept-wing mechanism, which could then be tested, and adjusted for any shape imperfection correction.
- Also, it is recommended that further verification experiments on the shape/force adjustment be carried out on other types of structures, for example tensegrity structures which are geometry dependent, or other three-dimensional truss structure with cable elements.
- Although some work on minimising the amount of actuation was carried out in the present work, it would be useful to have a technique to find exactly the theoretical minimum amount of actuation for controlling displacement, internal force and simultaneously controlling of external nodal displacement and internal bar force.
- Lastly, since many of the structures requiring shape/force control are fairly flexible and thus exhibit geometric nonlinearity, it is recommended that the current technique for adjustment of linear structures be extended to include geometric nonlinearity, and that validation work also be carried out on geometrically non-linear structural models.

References

Akgün, Y. 2010. *A novel transformation model for deployable scissor-hinge structures.* PhD Thesis, Izmır Institute of Technology.

Akgün, Y., Gantes, C. J., Kalochairetis, K. E. and Kiper, G. 2010. A novel concept of convertible roofs with high transformability consisting of planar scissor-hinge structures. *Engineering Structures* 32(9), pp. 2873-2883.

Akgün, Y., Haase, W. and Sobek, W. 2007. *Proposal for a new scissor-hinge structure to create transformable and adaptive roofs*. Proceedings of International Symposium Shell and Spatial Structures-Architectural Engineering-Towards the future looking to the past. Venice, Italy, 3-6 September 2007.

Alegria Mira, L. 2010. *Design and analysis of a universal scissor component for mobile architectural applications.* MSc Dissertation, Vrije Universiteit Brussel.

Arbabi, S. 2012. *Engadget primed: Camera metering explained* [Online]. Available at: http://www.engadget.com/2012/03/23/engadget-primed-camera-metering-explained/ [Accessed: 2 August 2013].

Bar-Meir, G. 2013. *Basics of fluid mechanics* [Online]. Available at: www.potto.org/FM/intro.pdf [Accessed: 18 October 2013].

Bettini, P., Airoldi, A., Sala, G., Landro, L. D., Ruzzene, M. and Spadoni, A. 2010. Composite chiral structures for morphing airofoils: Numerical analyses and development of a manufacturing process. *Composites Part B: Engineering* 41(2), pp. 133-147.

Binette, P., Dano, M. L. and Gendron, G. 2009. Active shape control of composite structures under thermal loading. *Smart Materials and Structures* 18(2), pp. 1-12.

Brandt, S. A., Stiles, R. J., Bertin, J. J. and Whitford, R. 2004. *Introduction to Aeronautics: A Design Perspective*. 2nd ed. Reston, Virginia, USA: AIAA Education Series.

Burdisso, R. A. and Haftka, R. T. 1989. Optimal location of actuators for correcting distortions in large truss structures. *AIAA Journal* 27(10), pp. 1406-1411.

Burdisso, R. A. and Haftka, R. T. 1990. Statistical analysis of static shape control in space structures. *AIAA Journal* 28(8), pp. 1504-1508.

Chandrala, M., Choubey, A. and Gupta, B. 2012. Aerodynamic analysis of horizontal axis wind turbine blade. *International Journal of Engineering Research and Applications (IJERA)* 2(6), pp. 1244-1248.

Chee, C. Y. K., Tong, L. and Steven, G. P. 1998. A review on the modelling of piezoelectric sensors and actuators incorporated in intelligent structures. *Journal of Intelligent Material Systems and Structures* 9(1), pp. 3-19.

Chee, C. Y. K., Tong, L. and Steven, G. P. 2001. Static shape control of composite plates using a curvature–displacement based algorithm. *International Journal of Solids and Structures* 38(36), pp. 6381-6403.

Chee, C. Y. K., Tong, L. and Steven, G. P. 2002. Static shape control of composite plates using a slope-displacement-based algorithm. *AIAA Journal* 40(8), pp. 1611-1618.

Chen, G.-S., Bruno, R. J. and Salama, M. 1991. Optimal placement of active/passive members in truss structures using simulated annealing. *AIAA Journal* 29(8), pp. 1327-1334.

Chikahiro, Y., Ario, I., Nakazawa, M., Ono, S., Holnicki-Szulc, J., Pawlowski, P. and Graczykowski, C. 2014. *An experimental study on the design method of a real-sized Mobile Bridge for a moving vehicle*. Proceedings of Mobile and Rapidly Assembled Structures IV. Ostend, Belgium, 11–13 June 2014. WIT Press, pp. 93-103.

De Temmerman, N. 2007. *Design and analysis of deployable bar structures for mobile architectural applications.* PhD Thesis, Vrije Universiteit Brussel.

Dong, S. and Yuan, X. 2007. Pretension process analysis of prestressed space grid structures. *Journal of Constructional Steel Research* 63(3), pp. 406-411.

Du, J., Bao, H. and Cui, C. 2014. Shape adjustment of cable mesh reflector antennas considering modeling uncertainties. *Acta Astronautica* 97, pp. 164-171.

Du, J., Zong, Y. and Bao, H. 2013. Shape adjustment of cable mesh antennas using sequential quadratic programming. *Aerospace Science and Technology* 30(1), pp. 26-32.

Du, S. and Ang, H. 2012. Design and feasibility analyses of morphing airfoil used to control flight attitude. *Journal of Mechanical Engineering* 58(1), pp. 46-55.

Edberg, D. L. 1987. Control of flexible structures by applied thermal gradients. *AIAA Journal* 25(6), pp. 877-883.

Escrig, F. 1985. Expandable Space Structures. *Space Structures Journal* 1(2), pp. 79-91.

Furuya, H. and Haftka, R. T. 1995a. Placing actuators on space structures by genetic algorithms and effectiveness indices. *Structural Optimization* 9(2), pp. 69-75.

Furuya, H. and Haftka, R. T. 1995b. Static shape control of space trusses with partial measurements. *Journal of Spacecraft and Rockets* 32(5), pp. 856-865.

Gantes, C. J. 2001. *Deployable Structures: Analysis and Design*. Southampton, UK: WIT Press.

Glisic, B., Adriaenssens, S. and Szerzo, P. 2013. Structural analysis and validation of a smart pantograph mast concept. *Computer-Aided Civil and Infrastructure Engineering* 28(9), pp. 651-665.

Greene, W. H. and Haftka, R. T. 1990. Reducing distortion and internal forces in truss structures by member exchanges. *AIAA Journal* 28(9), pp. 1655-1662.

Hadjigeorgiou, E. P., Stavroulakis, G. E. and Massalas, C. V. 2006. Shape control and damage identification of beams using piezoelectric actuation and genetic optimization. *International Journal of Engineering Science* 44(7), pp. 409-421.

Haftka, R. T. 1984. Optimum placement of controls for static deformations of space structures. *AIAA Journal* 22(9), pp. 1293-1298.

Haftka, R. T. 1991. Limits on static shape control for space structures. *AIAA Journal* 29(11), pp. 1945-1950.

Haftka, R. T. and Adelman, H. M. 1985a. An analytical investigation of shape control of large space structures by applied temperatures. *AIAA Journal* 23(3), pp. 450-457.

Haftka, R. T. and Adelman, H. M. 1985b. Selection of actuator locations for static shape control of large space structures by heuristic integer programing. *Computers & Structures* 20(1), pp. 575-582.

Haftka, R. T. and Adelman, H. M. 1987. Effect of sensor and actuator errors on static shape control for large space structures. *AIAA Journal* 25(1), pp. 134-138.

Hoberman, C. 1990. Reversibly expandable doubly-curved truss structure. United States Patent no. 4, 942, 700.

Iannucci, L. and Fontanazza, A. 2008. *Design of morphing wing structures*. Proceedings of 3rd Systems Engineering for Autonomous Systems (SEAS) Defence Technology Centre (DTC) Technical Conference. Edinburgh, UK, 24–5 June 2008. pp. 24-25.

Inoue, F. 2007. *Development of adaptive construction structure by variable geometry truss*. Proceedings of International Symposium Shell and Spatial Structures-Architectural Engineering-Towards the future looking to the past. Venice, Italy, 3-6 September 2007. pp. 253-272.

Inoue, F., Moroto, R., Kurita, K. and Furuya, N. 2006. *Development of Adaptive Structure by Variable Geometry Truss (Application of Movable Monument in EXPO 2005)*. Proceedings of 23th International Symposium on Automation and Robotics in Construction. Tokyo, Japan, 3-5 October 2006. pp. 704-709.

Irschik, H. 2002. A review on static and dynamic shape control of structures by piezoelectric actuation. *Engineering Structures* 24(1), pp. 5-11.

Irschik, H. and Nader, M. 2009. Actuator placement in static bending of smart beams utilizing Mohr's analogy. *Engineering Structures* 31(8), pp. 1698-1706.

Irschik, H. and Ziegler, F. 2001. Eigenstrain without stress and static shape control of structures. *AIAA journal* 39(10), pp. 1985-1990.

Jacobs, E. N., Ward, K. E. and Pinkerton, R. M. 1933. *The characteristics of 78 related airfoil sections from tests in the variable-density wind tunnel*. Washington: DTIC Document.

Jensen, F. and Pellegrino, S. 2005. Expandable 'blob'structures. *Journal of the International Association for Shell and Spatial Structures* 46(149), pp. 151-158.

Kaveh, A. and Davaran, A. 1996. Analysis of pantograph foldable structures. *Computers & Structures* 59(1), pp. 131-140.

Kawaguchi, K.-I., Hangai, Y., Pellegrino, S. and Furuya, H. 1996. Shape and stress control analysis of prestressed truss structures. *Journal of Reinforced Plastics and Composites* 15(12), pp. 1226-1236.

Kincaid, R. K. 1993. Minimizing distortion in truss structures: A comparison of simulated annealing and tabu search. *Structural Optimization* 5(4), pp. 217-224.

Koconis, D. B., Kollar, L. P. and Springer, G. S. 1994a. Shape control of composite plates and shells with embedded actuators. I. Voltages specified. *Journal of Composite Materials* 28(5), pp. 415-458.

Koconis, D. B., Kollar, L. P. and Springer, G. S. 1994b. Shape control of composite plates and shells with embedded actuators. II. Desired shape specified. *Journal of Composite Materials* 28(3), pp. 262-285.

Korkmaz, S. 2011. A review of active structural control: challenges for engineering informatics. *Computers & Structures* 89(23), pp. 2113-2132.

Kwan, A. S. K. 1991. *A pantographic deployable mast.* PhD Thesis, University of Cambridge.

Kwan, A. S. K. and Pellegrino, S. 1993. Prestressing a space structure. *AIAA Journal* 31(10), pp. 1961-1963.

Kwan, A. S. K. and Pellegrino, S. 1994. Matrix formulation of macro-elements for deployable structures. *Computers & Structures* 50(2), pp. 237-254.

Lachenal, X., Weaver, P. M. and Daynes, S. 2012. Multi-stable composite twisting structure for morphing applications. *Proceedings of the Royal Society A: Mathematical, Physical and Engineering Science* 468(2141), pp. 1230-1251.

Levy, R., Hanaor, A. and Rizzuto, N. 1994. Experimental investigation of prestressing in double-layer grids. *International Journal of Space Structures* 9(1), pp. 21-26.

Livesley, R. K. 1975. *Matrix Methods of Structural Analysis*. Oxford, UK: Pergamon Press.

Maden, F., Korkmaz, K. and Akgün, Y. 2011. A review of planar scissor structural mechanisms: geometric principles and design methods. *Architectural Science Review* 54(3), pp. 246-257.

Maghami, P. G. and Joshi, S. M. 1993. Sensor/actuator placement for flexible space structures. *IEEE Transactions on Aerospace and Electronic Systems* 29(2), pp. 345-351.

Matunaga, S. and Onoda, J. 1995. Actuator placement with failure consideration for static shape control of truss structures. *AIAA Journal* 33(6), pp. 1161-1163.

Merchan, C. H. H. 1987. *Deployable structures.* MSc Dissertation, Massachusetts Institute of Technology, Department of Architecture.

Mitsugi, J., Yasaka, T. and Miura, K. 1990. Shape control of the tension truss antenna. *AIAA Journal* 28(2), pp. 316-322.

Nagaraj, B. P., Pandiyan, R. and Ghosal, A. 2010. A constraint Jacobian based approach for static analysis of pantograph masts. *Computers & Structures* 88(1), pp. 95-104.

Onoda, J. and Hanawa, Y. 1993. Actuator placement optimization by genetic and improved simulated annealing algorithms. *AIAA Journal* 31(6), pp. 1167-1169.

Pellegrino, S. 1993. Structural computations with the singular value decomposition of the equilibrium matrix. *International Journal of Solids and Structures* 30(21), pp. 3025-3035.

Pellegrino, S., Kwan, A. S. K. and Van Heerden, T. F. 1992. Reduction of equilibrium, compatibility and flexibility matrices, in the force method. *International Journal for Numerical Methods in Engineering* 35(6), pp. 1219-1236.

Peng, F., Jiang, X. X., Hu, Y. R. and Ng, A. 2008. Actuation precision control of SMA actuators used for shape control of inflatable SAR antenna. *Acta Astronautica* 63(5), pp. 578-585.

Pinero, E. P. 1961. A reticular movable theatre. *The Architects' Journal* 134, p. 299.

Rao, S. S., Pan, T. S. and Venkayya, V. B. 1991. Optimal placement of actuators in actively controlled structures using genetic algorithms. *AIAA Journal* 29(6), pp. 942-943.

Roovers, K. and De Temmerman, N. 2014. *The design of a foldable triangulated scissor grid for single-curvature surfaces*. Proceedings of Mobile and Rapidly Assembled Structures IV. Ostend, Belgium, 11–13 June 2014. WIT Press, pp. 195-206.

Salama, M., Umland, J., Bruno, R. and Garba, J. 1993. Shape adjustment of precision truss structures: analytical and experimental validation. *Smart Materials and Structures* 2(4), p. 240.

Sener, M., Utku, S. and Wada, B. K. 1994. Geometry control in prestressed adaptive space trusses. *Smart Materials and Structures* 3(2), p. 219.

Shea, K., Fest, E. and Smith, I. F. C. 2002. Developing intelligent tensegrity structures with stochastic search. *Advanced Engineering Informatics* 16(1), pp. 21-40.

Shen, L. Y., Li, G. Q. and Luo, Y. F. 2006. Displacement control of prestressed cable structures (in Chinese). *J. Tongji Univ. (Nat. Sci.)* 34(3), pp. 291-295.

Skelton, R. E. and DeLorenzo, M. L. 1983. Selection of noisy actuators and sensors in linear stochastic systems. *Large Scale Systems* 4(2), pp. 109-136.

Sofla, A. Y. N., Elzey, D. M. and Wadley, H. N. G. 2009. Shape morphing hinged truss structures. *Smart Materials and Structures* 18(6), p. 065012.

Song, G., Ma, N. and Li, H.-N. 2006. Applications of shape memory alloys in civil structures. *Engineering Structures* 28(9), pp. 1266-1274.

Subramanian, G. and Mohan, P. 1996. A fast algorithm for the static shape control of flexible structures. *Computers & Structures* 59(3), pp. 485-488.

Sunar, M. and Rao, S. S. 1999. Recent advances in sensing and control of flexible structures via piezoelectric materials technology. *Applied Mechanics Reviews* 52(1), pp. 1-16.

Susam, G. 2013. *A Research on a Reconfigurable Hypar Structure for Architectural Applications.* MSc Dissertation, İzmir Institute of Technology.

Taheri, P. 2013. *Numerical calculation of lift and drag coefficients for an ellipse aerofoil.* Course Project ENSC 283: Simon Fraser University.

Tanaka, H. 2011. Surface error estimation and correction of a space antenna based on antenna gainanalyses. *Acta Astronautica* 68(7), pp. 1062-1069.

Tanaka, H. and Natori, M. 2006. Shape control of cable-network structures based on concept of self-equilibrated stresses. *JSME International Journal Series C* 49, pp. 1067-1072.

Tanaka, H. and Natori, M. C. 2004. Shape control of space antennas consisting of cable networks. *Acta Astronautica* 55(3), pp. 519-527.

Trak, A. B. and Melosh, R. J. 1992. Passive shape control of space antennas with truss support structures. *Computers & Structures* 45(2), pp. 297-305.

Wang, Z., Chen, S. h. and Han, W. 1997. The static shape control for intelligent structures. *Finite Elements in Analysis and Design* 26(4), pp. 303-314.

Wang, Z., Li, T. and Cao, Y. 2013. Active shape adjustment of cable net structures with PZT actuators. *Aerospace Science and Technology* 26(1), pp. 160-168.

Weeks, C. J. 1984a. Static shape determination and control of large space structures: I. The flexible beam. *Journal of Dynamic Systems, Measurement, and Control* 106(4), pp. 261-266.

Weeks, C. J. 1984b. Static shape determination and control of large space structures: II. A large space antenna. *Journal of Dynamic Systems, Measurement, and Control* 106(4), pp. 267-272.

White, F. M. 2011. *Fluid mechanics*. 7th ed. McGraw-Hill.

Wolfe, M. H. 2013. *Analysis of deployable strut roof structures*. MSc Dissertation, Massachusetts Institute of Technology.

Wujun, C., Gongyi, F., Jinghai, G., Yanli, H. and Shilin, D. 2002. A new design conception for large span deployable flat grid structures. *International Journal of Space Structures* 17(4), pp. 293-299.

Xu, X. and Luo, Y. 2009. Non-linear displacement control of prestressed cable structures. *Proceedings of the Institution of Mechanical Engineers, Part G: Journal of Aerospace Engineering* 223(7), pp. 1001-1007.

Xu, X. and Luo, Y. Z. 2008. Multi-objective shape control of prestressed structures with genetic algorithms. *Proceedings of the Institution of Mechanical Engineers, Part G: Journal of Aerospace Engineering* 222(8), pp. 1139-1147.

Yang, S. and Ngoi, B. 2000. Shape control of beams by piezoelectric actuators. *AIAA Journal* 38(12), pp. 2292-2298.

You, Z. 1997. Displacement control of prestressed structures. *Computer Methods in Applied Mechanics and Engineering* 144(1), pp. 51-59.

You, Z. and Pellegrino, S. 1997. Foldable bar structures. *International Journal of Solids and Structures* 34(15), pp. 1825-1847.

Yu, Y., Zhang, X. N. and Xie, S. L. 2009. Optimal shape control of a beam using piezoelectric actuators with low control voltage. *Smart Materials and Structures* 18(9), p. 095006.

Zadeh, O. S. 2012. *Comparison between three types of cable stayed bridges using structural optimization.* MSc Dissertation, The University of Western Ontario.

Ziegler, F. 2005. Computational aspects of structural shape control. *Computers & Structures* 83(15), pp. 1191-1204.

Appendix A

MATLAB Programs

A.1 MATLAB Program for Tables 3.1 and 3.2

```
clear; clc;
coor=100*[0 1; 0 0; 1 1; 1 0; 2 1; 2 0]; %sets up coordinates in mm
bar=[1 2; 1 3; 2 3; 1 4; 2 4; 3 4; 3 5; 3 6; 4 6; 5 6]; %sets up matrix of
connectivity
EA=400000*[1 1 1 1 1 1 1 1 1 1]; %EA for each bar in N
H=zeros(12, 10);     %sets up 12x8 structural equilibrium matrix
F=zeros(10, 10);     %sets up 10x10 structural flexibility matrix
for i=1:10,
  j1=bar(i, 1); j2=bar(i, 2);
  hor=coor(j2, 1)-coor(j1, 1); ver=coor(j2, 2)-coor(j1, 2);
  L=sqrt(hor^2+ver^2); l=hor/L; m=ver/L; %l & m are the cos & sin of bar angle
  h=[-hor; -ver; hor; ver]/L; f=L/EA(i);
  H((j1-1)*2+1:(j1-1)*2+2,i)=H((j1-1)*2+1:(j1-1)*2+2,i)+h(1:2,1);
  H((j2-1)*2+1:(j2-1)*2+2,i)=H((j2-1)*2+1:(j2-1)*2+2,i)+h(3:4,1);
  F(i,i)=f;
end;
H=H([4:12],:);          %selecting rows relating to non-supports
e0=zeros(10,1);         %vector of initial bar elongation
P=[0 0 -1000 0 0 0 -3000 0 0]';%Force vector, with rows for supports taken out
already
S=null(H);          %state of self-stress, will explain "null"
tH=pinv(H)*P;       %tH is a vector of t that is in eqm with applied P
alpha=inv(S'*F*S)*(-S'*(e0+F*tH));    %alpha is the "redundancies"
t=tH+S*alpha;           %t is the vector of bar tensions
e=e0+F*t;               %e is vector of bar elongations
dp=pinv(H')*e;       %d is vector of displacements
dp1=dp([3,7],1) ; d1=[-2;-2];
B=H' ;
Y=pinv(B)-pinv(B)*F*S*inv(S'*F*S)*S' ;
Y1=Y([3,7],:) ;
e0a=pinv(Y1)*(d1-dp1);
dpa=Y*e0a+dp ;
Y4=Y([3,7],[2:5]);
e04=pinv(Y4)*(d1-dp1);
```

```
e0(2:5,1)=e04 ;
e04=e0 ;
dp4=Y*e04+dp;
Y2=Y([3,7],[2:3]);
e02=pinv(Y2)*(d1-dp1);
e0=zeros(10,1);
e0(2:3,1)=e02 ;
e02=e0 ;
dp2=Y*e02+dp ;
Table 3.1=[dp,dpa,dp4,dp2]
%%%%%%%%%%%%%%%%%%
Z=S*inv(S'*F*S)*S';
e0=zeros(10,1);
tp3=t([2,5,8],:);
Z3=Z([2,5,8],:);
e0=zeros(10,1);
tp2=t([2,5],:);
tc2=[6000;-4000];
Z2=Z([2,5],:);
e02=pinv(Z2)*(tp2-tc2);
t2=t-Z*e02;
e0=zeros(10,1);
tp1=t(5,:);
tc1=[-4000];
Z1=Z([5],:) ;
e01=pinv(Z1)*(tp1-tc1);
t1=t-Z*e01;
Table 3.2=[t, t2, t1]
```

A.2 MATLAB Program for Tables 3.3 and 3.4

```
clear; clc;
coor=100*[0 0; 3 0; 2 0; 1 0; 0 1; 1 1; 2 1; 3 1]; %sets up coordinates in mm
bar=[1 4; 4 6;5 6; 1 5; 1 6; 4 5; 3 4; 3 7; 6 7; 4 7; 3 6; 2 3; 2 8; 7 8; 3 8;
2 7; 1 7; 3 5; 4 8; 2 6]; %sets up matrix of connectivity
EA=40000*[1 1 1 1 1 1 1 1 1 1 1 1 1 1 1 1 1 1 1 1];%EA for each bar in N
P=[0 0 0 0 0 0 0 0 -1000 0 -3000 0 0]';
H=zeros(16,20);    %sets up 10x8 structural equilibrium matrix
F=zeros(20,20);    %sets up 8x8 structural flexibility matrix
for i=1:20,
  j1=bar(i,1); j2=bar(i,2);
  hor=coor(j2,1)-coor(j1,1); ver=coor(j2,2)-coor(j1,2);
  L=sqrt(hor^2+ver^2); l=hor/L; m=ver/L;%l & m are the cos & sin of bar angle
  h=[-hor; -ver; hor; ver]/L; f=L/EA(i);
  H((j1-1)*2+1:(j1-1)*2+2,i)=H((j1-1)*2+1:(j1-1)*2+2,i)+h(1:2,1);
  H((j2-1)*2+1:(j2-1)*2+2,i)=H((j2-1)*2+1:(j2-1)*2+2,i)+h(3:4,1);
  F(i,i)=f;
end;
dp=zeros(16,1);
H=H([3,5:16],:);         %selecting rows relating to non-supports
e0=zeros(20,1);          %vector of initial bar elongation
S=null(H);               %state of self-stress, will explain "null"
tH=pinv(H)*P;            %tH is a vector of t that is in eqm with applied P
```

225

```
alpha=inv(S'*F*S)*(-S'*(e0+F*tH)); %alpha is the "redundancies"
t=tH+S*alpha;           %t is the vector of bar tensions
e=e0+F*t;               %e is vector of bar elongations
dp=pinv(H')*e ;         %d is vector of displacements
dp1=dp([7,9,11,13],1) ; d1=[-8;-8;-8;-8];  dd1=d1-dp1;   B=H';
Y=pinv(B)-pinv(B)*F*S*inv(S'*F*S)*S';
Y1=Y([7,9,11,13],:) ;
Z=S*inv(S'*F*S)*S';
e01=pinv(Y1)*dd1 ;
dpe01=Y*e01+dp;
tpe01=t-Z*e01;
%%%%%%%%%%%%%%%%%%%%%
dp2=dp([7,9,11,13],1) ;  d2=[-8;-8;-8;-8];   dd2=d2-dp2;
Y=pinv(B)-pinv(B)*F*S*inv(S'*F*S)*S' ;
Y2=Y([7,9,11,13],:) ;
tp2=t([7,12, 16],:);
tc2=[1500;1500;-1500];
tt2=tp2-tc2;
Z=S*inv(S'*F*S)*S';
Z2=Z([7, 12,16],:);
A2=[dd2;tt2];
B2=[Y2;Z2];
e02=pinv(B2)*A2 ;
dpe02=Y*e02+dp;
tpe02=t-Z*e02;
%%%%%%%%%%%%%%%%%%
dp3=dp([7,9,11,13],1) ; d3=[-8;-8;-8;-8]; dd3=d3-dp3;
Y=pinv(B)-pinv(B)*F*S*inv(S'*F*S)*S' ;
Y3=Y([7, 9, 11,13], :) ;
tp3=t([7,9, 12,16], :);
tc3=[1500;-1500;1500;-1500];
tt3=tp3-tc3;
Z=S*inv(S'*F*S)*S';
Z3=Z([7, 9, 12,16], :);
A3=[dd3; tt3];
B3=[Y3; Z3];
e03=pinv(B3)*A3;
dpe03=Y*e03+dp;
tpe03=t-Z*e03;
%%%%%%%%%%%%%%%%
dp4=dp([7,9,11,13],1) ; d4=[-8;-8;-8;-8]; dd4=d4-dp4;
Y=pinv(B)-pinv(B)*F*S*inv(S'*F*S)*S';
Y4=Y([7,9, 11,13],[4,7:9, 13,16:17,20]) ;
tp4=t([7, 9, 12,16], :);
tc4=[1500;-1500;1500;-1500];
tt4=tp4-tc4;
Z=S*inv(S'*F*S)*S';
Z4=Z([7, 9, 12,16], [4,7:9, 13,16:17,20]);
```

```
A4=[dd4; tt4];
B4=[Y4; Z4];
e04=zeros(20,1);
e04a=pinv(B4)*A4;
e04([4,7:9, 13,16:17,20] ,1)=e04a;
dpe04=Y*e04+dp;
tpe04=t-Z*e04;
%%%%%%%%%%%%%%%%%%
dp5=dp([7,9,11,13],1) ; d5=[-8;-8;-8;-8]; dd5=d5-dp5;
Y=pinv(B)-pinv(B)*F*S*inv(S'*F*S)*S';
Y5=Y([7, 9, 11,13], [4,6:9,13:14, 16,20]) ;
tp5=t([1, 7, 9, 12,16], :);
tc5=[1500;1500;-1500;1500;-1500];
tt5=tp5-tc5;
Z=S*inv(S'*F*S)*S';
Z5=Z([1, 7, 9, 12,16], [4,6:9,13:14, 16,20]);
A5=[dd5; tt5];
B5=[Y5; Z5];
e05=zeros(20,1);
e05a=pinv(B5)*A5;
e05([4,6:9,13:14, 16,20] ,1)=e05a;
dpe05=Y*e05+dp;
tpe05=t-Z*e05;
%%%%%%%%%%%%%%%%%%
dp6=dp([7,9,11,13],1) ; d6=[-8;-8;-8;-8]; dd6=d6-dp6;
Y=pinv(B)-pinv(B)*F*S*inv(S'*F*S)*S';
Y6=Y([7, 9, 11,13], [3:4,7:9,12:14,16]) ;
tp6=t([1, 7, 9, 12,16], :);
tc6=[1500;1500;-1500;1500;-1500];
tt6=tp6-tc6;
Z=S*inv(S'*F*S)*S';
Z6=Z([1, 7, 9, 12,16], [3:4,7:9,12:14,16]);
A6=[dd5;tt5];
B6=[Y6; Z6];
e06=zeros(20,1);
e06a=pinv(B6)*A6;
e06([3:4,7:9,12:14,16] ,1)=e06a;
dpe06=Y*e06+dp;
tpe06=t-Z*e06;
D=[dp,dpe01,dpe02,dpe03,dpe04,dpe05,dpe06]
T=[t,tpe01,tpe02,tpe03,tpe04,tpe05,tpe06]
T=[e04,e05,e06]
```

A.3 MATLAB Program for Tables 3.5, 3.6 and 3.7

```
clear; clc
coor=[0 200; 0 0; 200 200; 200 0; 100 100; 100 100];%sets up coordinates in mm
bar=[2 5; 5 3; 1 6; 6 4; 1 3; 1 2; 2 4; 3 4];%sets up matrix of connectivity
hold on; for i=1:8, j1=bar(i,1); j2=bar(i,2);
    plot([coor(j1,1) coor(j2,1)], [coor(j1,2) coor(j2,2)],'b-'); end;
area=[36 36 36 36 36 36 36 36 ];%bar area for each bar in mm2
inertia=[108 108 108 108 108 108 108 108 ];%bar moment of inertia for each bar
in mm4
E=10000*[1 1 1 1 1 1 1 1]; %young's modulus in N/mm2
H=zeros(18,24);%sets up 18x24 structural equilibrium matrix
F=zeros(24,24);%sets up 24x24 structural flexibility matrix
for i=1:8,
  j1=bar(i,1); j2=bar(i,2);
  hor=coor(j2,1)-coor(j1,1); ver=coor(j2,2)-coor(j1,2);
  L=sqrt(hor^2+ver^2) ;
  l=hor/L; m=ver/L;          %l & m are the cos & sin of bar angle
  h=[-l m/L -m/L;-m -l/L l/L; 0 -1 0;l -m/L m/L;m l/L -l/L;0 0 1];
  f=[(L/(E(i)*area(i))) 0 0; 0 (L/(3*E(i)*inertia(i)))
(L/(6*E(i)*inertia(i)));...
      0 (L/(6*E(i)*inertia(i))) (L/(3*E(i)*inertia(i)))];
  H((j1-1)*3+1:(j1-1)*3+3,i*3-2:i*3)= H((j1-1)*3+1:(j1-1)*3+3,i*3-
2:i*3)+h(1:3,:);
  H((j2-1)*3+1:(j2-1)*3+3,i*3-2:i*3)= H((j2-1)*3+1:(j2-1)*3+3,i*3-
2:i*3)+h(4:6,:);
  F((i-1)*3+1:(i-1)*3+3,(i-1)*3+1:(i-1)*3+3)=f;
end;
H=H([3 5:18 ],:);%selecting rows relating to non-supports
H=[H(:,[1 2 4 6 7 8 10 12:24]) H(:,3)+H(:,5)  H(:,9)+H(:,11)];%mI.II=mI2+mII1
H=H(:,[1 3 5 7 9 12 15 18 21 22]);%removing mI1=mII2=mIII1=mIV2=0
H=H([2 4 5 7 8 10 11 13 14],:);%M1=M2=M3=M4=M5=M6 no moment on mid and end
joints of pantographic
H=[H(1:5,:); H(6,:)+H(8,:); H(7,:)+H(9,:)]; %Px5+Px6=0,Py5+Py6=0, no load on
mid joint of pantographic
Amn=H(1:5,1:8); Amp=H(1:5,9:10); Apn=H(6:7,1:8); App=H(6:7,9:10);
A=Amn-Amp*pinv(App)*Apn;
F=[F(:,[1 4 7 10 13 16 19 22]) F(:,3)+F(:,5)  F(:,9)+F(:,11)];
%mI.II=mI2+mII1
F=[F([1 4 7 10 13 16 19 22],:); F(3,:)+F(5,:) ; F(9,:)+F(11,:)];
%mI.II=mI2+mII1
Fnn=F(1:8,1:8);  Fnp=F(1:8,9:10);  Fpn=F(9:10,1:8);  Fpp=F(9:10,9:10);
F=Fnn-Fnp*pinv(App)*Apn-Apn'*pinv(App')*Fpn+Apn'*pinv(App')*Fpp*pinv(App)*Apn;
e0n=zeros(8,1);%vector of initial bar elongation
e0p=zeros(2,1);
e0t=[e0n; e0p];
r=Apn'*pinv(App');
e0=e0n-r*e0p;
```

```
p1=-10000;
P=1*[0 0 p1 0 0]';%Force vector, with rows for supports taken out already
S=null(A);%state of self-stress
tH=pinv(A)*P;%tH is a vector of t that is in eqm with applied P
alpha=inv(S'*F*S)*(-S'*(e0+F*tH));%alpha is the "redundancies"
tn=tH+S*alpha;%t is the vector of bar tensions
tp=-pinv(App)*Apn*tn;
TT=[tn; tp];
e=e0+F*tn;%e is vector of bar elongations
en=(Fnn-Fnp*pinv(App)*Apn)*tn;
ep=(Fpn-Fpp*pinv(App)*Apn)*tn;
et=[en; ep];
dm=pinv(A')*e;%d is vector of displacements
dp=pinv(App')*ep-pinv(App')*Amp'*dm;
%2222222222222222222222222222222222222222
x=Fnn-Fnp*pinv(App)*Apn;
z=Fpn-Fpp*pinv(App)*Apn;
r=Apn'*pinv(App');
m=[pinv(A')-pinv(A')*F*S*inv(S'*F*S)*S'];
m1=m*F;
m2=m;
m3=m*-r;
k=S*inv(S'*F*S)*S';
k1=(-pinv(App')*z*k*F+pinv(App')*Amp'*pinv(A')*F*k*F-
pinv(App')*Amp'*pinv(A')*F+pinv(App')*z);
k2=(-pinv(App')*z*k  +pinv(App')*Amp'*pinv(A')*F*k  -
pinv(App')*Amp'*pinv(A'));
k3=( pinv(App')*z*k*r-
pinv(App')*Amp'*pinv(A')*F*k*r+pinv(App')*Amp'*pinv(A')*r+pinv(App'));
MK1=[m1; k1];
MK2=[m2; k2];
MK3=[m3; k3];
dpc=MK1*tH;
Yc=[MK2 MK3];
D=MK1*tH+Yc*e0t
J=-pinv(App)*Apn;
tpc=[tH-k*F*tH; J*tH-J*k*F*tH]
Znc=[-k;  -J*k];
Zpc=[k*r;  J*k*r];
Zc=[Znc Zpc];
T=tpc+Zc*e0t;
%2222222222222222222222222222222222222222
%Joint Displacement Control Table 3.5
e0n1=zeros(8,1);
e0p1=zeros(2,1);
e0t1=[e0n1; e0p1];
dpn1=dm(3,:);
ddn1=[0];  %target displacement
```

```
DDn1=ddn1-dpn1;      %difference between target and Theoretical
Y1=Yc(3,[1:8]);
e0t1([1:8],:)=pinv(Y1)*DDn1;
Te0t1=sum(abs(e0t1));
DDnp1=Yc*e0t1+dpc
Check1=DDnp1(3,1);
Check1=[ddn1 Check1];
%%%%%%%%%%%%%%%%%%%%
e0n2=zeros(8,1);
e0p2=zeros(2,1);
e0t2=[e0n2; e0p2];
dpn2=dm(3,:);
ddn2=[0];   %target displacement
DDn2=ddn2-dpn2;      %difference between target and Theoretical
Y2=Yc(3,1);
e0t2(1,:)=pinv(Y2)*DDn2;
Te0t2=sum(abs(e0t2));
DDnp2=Yc*e0t2+dpc
Check2=DDnp2(3,1);
Check2=[ddn2 Check2];
%%%%%%%%%%%%%%%%%%%%%
e0n2=zeros(8,1);
e0p2=zeros(2,1);
e0t2=[e0n2; e0p2];
dpn2=dm(3,:);
ddn2=[0];   %target displacement
DDn2=ddn2-dpn2;        %difference between target and Theoretical
Y2=Yc(3,4);
e0t2(4,:)=pinv(Y2)*DDn2;
Te0t2=sum(abs(e0t2));
DDnp2=Yc*e0t2+dpc
Check2=DDnp2(3,1);
Check2=[ddn2 Check2];
%%%%%%%%%%%%%%%%%%%%%%%%%%%%%%%%%%%%%%%%%%%%%%%%%%%%%%%%%%%%%%
%Bar Force Control Table 3.6
e0p1=zeros(2,1);
e0t1=[e0n1; e0p1];
tpn1=tn([1,2],:);
tdn1=[-6000; -6000];  %target displacement
TTn1=tdn1-tpn1;        %difference between target and Theoretical
Z1=Zc([1,2],[1:8]);
e0t1([1:8],:)=pinv(Z1)*TTn1;
Te0t1=sum(abs(e0t1));
TTnp1=Zc*e0t1+tpc
Check1=TTnp1([1,2],1);
Check1=[tdn1 Check1];
%%%%%%%%%%%%%%%%%%%%%
e0n2=zeros(8,1);
```

```
e0p2=zeros(2,1);
e0t2=[e0n2; e0p2];
tpn2=tn([1,2],:);
tdn2=[-6000; -6000];   %target displacement
TTn2=tdn2-tpn2;        %difference between target and Theoretical
Z2=Zc([1,2],[1,2]);
e0t2([1,2],:)=pinv(Z2)*TTn2;
Te0t2=sum(abs(e0t2));
TTnp2=Zc*e0t2+tpc
Check2=TTnp2([1,2],1);
Check2=[tdn2 Check2];
%%%%%%%%%%%%%%%%%%%%%%%
e0n2=zeros(8,1);
e0p2=zeros(2,1);
e0t2=[e0n2; e0p2];
tpn2=tn([1,2],:);
tdn2=[-6000; -6000];  %target displacement
TTn2=tdn2-tpn2;        %difference between target and Theoretical
Z2=Zc([1,2],1);
e0t2(1,:)=pinv(Z2)*TTn2;
Te0t2=sum(abs(e0t2));
TTnp2=Zc*e0t2+tpc
Check2=TTnp2([1,2],1);
Check2=[tdn2 Check2];
%%%%%%%%%%%%%%%%%%%
e0n2=zeros(8,1);
e0p2=zeros(2,1);
e0t2=[e0n2; e0p2];
tpn2=tn([1,2],:);
tdn2=[-6000; -6000];  %target displacement
TTn2=tdn2-tpn2;        %difference between target and Theoretical
Z2=Zc([1,2],2);
e0t2(2,:)=pinv(Z2)*TTn2;
Te0t2=sum(abs(e0t2));
TTnp2=Zc*e0t2+tpc
Check2=TTnp2([1,2],1);
Check2=[tdn2 Check2];
%%%%%%%%%%%%%%%%%%%%%%%%%%%%%%%%%%%%%%%%%%%%%%%%%%%%%%%%%%%%%
% simultaneously Joint Displacement and Bar Force Control Table 3.7
e0n3=zeros(8,1);
e0p3=zeros(2,1);
e0t3=[e0n3; e0p3];
dpn3=dm(3,:);
ddn3=[0];  %target displacement
DDn3=ddn3-dpn3;    %difference between target and prcatical
Y3=Yc(3,[1:8]);
tpn3=tn([1,2],:);
tdn3=[-6000; -6000];  %target displacement
```

```
TTn3=tdn3-tpn3;    %difference between target and prcatical
Z3=Zc([1,2],[1:8]);
DT3=[DDn3;TTn3];
YZ3=[Y3;Z3];
e0t3([1:8],:)=pinv(YZ3)*DT3;
Te0t3=sum(abs(e0t3));
DDnp3=Yc*e0t3+dpc
Check3=DDnp3(3,1);
Check3=[ddn3 Check3];
TTnp3=Zc*e0t3+tpc
Check3=TTnp3([1,2],1);
Check3=[tdn3 Check3];
%%%%%%%%%%%%%%%%%%%%%%%
e0n5=zeros(8,1);
e0p5=zeros(2,1);
e0t5=[e0n5; e0p5];
dpn5=dm(3,:);
ddn5=[0];  %target displacement
DDn5=ddn5-dpn5;       %difference between target and prcatical
Y5=Yc(3,[1, 2, 4]);
tpn5=tn([1,2],:);
tdn5=[-6000; -6000];  %target displacement
TTn5=tdn5-tpn5;       %difference between target and prcatical
Z5=Zc([1,2],[1, 2, 4]);
DT5=[DDn5;TTn5];
YZ5=[Y5;Z5];
e0t5([1, 2, 4],:)=pinv(YZ5)*DT5;
Te0t5=sum(abs(e0t5))
DDnp5=Yc*e0t5+dpc
Check5=DDnp5(3,1);
Check5=[ddn5 Check5];
TTnp5=Zc*e0t5+tpc
Check5=TTnp5([1,2],1);
Check5=[tdn5 Check5];
```

A.4 MATLAB Program for Tables 4.2, 4.4 and 4.6

```
Clear; clc;
coor=[0 980;0 190; 0 0; -1403 190; -1053 190; -703 190; -353 190;...
    353 190; 703 190; 1053 190; 1403 190]; %sets up coordinates in mm
bar=[1 4; 1 5; 1 6; 1 7; 1 8; 1 9; 1 10; 1 11; 4 5;5 6; 6 7; 7 2; 2 8; 8 9; 9
10;10 11; 1 2; 2 3];          %sets up matrix of connectivity
area=1*[0.135265 0.135265 0.135265 0.135265 0.135265 0.135265 0.135265
0.135265 70.584 70.584 70.584 70.584 70.584 70.584 70.584 70.584 ...
      388.09 388.09];          %bar area for each bar in mm2
```

```matlab
inertia=[0.0233 0.0233 0.0233 0.0233 0.0233 0.0233 0.0233 0.0233 ...
        396.464 396.464 396.464 396.464 396.464 396.464 396.464 396.464
12551.154 12551.154];%bar moment of inertia for each bar in mm4
E=1000*[183.0549 183.7874 185.915 185.8874 187.7155 185.7842 184.7105 ...
181.9555  210 210 210 210 210 210 210 210 200 200]; % young's modulus in N/mm2
H=zeros(33,38);      %sets up 33x38 structural equilibrium matrix
F=zeros(38,38);      %sets up 38x38 structural flexibility matrix
for i=1:8,
  j1=bar(i,1); j2=bar(i,2);
  hor=coor(j2,1)-coor(j1,1); ver=coor(j2,2)-coor(j1,2);
  L=sqrt(hor^2+ver^2); l=hor/L; m=ver/L; %l & m are the cos & sin of bar angle
  h=[-hor; -ver; hor; ver]/L;
  f=L/(E(i)*area(i));
  H((j1-1)*3+1:(j1-1)*3+2,i)=H((j1-1)*3+1:(j1-1)*3+2,i)+h(1:2,1);
  H((j2-1)*3+1:(j2-1)*3+2,i)=H((j2-1)*3+1:(j2-1)*3+2,i)+h(3:4,1);
  F(i,i)=f;
end;
X=(i+1)*2; Y=X-3;
for i=9:18,
  j1=bar(i,1); j2=bar(i,2);
  hor=coor(j2,1)-coor(j1,1); ver=coor(j2,2)-coor(j1,2);
  L=sqrt(hor^2+ver^2);
  l=hor/L; m=ver/L;        %l & m are the cos & sin of bar angle
  h=[-l m/L -m/L;-m -l/L l/L; 0 -1 0;l -m/L m/L;m l/L -l/L;0 0 1];
  f=[(L/(E(i)*area(i))) 0 0; 0 (L/(3*E(i)*inertia(i)))
(L/(6*E(i)*inertia(i))); 0 (L/(6*E(i)*inertia(i))) (L/(3*E(i)*inertia(i)))];
  H((j1-1)*3+1:(j1-1)*3+3,i*3-X:i*3-(X-2))= H((j1-1)*3+1:(j1-1)*3+3,i*3-X:i*3-
(X-2))+h(1:3,:);
  H((j2-1)*3+1:(j2-1)*3+3,i*3-X:i*3-(X-2))= H((j2-1)*3+1:(j2-1)*3+3,i*3-X:i*3-
(X-2))+h(4:6,:);
  F((i-1)*3-Y:(i-1)*3-(Y-2),(i-1)*3-Y:(i-1)*3-(Y-2))=f;
end;
H=H([1:6 10:33],:);          %selecting rows relating to non-supports
e0=zeros(38,1);              %vector of initial bar elongation
P=zeros(30,1); %sets up Force vector, with rows for supports taken out already
yL1=1.142474725;             %weight of each load in N
yL=15*yL1;   zL=20*yL1;
P([8 11  14  17  20  23  26  29],1)=-1*[yL zL zL zL zL zL zL yL]; %Force
vector, with rows for supports taken out already
S=null(H);          %state of self-stress,
tH=pinv(H)*P;       %tH is a vector of t that is in eqm with applied P
alpha=inv(S'*F*S)*(-S'*(e0+F*tH)); %alpha is the "redundancies"
t=tH+S*alpha;               %t is the vector of bar tensions
e=e0+F*t;                   %e is vector of bar elongations
dp=pinv(H')*e ;             %d is vector of displacements
t([1:8],1);                 %Tension in Cables [1:8]
t([20,22],1);               %Moment of  beams in supports
e([1:8],1);                 %Elongation of Cables [1:8]
```

233

```matlab
dp([8 11 14 17 20 23 26 29 1],1);   %Displacement in y direction with
horizontal direction of the top point of column
Y=pinv(H')-pinv(H')*F*S*inv(S'*F*S)*S';
Z=S*inv(S'*F*S)*S';
%+++++++++++++++++++++++++++++++++++++++++++++++++++++++++++++++
% Joint Displacement Table 5.2
e0d=zeros(38,1);
dp([8 11 14 17 20 23 26 29],:)=[-4.618;-3.569;-2.214;-0.98;-0.973;-2.155;-
3.375;-4.512];  %from Practical
dpd=dp([8 11 14 17 20 23 26 29],:);
dtd=-1*[1;1;1;1;1;1;1;1];    %target displacement
Yd=Y([8 11 14 17 20 23 26 29],[1:8]);
DD=dtd-dpd;               %difference between target and practical
e0d([1:8],1)=pinv(Yd)*(dtd-dpd);
e0d([1:8],1)              %e0 required
Te0d=sum(abs(e0d));
dpdA=Y*e0d+dp;
ddd=dpdA([8 11 14 17 20 23 26 29],1)-dpd;
dpdA([8 11 14 17 20 23 26 29 1],1)
%+++++++++++++++++++++++++++
% Bar Force Table 5.4
% Selecting  bar force  1,2,3,4,5,6,7&8 and e01,e02,e03,e04,e05,e06,e07&e08
e0t=zeros(38,1);
t([1:8],:)=[35.968;33.768;34.625;18.784;16.843;33.308;36.054;34.195];
tpt=t([1:8],:);
tct=34*[1;1;1;1;1;1;1;1];  %target bar tension
Zt=Z([1:8],[1:8]);
TT=tpt-tct;                %difference between target and practical
e0t([1:8],1)=pinv(Zt)*(tpt-tct);
e0t([1:8],1)                %e0 required
ttA=t-Z*e0t;
ttA([1:8],1)
Te0t=sum(abs(e0t));
%+++++++++++++++++++++++++++++++
% Joint Deflection & Bar Force Table 5.6
% Eight points for displacement and eight cables for force CONTROLLING BY
EIGHT CABLES
e0B=zeros(38,1);
dp([8 11 14 17 20 23 26 29],:)=[-4.53;-3.525;-2.189;-0.951;-1.075;-2.242;-
3.549;-4.696]; %from Practical
dpB=dp([8 11 14 17 20 23 26 29],:);
dtB=-0*[1;1;1;1;1;1;1;1];  %target displacement
DDB=dtB-dpB;               %difference between target and practical
YB=Y([8 11 14 17 20 23 26 29],[1:8]);
t([1:8],:)=[35.195;33.243;36.436;17.476;15.266;28.878;36.132;32.111]; %from
Practical
tpB=t([1:8],:);
tcB=30*[1;1;1;1;1;1;1;1];     %target bar tension
```

```
TTB=tpB-tcB;                    %difference between target and practical
ZB=Z([1:8],[1:8]);
DTB=[DDB;TTB];
YZB=[YB;ZB];
e0B([1:8],1)=pinv(YZB)*DTB;
e0B([1:8],1)            %e0 required
Te0B=sum(abs(e0B));
dpe0B=Y*e0B+dp;
dpe0B([8 11 14 17 20 23 26 29 1],1)
tpe0B=t-Z*e0B;
tpe0B([1:8],1)
```

A.5 MATLAB Program for Tables 4.3, 4.5 and 4.7

```
clear; clc;
coor=[0 980;0 190; 0 0; -1403 190; -1053 190; -703 190; -353 190;...
    353 190; 703 190; 1053 190; 1403 190]; %sets up coordinates in mm
bar=[1 4; 1 5; 1 6; 1 7; 1 8; 1 9; 1 10; 1 11; 4 5;5 6; 6 7; 7 2; 2 8; 8 9; 9
10; 10 11; 1 2; 2 3];           %sets up matrix of connectivity
area=1*[0.135265 0.135265 0.135265 0.135265 0.135265 0.135265 0.135265
0.135265 70.584 70.584 70.584 70.584 70.584 70.584 70.584 70.584 ...
     388.09 388.09];           %bar area for each bar in mm2
inertia=[0.0233 0.0233 0.0233 0.0233 0.0233 0.0233 0.0233 0.0233 ...
      396.464 396.464 396.464 396.464 396.464 396.464 396.464 396.464
12551.154 12551.154];%bar moment of inertia for each bar in mm4
E=1000*[183.0549 183.7874 185.915 185.8874 187.7155 185.7842 184.7105 181.9555
210 210 210 210 210 210 210 210 200 200]; %young's modulus in N/mm2
H=zeros(33,38);          %sets up 33x38 structural equilibrium matrix
F=zeros(38,38);          %sets up 38x38 structural flexibility matrix
for i=1:8,
  j1=bar(i,1); j2=bar(i,2);
  hor=coor(j2,1)-coor(j1,1); ver=coor(j2,2)-coor(j1,2);
  L=sqrt(hor^2+ver^2); l=hor/L; m=ver/L; %l & m are the cos & sin of bar angle
  h=[-hor; -ver; hor; ver]/L;
  f=L/(E(i)*area(i));
  H((j1-1)*3+1:(j1-1)*3+2,i)=H((j1-1)*3+1:(j1-1)*3+2,i)+h(1:2,1);
  H((j2-1)*3+1:(j2-1)*3+2,i)=H((j2-1)*3+1:(j2-1)*3+2,i)+h(3:4,1);
  F(i,i)=f;
end;
X=(i+1)*2; Y=X-3;
for i=9:18,
  j1=bar(i,1); j2=bar(i,2);
  hor=coor(j2,1)-coor(j1,1); ver=coor(j2,2)-coor(j1,2);
  L=sqrt(hor^2+ver^2);
  l=hor/L; m=ver/L;        %l & m are the cos & sin of bar angle
```

```
  h=[-l m/L -m/L;-m -l/L l/L; 0 -1 0;l -m/L m/L;m l/L -l/L;0 0 1];
  f=[(L/(E(i)*area(i))) 0 0; 0 (L/(3*E(i)*inertia(i)))
(L/(6*E(i)*inertia(i)));...
     0 (L/(6*E(i)*inertia(i))) (L/(3*E(i)*inertia(i)))];
  H((j1-1)*3+1:(j1-1)*3+3,i*3-X:i*3-(X-2))= H((j1-1)*3+1:(j1-1)*3+3,i*3-X:i*3-
(X-2))+h(1:3,:);
  H((j2-1)*3+1:(j2-1)*3+3,i*3-X:i*3-(X-2))= H((j2-1)*3+1:(j2-1)*3+3,i*3-X:i*3-
(X-2))+h(4:6,:);
  F((i-1)*3-Y:(i-1)*3-(Y-2),(i-1)*3-Y:(i-1)*3-(Y-2))=f;
end;
H=H([1:6 10:33],:);        %selecting rows relating to non-supports
e0=zeros(38,1);            %vector of initial bar elongation
P=zeros(30,1);            %sets up Force vector, with rows for supports taken
out already
yL1=1.142474725;          %weight of each load in N
yL=15*yL1; zL=20*yL1;
P([8 11  14  17  20  23  26  29],1)=-1*[yL zL zL zL zL zL zL yL]; %Force
vector, with rows for supports taken out already
S=null(H);             %state of self-stress,
tH=pinv(H)*P;          %tH is a vector of t that is in eqm with applied P
alpha=inv(S'*F*S)*(-S'*(e0+F*tH));     %alpha is the "redundancies"
t=tH+S*alpha;                %t is the vector of bar tensions
e=e0+F*t;                    %e is vector of bar elongations
dp=pinv(H')*e ;              %d is vector of displacements
t([1:8],1);                  %Tension in Cables [1:8]
t([20,22],1);                %Moment of  beams in supports
e([1:8],1);                  %Elongation of Cables [1:8]
dp([8 11 14 17 20 23 26 29 1],1);  %Displacement in y direction with
horizontal direction of the top point of column
Y=pinv(H')-pinv(H')*F*S*inv(S'*F*S)*S';
Z=S*inv(S'*F*S)*S';
%+++++++++++++++++++++++++++++++++++++++++++++++++++++++++++
%Joint Displacement Table 5.3
e0d=zeros(38,1);
dp([8 11 14 17 20 23 26 29],:)=[-4.52;-3.515;-2.182;-0.96;-1.031;-2.205;-
3.49;-4.581]; %from Practical
dpd=dp([8 11 14 17 20 23 26 29],:);
dtd=-1*[1;1;1;1;1;1;1;1];          %target displacement
Yd=Y([8 11 14 17 20 23 26 29],[1,3,6,8]);
DD=dtd-dpd;            %difference between target and practical
e0d([1,3,6,8],1)=pinv(Yd)*(dtd-dpd);
e0d([1:8],1)            %e0 required
Te0d=sum(abs(e0d));
dpdA=Y*e0d+dp;
ddd=dpdA([8 11 14 17 20 23 26 29],1)-dpd;
dpdA([8 11 14 17 20 23 26 29 1],1)
%+++++++++++++++++++++++++++++++++++++++++++++++++++++++++++
%Bar Force; Table 5.5
```

```
%Selecting  bar force  1,2,3,4,5,6,7&8 and e01,e02,e03,e04,e05,e06,e07&e08
e0t=zeros(38,1);
t([1:8],:)=[35.11;33.65;34.09;18.47;16.52;33.80;35.56;33.37];
tpt=t([1:8],:);
tct=34*[1;1;1;1;1;1;1;1];        %target bar tension
Zt=Z([1:8],[1,3,6,8]);
TT=tpt-tct;                       %difference between target and practical
e0t([1,3,6,8],1)=pinv(Zt)*(tpt-tct);
e0t([1:8],1)           %e0 required
ttA=t-Z*e0t;
ttA([1:8],1)
Te0t=sum(abs(e0t));
%Eight points for displacement and eight cables for force CONTROLLING BY FOUR
CABLES Table 5.7
e0B=zeros(38,1);
dp([8 11 14 17 20 23 26 29],:)=[-4.519;-3.414;-2.194;-0.993;-1.046;-2.248;-
3.536;-4.642]; %from Practical
dpB=dp([8 11 14 17 20 23 26 29],:);
dtB=-0*[1;1;1;1;1;1;1;1];        %target displacement
DDB=dtB-dpB;                      %difference between target and practical
YB=Y([8 11 14 17 20 23 26 29],[1,3,6,8]);
t([1:8],:)=[35.968;36.785;34.216;19.815;17.398;35.764;37.03;34.711]; %from
Practical
tpB=t([1:8],:);
tcB=30*[1;1;1;1;1;1;1;1];    %target bar tension
TTB=tpB-tcB;                      %difference between target and practical
ZB=Z([1:8],[1,3,6,8]);

DTB=[DDB;TTB];
YZB=[YB;ZB];
e0B([1,3,6,8],1)=pinv(YZB)*DTB;
e0B([1:8],1)                %e0 required
Te0B=sum(abs(e0B));
dpe0B=Y*e0B+dp;
dpe0B([8 11 14 17 20 23 26 29 1],1)
tpe0B=t-Z*e0B;
tpe0B([1:8],1)
```

A.6 MATLAB Program for Tables 4.8, 4.9, 4.10 and 4.11

```
clear; clc;
coor=[0 980;0 190; 0 0; -1403 190; -1053 190; -703 190; -353 190;...
    353 190; 703 190; 1053 190; 1403 190]; %sets up coordinates in mm
bar=[1 4; 1 6; 1 9; 1 11; 4 5;5 6; 6 7; 7 2; 2 8; 8 9; 9 10;10 11;...
    1 2; 2 3];        %sets up matrix of connectivity
```

```matlab
area=1*[0.135265 0.135265 0.135265 0.135265 ...
        70.584 70.584 70.584 70.584 70.584 70.584 70.584 70.584 ...
        388.09 388.09];              %bar area for each bar in mm2
inertia=[0.0233 0.0233 0.0233 0.0233 396.464 396.464...
        396.464 396.464 396.464 396.464 396.464 396.464 12551.154 12551.154];
%bar moment of inertia for each bar in mm
E=1000*[183.0549 185.915 185.7842  181.9555 210 210...
        210 210 210 210 210 210 200 200] ;% young's modulus in N/mm2
H=zeros(33,34);       %sets up 33x34 structural equilibrium matrix
F=zeros(34,34);       %sets up 34x34 structural flexibility matrix
for i=1:4,
  j1=bar(i,1); j2=bar(i,2);
  hor=coor(j2,1)-coor(j1,1); ver=coor(j2,2)-coor(j1,2);
  L=sqrt(hor^2+ver^2); l=hor/L; m=ver/L;  %l & m are the cos & sin of bar
angle
  h=[-hor; -ver; hor; ver]/L;
  f=L/(E(i)*area(i));
  H((j1-1)*3+1:(j1-1)*3+2,i)=H((j1-1)*3+1:(j1-1)*3+2,i)+h(1:2,1);
  H((j2-1)*3+1:(j2-1)*3+2,i)=H((j2-1)*3+1:(j2-1)*3+2,i)+h(3:4,1);
  F(i,i)=f;
end;
X=(i+1)*2; Y=X-3;
for i=5:14,
  j1=bar(i,1); j2=bar(i,2);
  hor=coor(j2,1)-coor(j1,1); ver=coor(j2,2)-coor(j1,2);
  L=sqrt(hor^2+ver^2);
  l=hor/L; m=ver/L;     %l & m are the cos & sin of bar angle
  h=[-l m/L -m/L l/L; 0 -1 0;l -m/L m/L;m l/L -l/L;0 0 1];
  f=[(L/(E(i)*area(i))) 0 0; 0 (L/(3*E(i)*inertia(i)))
(L/(6*E(i)*inertia(i)));...
      0 (L/(6*E(i)*inertia(i))) (L/(3*E(i)*inertia(i)))];
  H((j1-1)*3+1:(j1-1)*3+3,i*3-X:i*3-(X-2))= H((j1-1)*3+1:(j1-1)*3+3,i*3-X:i*3-
(X-2))+h(1:3,:);
  H((j2-1)*3+1:(j2-1)*3+3,i*3-X:i*3-(X-2))= H((j2-1)*3+1:(j2-1)*3+3,i*3-X:i*3-
(X-2))+h(4:6,:);
  F((i-1)*3-Y:(i-1)*3-(Y-2),(i-1)*3-Y:(i-1)*3-(Y-2))=f;
end;
H=H([1:6 10:33],:);            %selecting rows relating to non-supports
e0=zeros(34,1);                %vector of initial bar elongation
P=zeros(30,1);                 %sets up Force vector, with rows for supports
taken out already
yL=1.142474725;                %weight of each load in N
zL=2*yL;
P([8 11  14  17  20  23  26  29],1)=-25*[yL 0 zL 0 0 zL 0 yL]; %Force vector,
with rows for supports taken out already
S=null(H);                          %state of self-stress,
tH=pinv(H)*P;                       %tH is a vector of t that is in eqm with
applied P
```

```matlab
alpha=inv(S'*F*S)*(-S'*(e0+F*tH)); %alpha is the "redundancies"
t=tH+S*alpha;                      %t is the vector of bar tensions
e=e0+F*t;                          %e is vector of bar elongations
dp=pinv(H')*e;                     %d is vector of displacements
t([1:4],1);                        %Tension in Cables [1:4]
t([16,18],1);                      %Moment of  beams in supports
e([1:4],1);                        %Elongation of Cables [1:4]
dp([8 11 14 17 20 23 26 29 1],1);  %Displacement in y direction with
horizontal direction of the top point of column
dp([8 14 23 29],1);
Y=pinv(H')-pinv(H')*F*S*inv(S'*F*S)*S';
Z=S*inv(S'*F*S)*S';
%+++++++++++++++++++++++++++++++++++++++++++++++++++++++++++++++
%Joint Displacement Table 5.8
%Selecting bars (1,2,3&4)
e0d=zeros(34,1);
dp([8,11,14,17,20,23,26,29],:)=[-7.268;-5.99;-4.005;-1.44;-1.57; -4.244;-6.3;
-7.618]; %First Iteration from Practical
%dp([8,14,23,29],:)=[-2.683;-2.475;-2.533;-2.64];  %Second Iteration from
Practical
dpd=dp([8 14 23 29],:);
dtd=[-2.5;-2.5;-2.5;-2.5];        %target displacement
Yd=Y([8,14,23,29],[1:4]);
DD=dtd-dpd;             %difference between target and practical
e0d(1:4,1)=pinv(Yd)*(dtd-dpd);
e0d([1:4],1)            %e0 required
Te0d=sum(abs(e0d));
dpdA=Y*e0d+dp;
ddd=dpdA([8 14 23 29],1)-dpd;
dpdA([8 14 23 29 1],1)
%++++++++++++++++++++++++++++++++
%Bar Force Table 5.9
%Selecting  bar force  1,2,3&4 and e01,e02,e03&e04
e0t=zeros(34,1);
t([1 2 3 4],:)=[57.915;67.89;68.149;57.126];%from Practical
tpt=t([1 2 3 4],:);
tct=[61;61;61;61];             %target bar tension
Zt=Z([1 2 3 4],[1:4]);
TT=tpt-tct;                    %difference between target and practical
e0t([1:4],1)=pinv(Zt)*(tpt-tct);
e0t([1:4],1)           %e0 required
ttA=t-Z*e0t;
ttA([1:4],1)
Te0t=sum(abs(e0t));

%++++++++++++++++++++++++++++++++
% Joint Deflection & Bar Force Table 5.10
```

```
%Four point for displacement and four cables for force CONTROLLING BY FOUR
CABLES
e0B=zeros(34,1);
dp([8,11,14,17,20,23,26,29],:)=[-8.266;-6.03;-4.04;-1.47;-1.57;-4.246; -6.26;
-7.592]; %from Practical used for Table 5.11
dpB=dp([8,14,23,29],:) ;
dtB=[-4;-4;-4;-4];              %target displacement
DDB=dtB-dpB;                    %difference between target and practical
YB=Y([8,14,23,29],[1:4]);
t([1 2 3 4],:)=[58.153;68.814;69.134;56.949];
tpB=t([1 2 3 4],:);
tcB=[61;61;61;61];             %target bar tension
TTB=tpB-tcB;                    %difference between target and practical
ZB=Z([1 2 3 4],[1:4]);
DTB=[DDB;TTB];
YZB=[YB;ZB];
e0B([1:4],1)=pinv(YZB)*DTB;
e0B([1:4],1)          %e0 required
Te0B=sum(abs(e0B));
dpe0B=Y*e0B+dp;
dpe0B([8 14 23 29 1],1)
tpe0B=t-Z*e0B;
tpe0B([1:4],1)
```

A.7 MATLAB Program for Table 6.1

```
clear; clc;
coor=[0.0000      25.8097;   31.8877          74.7896;   69.2926      15.0920
    181.8877     137.4954;  212.2653          22.9330;   381.8877    174.9123
    395.6891      53.9261;  581.8877         188.7024;   586.5517     68.7931
    781.8877     186.0357;  775.7805          66.1912;   981.8877    172.3276
    970.8177      48.5476; 1181.8877         150.9526; 1167.3160      30.5043
    1381.8877    123.1472; 1362.2205          0.0000; 1581.8877       89.3289
    1781.8877     31.7244;  104.8987          53.7998;   104.8987     53.7998
    292.0632      94.4307;  292.0632          94.4307;   487.3151    120.2478;
    487.3151     120.2478;  681.4841         125.7724;   681.4841    125.7724
    875.7975     117.6957;  875.7975         117.6957; 1076.6141      99.8769
    1076.6141     99.8769; 1271.8576          75.6409; 1271.8576      75.6409
  1471.7888              44.5566; 1471.7888     44.5566];%sets up coordinates in mm

bar=[1     2; 1    3; 3    20; 20    4; 2    21; 21    5; 5    22; 22    6; 4    23
     23    7; 7   24; 24    8; 6   25; 25    9; 9   26; 26   10; 8   27; 27   11
     11   28; 28  12; 10   29; 29   13; 13   30; 30   14; 12   31; 31   15; 15   32
     32   16; 14  33; 33   17; 17   34; 34   18; 16   35; 35   19; 18   19; 10
12];  %sets up matrix of connectivity
```

```
area=[54 54 54 54 54 54 54 54 54 54 54 54 54 54 54 54 54 54 54 54 54 54...
   54 54 54 54 54 54 54 54 54 54 54 54  54];%bar area for each bar in mm2
inertia=[364.5 364.5 364.5 364.5 364.5 364.5 364.5 364.5 364.5 364.5 ...
        364.5 364.5 364.5 364.5 364.5 364.5 364.5 364.5 364.5 ...
        364.5 364.5 364.5 364.5 364.5 364.5 364.5 364.5 364.5 ...
        364.5 364.5 364.5 364.5 364.5  364.5];        %bar moment of inertia
for each bar in mm4
E=1000*[70 70 70 70 70 70 70 70 70 70 70 70 70 70 70 70 70 70 70 70 70 70 ...
        70 70 70 70 70 70 70 70 70 70 70 70 70 70];%young's modulus in N/mm2
H=zeros(105,108);         %sets up 105x108 structural equilibrium matrix
F=zeros(108,108);         %sets up 108x108 structural flexibility matrix
for i=1:36,
  j1=bar(i,1); j2=bar(i,2);
  hor=coor(j2,1)-coor(j1,1); ver=coor(j2,2)-coor(j1,2);
  L=sqrt(hor^2+ver^2) ;
  l=hor/L; m=ver/L;          %l & m are the cos & sin of bar angle
  h=[-l m/L -m/L;-m -l/L l/L; 0 -1 0;l -m/L m/L;m l/L -l/L;0 0 1];
  f=[(L/(E(i)*area(i))) 0 0; 0 (L/(3*E(i)*inertia(i)))
(L/(6*E(i)*inertia(i)));...
      0 (L/(6*E(i)*inertia(i))) (L/(3*E(i)*inertia(i)))];
  H((j1-1)*3+1:(j1-1)*3+3,i*3-2:i*3)= H((j1-1)*3+1:(j1-1)*3+3,i*3-
2:i*3)+h(1:3,:);
  H((j2-1)*3+1:(j2-1)*3+3,i*3-2:i*3)= H((j2-1)*3+1:(j2-1)*3+3,i*3-
2:i*3)+h(4:6,:);
  F((i-1)*3+1:(i-1)*3+3,(i-1)*3+1:(i-1)*3+3)=f;
end;
H;
H=H([1:27 30:36 39:105],:);      %selecting rows relating to non-supports
H=[H(:,[1:8 10 12:14 16 18:20 22 24:26 28 30:32 34 36:38 40 42:44 46 48:50 52
...
    54:56 58 60:62 64 66:68 70 72:74 76 78:80 82 84:86 88 90:92 94 96:108])...
    H(:,9)+H(:,11)  H(:,15)+H(:,17) H(:,21)+H(:,23) H(:,27)+H(:,29) ...
    H(:,33)+H(:,35) H(:,39)+H(:,41) H(:,45)+H(:,47) H(:,51)+H(:,53)  ...
    H(:,57)+H(:,59) H(:,63)+H(:,65) H(:,69)+H(:,71) H(:,75)+H(:,77)  ...
    H(:,81)+H(:,83)  H(:,87)+H(:,89) H(:,93)+H(:,95)];   %mI.II=mI2+mII1
H=H(:,[1 4 7 9 11 13 15 17 19 21 23 25 27 29 31 33 35 37 39 41 43 45 47 49 51
...
    53 55 57 59 61 63 65 67 70 73 76 79:93]); %removing mI1=mII2=mIII1=mIV2=0
H=H([1 2 4 5 7 8 10 11 13 14 16 17 19 20 22 23 25 26 29 30 32 33 36 37 39...
 40 42 43 45 46 48 49 51 52 54 55 57 58 60 61 63 64 66 67 69 70 72 73 75...
  76 78 79 81 82 84 85 87 88 90 91 93 94 96 97 99 100],:);
         %M1=M2=M3=M4=M5=M6 no moment on mid and end joints of pantographic
H=[H(1:34,:); H(63,:)+H(65,:); H(64,:)+H(66,:); H(35,:)+H(37,:);
H(36,:)+H(38,:);...
            H(39,:)+H(41,:); H(40,:)+H(42,:); H(43,:)+H(45,:);
H(44,:)+H(46,:);...
            H(47,:)+H(49,:); H(48,:)+H(50,:); H(51,:)+H(53,:);
H(52,:)+H(54,:);...
```

```
                H(55,:)+H(57,:); H(56,:)+H(58,:); H(59,:)+H(61,:);
H(60,:)+H(62,:)];
                %Px5+Px6=0,Py5+Py6=0, no load on mid joint of pantographic
Amn=H(1:35,1:36); Amp=H(1:35,37:51); Apn=H(36:50,1:36); App=H(36:50,37:51);
A=Amn-Amp*pinv(App)*Apn;
F=[F(:,[1 4 7 10 13 16 19 22 25 28 31 34 37 40 43 46 49 52 55 58 61 64 67 ...
 70 73 76 79 82 85 88 91 94 97 100 103 106]) F(:,9)+F(:,11)  F(:,15)+F(:,17)
F(:,21)+F(:,23)...
    F(:,27)+F(:,29) F(:,33)+F(:,35) F(:,39)+F(:,41) F(:,45)+F(:,47)
F(:,51)+F(:,53)...
    F(:,57)+F(:,59) F(:,63)+F(:,65) F(:,69)+F(:,71) F(:,75)+F(:,77)
F(:,81)+F(:,83)...
    F(:,87)+F(:,89) F(:,93)+F(:,95)];  %mI.II=mI2+mII1
F=[F([1 4 7 10 13 16 19 22 25 28 31 34 37 40 43 46 49 52 55 58 61 64 67 70 73
76 79 ...
 82 85 88 91 94 97 100 103 106],:); F(9,:)+F(11,:) ; F(15,:)+F(17,:);
F(21,:)+F(23,:);...
  F(27,:)+F(29,:); F(33,:)+F(35,:); F(39,:)+F(41,:); F(45,:)+F(47,:);
F(51,:)+F(53,:);...
  F(57,:)+F(59,:); F(63,:)+F(65,:); F(69,:)+F(71,:); F(75,:)+F(77,:);
F(81,:)+F(83,:);...
  F(87,:)+F(89,:); F(93,:)+F(95,:)];        %mI.II=mI2+mII1
Fnn=F(1:36,1:36);  Fnp=F(1:36,37:51);  Fpn=F(37:51,1:36);  Fpp=F(37:51,37:51);
F=Fnn-Fnp*pinv(App)*Apn-Apn'*pinv(App')*Fpn+Apn'*pinv(App')*Fpp*pinv(App)*Apn;
e0n=zeros(36,1);      %vector of initial bar elongation
e0p=zeros(15,1);
e0t=[e0n; e0p];
r=Apn'*pinv(App');
e0=e0n-r*e0p;


p1=2*-1.1430; p2=2*-1.1430; p3=2*-1.1430; p4=2*-1.1430; p5=2*-1.1430;
p6=0*-1.1430; p7=2*-1.1430; p8=2*-1.1430; p9=2*-1.1430; p10=2*-1.1430;


P=1*[0 p1 0 p2 0 0 0 p3 0 0 0 p4 0 0 0 p5 0 0 0 0 0 p6 0 p7 0 0 0 p8 0 0 0 p9
0 p10 0]'; %Force vector, with rows for supports taken out already
S=null(A);                 %state of self-stress
tH=pinv(A)*P;              %tH is a vector of t that is in eqm with applied P
alpha=inv(S'*F*S)*(-S'*(e0+F*tH));   %alpha is the "redundancies"
tn=tH+S*alpha;                       %t is the vector of bar tensions
tn([33:36],:);                       %Check strain gauge testing
tp=-pinv(App)*Apn*tn;
TT=[tn; tp];
e=e0+F*tn;                           %e is vector of bar elongations
en=(Fnn-Fnp*pinv(App)*Apn)*tn;
ep=(Fpn-Fpp*pinv(App)*Apn)*tn;
et=[en; ep];
dm=pinv(A')*e;          %d is vector of displacements
dp=pinv(App')*ep-pinv(App')*Amp'*dm;
```

```matlab
%22222222222222222222222222222222222222222
dy=dm([2;4;6;8;10;12;14;16;18;20;22;24;26;28;30;32;34],:); %dmy
Test=dm([2;4;8;12;16;22;24;28;32;34],:)';
%22222222222222222222222222222222222222222
x=Fnn-Fnp*pinv(App)*Apn;
z=Fpn-Fpp*pinv(App)*Apn;
r=Apn'*pinv(App');
m=[pinv(A')-pinv(A')*F*S*inv(S'*F*S)*S'];
m1=m*F;
m2=m;
m3=m*-r;
k=S*inv(S'*F*S)*S';
k1=(-pinv(App')*z*k*F+pinv(App')*Amp'*pinv(A')*F*k*F-
pinv(App')*Amp'*pinv(A')*F+pinv(App')*z);
k2=(-pinv(App')*z*k  +pinv(App')*Amp'*pinv(A')*F*k  -
pinv(App')*Amp'*pinv(A'));
k3=( pinv(App')*z*k*r-
pinv(App')*Amp'*pinv(A')*F*k*r+pinv(App')*Amp'*pinv(A')*r+pinv(App'));

MK1=[m1; k1];
MK2=[m2; k2];
MK3=[m3; k3];
dpc=MK1*tH;
Yc=[MK2 MK3];
D=MK1*tH+Yc*e0t;

J=-pinv(App)*Apn;
tpc=[tH-k*F*tH; J*tH-J*k*F*tH];
Znc=[-k;   -J*k];
Zpc=[k*r;  J*k*r];
Zc=[Znc Zpc];
T=tpc+Zc*e0t;
%22222222222222222222222222222222222222222
%Joint Displacement
% Selecting bars (4,5,8,9,12,13,16,17,20,24,25,28,29,32,33,34&36) to control
% y of joints (1,2,4,6,8,12,14,16,18&19)
e0n1=zeros(36,1);
e0p1=zeros(15,1);
e0t1=[e0n1; e0p1];
dpn1=dm([2;4;8;12;16;22;24;28;32;34],:);
ddn1=[-9; -8; -5; -3; -1; 0; 0; -1; -2; -3];  %target displacement
DDn1=ddn1-dpn1;                %difference between target and practical
Y1=Yc([2 4 8 12 16 22 24 28 32 34],[4 5 12 13 17 20 24 25 28 29]);
e0t1([4 5 12 13 17 20 24 25 28 29],:)=pinv(Y1)*DDn1;
e0t1([4 5 12 13 17 20 24 25 28 29],:)
ee=15*ones(10,1)+e0t1([4 5 12 13 17 20 24 25 28 29],:);
Bn=[4; 5; 12; 13; 17; 20; 24; 25; 28; 29];
```

```
ee=[ee   Bn];
Te0t1=sum(abs(e0t1));
DDnp1=Yc*e0t1+D;
Check1=DDnp1([2 4 8 12 16 22 24 28 32 34],1)
Check2=[ddn1 Check1];
TH=DDnp1([2 4 8 12 16 22 24 28 32 34],1);
PR=D([2 4 8 12 16 22 24 28 32 34],1)+[3.990; 4.267; 4.457; 2.456; 0.999; -
0.340; 0.634; 1.180; 2.201; 4.236];
DF=TH-PR;
Both=[TH PR DF];
```

A.8 MATLAB Program for Table 6.2

```
clear; clc;
coor=[0.0000      25.8097;   31.8877        74.7896;   69.2926      15.0920
    181.8877    137.4954;  212.2653        22.9330;  381.8877     174.9123
    395.6891     53.9261;  581.8877       188.7024;  586.5517      68.7931
    781.8877    186.0357;  775.7805        66.1912;  981.8877     172.3276
    970.8177     48.5476; 1181.8877       150.9526; 1167.3160      30.5043
   1381.8877    123.1472; 1362.2205         0.0000; 1581.8877      89.3289
   1781.8877     31.7244;  104.8987        53.7998;  104.8987      53.7998
    292.0632     94.4307;  292.0632        94.4307;  487.3151     120.2478;
    487.3151    120.2478;  681.4841       125.7724;  681.4841     125.7724
    875.7975    117.6957;  875.7975       117.6957; 1076.6141      99.8769
   1076.6141     99.8769; 1271.8576        75.6409; 1271.8576      75.6409
   1471.7888     44.5566; 1471.7888        44.5566];%sets up coordinates in mm

bar=[1    2; 1    3; 3    20; 20    4; 2    21; 21    5; 5    22; 22    6; 4    23
     23    7; 7    24; 24    8; 6    25; 25    9; 9    26; 26    10; 8    27; 27   11
     11   28; 28   12; 10   29; 29   13; 13   30; 30   14; 12   31; 31   15; 15   32
     32   16; 14   33; 33   17; 17   34; 34   18; 16   35; 35   19; 18   19; 10
12];   %sets up matrix of connectivity
area=[54 54 54 54 54 54 54 54 54 54 54 54 54 54 54 54 54 54 54 54 54 54 54...
    54 54 54 54 54 54 54 54 54 54 54 54];%bar area for each bar in mm2
inertia=[364.5 364.5 364.5 364.5 364.5 364.5 364.5 364.5 364.5 364.5 ...
        364.5 364.5 364.5 364.5 364.5 364.5 364.5 364.5 364.5 364.5 ...
        364.5 364.5 364.5 364.5 364.5 364.5 364.5 364.5 364.5 364.5 ...
        364.5 364.5 364.5 364.5 364.5  364.5]; %bar moment of inertia for
each bar in mm4
E=1000*[70 70 70 70 70 70 70 70 70 70 70 70 70 70 70 70 70 70 70 70 70 70 70 ...
        70 70 70 70 70 70 70 70 70 70 70 70 70]; %young's modulus in N/mm2
H=zeros(105,108);     %sets up 105x108 structural equilibrium matrix
F=zeros(108,108);     %sets up 108x108 structural flexibility matrix
for i=1:36,
  j1=bar(i,1); j2=bar(i,2);
```

```matlab
  hor=coor(j2,1)-coor(j1,1); ver=coor(j2,2)-coor(j1,2);
  L=sqrt(hor^2+ver^2) ;
  l=hor/L; m=ver/L;          %l & m are the cos & sin of bar angle
  h=[-l m/L -m/L;-m -l/L l/L; 0 -1 0;l -m/L m/L;m l/L -l/L;0 0 1];
  f=[(L/(E(i)*area(i))) 0 0; 0 (L/(3*E(i)*inertia(i)))
(L/(6*E(i)*inertia(i)));...
      0 (L/(6*E(i)*inertia(i))) (L/(3*E(i)*inertia(i)))];
  H((j1-1)*3+1:(j1-1)*3+3,i*3-2:i*3)= H((j1-1)*3+1:(j1-1)*3+3,i*3-
2:i*3)+h(1:3,:);
  H((j2-1)*3+1:(j2-1)*3+3,i*3-2:i*3)= H((j2-1)*3+1:(j2-1)*3+3,i*3-
2:i*3)+h(4:6,:);
  F((i-1)*3+1:(i-1)*3+3,(i-1)*3+1:(i-1)*3+3)=f;
end;
H=H([1:27 30:36 39:105],:);     %selecting rows relating to non-supports
H=[H(:,[1:8 10 12:14 16 18:20 22 24:26 28 30:32 34 36:38 40 42:44 46 48:50 52
...
    54:56 58 60:62 64 66:68 70 72:74 76 78:80 82 84:86 88 90:92 94 96:108])...
    H(:,9)+H(:,11)  H(:,15)+H(:,17) H(:,21)+H(:,23) H(:,27)+H(:,29) ...
    H(:,33)+H(:,35) H(:,39)+H(:,41) H(:,45)+H(:,47) H(:,51)+H(:,53)  ...
    H(:,57)+H(:,59) H(:,63)+H(:,65) H(:,69)+H(:,71) H(:,75)+H(:,77)  ...
    H(:,81)+H(:,83)  H(:,87)+H(:,89) H(:,93)+H(:,95)];    %mI.II=mI2+mII1
H=H(:,[1 4 7 9 11 13 15 17 19 21 23 25 27 29 31 33 35 37 39 41 43 45 47 49 51
...
    53 55 57 59 61 63 65 67 70 73 76 79:93]);  %removing mI1=mII2=mIII1=mIV2=0
H=H([1 2 4 5 7 8 10 11 13 14 16 17 19 20 22 23 25 26 29 30 32 33 36 37 39 40
42 ...
  43 45 46 48 49 51 52 54 55 57 58 60 61 63 64 66 67 69 70 72 73 75 76 78 79
81 ...
  82 84 85 87 88 90 91 93 94 96 97 99 100],:);%M1=M2=M3=M4=M5=M6 no moment on
mid and end joints of pantographic
H=[H(1:34,:); H(63,:)+H(65,:); H(64,:)+H(66,:); H(35,:)+H(37,:);
H(36,:)+H(38,:);...
            H(39,:)+H(41,:); H(40,:)+H(42,:); H(43,:)+H(45,:);
H(44,:)+H(46,:);...
            H(47,:)+H(49,:); H(48,:)+H(50,:); H(51,:)+H(53,:);
H(52,:)+H(54,:);...
            H(55,:)+H(57,:); H(56,:)+H(58,:); H(59,:)+H(61,:);
H(60,:)+H(62,:)]; %Px5+Px6=0,Py5+Py6=0, no load on mid joint of pantographic
Amn=H(1:35,1:36); Amp=H(1:35,37:51); Apn=H(36:50,1:36); App=H(36:50,37:51);
A=Amn-Amp*pinv(App)*Apn;
F=[F(:,[1 4 7 10 13 16 19 22 25 28 31 34 37 40 43 46 49 52 55 58 61 64 67 70
73 76 ...
 79 82 85 88 91 94 97 100 103 106]) F(:,9)+F(:,11)  F(:,15)+F(:,17)
F(:,21)+F(:,23)...
    F(:,27)+F(:,29) F(:,33)+F(:,35) F(:,39)+F(:,41) F(:,45)+F(:,47)
F(:,51)+F(:,53)...
    F(:,57)+F(:,59) F(:,63)+F(:,65) F(:,69)+F(:,71) F(:,75)+F(:,77)
F(:,81)+F(:,83)...
```

```
   F(:,87)+F(:,89) F(:,93)+F(:,95)];           %mI.II=mI2+mII1
F=[F([1 4 7 10 13 16 19 22 25 28 31 34 37 40 43 46 49 52 55 58 61 64 67 70 73
76 79 ...
 82 85 88 91 94 97 100 103 106],:); F(9,:)+F(11,:) ; F(15,:)+F(17,:);
F(21,:)+F(23,:);...
  F(27,:)+F(29,:); F(33,:)+F(35,:); F(39,:)+F(41,:); F(45,:)+F(47,:);
F(51,:)+F(53,:);...
  F(57,:)+F(59,:); F(63,:)+F(65,:); F(69,:)+F(71,:); F(75,:)+F(77,:);
F(81,:)+F(83,:);...
  F(87,:)+F(89,:); F(93,:)+F(95,:)];           %mI.II=mI2+mII1
Fnn=F(1:36,1:36);  Fnp=F(1:36,37:51);  Fpn=F(37:51,1:36);  Fpp=F(37:51,37:51);
F=Fnn-Fnp*pinv(App)*Apn-Apn'*pinv(App')*Fpn+Apn'*pinv(App')*Fpp*pinv(App)*Apn;
e0n=zeros(36,1);                         %vector of initial bar elongation
e0n(36,1)=10;
e0p=zeros(15,1);
e0t=[e0n; e0p];
r=Apn'*pinv(App');
e0=e0n-r*e0p;


p1=2*-1.1430; p2=2*-1.1430; p3=2*-1.1430; p4=2*-1.1430; p5=2*-1.1430;
p6=0*-1.1430; p7=2*-1.1430; p8=2*-1.1430; p9=2*-1.1430; p10=2*-1.1430;
P=1*[0 p1 0 p2 0 0 0 p3 0 0 0 p4 0 0 0 p5 0 0 0 0 0 p6 0 p7 0 0 0 p8 0 0 0 p9
0 p10 0]'; %Force vector, with rows for supports taken out already
S=null(A);               %state of self-stress
tH=pinv(A)*P;            %tH is a vector of t that is in eqm with applied P
alpha=inv(S'*F*S)*(-S'*(e0+F*tH));   %alpha is the "redundancies"
tn=tH+S*alpha;                       %t is the vector of bar tensions
tn([33:36],:);                        %Check strain gauge testing
tp=-pinv(App)*Apn*tn;
TT=[tn; tp];
e=e0+F*tn;                           %e is vector of bar elongations
en=(Fnn-Fnp*pinv(App)*Apn)*tn;
ep=(Fpn-Fpp*pinv(App)*Apn)*tn;
et=[en; ep];
dm=pinv(A')*e;           %d is vector of displacements
dp=pinv(App')*ep-pinv(App')*Amp'*dm;


%2222222222222222222222222222222222222222
dy=dm([2;4;6;8;10;12;14;16;18;20;22;24;26;28;30;32;34],:); %dmy
Test=dm([2;4;8;12;16;22;24;28;32;34],:)';
%2222222222222222222222222222222222222222
x=Fnn-Fnp*pinv(App)*Apn;
z=Fpn-Fpp*pinv(App)*Apn;
r=Apn'*pinv(App');
m=[pinv(A')-pinv(A')*F*S*inv(S'*F*S)*S'];
m1=m*F;
m2=m;
m3=m*-r;
```

```
k=S*inv(S'*F*S)*S';
k1=(-pinv(App')*z*k*F+pinv(App')*Amp'*pinv(A')*F*k*F-
pinv(App')*Amp'*pinv(A')*F+pinv(App')*z);
k2=(-pinv(App')*z*k  +pinv(App')*Amp'*pinv(A')*F*k  -
pinv(App')*Amp'*pinv(A'));
k3=( pinv(App')*z*k*r-
pinv(App')*Amp'*pinv(A')*F*k*r+pinv(App')*Amp'*pinv(A')*r+pinv(App'));
MK1=[m1; k1];
MK2=[m2; k2];
MK3=[m3; k3];
dpc=MK1*tH;
Yc=[MK2 MK3];
D=MK1*tH+Yc*e0t;
J=-pinv(App)*Apn;
tpc=[tH-k*F*tH; J*tH-J*k*F*tH];
Znc=[-k;  -J*k];
Zpc=[k*r;  J*k*r];
Zc=[Znc Zpc];
T=tpc+Zc*e0t;
%2222222222222222222222222222222222222222
%Joint Displacement
% Selecting bars (4,5,8,9,12,13,16,17,20,24,25,28,29,32,33,34&36) to control
% y of joints (1,2,4,6,8,12,14,16,18&19)
e0n1=zeros(36,1);
e0p1=zeros(15,1);
e0t1=[e0n1; e0p1];
dpn1=dm([2;4;8;12;16;22;24;28;32;34],:);
ddn1=[15; 15; 15; 15; 10; -15; -30; -50; -75; -110];  %target displacement
DDn1=ddn1-dpn1;              %difference between target and practical
Y1=Yc([2 4 8 12 16 22 24 28 32 34],[4 5 12 13 17 20 24 25 28 29]);
e0t1([4 5 12 13 17 20 24 25 28 29],:)=pinv(Y1)*DDn1;
e0t1([4 5 12 13 17 20 24 25 28 29],:)

ee=15*ones(10,1)+e0t1([4 5 12 13 17 20 24 25 28 29],:);
Bn=[4; 5; 12; 13; 17; 20; 24; 25; 28; 29];
ee=[ee    Bn];
Te0t1=sum(abs(e0t1));
DDnp1=Yc*e0t1+D;
Check1=DDnp1([2 4 8 12 16 22 24 28 32 34],1)
Check2=[ddn1 Check1];

TH=DDnp1([2 4 8 12 16 22 24 28 32 34],1);
PR=D([2 4 8 12 16 22 24 28 32 34],1)+[-4.99; -3.76; -3.55; -3.26;  -1.92; 1.97
; 5.39; 6.96; 4.83; 7.53];
DF=TH-PR;
Both=[TH PR DF];
```

A.9 MATLAB Program for Table 6.3

```
clear; clc;
coor=[0.0000       25.8097;   31.8877        74.7896;   69.2926     15.0920
     181.8877     137.4954;  212.2653        22.9330;  381.8877    174.9123
      395.6891     53.9261;   581.8877      188.7024;  586.5517     68.7931
      781.8877     186.0357;  775.7805       66.1912;  981.8877    172.3276
      970.8177      48.5476; 1181.8877      150.9526; 1167.3160     30.5043
     1381.8877     123.1472; 1362.2205        0.0000; 1581.8877     89.3289
     1781.8877      31.7244;  104.8987       53.7998;  104.8987     53.7998
      292.0632            94.4307;  292.0632    94.4307;  487.3151   120.2478;
      487.3151          120.2478;  681.4841   125.7724;  681.4841   125.7724
      875.7975          117.6957;  875.7975   117.6957; 1076.6141    99.8769
     1076.6141           99.8769; 1271.8576    75.6409; 1271.8576    75.6409
     1471.7888           44.5566; 1471.7888    44.5566];%sets up coordinates in mm


bar=[1     2; 1    3; 3    20; 20   4; 2    21; 21    5; 5    22; 22    6; 4    23
      23    7; 7   24; 24    8; 6   25; 25    9; 9    26; 26   10; 8    27; 27   11
      11   28; 28  12; 10   29; 29   13; 13   30; 30   14; 12   31; 31   15; 15   32
      32   16; 14  33; 33   17; 17   34; 34   18; 16   35; 35   19; 18   19; 10
12]; %sets up matrix of connectivity
area=[54 54 54 54 54 54 54 54 54 54 54 54 54 54 54 54 54 54 54 54 54 54 54 54 ...
    54 54 54 54 54 54 54 54 54 54 54 54 54];%bar area for each bar in mm2
inertia=[364.5 364.5 364.5 364.5 364.5 364.5 364.5 364.5 364.5 364.5 ...
        364.5 364.5 364.5 364.5 364.5 364.5 364.5 364.5 364.5 364.5 ...
        364.5 364.5 364.5 364.5 364.5 364.5 364.5 364.5 364.5 364.5 ...
        364.5 364.5 364.5 364.5 364.5 364.5];%bar moment of inertia for each
bar in mm4
E=1000*[70 70 70 70 70 70 70 70 70 70 70 70 70 70 70 70 70 70 70 70 70 70 ...
        70 70 70 70 70 70 70 70 70 70 70 70 70 70]; %young's modulus in N/mm2
H=zeros(105,108);          %sets up 105x108 structural equilibrium matrix
F=zeros(108,108);          %sets up 108x108 structural flexibility matrix
for i=1:36,
  j1=bar(i,1); j2=bar(i,2);
  hor=coor(j2,1)-coor(j1,1); ver=coor(j2,2)-coor(j1,2);
  L=sqrt(hor^2+ver^2) ;
  l=hor/L; m=ver/L;          %l & m are the cos & sin of bar angle
  h=[-l m/L -m/L;-m -l/L l/L; 0 -1 0;l -m/L m/L;m l/L -l/L;0 0 1];
  f=[(L/(E(i)*area(i))) 0 0; 0 (L/(3*E(i)*inertia(i)))
(L/(6*E(i)*inertia(i)));...
      0 (L/(6*E(i)*inertia(i))) (L/(3*E(i)*inertia(i)))];
  H((j1-1)*3+1:(j1-1)*3+3,i*3-2:i*3)= H((j1-1)*3+1:(j1-1)*3+3,i*3-
2:i*3)+h(1:3,:);
  H((j2-1)*3+1:(j2-1)*3+3,i*3-2:i*3)= H((j2-1)*3+1:(j2-1)*3+3,i*3-
2:i*3)+h(4:6,:);
  F((i-1)*3+1:(i-1)*3+3,(i-1)*3+1:(i-1)*3+3)=f;
end;
```

```
H=H([1:27 30:36 39:105],:);                    %selecting rows relating to non-
supports
H=[H(:,[1:8 10 12:14 16 18:20 22 24:26 28 30:32 34 36:38 40 42:44 46 48:50 52
...
    54:56 58 60:62 64 66:68 70 72:74 76 78:80 82 84:86 88 90:92 94 96:108])...
    H(:,9)+H(:,11)  H(:,15)+H(:,17) H(:,21)+H(:,23) H(:,27)+H(:,29) ...
    H(:,33)+H(:,35) H(:,39)+H(:,41) H(:,45)+H(:,47) H(:,51)+H(:,53)   ...
    H(:,57)+H(:,59) H(:,63)+H(:,65) H(:,69)+H(:,71) H(:,75)+H(:,77)   ...
    H(:,81)+H(:,83)  H(:,87)+H(:,89) H(:,93)+H(:,95)];   %mI.II=mI2+mII1
H=H(:,[1 4 7 9 11 13 15 17 19 21 23 25 27 29 31 33 35 37 39 41 43 45 47 49...
   51 53 55 57 59 61 63 65 67 70 73 76 79:93]);%removing mI1=mII2=mIII1=mIV2=0
H=H([1 2 4 5 7 8 10 11 13 14 16 17 19 20 22 23 25 26 29 30 32 33 36 37 39...
   40 42 43 45 46 48 49 51 52 54 55 57 58 60 61 63 64 66 67 69 70 72 73 75...
   76 78 79 81 82 84 85 87 88 90 91 93 94 96 97 99 100],:); %M1=M2=M3=M4=M5=M6
no moment on mid and end joints of pantographic
H=[H(1:34,:); H(63,:)+H(65,:); H(64,:)+H(66,:); H(35,:)+H(37,:);
H(36,:)+H(38,:);...
 H(39,:)+H(41,:); H(40,:)+H(42,:); H(43,:)+H(45,:); H(44,:)+H(46,:);...
 H(47,:)+H(49,:); H(48,:)+H(50,:); H(51,:)+H(53,:); H(52,:)+H(54,:);...
           H(55,:)+H(57,:); H(56,:)+H(58,:); H(59,:)+H(61,:);
H(60,:)+H(62,:)]; %Px5+Px6=0,Py5+Py6=0, no load on mid joint of pantographic
Amn=H(1:35,1:36); Amp=H(1:35,37:51); Apn=H(36:50,1:36); App=H(36:50,37:51);
A=Amn-Amp*pinv(App)*Apn;
F=[F(:,[1 4 7 10 13 16 19 22 25 28 31 34 37 40 43 46 49 52 55 58 61 64 67...
 70 73 76 79 82 85 88 91 94 97 100 103 106]) F(:,9)+F(:,11)  F(:,15)+F(:,17)
F(:,21)+F(:,23)...
    F(:,27)+F(:,29) F(:,33)+F(:,35) F(:,39)+F(:,41) F(:,45)+F(:,47)
F(:,51)+F(:,53)...
    F(:,57)+F(:,59) F(:,63)+F(:,65) F(:,69)+F(:,71) F(:,75)+F(:,77)
F(:,81)+F(:,83)...
    F(:,87)+F(:,89) F(:,93)+F(:,95)];   %mI.II=mI2+mII1
F=[F([1 4 7 10 13 16 19 22 25 28 31 34 37 40 43 46 49 52 55 58 61 64 67 70...
73 76 79 82 85 88 91 94 97 100 103 106],:); F(9,:)+F(11,:) ; F(15,:)+F(17,:);
F(21,:)+F(23,:);...
F(27,:)+F(29,:); F(33,:)+F(35,:); F(39,:)+F(41,:); F(45,:)+F(47,:);
F(51,:)+F(53,:);...
  F(57,:)+F(59,:); F(63,:)+F(65,:); F(69,:)+F(71,:); F(75,:)+F(77,:);
F(81,:)+F(83,:);...
  F(87,:)+F(89,:); F(93,:)+F(95,:)];             %mI.II=mI2+mII1
Fnn=F(1:36,1:36);  Fnp=F(1:36,37:51); Fpn=F(37:51,1:36);  Fpp=F(37:51,37:51);
F=Fnn-Fnp*pinv(App)*Apn-Apn'*pinv(App')*Fpn+Apn'*pinv(App')*Fpp*pinv(App)*Apn;
e0n=zeros(36,1);                       %vector of initial bar elongation
e0p=zeros(15,1);
e0t=[e0n; e0p];
r=Apn'*pinv(App');
e0=e0n-r*e0p;
p1=9*-1.1430; p2=0*-1.1430; p3=0*-1.1430; p4=0*-1.1430; p5=0*-1.1430;
p6=0*-1.1430; p7=0*-1.1430; p8=0*-1.1430; p9=0*-1.1430; p10=0*-1.1430;
```

```
P=1*[0 p1 0 p2 0 0 0 p3 0 0 0 p4 0 0 0 p5 0 0 0 0 0 p6 0 p7 0 0 0 p8 0 0 0 p9
0 p10 0]'; %Force vector, with rows for supports taken out already
S=null(A);            %state of self-stress
tH=pinv(A)*P;         %tH is a vector of t that is in eqm with applied P
alpha=inv(S'*F*S)*(-S'*(e0+F*tH));    %alpha is the "redundancies"
tn=tH+S*alpha;                        %t is the vector of bar tensions
tn([33:36],:);                         %Check strain gauge testing
tp=-pinv(App)*Apn*tn;
TT=[tn; tp];
e=e0+F*tn;                            %e is vector of bar elongations
en=(Fnn-Fnp*pinv(App)*Apn)*tn;
ep=(Fpn-Fpp*pinv(App)*Apn)*tn;
et=[en; ep];
dm=pinv(A')*e;          %d is vector of displacements
dp=pinv(App')*ep-pinv(App')*Amp'*dm;

%2222222222222222222222222222222222222222
dy=dm([2;4;6;8;10;12;14;16;18;20;22;24;26;28;30;32;34],:); %dmy
Test=dm([2;4;8;12;16;22;24;28;32;34],:)';
%2222222222222222222222222222222222222222
x=Fnn-Fnp*pinv(App)*Apn;
z=Fpn-Fpp*pinv(App)*Apn;
r=Apn'*pinv(App);
m=[pinv(A')-pinv(A')*F*S*inv(S'*F*S)*S'];
m1=m*F;
m2=m;
m3=m*-r;
k=S*inv(S'*F*S)*S';
k1=(-pinv(App')*z*k*F+pinv(App')*Amp'*pinv(A')*F*k*F-
pinv(App')*Amp'*pinv(A')*F+pinv(App')*z);
k2=(-pinv(App')*z*k  +pinv(App')*Amp'*pinv(A')*F*k  -
pinv(App')*Amp'*pinv(A'));
k3=( pinv(App')*z*k*r-
pinv(App')*Amp'*pinv(A')*F*k*r+pinv(App')*Amp'*pinv(A')*r+pinv(App'));
MK1=[m1; k1];
MK2=[m2; k2];
MK3=[m3; k3];
dpc=MK1*tH;
Yc=[MK2 MK3];
D=MK1*tH+Yc*e0t;
J=-pinv(App)*Apn;
tpc=[tH-k*F*tH; J*tH-J*k*F*tH];
Znc=[-k;  -J*k];
Zpc=[k*r;  J*k*r];
Zc=[Znc Zpc];
T=tpc+Zc*e0t;
%2222222222222222222222222222222222222222
```

```
%Joint Displacement
% Selecting bars (4,5,8,9,12,13,16,17,20,24,25,28,29,32,33,34&36) to control
% y of joints (1,2,4,6,8,12,14,16,18&19)
e0n1=zeros(36,1);
e0p1=zeros(15,1);
e0t1=[e0n1; e0p1];
dpn1=dm([2;4;8;12;16;22;24;28;32;34],:)
ddn1=[0; 0; 0; 0; 0; 0; 0; 0; 0; 0];  %target displacement
DDn1=ddn1-dpn1;                        %difference between target and practical
Y1=Yc([2 4 8 12 16 22 24 28 32 34],[4 5 12 13 17 20]);
e0t1([4 5 12 13 17 20],:)=pinv(Y1)*DDn1;
e0t1([4 5 12 13 17 20],:)
ee=15*ones(6,1)+e0t1([4 5 12 13 17 20],:);
Bn=[4; 5; 12; 13; 17; 20];
ee=[ee   Bn];
Te0t1=sum(abs(e0t1));


DDnp1=Yc*e0t1+D;
Check1=DDnp1([2 4 8 12 16 22 24 28 32 34],1)
Check2=[ddn1 Check1];


TH=DDnp1([2 4 8 12 16 22 24 28 32 34],1);
PR=D([2 4 8 12 16 22 24 28 32 34],1)+[22.8980; 21.9391; 16.4163; 9.5580;
3.6345; -1.1229; -1.3364; -1.7648; -1.7332; -3.4908];
DF=TH-PR;
Both=[TH PR DF];
%2222222222222222222222222222222222222222222
%Joint Displacement
% Selecting bars (4,5,8,9,12,13,16,17,20,24,25,28,29,32,33,34&36) to control
% y of joints (1,2,4,6,8,12,14,16,18&19)
e0n2=zeros(36,1);
e0p2=zeros(15,1);
e0t2=[e0n1; e0p1];
dpn2=dm([2;4;8;12;16;22;24;28;32;34],:);
ddn2=[0; 0; 0; 0; -3; 0; 0; 0; 0; 0];  %target displacement
DDn2=ddn2-dpn2;            %difference between target and practical
Y2=Yc([2 4 8 12 16 22 24 28 32 34],[4 5 12 13 17 20]);
e0t2([4 5 12 13 17 20],:)=pinv(Y2)*DDn2;
e0t2([4 5 12 13 17 20],:)
ee2=15*ones(6,1)+e0t2([4 5 12 13 17 20],:);
Bn2=[4; 5; 12; 13; 17; 20];
ee2=[ee2   Bn2];
Te0t2=sum(abs(e0t2));


DDnp2=Yc*e0t2+D;
Check12=DDnp2([2 4 8 12 16 22 24 28 32 34],1)
Check22=[ddn2 Check12];
TH2=DDnp2([2 4 8 12 16 22 24 28 32 34],1);
```

```
PR2=D([2 4 8 12 16 22 24 28 32 34],1)+[24.2912; 23.3120; 17.2208; 9.7590;
0.9494; -1.3590; -1.33406; -1.7781; -2.2056; -3.5281];
DF2=TH2-PR2;
Both=[TH2 PR2 DF2];
```

A.10 MATLAB Program for Table 6.4

```
clear; clc;
coor=[0.0000      25.8097;   31.8877         74.7896;   69.2926      15.0920
     181.8877    137.4954;  212.2653         22.9330;  381.8877    174.9123
      395.6891    53.9261;  581.8877        188.7024;  586.5517      68.7931
      781.8877   186.0357;  775.7805         66.1912;  981.8877    172.3276
      970.8177    48.5476; 1181.8877        150.9526; 1167.3160      30.5043
     1381.8877   123.1472; 1362.2205          0.0000; 1581.8877      89.3289
     1781.8877    31.7244;  104.8987         53.7998;  104.8987      53.7998
      292.0632            94.4307;  292.0632    94.4307;  487.3151   120.2478;
      487.3151           120.2478;  681.4841   125.7724;  681.4841   125.7724
      875.7975           117.6957;  875.7975  117.6957; 1076.6141      99.8769
     1076.6141            99.8769; 1271.8576    75.6409; 1271.8576      75.6409
     1471.7888            44.5566; 1471.7888    44.5566];%sets up coordinates in mm


bar=[1      2; 1    3; 3    20; 20    4; 2    21; 21    5; 5    22; 22    6; 4    23
      23    7; 7   24; 24    8; 6    25; 25    9; 9    26; 26   10; 8    27; 27   11
      11   28; 28  12; 10   29; 29   13; 13   30; 30   14; 12   31; 31   15; 15   32
      32   16; 14  33; 33   17; 17   34; 34   18; 16   35; 35   19; 18   19; 10
12];   %sets up matrix of connectivity
area=[54 54 54 54 54 54 54 54 54 54 54 54 54 54 54 54 54 54 54 54 54 ...
    54 54 54 54 54 54 54 54 54 54 54 54 54 54  54];   %bar area for each bar in
mm2
inertia=[364.5 364.5 364.5 364.5 364.5 364.5 364.5 364.5 364.5 364.5 ...
        364.5 364.5 364.5 364.5 364.5 364.5 364.5 364.5 364.5 364.5 ...
        364.5 364.5 364.5 364.5 364.5 364.5 364.5 364.5 364.5 364.5 ...
        364.5 364.5 364.5 364.5 364.5  364.5]; %bar moment of inertia for
each bar in mm4
E=1000*[70 70 70 70 70 70 70 70 70 70 70 70 70 70 70 70 70 70 70 70 70 70 70...
        70 70 70 70 70 70 70 70 70 70 70 70 70 70]; %young's modulus in N/mm2
H=zeros(105,108);        %sets up 105x108 structural equilibrium matrix
F=zeros(108,108);        %sets up 108x108 structural flexibility matrix
for i=1:36,
  j1=bar(i,1); j2=bar(i,2);
  hor=coor(j2,1)-coor(j1,1); ver=coor(j2,2)-coor(j1,2);
  L=sqrt(hor^2+ver^2) ;
  l=hor/L; m=ver/L;            %l & m are the cos & sin of bar angle
  h=[-l m/L -m/L;-m -l/L l/L; 0 -1 0;l -m/L m/L;m l/L -l/L;0 0 1];
```

```matlab
  f=[(L/(E(i)*area(i))) 0 0; 0 (L/(3*E(i)*inertia(i)))
(L/(6*E(i)*inertia(i)));...
      0 (L/(6*E(i)*inertia(i))) (L/(3*E(i)*inertia(i)))];
  H((j1-1)*3+1:(j1-1)*3+3,i*3-2:i*3)= H((j1-1)*3+1:(j1-1)*3+3,i*3-
2:i*3)+h(1:3,:);
  H((j2-1)*3+1:(j2-1)*3+3,i*3-2:i*3)= H((j2-1)*3+1:(j2-1)*3+3,i*3-
2:i*3)+h(4:6,:);
  F((i-1)*3+1:(i-1)*3+3,(i-1)*3+1:(i-1)*3+3)=f;
end;
H=H([1:27 30:36 39:105],:);       %selecting rows relating to non-supports
H=[H(:,[1:8 10 12:14 16 18:20 22 24:26 28 30:32 34 36:38 40 42:44 46 48:50 52
...
    54:56 58 60:62 64 66:68 70 72:74 76 78:80 82 84:86 88 90:92 94 96:108])...
    H(:,9)+H(:,11)  H(:,15)+H(:,17) H(:,21)+H(:,23) H(:,27)+H(:,29) ...
    H(:,33)+H(:,35) H(:,39)+H(:,41) H(:,45)+H(:,47) H(:,51)+H(:,53)  ...
    H(:,57)+H(:,59) H(:,63)+H(:,65) H(:,69)+H(:,71) H(:,75)+H(:,77)  ...
    H(:,81)+H(:,83)  H(:,87)+H(:,89) H(:,93)+H(:,95)];    %mI.II=mI2+mII1
H=H(:,[1 4 7 9 11 13 15 17 19 21 23 25 27 29 31 33 35 37 39 41 43 45 47 49 51
...
    53 55 57 59 61 63 65 67 70 73 76 79:93]);%removing mI1=mII2=mIII1=mIV2=0
H=H([1 2 4 5 7 8 10 11 13 14 16 17 19 20 22 23 25 26 29 30 32 33 36 37 39 40
42 ...
  43 45 46 48 49 51 52 54 55 57 58 60 61 63 64 66 67 69 70 72 73 75 76 78 79
81 ...
  82 84 85 87 88 90 91 93 94 96 97 99 100],:); %M1=M2=M3=M4=M5=M6 no moment on
mid and end joints of pantographic
H=[H(1:34,:); H(63,:)+H(65,:); H(64,:)+H(66,:); H(35,:)+H(37,:);
H(36,:)+H(38,:);...
            H(39,:)+H(41,:); H(40,:)+H(42,:); H(43,:)+H(45,:);
H(44,:)+H(46,:);...
            H(47,:)+H(49,:); H(48,:)+H(50,:); H(51,:)+H(53,:);
H(52,:)+H(54,:);...
            H(55,:)+H(57,:); H(56,:)+H(58,:); H(59,:)+H(61,:);
H(60,:)+H(62,:)]; %Px5+Px6=0,Py5+Py6=0, no load on mid joint of pantographic
Amn=H(1:35,1:36); Amp=H(1:35,37:51); Apn=H(36:50,1:36); App=H(36:50,37:51);
A=Amn-Amp*pinv(App)*Apn;
F=[F(:,[1 4 7 10 13 16 19 22 25 28 31 34 37 40 43 46 49 52 55 58 61 64 67 70
73 76 ...
 79 82 85 88 91 94 97 100 103 106]) F(:,9)+F(:,11)  F(:,15)+F(:,17)
F(:,21)+F(:,23)...
    F(:,27)+F(:,29) F(:,33)+F(:,35) F(:,39)+F(:,41) F(:,45)+F(:,47)
F(:,51)+F(:,53)...
    F(:,57)+F(:,59) F(:,63)+F(:,65) F(:,69)+F(:,71) F(:,75)+F(:,77)
F(:,81)+F(:,83)...
    F(:,87)+F(:,89) F(:,93)+F(:,95)];        %mI.II=mI2+mII1
F=[F([1 4 7 10 13 16 19 22 25 28 31 34 37 40 43 46 49 52 55 58 61 64 67 70 73
76 79 ...
```

```
 82 85 88 91 94 97 100 103 106],:); F(9,:)+F(11,:) ; F(15,:)+F(17,:);
F(21,:)+F(23,:);...
  F(27,:)+F(29,:); F(33,:)+F(35,:); F(39,:)+F(41,:); F(45,:)+F(47,:);
F(51,:)+F(53,:);...
  F(57,:)+F(59,:); F(63,:)+F(65,:); F(69,:)+F(71,:); F(75,:)+F(77,:);
F(81,:)+F(83,:);...
  F(87,:)+F(89,:); F(93,:)+F(95,:)];                    %mI.II=mI2+mII1
Fnn=F(1:36,1:36);  Fnp=F(1:36,37:51);  Fpn=F(37:51,1:36);  Fpp=F(37:51,37:51);
F=Fnn-Fnp*pinv(App)*Apn-Apn'*pinv(App')*Fpn+Apn'*pinv(App')*Fpp*pinv(App)*Apn;
e0n=zeros(36,1);                         %vector of initial bar elongation

e0p=zeros(15,1);
e0t=[e0n; e0p];
r=Apn'*pinv(App');
e0=e0n-r*e0p;
   p1x=2*1.1430; p1=0*-1.1430; p2x=2*1.1430; p2=0*-1.1430; p3x=2*1.1430;
   p3=0*-1.1430; p4x=2*1.1430; p4=0*-1.1430; p5x=2*1.1430; p5=0*-1.1430;
   p6=0*-1.1430; p7=0*-1.1430; p8=0*-1.1430; p9=0*-1.1430; p10=0*-1.1430;

P=1*[p1x p1 p2x p2 0 0 p3x p3 0 0 p4x p4 0 0 p5x p5 0 0 0 0 p6 0 p7 0 0 0 p8
0 0 0 p9 0 p10 0]'; %Force vector, with rows for supports taken out already
S=null(A);                %state of self-stress
tH=pinv(A)*P;             %tH is a vector of t that is in eqm with applied P
alpha=inv(S'*F*S)*(-S'*(e0+F*tH)); %alpha is the "redundancies"
tn=tH+S*alpha;                      %t is the vector of bar tensions
tn([33:36],:);                      %Check strain gauge testing
tp=-pinv(App)*Apn*tn;
TT=[tn; tp];
e=e0+F*tn;                          %e is vector of bar elongations
en=(Fnn-Fnp*pinv(App)*Apn)*tn;
ep=(Fpn-Fpp*pinv(App)*Apn)*tn;
et=[en; ep];
dm=pinv(A')*e;           %d is vector of displacements
dp=pinv(App')*ep-pinv(App')*Amp'*dm;

%22222222222222222222222222222222222222222222
dy=dm([2;4;6;8;10;12;14;16;18;20;22;24;26;28;30;32;34],:); %dmy
Test=dm([2;4;8;12;16;22;24;28;32;34],:)';
%2222222222222222222222222222222222222222222
x=Fnn-Fnp*pinv(App)*Apn;
z=Fpn-Fpp*pinv(App)*Apn;
r=Apn'*pinv(App');
m=[pinv(A')-pinv(A')*F*S*inv(S'*F*S)*S'];
m1=m*F;
m2=m;
m3=m*-r;
k=S*inv(S'*F*S)*S';
```

```
k1=(-pinv(App')*z*k*F+pinv(App')*Amp'*pinv(A')*F*k*F-
pinv(App')*Amp'*pinv(A')*F+pinv(App')*z);
k2=(-pinv(App')*z*k  +pinv(App')*Amp'*pinv(A')*F*k  -
pinv(App')*Amp'*pinv(A'));
k3=( pinv(App')*z*k*r-
pinv(App')*Amp'*pinv(A')*F*k*r+pinv(App')*Amp'*pinv(A')*r+pinv(App'));

MK1=[m1; k1];
MK2=[m2; k2];
MK3=[m3; k3];
dpc=MK1*tH;
Yc=[MK2 MK3];
D=MK1*tH+Yc*e0t;

J=-pinv(App)*Apn;
tpc=[tH-k*F*tH; J*tH-J*k*F*tH];
Znc=[-k   -J*k];
Zpc=[k*r   J*k*r];
Zc=[Znc Zpc];
T=tpc+Zc*e0t;
%2222222222222222222222222222222222222222
%Joint Displacement
% Selecting bars (4,5,8,9,12,13,16,17,20,24,25,28,29,32,33,34&36) to control
% y of joints (1,2,4,6,8,12,14,16,18&19)
e0n1=zeros(36,1);
e0p1=zeros(15,1);
e0t1=[e0n1; e0p1];
dpn1=dm([1;3;7;11;15],:)
ddn1=[1; 0; 0; 0; 0];   %target displacement
DDn1=ddn1-dpn1 ;        %difference between target and practical
Y1=Yc([1 3 7 11 15],[4 5 12 13 17 20]);
e0t1([4 5 12 13 17 20],:)=pinv(Y1)*DDn1;
e0t1([4 5 12 13 17 20],:)

ee=15*ones(6,1)+e0t1([4 5 12 13 17 20],:);
Bn=[4; 5; 12; 13; 17; 20];
ee=[ee   Bn];
Te0t1=sum(abs(e0t1));

DDnp1=Yc*e0t1+D;
Check1=DDnp1([1 3 7 11 15],1)
Check2=[ddn1 Check1];
TH=DDnp1([1 3 7 11 15],1);
PR=D([1 3 7 11 15],1)+[-2.2612; -3.2207; -2.5815; -1.4971; -0.5204];
DF=TH-PR;
Both=[TH PR DF];
```

A.11 MATLAB Program for Table 6.5

```
clear; clc;
coor=[0.0000       25.8097;   31.8877        74.7896;   69.2926      15.0920
     181.8877      137.4954; 212.2653        22.9330; 381.8877    174.9123
     395.6891       53.9261; 581.8877       188.7024; 586.5517      68.7931
     781.8877      186.0357; 775.7805        66.1912; 981.8877    172.3276
     970.8177       48.5476; 1181.8877      150.9526; 1167.3160     30.5043
    1381.8877      123.1472; 1362.2205        0.0000; 1581.8877     89.3289
    1781.8877       31.7244; 104.8987        53.7998;  104.8987     53.7998
     292.0632           94.4307; 292.0632     94.4307;   487.3151  120.2478;
     487.3151          120.2478; 681.4841     125.7724;  681.4841  125.7724
     875.7975          117.6957; 875.7975     117.6957; 1076.6141     99.8769
    1076.6141           99.8769; 1271.8576     75.6409; 1271.8576    75.6409
    1471.7888           44.5566; 1471.7888     44.5566];%sets up coordinates in mm


bar=[1     2; 1    3; 3    20; 20    4; 2    21; 21    5; 5    22; 22    6; 4    23
      23    7; 7   24; 24    8; 6   25; 25    9; 9    26; 26   10; 8   27; 27   11
      11   28; 28  12; 10   29; 29   13; 13   30; 30   14; 12   31; 31   15; 15   32
      32   16; 14  33; 33   17; 17   34; 34   18; 16   35; 35   19; 18   19; 10 12
       2    4; 4    6; 6     8; 8   10; 12 14; 14 16; 16 18; 3     5; 5     7
       7    9; 9  11; 11 13; 13 15; 15 17; 17 19];%sets up matrix of connectivity
area=[54 54 54 54 54 54 54 54 54 54 54 54 54 54 54 54 54 54 54 54 54 54 54 54
...
     54 54 54 54 54 54 54 54 54 54 54 54 4 4 4 4 4 4 4 4 4 4 4 4 4 4]; %bar
area for each bar in mm2
inertia=[364.5 364.5 364.5 364.5 364.5 364.5 364.5 364.5 364.5 364.5 364.5 ...
        364.5 364.5 364.5 364.5 364.5 364.5 364.5 364.5 364.5 364.5 364.5 ...
        364.5 364.5 364.5 364.5 364.5 364.5 364.5 364.5 364.5 364.5 364.5 ...
        364.5 364.5  364.5 0.84375 0.84375 0.84375 0.84375 0.84375 0.84375...
         0.84375 0.84375 0.84375 0.84375 0.84375 0.84375 0.84375 0.84375...
          0.84375];     %bar moment of inertia for each bar in mm4
E=1000*[70 70 70 70 70 70 70 70 70 70 70 70 70 70 70 70 70 70 70 70 70 70 ...
       70 70 70 70 70 70 70 70 70 70 70 70 70 70 0.0025 0.0025 0.0025...
       0.0025 0.0025 0.0025 0.0025 0.0025 0.0025...
       0.0025 0.0025 0.0025 0.0025 0.0025 0.0025]; %young's modulus in N/mm2
H=zeros(105,153);       %sets up 105x108 structural equilibrium matrix
F=zeros(153,153);       %sets up 108x108 structural flexibility matrix
for i=1:51,
  j1=bar(i,1); j2=bar(i,2);
  hor=coor(j2,1)-coor(j1,1); ver=coor(j2,2)-coor(j1,2);
  L=sqrt(hor^2+ver^2) ;
  ll(i)=L;
  l=hor/L; m=ver/L;            %l & m are the cos & sin of bar angle
  h=[-l m/L -m/L;-m -l/L l/L; 0 -1 0;l -m/L m/L;m l/L -l/L;0 0 1];
```

```matlab
   f=[(L/(E(i)*area(i))) 0 0; 0 (L/(3*E(i)*inertia(i)))
(L/(6*E(i)*inertia(i)));...
      0 (L/(6*E(i)*inertia(i))) (L/(3*E(i)*inertia(i)))];
   H((j1-1)*3+1:(j1-1)*3+3,i*3-2:i*3)= H((j1-1)*3+1:(j1-1)*3+3,i*3-
2:i*3)+h(1:3,:);
   H((j2-1)*3+1:(j2-1)*3+3,i*3-2:i*3)= H((j2-1)*3+1:(j2-1)*3+3,i*3-
2:i*3)+h(4:6,:);
   F((i-1)*3+1:(i-1)*3+3,(i-1)*3+1:(i-1)*3+3)=f;
end;
H=H([1:27 30:36 39:105],:);     %selecting rows relating to non-supports
H=[H(:,[1:8 10 12:14 16 18:20 22 24:26 28 30:32 34 36:38 40 42:44 46 48:50 52
...
    54:56 58 60:62 64 66:68 70 72:74 76 78:80 82 84:86 88 90:92 94 96:153])...
    H(:,9)+H(:,11)  H(:,15)+H(:,17) H(:,21)+H(:,23) H(:,27)+H(:,29) ...
    H(:,33)+H(:,35) H(:,39)+H(:,41) H(:,45)+H(:,47) H(:,51)+H(:,53)   ...
    H(:,57)+H(:,59) H(:,63)+H(:,65) H(:,69)+H(:,71) H(:,75)+H(:,77)   ...
    H(:,81)+H(:,83)  H(:,87)+H(:,89) H(:,93)+H(:,95)];   %mI.II=mI2+mII1
H=H(:,[1 4 7 9 11 13 15 17 19 21 23 25 27 29 31 33 35 37 39 41 43 45 47 49 51
...
    53 55 57 59 61 63 65 67 70 73 76 79 82 85 88 91 94 97 100 103 106 ...
    109 112 115 118 121 124:138]);     %removing mI1=mII2=mIII1=mIV2=0
H=H([1 2 4 5 7 8 10 11 13 14 16 17 19 20 22 23 25 26 29 30 32 33 36 37 39 40
42 ...
  43 45 46 48 49 51 52 54 55 57 58 60 61 63 64 66 67 69 70 72 73 75 76 78 79
81 ...
  82 84 85 87 88 90 91 93 94 96 97 99 100],:); %M1=M2=M3=M4=M5=M6 no moment on
mid and end joints of pantographic
H=[H(1:34,:); H(63,:)+H(65,:); H(64,:)+H(66,:); H(35,:)+H(37,:);
H(36,:)+H(38,:);...
            H(39,:)+H(41,:); H(40,:)+H(42,:); H(43,:)+H(45,:);
H(44,:)+H(46,:);...
            H(47,:)+H(49,:); H(48,:)+H(50,:); H(51,:)+H(53,:);
H(52,:)+H(54,:);...
            H(55,:)+H(57,:); H(56,:)+H(58,:); H(59,:)+H(61,:);
H(60,:)+H(62,:)]; %Px5+Px6=0,Py5+Py6=0, no load on mid joint of pantographic
Amn=H(1:35,1:51); Amp=H(1:35,52:66); Apn=H(36:50,1:51); App=H(36:50,52:66);
A=Amn-Amp*pinv(App)*Apn;
F=[F(:,[1 4 7 10 13 16 19 22 25 28 31 34 37 40 43 46 49 52 55 58 61 64 67 70
73 76 ...
 79 82 85 88 91 94 97 100 103 106 109 112 115 118 121 124 127 130 133 136 139
142 ...
 145 148 151]) F(:,9)+F(:,11)  F(:,15)+F(:,17) F(:,21)+F(:,23) F(:,27)+F(:,29)
...
 F(:,33)+F(:,35) F(:,39)+F(:,41) F(:,45)+F(:,47) F(:,51)+F(:,53)
F(:,57)+F(:,59) ...
 F(:,63)+F(:,65) F(:,69)+F(:,71) F(:,75)+F(:,77) F(:,81)+F(:,83)
F(:,87)+F(:,89) ...
 F(:,93)+F(:,95)];                                 %mI.II=mI2+mII1
```

```
F=[F([1 4 7 10 13 16 19 22 25 28 31 34 37 40 43 46 49 52 55 58 61 64 67 70 73
76 79 ...
 82 85 88 91 94 97 100 103 106 109 112 115 118 121 124 127 130 133 136 139 142
...
 145 148 151],:); F(9,:)+F(11,:) ; F(15,:)+F(17,:); F(21,:)+F(23,:);
F(27,:)+F(29,:);...
 F(33,:)+F(35,:); F(39,:)+F(41,:); F(45,:)+F(47,:); F(51,:)+F(53,:);
F(57,:)+F(59,:);...
 F(63,:)+F(65,:); F(69,:)+F(71,:); F(75,:)+F(77,:); F(81,:)+F(83,:);
F(87,:)+F(89,:);...
 F(93,:)+F(95,:)];                                    %mI.II=mI2+mII1
Fnn=F(1:51,1:51);  Fnp=F(1:51,52:66);  Fpn=F(52:66,1:51);  Fpp=F(52:66,52:66);
F=Fnn-Fnp*pinv(App)*Apn-Apn'*pinv(App')*Fpn+Apn'*pinv(App')*Fpp*pinv(App)*Apn;

e0n=zeros(51,1);                          %vector of initial bar elongation

e0n([37:51],1)=-
0.205*100*[1.625792648330038;2.034699594672639;2.004748534305737;...
2.000177774321323;2.011389833547938;2.019236000797331; 2.028390431225951;...
1.431875491315149;1.860238228132354; 1.914407474070241;1.892466872445856;...
1.958336181680765; 1.973249669397667;1.972771564037255;4.208645819158463];
Elastic=0.795*[162.5793; 203.4700; 200.4749; 200.0178; 201.1390; 201.9236;...
    202.8390; 143.1875; 186.0238; 191.4407; 189.2467; 195.8336; 197.3250;...
    197.2772; 420.8646];
e0p=zeros(15,1);
e0t=[e0n; e0p];
r=Apn'*pinv(App');
e0=e0n-r*e0p;

p1=2*-1.1430; p2=2*-1.1430; p3=2*-1.1430; p4=2*-1.1430; p5=2*-1.1430;
p6=0*-1.1430; p7=2*-1.1430; p8=2*-1.1430; p9=2*-1.1430; p10=2*-1.1430;

P=1*[0 p1 0 p2 0 0 0 p3 0 0 0 p4 0 0 0 p5 0 0 0 0 0 p6 0 p7 0 0 0 p8 0 0 0 p9
0 p10 0]'; %Force vector, with rows for supports taken out already
S=null(A);           %state of self-stress
M=null(A');
tH=pinv(A)*P;        %tH is a vector of t that is in eqm with applied P
alpha=inv(S'*F*S)*(-S'*(e0+F*tH));   %alpha is the "redundancies"
tn=tH+S*alpha;                       %t is the vector of bar tensions
tn([37:51],:) ;                      %Check strain gauge testing
tp=-pinv(App)*Apn*tn;
TT=[tn; tp];
e=e0+F*tn;                           %e is vector of bar elongations
en=(Fnn-Fnp*pinv(App)*Apn)*tn;
ep=(Fpn-Fpp*pinv(App)*Apn)*tn;
et=[en; ep];
dm=pinv(A')*e;           %d is vector of displacements
dp=pinv(App')*ep-pinv(App')*Amp'*dm;
```

```
%222222222222222222222222222222222222222222
dy=dm([2;4;6;8;10;12;14;16;18;20;22;24;26;28;30;32;34],:); %dmy
Test=dm([2;4;8;12;16;22;24;28;32;34],:)';
%222222222222222222222222222222222222222222
x=Fnn-Fnp*pinv(App)*Apn;
z=Fpn-Fpp*pinv(App)*Apn;
r=Apn'*pinv(App');
m=[pinv(A')-pinv(A')*F*S*inv(S'*F*S)*S'];
m1=m*F;
m2=m;
m3=m*-r;
k=S*inv(S'*F*S)*S';
k1=(-pinv(App')*z*k*F+pinv(App')*Amp'*pinv(A')*F*k*F-
pinv(App')*Amp'*pinv(A')*F+pinv(App')*z);
k2=(-pinv(App')*z*k  +pinv(App')*Amp'*pinv(A')*F*k  -
pinv(App')*Amp'*pinv(A'));
k3=( pinv(App')*z*k*r-
pinv(App')*Amp'*pinv(A')*F*k*r+pinv(App')*Amp'*pinv(A')*r+pinv(App'));

MK1=[m1; k1];
MK2=[m2; k2];
MK3=[m3; k3];
dpc=MK1*tH;
Yc=[MK2 MK3];
D=MK1*tH+Yc*e0t;

J=-pinv(App)*Apn;
tpc=[tH-k*F*tH; J*tH-J*k*F*tH];
Znc=[-k;  -J*k];
Zpc=[k*r;  J*k*r];
Zc=[Znc Zpc];
T=tpc+Zc*e0t;
%222222222222222222222222222222222222222222
%Joint Displacement
% Selecting bars (4,5,8,9,12,13,16,17,20,24,25,28,29,32,33,34&36) to control
% y of joints (1,2,4,6,8,12,14,16,18&19)
e0n1=zeros(51,1);
e0p1=zeros(15,1);
e0t1=[e0n1; e0p1];
dpn1=dm([2;4;8;12;16;22;24;28;32;34],:)
ddn1=[-1; -1; -1; -1; -1; 0; 0; -1; -1; -1];  %target displacement
DDn1=ddn1-dpn1;       %difference between target and practical
Y1=Yc([2 4 8 12 16 22 24 28 32 34],[4 5 8 12 16 20 25 29 33 34]);
e0t1([4 5 8 12 16 20 25 29 33 34],:)=pinv(Y1)*DDn1;
e0t1([4 5 8 12 16 20 25 29 33 34],:)
ee=15*ones(10,1)+e0t1([4 5 8 12 16 20 25 29 33 34],:);
Bn=[4; 5; 8; 12; 16; 20; 25; 29; 33; 34];
```

```
ee=[ee   Bn];
Te0t1=sum(abs(e0t1));

DDnp1=Yc*e0t1+D;
Check1=DDnp1([2 4 8 12 16 22 24 28 32 34],1)
Check2=[ddn1 Check1];

TH=DDnp1([2 4 8 12 16 22 24 28 32 34],1);
PR=D([2 4 8 12 16 22 24 28 32 34],1)+[ 11.2335;11.1530;8.7709;4.6105;1.3939;-
0.4157;0.7418;1.0121 ;3.3320;6.1480];
DF=TH-PR;
Both=[TH PR DF];
```

A.12 MATLAB Program for Table 6.6

```
clear; clc;
coor=[0.0000      25.8097;   31.8877        74.7896;    69.2926     15.0920
    181.8877    137.4954; 212.2653        22.9330; 381.8877    174.9123
    395.6891     53.9261; 581.8877       188.7024; 586.5517      68.7931
    781.8877    186.0357; 775.7805        66.1912; 981.8877    172.3276
    970.8177     48.5476; 1181.8877      150.9526; 1167.3160     30.5043
    1381.8877   123.1472; 1362.2205        0.0000; 1581.8877     89.3289
    1781.8877    31.7244; 104.8987        53.7998; 104.8987      53.7998
    292.0632             94.4307; 292.0632       94.4307; 487.3151    120.2478;
    487.3151            120.2478; 681.4841    125.7724; 681.4841    125.7724
    875.7975            117.6957; 875.7975    117.6957; 1076.6141      99.8769
    1076.6141            99.8769; 1271.8576    75.6409; 1271.8576      75.6409
    1471.7888            44.5566; 1471.7888     44.5566];%sets up coordinates in mm

bar=[1      2; 1    3; 3    20; 20    4; 2    21; 21    5; 5    22; 22    6; 4    23
      23    7; 7    24; 24    8; 6    25; 25    9; 9    26; 26    10; 8    27; 27   11
      11    28; 28  12; 10   29; 29   13; 13   30; 30   14; 12   31; 31   15; 15   32
      32    16; 14  33; 33   17; 17   34; 34   18; 16   35; 35   19; 18   19; 10  12
    2    4; 4    6; 6    8; 8    10; 12  14; 14  16; 16  18; 3      5; 5      7
    7    9; 9  11; 11  13; 13  15; 15  17; 17  19]; %sets up matrix of connectivity
area=[54 54 54 54 54 54 54 54 54 54 54 54 54 54 54 54 54 54 54 54 54 54 54 ...
    54 54 54 54 54 54 54 54 54 54 54 54 4 4 4 4 4 4 4 4 4 4 4 4 4 4 4 4];
%bar area for each bar in mm2
inertia=[364.5 364.5 364.5 364.5 364.5 364.5 364.5 364.5 364.5 364.5 364.5 ...
        364.5 364.5 364.5 364.5 364.5 364.5 364.5 364.5 364.5 364.5 364.5 ...
        364.5 364.5 364.5 364.5 364.5 364.5 364.5 364.5 364.5 364.5 364.5 ...
        364.5 364.5 364.5 0.84375 0.84375 0.84375 0.84375 0.84375 0.84375...
         0.84375 0.84375 0.84375 0.84375 0.84375 0.84375 0.84375 0.84375...
           0.84375];         %bar moment of inertia for each bar in mm4
E=1000*[70 70 70 70 70 70 70 70 70 70 70 70 70 70 70 70 70 70 70 70 70 70 ...
```

```matlab
        70 70 70 70 70 70 70 70 70 70 70 70 70 70 0.0025 0.0025 0.0025...
        0.0025 0.0025 0.0025 0.0025 0.0025 0.0025...
        0.0025 0.0025 0.0025 0.0025 0.0025 0.0025]; %young's modulus in N/mm2
H=zeros(105,153);         %sets up 105x108 structural equilibrium matrix
F=zeros(153,153);         %sets up 108x108 structural flexibility matrix
for i=1:51,
  j1=bar(i,1); j2=bar(i,2);
  hor=coor(j2,1)-coor(j1,1); ver=coor(j2,2)-coor(j1,2);
  L=sqrt(hor^2+ver^2) ;
  ll(i)=L;
  l=hor/L; m=ver/L;        %l & m are the cos & sin of bar angle
  h=[-l m/L -m/L;-m -l/L l/L; 0 -1 0;l -m/L m/L;m l/L -l/L;0 0 1];
  f=[(L/(E(i)*area(i))) 0 0; 0 (L/(3*E(i)*inertia(i)))
(L/(6*E(i)*inertia(i)));...
      0 (L/(6*E(i)*inertia(i))) (L/(3*E(i)*inertia(i)))];
  H((j1-1)*3+1:(j1-1)*3+3,i*3-2:i*3)= H((j1-1)*3+1:(j1-1)*3+3,i*3-
2:i*3)+h(1:3,:);
  H((j2-1)*3+1:(j2-1)*3+3,i*3-2:i*3)= H((j2-1)*3+1:(j2-1)*3+3,i*3-
2:i*3)+h(4:6,:);
  F((i-1)*3+1:(i-1)*3+3,(i-1)*3+1:(i-1)*3+3)=f;
end;
H=H([1:27 30:36 39:105],:);    %selecting rows relating to non-supports
H=[H(:,[1:8 10 12:14 16 18:20 22 24:26 28 30:32 34 36:38 40 42:44 46 48:50 52
...
    54:56 58 60:62 64 66:68 70 72:74 76 78:80 82 84:86 88 90:92 94 96:153])...
    H(:,9)+H(:,11)  H(:,15)+H(:,17) H(:,21)+H(:,23) H(:,27)+H(:,29) ...
    H(:,33)+H(:,35) H(:,39)+H(:,41) H(:,45)+H(:,47) H(:,51)+H(:,53)  ...
    H(:,57)+H(:,59) H(:,63)+H(:,65) H(:,69)+H(:,71) H(:,75)+H(:,77)  ...
    H(:,81)+H(:,83)  H(:,87)+H(:,89) H(:,93)+H(:,95)];   %mI.II=mI2+mII1
H=H(:,[1 4 7 9 11 13 15 17 19 21 23 25 27 29 31 33 35 37 39 41 43 45 47 49 51
...
    53 55 57 59 61 63 65 67 70 73 76 79 82 85 88 91 94 97 100 103 106 ...
    109 112 115 118 121 124:138]);   %removing mI1=mII2=mIII1=mIV2=0
H=H([1 2 4 5 7 8 10 11 13 14 16 17 19 20 22 23 25 26 29 30 32 33 36 37 39 40
42 ...
  43 45 46 48 49 51 52 54 55 57 58 60 61 63 64 66 67 69 70 72 73 75 76 78 79
81 ...
  82 84 85 87 88 90 91 93 94 96 97 99 100],:); %M1=M2=M3=M4=M5=M6 no moment on
mid and end joints of pantographic
H=[H(1:34,:); H(63,:)+H(65,:); H(64,:)+H(66,:); H(35,:)+H(37,:);
H(36,:)+H(38,:);...
          H(39,:)+H(41,:); H(40,:)+H(42,:); H(43,:)+H(45,:);
H(44,:)+H(46,:);...
          H(47,:)+H(49,:); H(48,:)+H(50,:); H(51,:)+H(53,:);
H(52,:)+H(54,:);...
          H(55,:)+H(57,:); H(56,:)+H(58,:); H(59,:)+H(61,:);
H(60,:)+H(62,:)]; %Px5+Px6=0,Py5+Py6=0, no load on mid joint of pantographic
Amn=H(1:35,1:51); Amp=H(1:35,52:66); Apn=H(36:50,1:51); App=H(36:50,52:66);
```

```
A=Amn-Amp*pinv(App)*Apn;
F=[F(:,[1 4 7 10 13 16 19 22 25 28 31 34 37 40 43 46 49 52 55 58 61 64 67 70
73 76 ...
 79 82 85 88 91 94 97 100 103 106 109 112 115 118 121 124 127 130 133 136 139
142 ...
 145 148 151]) F(:,9)+F(:,11)  F(:,15)+F(:,17) F(:,21)+F(:,23) F(:,27)+F(:,29)
...
 F(:,33)+F(:,35) F(:,39)+F(:,41) F(:,45)+F(:,47) F(:,51)+F(:,53)
F(:,57)+F(:,59) ...
 F(:,63)+F(:,65) F(:,69)+F(:,71) F(:,75)+F(:,77) F(:,81)+F(:,83)
F(:,87)+F(:,89) ...
 F(:,93)+F(:,95)];              %mI.II=mI2+mII1
F=[F([1 4 7 10 13 16 19 22 25 28 31 34 37 40 43 46 49 52 55 58 61 64 67 70 ...
 73 76 79 82 85 88 91 94 97 100 103 106 109 112 115 118 121 124 127 130 133
136 139 142 145 148 151],:); F(9,:)+F(11,:) ; F(15,:)+F(17,:);
F(21,:)+F(23,:); F(27,:)+F(29,:);...
 F(33,:)+F(35,:); F(39,:)+F(41,:); F(45,:)+F(47,:); F(51,:)+F(53,:);
F(57,:)+F(59,:);...
 F(63,:)+F(65,:); F(69,:)+F(71,:); F(75,:)+F(77,:); F(81,:)+F(83,:);
F(87,:)+F(89,:);...
 F(93,:)+F(95,:)];                         %mI.II=mI2+mII1
Fnn=F(1:51,1:51);  Fnp=F(1:51,52:66);  Fpn=F(52:66,1:51);  Fpp=F(52:66,52:66);
F=Fnn-Fnp*pinv(App)*Apn-Apn'*pinv(App')*Fpn+Apn'*pinv(App')*Fpp*pinv(App)*Apn;
e0n=zeros(51,1);               %vector of initial bar elongation
e0n([37:51],1)=-
0.205*100*[1.625792648330038;2.034699594672639;2.004748534305737;...
2.000177774321323;2.011389833547938;2.019236000797331;...
2.028390431225951;1.431875491315149;1.860238228132354;...
1.914407474070241;1.892466872445856;1.958336181680765;...
1.973249669397667;1.972771564037255;4.208645819158463];
Elastic=0.795*[162.5793; 203.4700; 200.4749; 200.0178; 201.1390; 201.9236;...
    202.8390; 143.1875; 186.0238; 191.4407; 189.2467; 195.8336; 197.3250;...
    197.2772; 420.8646];
e0p=zeros(15,1); e0t=[e0n; e0p]; r=Apn'*pinv(App'); e0=e0n-r*e0p;
p1=2*-1.1430; p2=2*-1.1430; p3=2*-1.1430; p4=2*-1.1430; p5=2*-1.1430;
p6=0*-1.1430; p7=2*-1.1430; p8=2*-1.1430; p9=2*-1.1430; p10=2*-1.1430;

P=1*[0 p1 0 p2 0 0 0 p3 0 0 0 p4 0 0 0 p5 0 0 0 0 0 p6 0 p7 0 0 0 p8 0 0 0 p9
0 p10 0]'; %Force vector, with rows for supports taken out already
S=null(A);      %state of self-stress
M=null(A');
tH=pinv(A)*P;   %tH is a vector of t that is in eqm with applied P
alpha=inv(S'*F*S)*(-S'*(e0+F*tH));   %alpha is the "redundancies"
tn=tH+S*alpha;                       %t is the vector of bar tensions
tn([37:51],:) ;                      %Check strain gauge testing
tp=-pinv(App)*Apn*tn;
TT=[tn; tp];
e=e0+F*tn;                           %e is vector of bar elongations
```

```
en=(Fnn-Fnp*pinv(App)*Apn)*tn;
ep=(Fpn-Fpp*pinv(App)*Apn)*tn;
et=[en; ep];
dm=pinv(A')*e;              %d is vector of displacements
dp=pinv(App')*ep-pinv(App')*Amp'*dm;


%222222222222222222222222222222222222222222
dy=dm([2;4;6;8;10;12;14;16;18;20;22;24;26;28;30;32;34],:); %dmy
Test=dm([2;4;8;12;16;22;24;28;32;34],:)';
%222222222222222222222222222222222222222222
x=Fnn-Fnp*pinv(App)*Apn;
z=Fpn-Fpp*pinv(App)*Apn;
r=Apn'*pinv(App');
m=[pinv(A')-pinv(A')*F*S*inv(S'*F*S)*S'];
m1=m*F; m2=m; m3=m*-r;
k=S*inv(S'*F*S)*S';
k1=(-pinv(App')*z*k*F+pinv(App')*Amp'*pinv(A')*F*k*F-
pinv(App')*Amp'*pinv(A')*F+pinv(App')*z);
k2=(-pinv(App')*z*k  +pinv(App')*Amp'*pinv(A')*F*k  -
pinv(App')*Amp'*pinv(A'));
k3=( pinv(App')*z*k*r-
pinv(App')*Amp'*pinv(A')*F*k*r+pinv(App')*Amp'*pinv(A')*r+pinv(App'));
MK1=[m1; k1];
MK2=[m2; k2];
MK3=[m3; k3];
dpc=MK1*tH;
Yc=[MK2 MK3];
D=MK1*tH+Yc*e0t;
J=-pinv(App)*Apn;
tpc=[tH-k*F*tH; J*tH-J*k*F*tH];
Znc=[-k;  -J*k];
Zpc=[k*r;  J*k*r];
Zc=[Znc Zpc];
T=tpc+Zc*e0t;
%222222222222222222222222222222222222222222
%Joint Displacement
% Selecting bars (4,5,8,9,12,13,16,17,20,24,25,28,29,32,33,34&36) to control
% y of joints (1,2,4,6,8,12,14,16,18&19)
e0n1=zeros(51,1);  e0p1=zeros(15,1);
e0t1=[e0n1; e0p1];
dpn1=dm([2;4;8;12;16;22;24;28;32;34],:)
ddn1=[0; 0; 0; 0; 0; 0; 0; 0; 0; 0];  %target displacement
DDn1=ddn1-dpn1;                %difference between target and practical
Y1=Yc([2 4 8 12 16 22 24 28 32 34],[4 5 8 12 16 20 25 29 33 34]);
e0t1([4 5 8 12 16 20 25 29 33 34],:)=pinv(Y1)*DDn1;
e0t1([4 5 8 12 16 20 25 29 33 34],:)
ee=15*ones(10,1)+e0t1([4 5 8 12 16 20 25 29 33 34],:);
Bn=[4; 5; 8; 12; 16; 20; 25; 29; 33; 34];
```

```
ee=[ee   Bn];
Te0t1=sum(abs(e0t1));
DDnp1=Yc*e0t1+D;
Check1=DDnp1([2 4 8 12 16 22 24 28 32 34],1)
Check2=[ddn1 Check1];
TH=DDnp1([2 4 8 12 16 22 24 28 32 34],1);
PR=dpn1+[13.3790;13.1844;10.20781;5.9651;2.2739;-0.41063;0.5540;2.4496
;3.9245;6.4002];
DF=TH-PR;
Both=[TH PR DF];
%22222222222222222222222222222222222222222
e0n1=zeros(51,1); e0p1=zeros(15,1);
e0t1=[e0n1; e0p1];
dm([2;4;8;12;16;22;24;28;32;34],:)=PR;
D([2;4;8;12;16;22;24;28;32;34],:)=dm([2;4;8;12;16;22;24;28;32;34],:);
dpn1=dm([2;4;8;12;16;22;24;28;32;34],:)
ddn1=[0; 0; 0; 0; 0; 0; 0; 0; 0; 0];  %target displacement
DDn1=ddn1-dpn1;                 %difference between target and practical
Y1=Yc([2 4 8 12 16 22 24 28 32 34],[4 5 8 12 16 20 25 29 33 34]);
e0t1([4 5 8 12 16 20 25 29 33 34],:)=pinv(Y1)*DDn1;
e0t1([4 5 8 12 16 20 25 29 33 34],:)
ee=[14.7974;14.7853;14.6036;14.2431;13.9911;14.6366;14.6221;14.4582;14.5980;15
.0969]+e0t1([4 5 8 12 16 20 25 29 33 34],:);
Bn=[4; 5; 8; 12; 16; 20; 25; 29; 33; 34];
ee=[ee   Bn];
Te0t1=sum(abs(e0t1));
DDnp1=Yc*e0t1+D;
Check1=DDnp1([2 4 8 12 16 22 24 28 32 34],1)
Check2=[ddn1 Check1];
TH=DDnp1([2 4 8 12 16 22 24 28 32 34],1);
PR=dpn1+[ 0.3283;-0.0971;-0.5011;-0.0205;0.0102;-0.3932;-0.4756;-0.9599;-
0.5551;-0.9763];
DF=TH-PR;
Both=[TH PR DF];
```

A.13 MATLAB Program for Non-Linear Calculation Method (Coordinate Update Method) of Morphing

```
Clear; clc; dm=zeros(35,1); dp=zeros(15,1); y=0;
for w=1:300;
 u=0.1; y=y+u;
coor=[0.0000+dm(1)        25.8097+dm(2); 31.8877+dm(3)       74.7896+dm(4)
     69.2926+dm(5)        15.0920+dm(6); 181.8877+dm(7)    137.4954+dm(8)
    212.2653+dm(9)        22.9330+dm(10); 381.8877+dm(11)  174.9123+dm(12)
    395.6891+dm(13)       53.9261+dm(14); 581.8877+dm(15)  188.7024+dm(16)
```

```
     586.5517+dm(17)            68.7931+dm(18); 781.8877                186.0357
     775.7805+dm(19)            66.1912+dm(20); 981.8877+dm(21)   172.3276+dm(22)
     970.8177             48.5476; 1181.8877+dm(23)     150.9526+dm(24)
   1167.3160+dm(25)            30.5043+dm(26); 1381.8877+dm(27)
123.1472+dm(28) ; 1362.2205+dm(29)            0.0000+dm(30)
   1581.8877+dm(31)            89.3289+dm(32) ; 1781.8877+dm(33)
31.7244+dm(34)
     104.8987+dp(2)             53.7998+dp(3) ; 104.8987+dp(2)     53.7998+dp(3)
     292.0632+dp(4)             94.4307+dp(5) ; 292.0632+dp(4)     94.4307+dp(5)
     487.3151+dp(6)            120.2478+dp(7) ; 487.3151+dp(6)    120.2478+dp(7)
     681.4841+dp(8)            125.7724+dp(9) ; 681.4841+dp(8)    125.7724+dp(9)
     875.7975+dp(10)           117.6957+dp(11); 875.7975+dp(10)   117.6957+dp(11)
    1076.6141+dp(12)            99.8769+dp(13); 1076.6141+dp(12)    99.8769+dp(13)
    1271.8576+dp(14)           75.6409+dp(15); 1271.8576+dp(14)    75.6409+dp(15)
    1471.7888+dm(35)            44.5566+dp(1); 1471.7888+dm(35)    44.5566+dp(1)];
%sets up coordinates in mm
bar=[1   2; 1      3; 3     20; 20  4; 2     21; 21   5; 5    22; 22  6; 4      23
23        7; 7     24; 24  8; 6     25; 25  9; 9     26; 26  10; 8    27; 27  11
11     28; 28     12; 10  29; 29  13; 13    30; 30  14; 12  31; 31  15; 15   32
32     16; 14 33; 33     17; 17 34; 34 18; 16 35; 35 19; 18 19; 10 12];
area=[54 54 54 54 54 54 54 54 54 54 54 54 54 54 54 54 54 54 54 54 54 54 54 ...
     54 54 54 54 54 54 54 54 54 54 54 54 54];
inertia=[364.5 364.5 364.5 364.5 364.5 364.5 364.5 364.5 364.5 364.5 364.5 ...
        364.5 364.5 364.5 364.5 364.5 364.5 364.5 364.5 364.5 364.5 364.5 ...
        364.5 364.5 364.5 364.5 364.5 364.5 364.5 364.5 364.5 364.5 364.5 ...
        364.5 364.5 364.5];
E=1000*[70 70 70 70 70 70 70 70 70 70 70 70 70 70 70 70 70 70 70 70 70 70 ...
        70 70 70 70 70 70 70 70 70 70 70 70 70 70];
H=zeros(105,108);  F=zeros(108,108);
for i=1:36,
  j1=bar(i,1); j2=bar(i,2);
  hor=coor(j2,1)-coor(j1,1); ver=coor(j2,2)-coor(j1,2);
  L=sqrt(hor^2+ver^2) ;
  l=hor/L; m=ver/L;
  h=[-l m/L -m/L;-m -l/L l/L; 0 -1 0;l -m/L m/L;m l/L -l/L;0 0 1];
  f=[(L/(E(i)*area(i))) 0 0; 0 (L/(3*E(i)*inertia(i)))
(L/(6*E(i)*inertia(i)));...
      0 (L/(6*E(i)*inertia(i))) (L/(3*E(i)*inertia(i)))];
  H((j1-1)*3+1:(j1-1)*3+3,i*3-2:i*3)= H((j1-1)*3+1:(j1-1)*3+3,i*3-
2:i*3)+h(1:3,:);
  H((j2-1)*3+1:(j2-1)*3+3,i*3-2:i*3)= H((j2-1)*3+1:(j2-1)*3+3,i*3-
2:i*3)+h(4:6,:);
  F((i-1)*3+1:(i-1)*3+3,(i-1)*3+1:(i-1)*3+3)=f;
end;
H=H([1:27 30:36 39:105],:);    %selecting rows relating to non-supports
H=[H(:,[1:8 10 12:14 16 18:20 22 24:26 28 30:32 34 36:38 40 42:44 46 48:50...
    52 54:56 58 60:62 64 66:68 70 72:74 76 78:80 82 84:86 88 90:92 94
96:108])...
```

```
   H(:,9)+H(:,11)  H(:,15)+H(:,17) H(:,21)+H(:,23) H(:,27)+H(:,29) ...
   H(:,33)+H(:,35) H(:,39)+H(:,41) H(:,45)+H(:,47) H(:,51)+H(:,53)  ...
   H(:,57)+H(:,59) H(:,63)+H(:,65) H(:,69)+H(:,71) H(:,75)+H(:,77)  ...
   H(:,81)+H(:,83)  H(:,87)+H(:,89) H(:,93)+H(:,95)];   %mI.II=mI2+mII1
H=H(:,[1 4 7 9 11 13 15 17 19 21 23 25 27 29 31 33 35 37 39 41 43 45 47 49...
   51 53 55 57 59 61 63 65 67 70 73 76 79:93]);      %removing
mI1=mII2=mIII1=mIV2=0
H=H([1 2 4 5 7 8 10 11 13 14 16 17 19 20 22 23 25 26 29 30 32 33 36 37 39...
  40 42 43 45 46 48 49 51 52 54 55 57 58 60 61 63 64 66 67 69 70 72 73 75...
  76 78 79 81 82 84 85 87 88 90 91 93 94 96 97 99 100], :);
       %M1=M2=M3=M4=M5=M6 no moment on mid and end joints of pantographic
H=[H(1:34,:); H(63,:)+H(65,:); H(64,:)+H(66,:); H(35,:)+H(37,:);
H(36,:)+H(38,:);...
           H(39,:)+H(41,:); H(40,:)+H(42,:); H(43,:)+H(45,:);
H(44,:)+H(46,:);...
           H(47,:)+H(49,:); H(48,:)+H(50,:); H(51,:)+H(53,:);
H(52,:)+H(54,:);...
           H(55,:)+H(57,:); H(56,:)+H(58,:); H(59,:)+H(61,:);
H(60,:)+H(62,:)]; %Px5+Px6=0,Py5+Py6=0, no load on mid joint of pantographic
Amn=H(1:35,1:36); Amp=H(1:35,37:51); Apn=H(36:50,1:36); App=H(36:50,37:51);
A=Amn-Amp*pinv(App)*Apn;
F=[F(:,[1 4 7 10 13 16 19 22 25 28 31 34 37 40 43 46 49 52 55 58 61 64 67...
 70 73 76 79 82 85 88 91 94 97 100 103 106]) F(:,9)+F(:,11)  F(:,15)+F(:,17)
F(:,21)+F(:,23)...
   F(:,27)+F(:,29) F(:,33)+F(:,35) F(:,39)+F(:,41) F(:,45)+F(:,47)
F(:,51)+F(:,53)...
   F(:,57)+F(:,59) F(:,63)+F(:,65) F(:,69)+F(:,71) F(:,75)+F(:,77)
F(:,81)+F(:,83)...
   F(:,87)+F(:,89) F(:,93)+F(:,95)];             %mI.II=mI2+mII1
F=[F([1 4 7 10 13 16 19 22 25 28 31 34 37 40 43 46 49 52 55 58 61 64 67 70 ...
 73 76 79 82 85 88 91 94 97 100 103 106],:); F(9,:)+F(11,:) ; F(15,:)+F(17,:);
F(21,:)+F(23,:);...
  F(27,:)+F(29,:); F(33,:)+F(35,:); F(39,:)+F(41,:); F(45,:)+F(47,:);
F(51,:)+F(53,:);...
  F(57,:)+F(59,:); F(63,:)+F(65,:); F(69,:)+F(71,:); F(75,:)+F(77,:);
F(81,:)+F(83,:);...
  F(87,:)+F(89,:); F(93,:)+F(95,:)];             %mI.II=mI2+mII1
Fnn=F(1:36,1:36); Fnp=F(1:36,37:51); Fpn=F(37:51,1:36); Fpp=F(37:51,37:51);
F=Fnn-Fnp*pinv(App)*Apn-Apn'*pinv(App')*Fpn+Apn'*pinv(App')*Fpp*pinv(App)*Apn;
e0n=zeros(36,1);           %vector of initial bar elongation
e0n(36,1)=u;
e0p=zeros(15,1);
e0t=[e0n; e0p];
r=Apn'*pinv(App');
e0=e0n-r*e0p;
   p1x=0*1.1430; p1y=0*-1.1430;   p2x=0*1.1430; p2y=0*-1.1430; p3x=0*1.1430;
   p3y=0*-1.1430; p4x=0*1.1430;     p4y=0*-1.1430; p5x=0*1.1430; p5y=0*-1.1430;
   p6y=0*-1.1430; p7y=0*-1.1430; p8y=0*-1.1430; p9y=0*-1.1430; p10y=0*-1.1430;
```

```
P=1*[p1x p1y p2x p2y 0 0 p3x p3y 0 0 p4x p4y 0 0 p5x p5y 0 0 0 0 0 p6y 0 p7y 0
0 0 p8y 0 0 0 p9y 0 p10y 0]';
S=null(A);
tH=pinv(A)*P;
alpha=inv(S'*F*S)*(-S'*(e0+F*tH));
tn=tH+S*alpha;
tn([33:36],:);
tp=-pinv(App)*Apn*tn;
e=e0+F*tn;
en=(Fnn-Fnp*pinv(App)*Apn)*tn;
ep=(Fpn-Fpp*pinv(App)*Apn)*tn;
dm=dm+pinv(A')*e;
dm1=pinv(A')*e;
dp=dp+(pinv(App')*ep-pinv(App')*Amp'*dm1); end;
dmx=dm([1;3;7;11;15;21;23;27;31;33],:)
dmy=dm([2;4;8;12;16;22;24;28;32;34],:)
```